ROLE OF METABOLIC OVERLOAD AND METABOLIC INFLAMMATION IN THE DEVELOPMENT OF NASH Wen Liang

ROLE OF METABOLIC OVERLOAD AND METABOLIC INFLAMMATION IN THE DEVELOPMENT OF NONALCOHOLIC STEATOHEPATITIS (NASH)

Wen Liang

ROLE OF METABOLIC OVERLOAD AND METABOLIC INFLAMMATION IN THE DEVELOPMENT OF NONALCOHOLIC STEATOHEPATITIS (NASH)

WEN LIANG

Role of metabolic overload and metabolic inflammation in the development of Nonalcoholic Steatohepatitis (NASH)
Wen Liang

Cover illustration: © iStock signature
Cover design: Rob Koster & Wen Liang
Layout: Wen Liang
Printing: Gildeprint Drukkerijen, Enschede
ISBN: 978-94-6108-920-5

ROLE OF METABOLIC OVERLOAD AND METABOLIC INFLAMMATION IN THE DEVELOPMENT OF NONALCOHOLIC STEATOHEPATITIS (NASH)

Proefschrift

ter verkrijging van
de graad van Doctor aan de Universiteit Leiden,
op gezag van Rector Magnificus prof.mr. C.J.J.M. Stolker,
volgens besluit van het College voor Promoties
te verdediging op dinsdag 31 maart 2015
klokke 16.15 uur

door

Wen Liang

geboren te Xi'an, China
in 1981

PROMOTIECOMMISSIE

Promotor	Prof. dr. L.M. Havekes
Copromotors	Dr. A.M. van den Hoek (TNO, Leiden) Dr. R. Kleemann (TNO, Leiden)
Overige leden	Prof. dr. J.A.P. Willems van Dijk Prof. dr. P. Heeringa (UMCG, Groningen) Prof. dr. M.H. Hofker (UMCG, Groningen) Prof. dr. A. Biggeri (University of Florence, Italy)

The work described in this thesis was performed at the department of Metabolic Health Research at the Gaubius Laboratory of TNO, Leiden, The Netherlands.

The studies were performed within the framework of CTMM, the Center for Translational Molecular Medicine (www.ctmm.nl), project PREDICCT. This work was financially supported by CTMM, and TNO research programs 'Personalized Prevention and Therapy - Op Maat' and 'Enabling Technology Systems Biology'.

The printing of this thesis was kindly supported by TNO MHR, Daan Traas fonds and Dept. Medicine, Div. Endocrinology, LUMC.

To my parents

Sharing beauty and make life fun

TABLE OF CONTENTS

GENERAL INTRODUCTION

HUMAN NASH

Prevalence and risk factors

Nonalcoholic fatty liver disease (NAFLD) is emerging as one of the most common chronic liver diseases during the last decades (1). In US, a dramatic increase in patients with NAFLD has been observed from 30% in 2008 to 46% in 2011 (2) and the prevalence of NAFLD in Asian countries is alarmingly high with 17% in China, 32% in India, 18% in Japan, 32% in Malaysia and 55% in Indonesia (3, 4). Depending on the study population and the diagnosis approach used, the prevalence of NAFLD is estimated between 20% and 40% in the general population (1, 5, 6).

NAFLD is strongly associated with metabolic comorbidities, such as obesity, diabetes mellitus, and dyslipidemia (1). Most recent studies report that NASH has a prevalence of 2-3% in the lean non-Asian population (7) and the prevalence markedly increases in obese (up to 20%) and morbidly obese subjects (up to 50%) (8, 9). However, Asian people with a low body mass index or BMI (~23.5) but higher proportion body fat already has an increased risk for NAFLD. Recent reports have shown that 15%-21% of Asian patients with NAFLD are non-obese (4), suggesting that the other risk factors or the distribution of body fat may be important for NAFLD development as well. Globally, there is a 60% to 76% prevalence of NAFLD in diabetic patients and 22% of those further develop NASH (2, 3). Histopathological evaluation showed that patients with diabetic NAFLD have more severe inflammation than non-diabetic NAFLD patients and are susceptible for rapid progression to fibrosis (8, 9). Furthermore, dyslipidemia is also associated with an increased prevalence to develop NAFLD, for instance in patients with the metabolic syndrome (10). In 2002, the National Institute of Health (NIH) reported that the presence of dyslipidemia (hypertriglyceridemia, hypercholesterolemia, or both), was associated with NAFLD in 20% to 80% of the cases (11). A South Korean study in nonobese, nondiabetic adults showed that insulin resistance and triglyceride levels are independently associated with NAFLD (12).

Diagnosis

Most persons with NAFLD are asymptomatic and the disease is usually discovered when laboratory examination shows abnormal and persistently high levels of liver enzymes, that is alanine aminotransferase (ALT) and aspartate aminotransferase (AST), during screening. However, ALT and AST are also frequently elevated in obese subjects, and it is very difficult to define the upper limits of ‘normal’ for these routine liver enzymes tests (13). Alternatively, NAFLD with bland steatosis can be diagnosed by non-invasive imaging techniques, such as ultrasound, computed tomography (CT) and magnetic resonance imaging (MRI), however, imaging approaches are unable to detect inflammation, a required criteria for NASH diagnosis. Currently, liver biopsy is still the ‘golden standard’ for NASH diagnosis in the clinic and there is an urgent need for alternative diagnostic tools. The procedure of patient selection for biopsy-based diagnosis is illustrated in **Figure 1**. However, since liver biopsy is expensive and invasive and clearly cannot be employed for population screening, accurate noninvasive tests would be of tremendous benefit. The

apoptosis marker CK-18 has been reported recently to be a most promising noninvasive diagnostic test for NASH. In 2006, Wieckpwski et al (14) found that measurement of caspase-cleaved CK-18 levels showed a specificity of 99.9%, and a sensitivity of 85.7% for the diagnosis of NASH. Further validation studies are still needed to clarify the cut-off value for NASH detection when a commercial test for CK-18 would be employed in clinical settings.

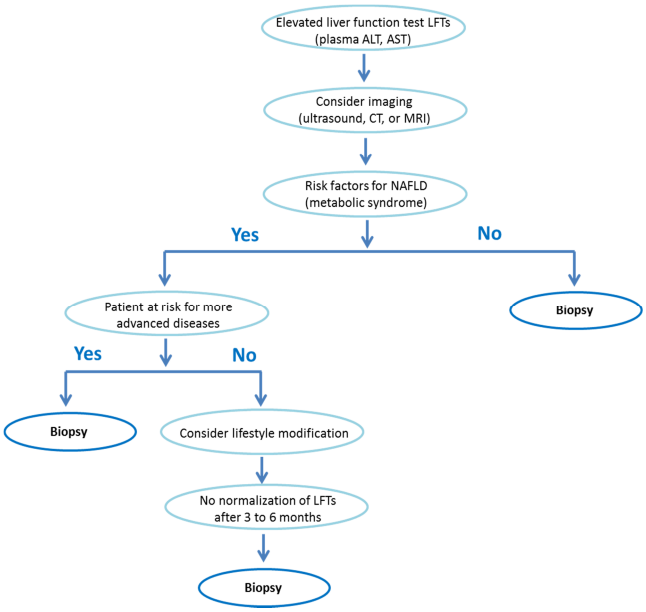

Figure 1: Selection algorithm for assigning patient to biopsy-based diagnosis. Copyright 2009, 2010 The Cleveland Clinic Foundation. All rights reserved.

Histopathology

Histopathologic features

The hallmarks of NASH are steatosis and inflammation (**Figure 2**). Steatosis is always a component of NAFLD and is characterized as an accumulation of intrahepatic lipids in the form of triglycerides and cholesterylesters within hepatocytes (15). Using hematoxylin and eosin (HE) staining or specific stainings for lipids identification such as Oil Red O, intrahepatic fat accumulation can be observed in different forms, namely: 1) macrovesicular steatosis: large fat droplets fill the cytoplasm of hepatocytes, displacing the remaining contents of the cell and the nucleus to the periphery, or 2) microvesicular steatosis: small fat droplets accumulate around the nucleus of the hepatocytes (16). Lobular inflammation is a defining characteristic of NASH livers and foci of inflammatory cell infiltrates, which consist of Kupffer cells, monocytes, and polymorphonuclear leukocytes, are typically detected. Hepatocellular injury is another important feature of NASH and is usually identified as cellular ballooning. Hepatocellular ballooning refers to enlarged hepatocytes, with rarefied and reticulated-like cytoplasm. The ballooned hepatocytes are predominantly located in the neighborhood of steatotic hepatocytes.

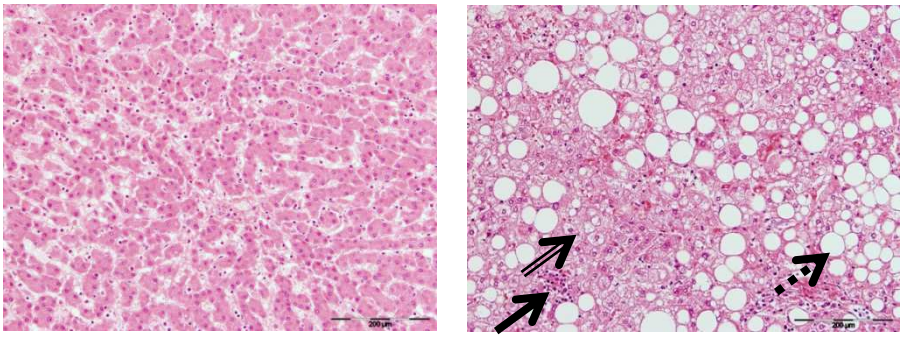

Figure 2: characterization of steatosis and inflammation in human NASH. Macrovesicular steatosis (⇢), microvesicular steatosis (⟹), foci of inflammatory cell infiltrates indicates inflammation (→)

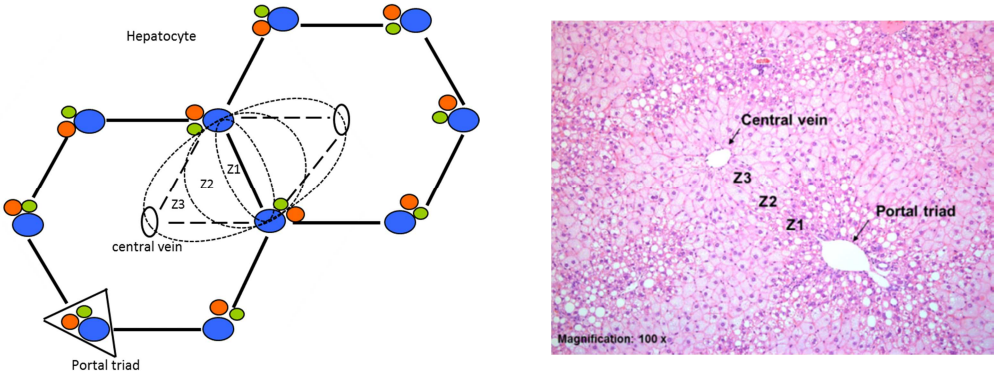

Figure 3: zonation of the liver: schematic diagram (left) and histological (HE) cross- section (right).

The liver parenchyma can be functionally divided into three zones, Z1, Z2 and Z3 (**Figure 3**), which differ with respect to oxygen supply. Z1 is the periportal area, where oxygen- and nutrient enriched blood enters the tissue via the hepatic artery and the portal vein. Z2 is the midzonal area, and Z3 is the pericentral area. The incoming blood flows through sinuses to the central vein. Adult and pediatric patients (2-19 years old) show a different zonal steatosis pattern as shown in **Table 1**.

Table 1: Different steatosis pattern in adult and pediatric patients (2-19 years old).

Patient	Steatosis		
	Predominant pattern	**Zonal location**	**Severity**
Adult	mixed macro- and microvesicular steatosis	pericentral, Z3	+
Pediatric	macrovesicular steatosis	periportal, Z1	++

Scoring system for pathologic evaluation

In 2005, the NASH Clinical Research Network (NASH-CRN) has developed and validated a system of histological evaluation for the full spectrum of NAFLD that could be useful in clinical trials (17). This scoring system of Kleiner et al. (17) separates the grading (activity) from staging (fibrosis) and is also called NAFLD activity score (NAS). The grading is feature-based and encompasses steatosis, inflammation and hepatocellular ballooning (18). Notably, this scoring system of NASH not only relies on the presence of the different features mentioned above, but also on the zonal pattern that develops within the liver. The NAFLD activity score is however not applicable for diagnosis of NASH, but developed for monitoring the severity of the disease in order to assess putative changes in disease progression during the duration of a clinical trial.

Regular intervention and treatment

Lifestyle modification

In clinical practice, the approach for NAFLD and NASH treatment begins with advices on lifestyle modification to induce weight loss. The goal of this primary treatment is to improve steatosis (which is often a reversible condition) and prevent the development of fibrosis, which can lead to cirrhosis and its complications. A Randomized controlled trial (RCT) with 31 obese NASH patients receiving intensive lifestyle changes for 48 weeks showed that subjects with ≥7% weight loss had significant improvement in steatosis, lobular inflammation and ballooning (19). It has been suggested that body weight loss between 5~10% is beneficial for improvement of hepatic steatosis and liver histology (19, 20). Weight loss is commonly achievable by calorie restriction, especially the reduction of calories from dietary carbohydrates, combined with regular exercise. In 2012, the American Association for the Study of Liver Disease (AASLD) proposed a dietary guideline for patients with NAFLD, which recommends an approach of calorie restriction with a low-carbohydrate (40%-45%) or low-fat (<30%) daily calorie intake, to reduce hepatic triglyceride content and to improve insulin resistance (21, 22). A mild and significant reduction in intrahepatic triglyceride content was reported in a recent randomized clinical trial (RTC) after 16 weeks of 150-300 min (per week) of moderate intensity exercise (23). Another RCT showed similar reduction in hepatic fat content, as well as an improvement of BMI and insulin resistance after following aerobic exercise and anaerobic resistance training for 4 months (24). In practice, the initiation of an exercise program is recommended based on the current activity level of the patient, however, it is hard to reach a consensus on the type, intensity and duration of exercise which are optimal for patients with NAFLD or NASH.

Vitamin E

Although the most safe treatment for NAFLD or NASH is lifestyle modification, weight loss is still difficult to maintain in the long term (25). Therefore, additional supplementary therapy is often necessary. Vitamin E (α-tocopherol) is an antioxidant and vitamin E-800 international units (IU)/day is currently considered as a first-line treatment for non-diabetic, non-cirrhotic NASH patients (21). The largest clinical trial to date, PIVENS, which

tested 800 IU/day vitamin E in 84 subjects with NASH for 96 weeks, showed significant reductions in ALT (P<0.001), AST (P<0.001), hepatic steatosis (P<0.005), and lobular inflammation (P<0.02), but no significant improvement in fibrosis (P<0.24) (26). After 2 years, the follow-up analysis showed that beneficial changes in ALT were more frequent among vitamin E treated subjects (48%) than placebo (16%) recipients (P<0.001). Among vitamin E recipients, ALT responses were associated with decreases in NAS (P<0.001), but not with fibrosis scores (P=0.34) (27). Although vitamin E has consistently shown to have an effect in improving serum ALT and AST as well as liver histology in patients with NASH, one concern is whether it increases all-cause mortality. Since there are conflicting data from different clinical trials, additional RCTs are needed to determine long-term efficacy and safety of vitamin E (28).

Thiazolidinediones

When vitamin E is not effective, administration of pharmacological agents (e.g. pioglitazone rosiglitazone) as adjunctive therapy is widely applied in the clinic. Pioglitazone and rosiglitazone belong to the class of thiazolidinediones (TZDs). TZDs can improve insulin sensitivity by activating the nuclear transcription factor peroxisome proliferator activated-receptor-gamma (PPAR-γ), thereby upregulating gene transcription for several proteins involved in glucose and lipid metabolism (29). A pilot study in 18 non-diabetic NASH patients showed that 30 mg/day pioglitazone for 48 weeks led to a significant reduction in transaminases (ALT, AST), and a significant improvement in NAS (P<0.05) (30). A recent meta-analysis that included 5 RCTs showed that pioglitazone significantly improved steatosis (OR 4.05, 95% CI 2.58-6.35) and inflammation (OR 3.53, 95 % CI 2.21-5.64), but not fibrosis (OR 1.40, 95% CI 0.87-2.24) (3). The long-term safety of TZDs has been debated regarding the risk of cardiovascular disease (31), congestive heart failure (32) and bladder cancer (33). In a recent meta-analysis (32) of 19 trials enrolling a total of 16.390 patients with T2DM, pioglitazone treatment was associated with a significant reduction (18%) in the primary outcome of death, myocardial infarction or stroke (P<0.005), however, there was also a higher rate of congestive heart failure with pioglitazone (2.3% vs.1.8% in the control group, P<0.002). Therefore, in September 2010, the European Medicines Agency (EMA) recommended that the drug should be suspended from the European market because the benefits of rosiglitazone no longer outweighed the risks. In US, rosiglitazone only could be sold with a prescription from a certified doctor and patients were required to be informed of the risks associated with its use through specified pharmacies. Until November 2013, the FDA lifted its earlier restrictions on rosiglitazone after reviewing the results of several other clinical trials, which did not provide evidence for an increased risk of heart infarct associated with the use of the drug.

Agents in clinical trials

Ezetimibe

Ezetimibe, as a potent inhibitor of cholesterol absorption, inhibits Niemann–Pick C1-like 1 (NPC1L1)-dependent cholesterol transport in liver (34). The beneficial effects of ezetimibe on improvement of liver steatosis and insulin resistance have been observed in mice fed a high fat diet (35) and Zucker obese fatty rats (36). An open-label study enrolled 45

patients with liver biopsy-proven NAFLD for treatment with ezetimibe (10 mg/day) for 24 months. It was found that ezetimibe therapy significantly lowered serum ALT and CRP levels, whereas no significant changes were observed in adiponectin, leptin, and resistin levels. Histological features of steatosis score (P=0.0003), necro-inflammatory score (P=0.0456), ballooning score (P=0.0253) and NAS (P=0.0007) were significantly improved relative to baseline (the trial had no placebo control group). However, the fibrosis stage was not significantly (P=0.6547) changed (37). A recent RCT trail showed that ezetimibe (10 mg/day) treatment for 6 months significantly lowered the level of serum total cholesterol and also improved hepatic ballooning score and fibrosis stage, but significantly increased hepatic long-chain fatty acids and HbA_{1c} compared to the control group (38). Collectively, the effect of ezetimibe on NASH still needs further examination in future studies.

Metreleptin

In February 2014, the US Food and Drug Administration (FDA) approved orphan drug MYALEPT™ (metreleptin for injection), which is indicated as an adjunct to diet as replacement therapy for the treatment of complications of leptin deficiency in patients with lipodystrophy. Metreleptin is recombinant human leptin. In a recent human study, NASH patients received subcutaneous administration of metreleptin daily for 2 years (39). Besides a significant improvement in metabolic profile, ALT and AST, patients treated with metreleptin also showed significant improvements in steatosis (reduction of mean score from 1.8 to 0.9) and ballooning injury scores (from 1.2 to 0.4), as well as a 44.2% reduction in NAS ($p<0.0001$) while fibrosis remained stable (39). Another ongoing RCT has been performed by the University of Michigan and is expected to complete in September 2015. The aim of this trail is to determine if the one-year treatment of metreleptin can improve NAFLD or NASH in patients with concurrent lipodystrophy, By taking pre-treatment and post-treatment liver biopsies and measuring various metabolic markers, this trial will evaluate the safety and effectiveness of metreleptin for the treatment of NAFLD/NASH.

L-carnitine

In mammals, L-carnitine is a conditionally essential nutrient that can be synthesized endogenously from lysine and methionine or obtained from the diet, primarily from red meat (40). L-carnitine is indispensable for energy metabolism and has been proposed as a supplement to treat a variety of health conditions including heart attack and heart failure (41, 42). *In vitro* and *in vivo* studies found that L-carnitine enhances both lipolysis and fatty acid oxidation (43) and that it reduces serum fatty acid levels by increasing beta-oxidation in hepatocytes (44, 45). Recently, dietary supplementation of L-carnitine (1000 mg/day) was investigated in 74 NASH patients, over a period of 6 months (46). Laboratory parameters in patients treated with L-carnitine showed significant improvements in plasma risk factors, among which a decrease of serum ALT/AST, TNF and CRP levels, and an improvement of insulin resistance. All patients (36) showed a significant reduction in steatosis, parenchymal inflammation, and hepatocellular injury, and 32 patients (86%) had improvement in fibrosis. Another recent RCT trail has been performed by Tehran University of Medical Sciences with the estimated completion year of 2015. After 2 years

treatment of L-carnitine (1000 mg/day), the level of ALT, AST and liver elasticity in NASH patients will be measured to evaluate the effect of L-carnitine on NASH (28).

Polyphenols

Polyphenols are often concentrated in leaf tissue and consist of 1-25% of the dry green leaf mass (47). A high amount of polyphenols has been found in green tea (about 35% of its total dry weight) (48). Studies from Park HJ et al. indicate that green tea extract attenuated hepatic steatosis by decreasing adipose lipogenesis and enhancing hepatic anti-oxidant defenses in ob/ob mice (49), as well as that it suppressed hepatic NFκB activation and inflammatory responses in diet-induced obese rats (50). Although several human studies have been conducted on the anti-obesity effects of dietary polyphenols (51, 52), the effects of dietary polyphenols on NAFLD are missing. In a recent RCT study, 44 participants (age 18–25 y, BMI ≥23.1 kg/m^2) were given 250 mL of either bayberry juice or placebo twice daily for 4 weeks. Compared with placebo, the consumption of bayberry juice significantly decreased the plasma levels of TNF-α ($P<0.001$) and IL-8 ($P=0.022$), although no significant changes in plasma TGs, TC, LDL-C, fasting glucose level, insulin concentration, or HOMA-IR were found (53). Due to variation among subjects (age, gender, ethnicity), chemical forms of the dietary polyphenols used and confounding factors such as other weight-reducing agents, future RCT are warranted to evaluate the efficacy of dietary polyphenols on NAFLD/NASH.

EXPERIMENTAL NASH

Taken together, the major current challenges for the study of human NASH are: 1) lack of specific and efficient non-invasive methods that detect inflammation and fibrosis in the liver and 2) lack of effective and reliable therapeutic approaches that are based on understanding the pathogenesis of NASH. Furthermore, studies of NASH in humans have limitations or ethical issues regarding the collection of liver biopsies from patients and the administration of drugs to patients because of safety concerns. Animal models of NASH that mimic human disease can thus provide crucial mechanistic information, not only for elucidating the pathogenesis of NASH but also for examining therapeutic effects of various agents.

Available diet-inducible animal NASH models

Ideally, animal models should mimic both histopathology and pathophysiology of human NASH. Recently, several review articles on animal models of NAFLD/NASH have been published (54-56). An overview of the metabolic and hepatic characteristics of current diet-inducible NASH animal models is provided in **Table 2**. C57BL6 mice fed a HFD acquire a human NASH-like metabolic and histological phenotype, but a very long feeding period (>50 weeks) is required. MCD diet-induced NASH shows similar pathohistological features as human NASH, but does not develop the metabolic syndrome characteristics of human risk groups and therefore do not exhibit the metabolic context which is seen in most human NASH patients. Fructose with/without HFD or ALIOS diet feeding leads to elevated plasma insulin, resistin, and leptin levels, as well as increased plasma ALT levels, liver TNF-

α and procollagen mRNA, indicating an inflammatory and profibrogenic response to injury. These diets also lead to hepatic steatosis and inflammation with a similar histological featuresas observed in patients with NASH. LDLR$^{-/-}$ mice fed a HFD or HFC also develop a human-like NASH with respect to the metabolic context and histological phenotype, and this strain of mice is prone to develop fibrosis. Although the available animal models do not reflect the full spectrum of human NAFLD pathology, they are useful for verifying hypotheses on the pathogenesis of NASH and for testing pharmaceutical compounds in intervention studies.

Table 2: Metabolic and pathological characteristics of animal NAFLD/NASH models. Important phenotypic and histological hallmarks are compared and the severity of a particular parameter is indicated as "+", "++", "+++", absence of a particular feature is indicated as"-".

	Phenotypic hallmarks			Histological hallmarks				
Model	Obesity	IR	Hypertriglyceridemia	Steatosis		Inflammation	Fibrosis	Ref.
				Predominate pattern	Severity			
C57BL6, HFD*	+	+	+	microvesicular	++	+	+	(57)
C57BL6, HFD+fructose**	+++	++	+++	macrovesicular	+++	+	not described	(58)
C57BL6, ALIOS diet	+++	++	++	macrovesicular	++	+	not described	(59)
C57BL6, MCD diet	-	-	-	macrovesicular	+++	+++, lymphocytes & neutrophils	++	(60-62)
Ob/ob, HFD	+++	++	++	not described	++	-	-	(63, 64)
ApoE2 knock-in, HFC	+	-	++	not described	++	++, macrophages	upregulation of collagen synthesis genes	(65, 66)
ApoE$^{-/-}$, HFC	+	+	++	macrovesicular	++	++, macrophages	not described	(67, 68)
LDLR$^{-/-}$, HFD	++	++	++	not described	++	++	+	(69)
LDLR$^{-/-}$, HFC	+++	++	+++	macrovesicular	+++	+++, macrophages	++	(66, 70)
hCRP, HFD	++	++	++	macrovesicular	++	++	+	(71)

IR: insulin resistance; HFD: high fat diet; HFC: high fat high cholesterol diet; MCD: methionine choline deficient diet

**C57BL6 wild type mice hardly develop NASH, the features shown in the table were present only when they were fed for up to 50 weeks.*

***Alios diet: 45% kcal from fat (30% from partially hydrogenated vegetable oil (28% saturated fatty acids, 57% monounsaturated fatty acids, 13% polyunsaturated fatty acids) + high fructose corn syrup equivalent (55% fructose, 45% glucose by weight) (42 g/l as gel-water)*

Note: Since the severity of NASH largely depends on how long a study is performed, studies with 8-15 weeks feeding period are included in the table (except for C57BL6 on MCD diet, which were fed the MCD diet for 50 weeks).

Pathogenesis of NASH

Intrahepatic effects of lipid imbalance on NASH

Triglycerides (TGs) are utilized as metabolic fuel via fatty acids oxidation. In liver, TGs can either be stored in hepatocytes or can be exported as very low density lipoprotein (VLDL). An increase of TGs in hepatocytes, which ultimately leads to hepatic steatosis, can be due to 1) increased dietary intake of free fatty acids, 2) increased *de novo* lipogenesis, 3) increased recirculation of non-esterified fatty acids to the liver from the peripheral tissues (e.g. adipose tissue or skeletal muscle), or 4) failure of hepatic clearance of fatty acids due to either impaired esterification to TGs and export as VLDL, or impaired hepatic mitochondrial β-oxidation (16). In the next paragraphs, the dietary intake and the contribution of different dietary components (HFD, dietary cholesterol and dietary carbohydrate) on NASH development will be discussed.

HFD

Studies in humans (15) and animals (72) have shown that different types of fatty acids can lead to different outcomes with respect to liver injury. Nutritional surveys showed that the dietary intake of saturated fats (SF) was significantly higher in NAFLD and NASH patients than in healthy controls (73, 74). Consistent with this, a high fat diet (HFD), that consists of >24% of energy from fat, is commonly used to induce hepatic steatosis in animal NASH models. In a high fat diet rat model, Buettner et al. (72) compared different high fat diets: coconut oil (primarily SF), olive oil (primarily monounsaturated fatty acids, MUFA), lard (mixture of SF and MUFA), and fish oil (primarily polyunsaturated fatty acids, PUFA). After 12 weeks, the first three diets significantly worsened hepatic steatosis as well as elevated plasma TG, whereas the fish oil (PUFA)-based diet did not.

However, growing evidence suggests that HFD alone is not sufficient to induce NASH (75, 76). A refined time course analysis (77) of HFD feeding in rodents showed that the inflammatory response of the liver is transient and that the liver can adapt its metabolic program to the HFD overload. Therefore experimental steatosis hardly progresses into the extensively inflamed conditions of NASH as they are observed in patients. This suggests that additional inflammatory triggers are important to experimentally induce an inflamed fatty liver.

Dietary cholesterol

The role of cholesterol on the development of NASH is recently getting more attention. In a large, nationally epidemiological study in the United States, dietary cholesterol consumption was independently associated with the development of cirrhosis (78). Another recent, pilot trial of ezetimibe, as an intestinal cholesterol absorption inhibitor, found improvements in hepatic steatosis and inflammation in humans with NASH (37, 79). Animal data are also emerging to support a role for dietary cholesterol in the progression

towards NASH. Hofker MH and colleagues (66) suggested that dietary cholesterol induced hepatic inflammation independently of hepatic steatosis in a hyperlipidemic mouse model with NASH. A study by Ioannou at al. (80) recently compared different diets (high fat, high cholesterol and high fat+high cholesterol) to examine their effects on NASH development. After 30 weeks of diet feeding using C57BL/6J mice, only high fat+high cholesterol diet led to significant levels of hepatic steatosis, hepatic inflammation, and perisinusoidal fibrosis with a similar profile of risk factors as seen in human NASH. These effects were associated with adipose tissue inflammation and a reduction in plasma adiponectin levels. Interestingly, an investigation of dietary records by Yasutake et al. (81) revealed that cholesterol intake was significantly greater in both obese and non-obese NAFLD patients than in healthy controls. Surprisingly, non-obese NAFLD patients even had higher cholesterol consumption than obese NAFLD patients, suggesting that cholesterol intake may cause NAFLD independent of obesity. Based on available human and animal data, it has been hypothesized that cholesterol-induced liver injury could be an important cause of NASH independent of obesity, insulin resistance or even steatosis as proposed recently (82). However, the exact molecular mechanism of the effects of dietary cholesterol on NASH pathogenesis is still unknown.

Dietary carbohydrate

Several human and animal studies suggest that carbohydrates, such as sucrose and fructose, are possibly causative to NAFLD development (83). Nutrition reports have shown that the mean daily consumption and mean frequency of soft drinks is at least two fold higher in NAFLD patients than in healthy subjects (84, 85). High amount of fructose consumption is thought to be one of the most important dietary contributors to the pathogenesis of NAFLD. In a large clinical study performed by the NASH Clinical Research Network, dietary fructose consumption was found to be associated with induction of histological features of NASH, including hepatic inflammation and hepatocyte ballooning and fibrosis stage (86). Animal studies have shown that excess intake of fructose is closely associated with obesity and steatosis, through the activation of sterol regulatory element-binding protein-1c (SREBP-1c), a transcription factor that enhances the expression of enzymes associated with fatty acid synthesis (87, 88), and with increased visceral adiposity (89) and insulin resistance (58). Some animal studies have shown that high-fructose feeding is associated with upregulation of markers of inflammation, macrophage activation and oxidative stress. A recent study form Bhattacharjee demonstrated that fructose-induced NAFLD is associated with recruitment of T cells and NK cells in mice (90).

Intrahepatic effects of inflammation leading to NASH

Pro-inflammatory cytokines

Pro-inflammatory cytokines are important contributors to the development of NASH (91). TNF-α secreted by adipocytes and hepatocytes, was the first cytokine known to be elevated in NAFLD patients (92). Human data has shown that TNF-α is elevated in NAFLD patients compared with both obese and non-obese controls (93). Crespo et al. (94) identified increased mRNA expression of TNF-α and TNF-α receptor, p55, and showed that circulating levels of these molecules are associated with fibrosis in NAFLD patients. In

leptin-deficient (ob/ob) mice fed a high-fat diet, dietary manipulations that favor pathways which quench TNF-α improved insulin sensitivity, hepatic steatosis, and inflammatory cells infiltration in the liver (95).

Data from human studies have shown that increased systemic IL-6 levels are associated with increased inflammation and fibrosis in NAFLD patients (96). Wieckowska et al. found that IL-6 expression was increased in both hepatocytes and Kupffer cells and these levels positively correlated with both the inflammatory activity and the stage of fibrosis in NAFLD patients (97). Evidence from human and animal studies indicate that pro-inflammatory (TNF-α, IL-6)-induced insulin resistance and lipid overloading of liver cells both involve activation of stress-related protein kinases such as IKKβ, an activator of the proinflammatory transcription factor NFκB) and Jun N-terminal kinase (JNK), an activator of AP-1. These pathways subsequently increase inflammatory mediators like CRP, TNF-α, IL-6, and IL-1β, which further can contribute to liver injury (16, 98). IKKβ activation leads to NFκB translocation to the nucleus, resulting in a feed–forward loop that promotes increased expression of pro-inflammatory cytokines and other mediators of inflammation that augment hepatic inflammation and insulin resistance (99). Activation of NFκB has been observed in human NASH (100) and NASH mouse models (101). Animal studies have shown that pro-inflammatory cytokines (e.g. TNF-α, IL-1β) released from NFκB-activated Kupffer cells could also activate NFκB in adjacent hepatocytes (102). The involvement of hepatic NFκB in the progression of bland steatosis to NASH has recently been proposed in transgenic mice selectively expressing constitutively active IKKβ in hepatocytes (98). The JNKs (1 and 2) can be stimulated via activation of TNF superfamily death-signaling receptors (e.g. Fas, TNF-R1, TNF-related apoptosis-inducing ligand death receptors) and TLRs, or they can directly activated by lipotoxic molecules and oxidative stress (103). Videla et al. (100) showed that, in liver, NFκB and AP-1 DNA binding is significantly increased in NASH patients. In animal studies, removal of JNK1 or IKKβ suppressed pro-inflammatory gene expression and cytokine release (104, 105). Farrell et al. (106). showed that both JNK1 and JNK2 are activated in a NASH mouse model and, conversely, italso been shown that abolishing JNK activation can attenuate macrophage accumulation, hepatocyte apoptosis and liver injury in the context of NAFLD (102). However, the exact nature of most of the inflammatory mediators that cause the transition from bland steatosis to NASH is still largely unknown.

Oxidative stress

Oxidative stress, refers to an imbalance in the production of reactive oxygen species (ROS) and protective antioxidants, and has been considered to be an important contributor to the development of NASH (16). Oxidative damage is significantly correlated with inflammation and increased in the livers of patients with NAFLD when compared with controls (107). Sanyal et al. (108) demonstrated that immunohistochemical staining for 3-nitrotyrosine, a marker for oxidative stress, was elevated in NAFLD patients as compared to controls and was markedly higher in NASH patients than in patients with bland steatosis. Mitochondrial dysfunction leading to uncoupling of oxidative phosphorylation and resulting in ROS generation has been reported in NASH subjects (108, 109). Furthermore, in NASH patients increased activity of the mitochondrial cytochrome P450 2E1 (CYP2E1) has been observed (110). Studies in rats using the methionine choline

deficient diet to induce NASH found increased CYP2E1 activity (111). Using CYP2E1 knock-out mice, Abdelmegeed et al. recently showed that CYP2E1 plays a role in NASH development (112) and the authors suggest that the CYP2E1 enzyme may have a capacity of directly generating ROS. Moreover, upregulaton of cytokine receptors, especially TNF-α and antigens derived from gut flora via activation of NADPH oxidase system, also may play a role in the progression of NASH (16, 113).

In 1998, Day and James proposed the 'two-hit theory' (114) and described a possible pathogenic mechanism for the development of NASH: extensive lipid accumulation as a 'first hit' is followed by inflammation (as 'second hit') causes the progression of the disease towards NASH. On the other hand, clinical researchers occasionally found patients with NASH without obvious steatosis. Furthermore, steatosis could be improved in ob/ob mice when treated with anti-tumor necrosis (TNF)-α antibody (95). After a series of debates on the proposed sequence of events, either sequentially or in parallel, the concept of 'multiple parallel hits' has recently been considered (115). More recently, Jou et al. (116) proposed hepatocyte death and lack of repair as a possible 'third hit'. This theory proposes that combined oxidative/metabolic stress and in imbalanced cytokine production, may lead to an increase of hepatocytes death. These multiple hits can occur simultaneously and are intertwined; this may eventually lead to NASH (16, 117).

OUTLINE OF THE THESIS

Metabolic stress caused by excess dietary intake is considered to be an important contributor to NASH in humans, but the exact molecular mechanism of metabolic overload-induced NASH is largely unknown. Therefore, the aim of this thesis was to better understand the role of metabolic overload and metabolic inflammation in the development of NASH.

The NAFLD activity score (NAS) used in clinical studies has not been validated for animal models of NASH. In ***Chapter 2***, we developed a generic scoring system for the assessment of NAFLD in mice. This new scoring system allows to grade the histological features present in the various NASH mouse models currently used in preclinic research. Our scoring system is based on the human NAS system, and the inter- and intra-observer reproducibility was analyzed and found to be reliable.

After this methodological optimization and in order to get insight into the nature of the chronic inflammatory component that drives the development of NASH, we examined in ***Chapter 3*** the effect of non-metabolic triggers (LPS, IL-1β administered by slow-release minipumps) and metabolic dietary triggers (carbohydrate, cholesterol) of inflammation on the progression of bland steatosis to NASH. We showed that HFD feeding followed by metabolic triggers induced extensive steatosis and specific inflammatory components (neutrophils, AP-1) which results in a human-like NASH phenotype, while long-term LPS and IL-1β stimulation on top of HFD feeding did not. We next analyzed the distinct types of steatosis, microvesicular and macrovesicular steatosis, during NAFLD development over time, and investigated how steatosis is related to the onset of hepatic inflammation. More specifically, we performed in ***Chapter 4*** a time-course study using a metabolic inflammatory trigger (HFD+cholesterol). Histological hallmarks of NASH, such as macro-

vesicular/micro-vesicular steatosis, inflammatory cell infiltrates, NFκB activation and fibrosis were evaluated, and the correlations between the specific forms of steatosis, hepatic inflammation and activation of inflammatory transcription factors were established.

Next, we examined specific nutritional and pharmacological interventions that may attenuate diet-induced experimental NASH. In ***Chapter 5***, the effect of Mirtoselect, a standardized anthocyanin-rich bilberry extract was evaluated on the progression of NASH. We showed that Mirtoselect has profound effects on intrahepatic inflammatory processes resulting in a significant attenuation of NASH and associated fibrosis. In ***Chapter 6***, we studied the effect of an anti-inflammatory drug, salsalate, on diet-induced NASH in a short-term and a long-term study. Salsalate exhibited strong NASH-reducing properties and almost fully attenuated hepatic steatosis and inflammation.

Besides in liver, chronic metabolic overload may also develop in other organs which potentially contribute to NAFLD development. In ***Chapter 7***, we analyzed the development of metabolic stress in white adipose tissue and liver over time and found that white adipose inflammation preceded liver inflammation and NAFLD. The nature of the metabolic adaptations in WAT and liver were remarkably similar. The same transcriptional regulators were found to be activated to orchestrate the complex responses to metabolic overload. Finally, we investigated how long-term HFD-induced metabolic overload (t=42 weeks) would affect metabolic and inflammatory processes in the kidney in ***Chapter 8***. Drugs with established anti-inflammatory properties (rosuvastatin and rosiglitazone) were tested regarding their potency to reduce metabolically-induced organ inflammation and to improve kidney function.

Finally, the findings from the above studies and their implications are discussed in ***Chapter 9***.

REFERENCES

1. Lazo M, Clark JM. The epidemiology of nonalcoholic fatty liver disease: A global perspective. *Semin Liver Dis* 2008;28(4):339-50.

2. Williams CD, Stengel J, Asike MI, et al. Prevalence of nonalcoholic fatty liver disease and nonalcoholic steatohepatitis among a largely middle-aged population utilizing ultrasound and liver biopsy: A prospective study. *Gastroenterology* 2011;140(1):124-31.

3. Vernon G, Baranova A, Younossi ZM. Systematic review: The epidemiology and natural history of non-alcoholic fatty liver disease and non-alcoholic steatohepatitis in adults. *Aliment Pharmacol Ther* 2011;34(3):274-85.

4. Chitturi S, Wong VW, Farrell G. Nonalcoholic fatty liver in asia: Firmly entrenched and rapidly gaining ground. *J Gastroenterol Hepatol* 2011;26 Suppl 1:163-72.

5. WHO fact files: Ten facts on obesity [homepage on the Internet]. Geneva: WHO. 2010. Available from: http://www.who.int/features/facfiles/obesity/en/index.html.

6. Bellentani S, Scaglioni F, Marino M, et al. Epidemiology of non-alcoholic fatty liver disease. *Dig Dis* 2010;28(1):155-61.

7. Neuschwander-Tetri BA, Bacon BR. Nonalcoholic steatohepatitis. *Med Clin North Am* 1996;80(5):1147-66.

8. Adams LA, Sanderson S, Lindor KD, et al. The histological course of nonalcoholic fatty liver disease: A longitudinal study of 103 patients with sequential liver biopsies. *J Hepatol* 2005;42(1):132-8.

9. Angulo P, Keach JC, Batts KP, et al. Independent predictors of liver fibrosis in patients with nonalcoholic steatohepatitis. *Hepatology* 1999;30(6):1356-62.

10. Targher G, Bertolini L, Padovani R, et al. Prevalence of nonalcoholic fatty liver disease and its association with cardiovascular disease among type 2 diabetic patients. *Diabetes Care* 2007;30(5):1212-8.

11. National Cholesterol Education Program (NCEP) Expert Panel on Detection, Evaluation, and Treatment of High Blood Cholesterol in Adults (Adult Treatment Panel III). Third report of the national cholesterol education program (NCEP) expert panel on detection, evaluation, and treatment of high blood cholesterol in adults (adult treatment panel III) final report. *Circulation* 2002;106(25):3143-421.

12. Kim HJ, Kim HJ, Lee KE, et al. Metabolic significance of nonalcoholic fatty liver disease in nonobese, nondiabetic adults. *Arch Intern Med* 2004;164(19):2169-75.

13. Pacifico L, Poggiogalle E, Cantisani V, et al. Pediatric nonalcoholic fatty liver disease: A clinical and laboratory challenge. *World J Hepatol* 2010;2(7):275-88.

14. Wieckowska A, Zein NN, Yerian LM, et al. In vivo assessment of liver cell apoptosis as a novel biomarker of disease severity in nonalcoholic fatty liver disease. *Hepatology* 2006;44(1):27-33.

15. Puri P, Baillie RA, Wiest MM, et al. A lipidomic analysis of nonalcoholic fatty liver disease. *Hepatology* 2007;46(4):1081-90.

16. Tiniakos DG, Vos MB, Brunt EM. Nonalcoholic fatty liver disease: Pathology and pathogenesis. *Annu Rev Pathol* 2010;5:145-71.

17. Kleiner DE, Brunt EM, Van Natta M, et al. Design and validation of a histological scoring system for nonalcoholic fatty liver disease. *Hepatology* 2005;41(6):1313-21.

18. Brunt EM, Janney CG, Di Bisceglie AM, et al. Nonalcoholic steatohepatitis: A proposal for grading and staging the histological lesions. *Am J Gastroenterol* 1999;94(9):2467-74.

19. Promrat K, Kleiner DE, Niemeier HM, et al. Randomized controlled trial testing the effects of weight loss on nonalcoholic steatohepatitis. *Hepatology* 2010;51(1):121-9.

20. Suzuki A, Lindor K, St Saver J, et al. Effect of changes on body weight and lifestyle in nonalcoholic fatty liver disease. *J Hepatol* 2005;43(6):1060-6.

21. Chalasani N, Younossi Z, Lavine JE, et al. The diagnosis and management of non-alcoholic fatty liver disease: Practice guideline by the american association for the study of liver diseases, american college of gastroenterology, and the american gastroenterological association. *Hepatology* 2012;55(6):2005-23.

22. Kirk E, Reeds DN, Finck BN, et al. Dietary fat and carbohydrates differentially alter insulin sensitivity during caloric restriction. *Gastroenterology* 2009;136(5):1552-60.

23. Sullivan S, Kirk EP, Mittendorfer B, et al. Randomized trial of exercise effect on intrahepatic triglyceride content and lipid kinetics in nonalcoholic fatty liver disease. *Hepatology* 2012;55(6):1738-45.

24. Bacchi E, Negri C, Targher G, et al. Both resistance training and aerobic training reduce hepatic fat content in type 2 diabetic subjects with nonalcoholic fatty liver disease (the RAED2 randomized trial). *Hepatology* 2013;58(4):1287-95.

25. Torres DM, Williams CD, Harrison SA. Features, diagnosis, and treatment of nonalcoholic fatty liver disease. *Clin Gastroenterol Hepatol* 2012;10(8):837-58.

26. Violi F, Cangemi R. Pioglitazone, vitamin E, or placebo for nonalcoholic steatohepatitis. *N Engl J Med* 2010;363(12):1185-86.

27. Hoofnagle JH, Van Natta ML, Kleiner DE, et al. Vitamin E and changes in serum alanine aminotransferase levels in patients with non-alcoholic steatohepatitis. *Aliment Pharmacol Ther* 2013;38(2):134-43.

28. Pearlman M, Loomba R. State of the art: Treatment of nonalcoholic steatohepatitis. *Curr Opin Gastroenterol* 2014;30(3):223-37.

29. Smith U. Pioglitazone: Mechanism of action. *Int J Clin Pract Suppl* 2001;(121)(121):13-8.

30. Promrat K, Lutchman G, Uwaifo GI, et al. A pilot study of pioglitazone treatment for nonalcoholic steatohepatitis. *Hepatology* 2004;39(1):188-96.

31. Ratziu V, Caldwell S, Neuschwander-Tetri BA. Therapeutic trials in nonalcoholic steatohepatitis: Insulin sensitizers and related methodological issues. *Hepatology* 2010;52(6):2206-15.

32. Lincoff AM, Wolski K, Nicholls SJ, et al. Pioglitazone and risk of cardiovascular events in patients with type 2 diabetes mellitus: A meta-analysis of randomized trials. *JAMA* 2007;298(10):1180-8.

33. Neumann A, Weill A, Ricordeau P, et al. Pioglitazone and risk of bladder cancer among diabetic patients in france: A population-based cohort study. *Diabetologia* 2012;55(7):1953-62.

34. Garcia-Calvo M, Lisnock J, Bull HG, et al. The target of ezetimibe is niemann-pick C1-like 1 (NPC1L1). *Proc Natl Acad Sci U S A* 2005;102(23):8132-7.

35. de Bari O, Neuschwander-Tetri BA, Liu M, et al. Ezetimibe: Its novel effects on the prevention and the treatment of cholesterol gallstones and nonalcoholic fatty liver disease. *J Lipids* 2012;2012:3028-47.

36. Deushi M, Nomura M, Kawakami A, et al. Ezetimibe improves liver steatosis and insulin resistance in obese rat model of metabolic syndrome. *FEBS Lett* 2007;581(29):5664-70.

37. Park H, Shima T, Yamaguchi K, et al. Efficacy of long-term ezetimibe therapy in patients with nonalcoholic fatty liver disease. *J Gastroenterol* 2011;46(1):101-7.

38. Takeshita Y, Takamura T, Honda M, et al. The effects of ezetimibe on non-alcoholic fatty liver disease and glucose metabolism: A randomised controlled trial. *Diabetologia* 2014;57(5):878-90.

39. Safar Zadeh E, Lungu AO, Cochran EK, et al. The liver diseases of lipodystrophy: The long-term effect of leptin treatment. *J Hepatol* 2013;59(1):131-7.

40. Strijbis K, van Roermund CW, Hardy GP, et al. Identification and characterization of a complete carnitine biosynthesis pathway in candida albicans. *FASEB J* 2009;23(8):2349-59.

41. Koeth RA, Wang Z, Levison BS, et al. Intestinal microbiota metabolism of L-carnitine, a nutrient in red meat, promotes atherosclerosis. *Nat Med* 2013;19(5):576-85.

42. DiNicolantonio JJ, Lavie CJ, Fares H, et al. L-carnitine in the secondary prevention of cardiovascular disease: Systematic review and meta-analysis. *Mayo Clin Proc* 2013;88(6):544-51.
43. Murosaki S, Lee TR, Muroyama K, et al. A combination of caffeine, arginine, soy isoflavones, and L-carnitine enhances both lipolysis and fatty acid oxidation in 3T3-L1 and HepG2 cells in vitro and in KK mice in vivo. *J Nutr* 2007;137(10):2252-7.
44. Lin X, Shim K, Odle J. Carnitine palmitoyltransferase I control of acetogenesis, the major pathway of fatty acid {beta}-oxidation in liver of neonatal swine. *Am J Physiol Regul Integr Comp Physiol* 2010;298(5):R1435-43.
45. Noland RC, Koves TR, Seiler SE, et al. Carnitine insufficiency caused by aging and overnutrition compromises mitochondrial performance and metabolic control. *J Biol Chem* 2009;284(34):22840-52.
46. Malaguarnera M, Gargante MP, Russo C, et al. L-carnitine supplementation to diet: A new tool in treatment of nonalcoholic steatohepatitis--a randomized and controlled clinical trial. *Am J Gastroenterol* 2010;105(6):1338-45.
47. Hattenschwiler S, Vitousek PM. The role of polyphenols in terrestrial ecosystem nutrient cycling. *Trends Ecol Evol* 2000;15(6):238-43.
48. Wang S, Noh SK, Koo SI. Green tea catechins inhibit pancreatic phospholipase A(2) and intestinal absorption of lipids in ovariectomized rats. *J Nutr Biochem* 2006;17(7):492-8.
49. Park HJ, DiNatale DA, Chung MY, et al. Green tea extract attenuates hepatic steatosis by decreasing adipose lipogenesis and enhancing hepatic antioxidant defenses in ob/ob mice. *J Nutr Biochem* 2011;22(4):393-400.
50. Park HJ, Lee JY, Chung MY, et al. Green tea extract suppresses NFkappaB activation and inflammatory responses in diet-induced obese rats with nonalcoholic steatohepatitis. *J Nutr* 2012;142(1):57-63.
51. Suliburska J, Bogdanski P, Szulinska M, et al. Effects of green tea supplementation on elements, total antioxidants, lipids, and glucose values in the serum of obese patients. *Biol Trace Elem Res* 2012;149(3):315-22.
52. Esfahani A, Wong JM, Truan J, et al. Health effects of mixed fruit and vegetable concentrates: A systematic review of the clinical interventions. *J Am Coll Nutr* 2011;30(5):285-94.
53. Guo H, Zhong R, Liu Y, et al. Effects of bayberry juice on inflammatory and apoptotic markers in young adults with features of non-alcoholic fatty liver disease. *Nutrition* 2014;30(2):198-203.
54. Schattenberg JM, Galle PR. Animal models of non-alcoholic steatohepatitis: Of mice and man. *Dig Dis* 2010;28(1):247-54.
55. Hebbard L, George J. Animal models of nonalcoholic fatty liver disease. *Nat Rev Gastroenterol Hepatol* 2011;8(1):35-44.
56. Takahashi Y, Soejima Y, Fukusato T. Animal models of nonalcoholic fatty liver disease/nonalcoholic steatohepatitis. *World J Gastroenterol* 2012;18(19):2300-8.
57. Ito M, Suzuki J, Tsujioka S, et al. Longitudinal analysis of murine steatohepatitis model induced by chronic exposure to high-fat diet. *Hepatol Res* 2007;37(1):50-7.
58. Tsuchiya H, Ebata Y, Sakabe T, et al. High-fat, high-fructose diet induces hepatic iron overload via a hepcidin-independent mechanism prior to the onset of liver steatosis and insulin resistance in mice. *Metabolism* 2013;62(1):62-9.
59. Tetri LH, Basaranoglu M, Brunt EM, et al. Severe NAFLD with hepatic necroinflammatory changes in mice fed trans fats and a high-fructose corn syrup equivalent. *Am J Physiol Gastrointest Liver Physiol* 2008;295(5):G987-95.
60. Rinella ME, Green RM. The methionine-choline deficient dietary model of steatohepatitis does not exhibit insulin resistance. *J Hepatol* 2004;40(1):47-51.
61. Rizki G, Arnaboldi L, Gabrielli B, et al. Mice fed a lipogenic methionine-choline-deficient diet develop hypermetabolism coincident with hepatic suppression of SCD-1. *J Lipid Res* 2006;47(10):2280-90.
62. Nagasawa T, Inada Y, Nakano S, et al. Effects of bezafibrate, PPAR pan-agonist, and GW501516,

PPARdelta agonist, on development of steatohepatitis in mice fed a methionine- and choline-deficient diet. *Eur J Pharmacol* 2006;536(1-2):182-91.
63. Pelleymounter MA, Cullen MJ, Baker MB, et al. Effects of the obese gene product on body weight regulation in ob/ob mice. *Science* 1995;269(5223):540-3.
64. Utzschneider KM, Kahn SE. Review: The role of insulin resistance in nonalcoholic fatty liver disease. *J Clin Endocrinol Metab* 2006;91(12):4753-61.
65. Shiri-Sverdlov R, Wouters K, van Gorp PJ, et al. Early diet-induced non-alcoholic steatohepatitis in APOE2 knock-in mice and its prevention by fibrates. *J Hepatol* 2006;44(4):732-41.
66. Wouters K, van Gorp PJ, Bieghs V, et al. Dietary cholesterol, rather than liver steatosis, leads to hepatic inflammation in hyperlipidemic mouse models of nonalcoholic steatohepatitis. *Hepatology* 2008;48(2):474-86.
67. Tous M, Ferre N, Camps J, et al. Feeding apolipoprotein E-knockout mice with cholesterol and fat enriched diets may be a model of non-alcoholic steatohepatitis. *Mol Cell Biochem* 2005;268(1-2):53-8.
68. Ma KL, Ruan XZ, Powis SH, et al. Inflammatory stress exacerbates lipid accumulation in hepatic cells and fatty livers of apolipoprotein E knockout mice. *Hepatology* 2008;48(3):770-81.
69. Bieghs V, Van Gorp PJ, Wouters K, et al. LDL receptor knock-out mice are a physiological model particularly vulnerable to study the onset of inflammation in non-alcoholic fatty liver disease. *PLoS One* 2012;7(1):e30668.
70. Subramanian S, Goodspeed L, Wang S, et al. Dietary cholesterol exacerbates hepatic steatosis and inflammation in obese LDL receptor-deficient mice. *J Lipid Res* 2011;52(9):1626-35.
71. Kaneko H, Anzai T, Nagai T, et al. Human C-reactive protein exacerbates metabolic disorders in association with adipose tissue remodelling. *Cardiovasc Res* 2011;91(3):546-55.
72. Buettner R, Parhofer KG, Woenckhaus M, et al. Defining high-fat-diet rat models: Metabolic and molecular effects of different fat types. *J Mol Endocrinol* 2006;36(3):485-501.
73. Musso G, Gambino R, De Michieli F, et al. Dietary habits and their relations to insulin resistance and postprandial lipemia in nonalcoholic steatohepatitis. *Hepatology* 2003;37(4):909-16.
74. Toshimitsu K, Matsuura B, Ohkubo I, et al. Dietary habits and nutrient intake in non-alcoholic steatohepatitis. *Nutrition* 2007;23(1):46-52.
75. Buettner R, Scholmerich J, Bollheimer LC. High-fat diets: Modeling the metabolic disorders of human obesity in rodents. *Obesity (Silver Spring)* 2007;15(4):798-808.
76. Vilar L, Oliveira CP, Faintuch J, et al. High-fat diet: A trigger of non-alcoholic steatohepatitis? preliminary findings in obese subjects. *Nutrition* 2008;24(11-12):1097-102.
77. Wielinga PY, Yakala GK, Heeringa P, et al. Beneficial effects of alternate dietary regimen on liver inflammation, atherosclerosis and renal activation. *PLoS One* 2011;6(3):e18432.
78. Ioannou GN, Morrow OB, Connole ML, et al. Association between dietary nutrient composition and the incidence of cirrhosis or liver cancer in the united states population. *Hepatology* 2009;50(1):175-84.
79. Yoneda M, Fujita K, Nozaki Y, et al. Efficacy of ezetimibe for the treatment of non-alcoholic steatohepatitis: An open-label, pilot study. *Hepatol Res* 2010;40(6):566-73.
80. Savard C, Tartaglione EV, Kuver R, et al. Synergistic interaction of dietary cholesterol and dietary fat in inducing experimental steatohepatitis. *Hepatology* 2013;57(1):81-92.
81. Yasutake K, Nakamuta M, Shima Y, et al. Nutritional investigation of non-obese patients with non-alcoholic fatty liver disease: The significance of dietary cholesterol. *Scand J Gastroenterol* 2009;44(4):471-7.
82. Van Rooyen DM, Larter CZ, Haigh WG, et al. Hepatic free cholesterol accumulates in obese, diabetic mice and causes nonalcoholic steatohepatitis. *Gastroenterology* 2011;141(4):1393-1403.

83. Yasutake K, Kohjima M, Kotoh K, et al. Dietary habits and behaviors associated with nonalcoholic fatty liver disease. *World J Gastroenterol* 2014;20(7):1756-67.
84. Ouyang X, Cirillo P, Sautin Y, et al. Fructose consumption as a risk factor for non-alcoholic fatty liver disease. *J Hepatol* 2008;48(6):993-9.
85. Abid A, Taha O, Nseir W, et al. Soft drink consumption is associated with fatty liver disease independent of metabolic syndrome. *J Hepatol* 2009;51(5):918-24.
86. Gregor MF, Yang L, Fabbrini E, et al. Endoplasmic reticulum stress is reduced in tissues of obese subjects after weight loss. *Diabetes* 2009;58(3):693-700.
87. Denechaud PD, Dentin R, Girard J, et al. Role of ChREBP in hepatic steatosis and insulin resistance. *FEBS Lett* 2008;582(1):68-73.
88. Koo HY, Miyashita M, Cho BH, et al. Replacing dietary glucose with fructose increases ChREBP activity and SREBP-1 protein in rat liver nucleus. *Biochem Biophys Res Commun* 2009;390(2):285-9.
89. Neuschwander-Tetri BA. Carbohydrate intake and nonalcoholic fatty liver disease. *Curr Opin Clin Nutr Metab Care* 2013;16(4):446-52.
90. Bhattacharjee J, Kumar JM, Arindkar S, et al. Role of immunodeficient animal models in the development of fructose induced NAFLD. *J Nutr Biochem* 2014;25(2):219-26.
91. Diehl AM, Li ZP, Lin HZ, et al. Cytokines and the pathogenesis of non-alcoholic steatohepatitis. *Gut* 2005;54(2):303-6.
92. Kern PA, Saghizadeh M, Ong JM, et al. The expression of tumor necrosis factor in human adipose tissue. regulation by obesity, weight loss, and relationship to lipoprotein lipase. *J Clin Invest* 1995;95(5):2111-9.
93. Jarrar MH, Baranova A, Collantes R, et al. Adipokines and cytokines in non-alcoholic fatty liver disease. *Aliment Pharmacol Ther* 2008;27(5):412-21.
94. Crespo J, Fernandez-Gil P, Hernandez-Guerra M, et al. Are there predictive factors of severe liver fibrosis in morbidly obese patients with non-alcoholic steatohepatitis?. *Obes Surg* 2001;11(3):254-7.
95. Li Z, Yang S, Lin H, et al. Probiotics and antibodies to TNF inhibit inflammatory activity and improve nonalcoholic fatty liver disease. *Hepatology* 2003;37(2):343-50.
96. van der Poorten D, Milner KL, Hui J, et al. Visceral fat: A key mediator of steatohepatitis in metabolic liver disease. *Hepatology* 2008;48(2):449-57.
97. Wieckowska A, Papouchado BG, Li Z, et al. Increased hepatic and circulating interleukin-6 levels in human nonalcoholic steatohepatitis. *Am J Gastroenterol* 2008;103(6):1372-9.
98. Cai D, Yuan M, Frantz DF, et al. Local and systemic insulin resistance resulting from hepatic activation of IKK-beta and NF-kappaB. *Nat Med* 2005;11(2):183-90.
99. Steinberg GR. Inflammation in obesity is the common link between defects in fatty acid metabolism and insulin resistance. *Cell Cycle* 2007;6(8):888-94.
100. Videla LA, Tapia G, Rodrigo R, et al. Liver NF-kappaB and AP-1 DNA binding in obese patients. *Obesity (Silver Spring)* 2009;17(5):973-9.
101. Shoelson SE, Lee J, Yuan M. Inflammation and the IKK beta/I kappa B/NF-kappa B axis in obesity- and diet-induced insulin resistance. *Int J Obes Relat Metab Disord* 2003;27 Suppl 3:S49-52.
102. Farrell GC, van Rooyen D, Gan L, et al. NASH is an inflammatory disorder: Pathogenic, prognostic and therapeutic implications. *Gut Liver* 2012;6(2):149-71.
103. Brenner DA, Seki E, Taura K, et al. Non-alcoholic steatohepatitis-induced fibrosis: Toll-like receptors, reactive oxygen species and jun N-terminal kinase. *Hepatol Res* 2011;41(7):683-6.
104. Greten FR, Eckmann L, Greten TF, et al. IKKbeta links inflammation and tumorigenesis in a mouse model of colitis-associated cancer. *Cell* 2004;118(3):285-96.
105. Solinas G, Vilcu C, Neels JG, et al. JNK1 in hematopoietically derived cells contributes to diet-induced inflammation and insulin resistance

without affecting obesity. *Cell Metab* 2007;6(5):386-97.
106. Larter CZ, Yeh MM, Van Rooyen DM, et al. Peroxisome proliferator-activated receptor-alpha agonist, wy 14,643, improves metabolic indices, steatosis and ballooning in diabetic mice with non-alcoholic steatohepatitis. *J Gastroenterol Hepatol* 2012;27(2):341-50.
107. Videla LA, Rodrigo R, Orellana M, et al. Oxidative stress-related parameters in the liver of non-alcoholic fatty liver disease patients. *Clin Sci (Lond)* 2004;106(3):261-8.
108. Sanyal AJ, Campbell-Sargent C, Mirshahi F, et al. Nonalcoholic steatohepatitis: Association of insulin resistance and mitochondrial abnormalities. *Gastroenterology* 2001;120(5):1183-92.
109. Gambino R, Musso G, Cassader M. Redox balance in the pathogenesis of nonalcoholic fatty liver disease: Mechanisms and therapeutic opportunities. *Antioxid Redox Signal* 2011;15(5):1325-65.
110. Chalasani N, Gorski JC, Asghar MS, et al. Hepatic cytochrome P450 2E1 activity in nondiabetic patients with nonalcoholic steatohepatitis. *Hepatology* 2003;37(3):544-50.
111. Weltman MD, Farrell GC, Liddle C. Increased hepatocyte CYP2E1 expression in a rat nutritional model of hepatic steatosis with inflammation. *Gastroenterology* 1996;111(6):1645-53.
112. Abdelmegeed MA, Banerjee A, Yoo SH, et al. Critical role of cytochrome P450 2E1 (CYP2E1) in the development of high fat-induced non-alcoholic steatohepatitis. *J Hepatol* 2012;57(4):860-6.
113. Crespo J, Cayon A, Fernandez-Gil P, et al. Gene expression of tumor necrosis factor alpha and TNF-receptors, p55 and p75, in nonalcoholic steatohepatitis patients. *Hepatology* 2001;34(6):1158-63.
114. Day CP, James OF. Steatohepatitis: A tale of two "hits"?. *Gastroenterology* 1998;114(4):842-5.
115. Tilg H, Moschen AR. Evolution of inflammation in nonalcoholic fatty liver disease: The multiple parallel hits hypothesis. *Hepatology* 2010;52(5):1836-46.
116. Jou J, Choi SS, Diehl AM. Mechanisms of disease progression in nonalcoholic fatty liver disease. *Semin Liver Dis* 2008;28(4):370-9.
117. Takaki A, Kawai D, Yamamoto K. Multiple hits, including oxidative stress, as pathogenesis and treatment target in non-alcoholic steatohepatitis (NASH). *Int J Mol Sci* 2013;14(10):20704-28.

ESTABLISHMENT OF A GENERAL NAFLD SCORING SYSTEM FOR RODENT MODELS AND COMPARISON TO HUMAN LIVER PATHOLOGY

Wen Liang
Aswin L. Menke
Ann Driessen
Ger H. Koek
Jan. H. Lindeman
Reinout Stoop
Louis M. Havekes
Robert Kleemann
Anita M. van den Hoek

PLoS One 2014; 9(12):e115922

ABSTRACT

Background and aims: The recently developed histological scoring system for non-alcoholic fatty liver disease (NAFLD) by the NASH Clinical Research Network (NASH-CRN) has been widely used in clinical settings, but is increasingly employed in preclinical research as well. However, it has not been systematically analyzed whether the human scoring system can directly be converted to preclinical rodent models. To analyze this, we systematically compared human NAFLD liver pathology, using human liver biopsies, with liver pathology of several NAFLD mouse models. Based upon the features pertaining to mouse NAFLD, we aimed at establishing a modified generic scoring system that is applicable to broad spectrum of rodent models.

Methods: The histopathology of NAFLD was analyzed in several different mouse models of NAFLD to define generic criteria for histological assessment (preclinical scoring system). For validation of this scoring system, 36 slides of mouse livers, covering the whole spectrum of NAFLD, were blindly analyzed by ten observers. Additionally, the livers were blindly scored by one observer during two separate assessments longer than 3 months apart.

Results: The criteria macrovesicular steatosis, microvesicular steatosis, hepatocellular hypertrophy, inflammation and fibrosis were generally applicable to rodent NAFLD. The inter-observer reproducibility (evaluated using the Intraclass Correlation Coefficient) between the ten observers was high for the analysis of macrovesicular steatosis and microvesicular steatosis (ICC=0.784 and 0.776, all $p<0.001$, respectively) and moderate for the analysis of hypertrophy and inflammation (ICC=0.685 and 0.650, all $p<0.001$, respectively). The intra-observer reproducibility between the different observations of one observer was high for the analysis of macrovesicular steatosis, microvesicular steatosis and hypertrophy (ICC=0.871, 0.871 and 0.896, all $p<0.001$, respectively) and very high for the analysis of inflammation (ICC=0.931, $p<0.001$).

Conclusions: We established a simple NAFLD scoring system with high reproducibility that is applicable for different rodent models and for all stages of NAFLD etiology.

INTRODUCTION

Non-alcoholic fatty liver disease (NAFLD) has become the most common chronic liver disease in developed countries, paralleling the increased prevalence of obesity during the last decades [1-3]. NAFLD encompasses a wide spectrum of liver pathology ranging from non-alcoholic hepatic steatosis to steatohepatitis (NASH), which can evolve into liver fibrosis, cirrhosis and its life threatening complications or hepatocellular cancer [4].

Currently, liver biopsy is still the 'golden standard' for NASH diagnosis in clinical setting. Liver biopsies will however often be taken in subjects at high risk, leading to a bias in the samples towards the more severe forms of NAFLD. Histological scoring systems designed for human diagnostic purposes therefore usually concentrate on facets of the later stages of NAFLD, making them less applicable for scoring early stages of NAFLD. However, in 2005, the NASH Clinical Research Network (NASH-CRN) established and validated a system of histological evaluation for the full spectrum of NAFLD that could be useful in clinical trials [5]. Importantly, this scoring system of Kleiner *et al.* was not developed for diagnosing NASH, but for monitoring histopathological changes during clinical trials. The semi-quantitative scoring system separates the grading (activity) from staging (fibrosis) [5]. The grading or NAFLD activity score (NAS) encompasses steatosis, lobular inflammation and ballooning [5, 6]. The methodology proposed for scoring the different features of NAFLD has now been widely utilized, as evidenced by its application in numerous studies. Among the studies that use the Kleiner scoring system are several preclinical animal studies. However, despite this widespread use of the scoring system in different mouse models of NAFLD, the original scoring system was intended for human samples and has never been validated for experimental rodent samples.

To this end, by comparing human liver biopsies with the liver samples of different NAFLD mouse models (HFD-fed C57BL6, MCD-diet fed C57BL6, HC-diet fed APOE*3Leiden, HFD-fed and HFC-diet fed APOE*3Leiden.CETP, HFD-fed and HFC-diet fed $LDLR^{-/-}$.Leiden and HFD-fed KKA^{y} mice), we first assessed whether specific features of human NAFLD pathology are present in NAFLD mouse models. Additionally, and based upon the features pertaining to mouse NAFLD, we defined a set of robust histological criteria to analyze NAFLD in rodents and propose a modified Kleiner scoring system that is applicable to all stages of NAFLD etiology and that could generally be used in preclinical rodent studies because of its low inter- and intra-observer variability.

MATERIALS AND METHODS

Human NAFLD samples

Thirty human liver biopsies were obtained during autopsy for postmortem histological analysis (Department of Pathology; Leiden University Medical Center/LUMC, Leiden, The Netherlands). Sample collection and handling was performed in accordance with the guidelines of the Committee Medical Ethics (CME, Leiden, The Netherlands) and the code of conduct of the Dutch Federation of Biomedical Scientific Societies and after permission of the institutional review board. The LUMC review board does not require ethical consent for this study as the human material in the study fulfils the criteria for 'further use' i.e. the

material is collected in the context of patient care and is later made available for scientific use provided that the material is used anonymously, not required for clinical use, that the patient has not objected to the further use, and that tissue handling is performed in accordance with the local and national guidelines. Cardiovascular disease was the predominant cause of death. Cases with a known or suspected alcohol abuse were excluded. Forty percent of the subjects were female and sixty percent male. The average age was 63 years. Liver samples were fixed in formalin, paraffin embedded and sections were stained with hematoxylin and eosin (H&E) and Sirius Red. Samples were scored for NAFLD (using NAS) and fibrosis stage and subsequently diagnosed as no evidence of fatty liver disease, steatosis or steatohepatitis by a clinical pathologist (A.D). In **Table 1** the most important histological characteristics for the human samples are listed per diagnosed category, additional histological features are listed in **Supplemental Table 1**.

Table 1: Histological characteristics of human samples per diagnosed category.

Histological feature	Score/code	Healthy (n=9)	NAFLD (n=11)	NASH (n=10)
Steatosis grade	0	9	0	0
	1	0	4	4
	2	0	6	4
	3	0	1	2
Lobular inflammation	0	9	11	0
	1	0	0	10
	2	0	0	0
	3	0	0	0
Ballooning	0	8	11	0
	1	1	0	8
	2	0	0	2
Fibrosis stage	0	6	6	2
	1	1	0	0
	1A	0	4	2
	1B	1	0	4
	1C	0	0	0
	2	1	1	1
	3	0	0	0
	4	0	0	1

Number of subjects per score/code are shown for the indicated histological features.

Animals and induction of NAFLD

Several animal models, covering the spectrum of NAFLD from simple steatosis to NASH without or with fibrosis, were used to define robust histological criteria for experimental disease and to validate the rodent scoring system. In **Table 2** the metabolic and histological characteristics of the different animal models and diet combinations are shown.

Table 2: Metabolic and histological characteristics of the used NAFLD mouse models.

Model	Obesity	IR	HTG	Steatosis	Hepatic inflammation	Fibrosis
C57BL6, HFD	+	+	-	+	+	-
C57BL6, MCD	-	-	-	++	++	++
E3L, HC	-	-	-	+	++	++
E3L.CETP, HFD	+	+	-	++	-	-
E3L.CETP, HFC	+	+	+	++	++	+
$LDLR^{-/-}$.Leiden, HFD	++	++	+	++	++	++
$LDLR^{-/-}$,Leiden, HFC	+	+	++	++	++	++
KKA^{y}, HFD	++	++	+	++	-	-

Severity is indicated as + or ++, absence is indicated as -. IR: insulin resistance; HGT: hypertriglyceridemia; HFD: high fat diet; MCD: methionine and choline deficient diet; HC: high cholesterol diet; HFC: high fat and cholesterol diet.

Male C57BL/6J mice, 12 weeks of age, were obtained from Charles River and were fed a high fat diet (HFD: 45 energy% fat derived from lard, Research Diets, New Brunswick, NJ, USA) for 24 weeks (n=10).

Male C57BL/6J mice, 4-8 weeks of age, were obtained from Charles River and were fed a methionine choline deficient diet (MCD: cat#960439; MP Biomedicals, Eindhoven, The Netherlands) for 8 weeks (n=10).

Female APOE*3Leiden (E3L) mice [7], 17-20 weeks of age were obtained from the in-house breeding colony (TNO Metabolic Health Research, Leiden, The Netherlands) and were fed a high cholesterol diet (HC: 35 energy% fat primarily as cocoa butter, 40 energy% sucrose and 1% cholesterol, modified semi-synthetic diet based on Nishina et al., [8]) for 20 weeks (n=10).

Human CETP transgenic mice that express cholesteryl ester transfer protein (CETP) under control of its natural flanking regions (strain 5203) [9] were obtained from Jackson Laboratories (Bar Harbor, MC) and cross-bred with APOE*3Leiden mice in our local animal facility at TNO to obtain heterozygous E3L.CETP mice [10, 11]. Male E3L.CETP mice, 10-14 weeks of age, were either fed a HFD for 16 weeks (n=10) to induce steatosis without steatohepatitis or were fed the HFD for 10 weeks, followed by 6 weeks of the HFD supplemented with 1% cholesterol (n=10), to induce steatohepatitis.

Male $LDLR^{-/-}$ mice [12], 13-17 weeks of age, were obtained from the in-house breeding colony ($LDLR^{-/-}$. Leiden strain; TNO Metabolic Health Research, Leiden, The Netherlands). This strain is more sensitive to diet-induced obesity and comorbidities than regular $LDLR^{-/-}$ mice. Mice were fed a HFD for 10 weeks, followed by 6 weeks of the HFD supplemented with 1% cholesterol (n=10), or in a separate experiment, fed a HFD for 21 weeks (n=10).

Male KKA^{y} mice, 5-7 weeks of age, were obtained from Jackson Laboratories and were fed a HFD for 16 weeks (n=10).

All animals were housed in a temperature-controlled room on a 12 hour light-dark cycle and had free access to food and water. Mice were sacrificed using CO_2 asphyxiation. Liver samples (of lobus sinister medialis hepatis and lobus dexter medialis hepatis) were

collected, fixed in formalin, paraffin embedded and sections were stained with hematoxylin and eosin (H&E) and Sirius Red. Animal experiments were approved by the Ethical Committee on Animal Care and Experimentation (Zeist, The Netherlands), and were in compliance with European Community specifications regarding the use of laboratory animals.

Defining the overlapping features of NAFLD in humans and mice

Using the histological scoring system of Kleiner *et al.*, tissue samples from mouse NAFLD models were compared to liver biopsy samples obtained from NAFLD patients to examine whether recognized features of human NAFLD were present in any of the experimental NAFLD models (**Table 3**). Liver histology photomicrographs were taken to compare histological features from human and mouse (control vs. NASH) (**Figure 1**).

Table 3: Histological features of NAFLD in humans and presence or absence in mice.

Histological feature	Human NAFLD	Mouse NAFLD
Steatosis		
Steatosis	√	√
Microvesicular steatosis	√	√
Inflammation		
Lobular inflammation	√	√
(overall assessment of all inflammatory foci)		
Microgranulomas (small aggregates of macrophages)	√	√
Large lipogranulomas	√	√
Portal inflammation	√	√
Fibrosis	√	√
Liver cell injury		
Ballooning cells	√	√*
Acidophil bodies (hepatic apoptosis)	√	-
Pigmented macrophages	√	-
Megamitochondria	√	-
Other findings		
Mallory-Denk bodies	√	-
Nuclear glycogenation	√	-

The presence or absence of the main histological features of NAFLD as identified in humans was evaluated in several different mouse models for NAFLD (C57BL6 mice on a high fat diet or on methionine choline deficient (MCD) diet, E3L, E3L.CETP, LDLR-/-.Leiden, KKAy mice): "√" presence; "-" absence of features. Ballooning cells were occasionally observed in the models.*

Definition of histological NAFLD score

Briefly, the two key features of NASH, steatosis and inflammation, were categorized as follows: steatosis was determined by analyzing hepatocellular vesicular steatosis, i.e. macrovesicular steatosis and microvesicular steatosis separately, and by hepatocellular

hypertrophy as defined below (**Figure 2**). Inflammation was scored by analyzing the amount of inflammatory cell aggregates (**Figure 2**). The proposed rodent scoring system is shown in **Table 4** and options for its use in diagnosis are shown in **Supplemental Figure 1**.

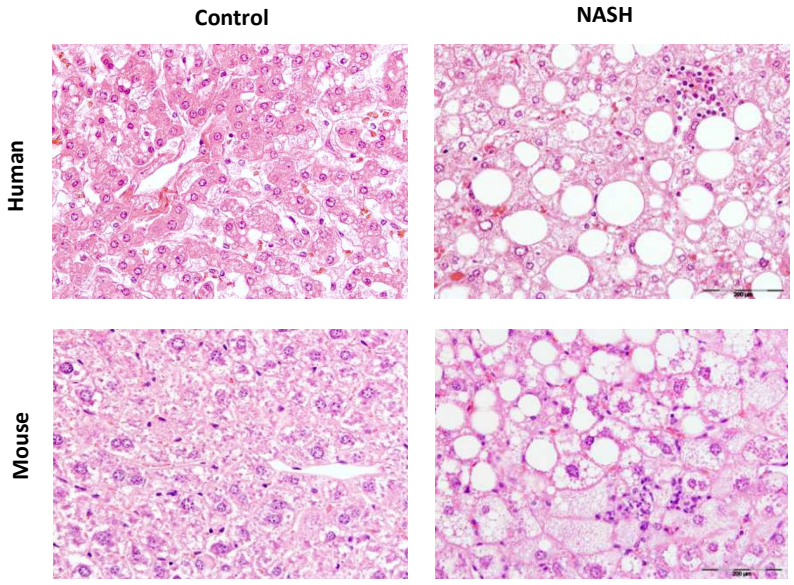

Figure 1: Histological photomicrographs of human NASH and NASH in mice. Liver histological cross-sections from a healthy control subject (A) and a NASH patient (B). Liver histological cross-sections from a healthy control (C) and a NASH E3L.CETP mouse (D). All photomicrographs: Hematoxylin and eosin; magnification 200x.

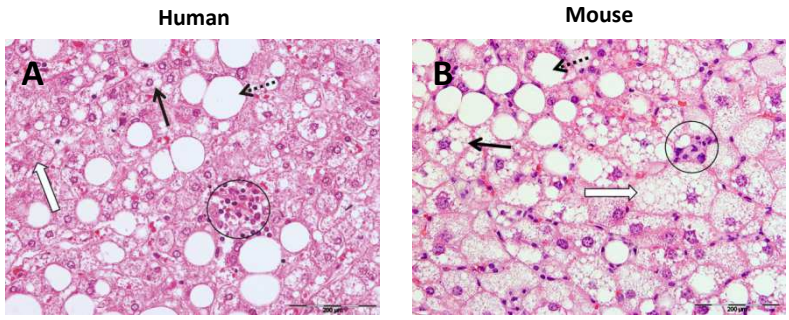

Figure 2: Hepatocellular steatosis, hypertrophy and inflammation. Liver cross-sections are from a NASH patient (A) or a E3L.CETP mouse fed a high fat diet supplemented with cholesterol to induce NASH (B). Macrovesicular steatosis (dotted line arrow): large lipid droplets are present in hepatocytes; microvesicular steatosis (bold arrow): small lipid droplets are present in hepatocytes. Hypertrophy (open arrow): the representative cell is much larger than the surrounding steatotic hepatocytes but has the same cytoplasmic characteristics. Clusters (aggregates) of inflammatory cells (within circles). All photomicrographs: Hematoxylin and eosin; magnification 200x.

Table 4: Grading system for rodent NAFLD.

Histological feature	Score			
	0	1	2	3
Steatosis:				
Macrovesicular steatosis	<5%	5-33%	33-66%	>66%
Microvesicular steatosis	<5%	5-33%	33-66%	>66%
Hypertrophy	<5%	5-33%	33-66%	>66%
Inflammation:				
Number of inflammatory foci/field	<0.5	0.5-1.0	1.0-2.0	>2.0

The purpose of this scoring system is however not to derive a single score, but to score the individual features.

Macrovesicular steatosis and microvesicular steatosis were both separately scored and the severity was graded, based on the percentage of the total area affected, into the following categories: 0 (<5%), 1 (5-33%), 2 (34-66%) and 3 (>66%). The difference between macrovesicular and microvesicular steatosis was defined by whether the vacuoles displaced the nucleus to the side (macrovesicular) or not (microvesicular). Similarly, the level of hepatocellular hypertrophy, defined as cellular enlargement more than 1.5 times the normal hepatocyte diameter, was scored, based on the percentage of the total area affected, into the following categories: 0 (<5%), 1 (5-33%), 2 (34-66%) and 3 (>66%). For hepatocellular hypertrophy the evaluation was merely based on abnormal enlargement of the cells, irrespective of rounding of the cells and/or changes in cytoplasm or the number of vacuoles, and is therefore not a substitute of ballooning. The unweight sum of the scores for steatosis (macrovesicular steatosis, microvesicular steatosis and hypertrophy) thus ranged from 0-9. Both steatosis and hypertrophy were evaluated at a 40 to 100 × magnification and only the sheets of hepatocytes were taken into account (terminal hepatic venules and portal tracts etc were excluded).

Inflammation was evaluated by counting the number of inflammatory foci per field using a 100 x magnification (view size of 3.1 mm^2). A focus was defined a cluster, not a row, of ≥5 inflammatory cells. Five different fields were counted and the average was subsequently scored into the following categories: normal (<0.5 foci), slight (0.5-1.0 foci), moderate (1.0-2.0 foci), severe (>2.0 foci).

Hepatic fibrosis was identified using Sirius Red stained slides at 40 x magnification and evaluated by scoring whether pathologic collagen staining was absent (only in vessels) or collagen staining observed within the liver slide, the latter further defined as mild, moderate or massive. In addition, the percentage of the total area affected was evaluated using using image analysis of surface area on Sirius red stained slides.

Validation of histological NAFLD scoring system in mice

To validate the scoring system, 36 slides of mouse livers covering the whole spectrum of NAFLD, were blindly analyzed by a board-certified pathologist (A.L.M), a clinical pathologist (A.D.) and nine scientists with basic histological experience. For the validation, the observers estimated the percentage of macrovesicular steatosis, microvesicular

steatosis and hypertrophy (relative scale) and the number of inflammatory foci per field (absolute scale), instead of using the different categories for steatosis and inflammation (ordinal measure). Additionally, quantification of the steatosis and inflammation was determined by one observer during two separate assessments that were separated by an interval longer than 3 months.

Statistical analysis

The reproducibility of the scoring system was determined by calculating the Intraclass Correlation Coefficient (ICC) to determine inter-observer reliability among ten observers or the intra-observer reliability among two separate scoring assessments of one observer. Using two-way random model with absolute agreement and the 95% confidence interval (CI), ICCs were calculated for the agreement on NAFLD/NASH criteria of macrovesicular steatosis, microvesicular steatosis, hypertrophy and inflammation.

The ICC was interpreted as follows, according to the Munro classification system little or no correlation for values below 0.25, low correlation for values between 0.26–0.49, moderate correlation for values between 0.50–0.69 high correlation for values between 0.70–0.89 and very good correlation for values between 0.90–1.00 [13]. The Bland-Altman plot [14] was used to analyze inter- and intra-observer reproducibility to permit a better visualization of the correlation between individual measures. Results were considered significant at P-value <0.05 and statistical analyses were performed using SPSS version 20.0 (IBM, Somers, NY, USA).

RESULTS

Development of histological NAFLD scoring system in mice

To define the overlapping NAFLD features in humans and mice, histological samples from several mouse NAFLD models were compared to human tissue biopsies of NAFLD patients. A summary of the main features of human NAFLD according to the Kleiner's scoring system and their presence or absence in the mouse NAFLD models is shown in **Table 1**. Overall, the histological cross-sections of the mouse NAFLD looked similar to those of the human NAFLD patients (**Figure 1**), but not all main features of human NAFLD were present in the mouse NAFLD models. The most important features of steatosis and inflammation, as well as fibrosis, were all found to be present in mouse NAFLD models as well. However, the features for hepatocellular injury, like apoptosis, pigmented macrophages and megamitochondria, were not found in any of the mouse NAFLD models. Ballooning, defined as enlarged and rounded hepatocytes with clear cytoplasm, was only occasionally found in the experimental NAFLD models, and did not prominently exist. Although enlarged hepatocytes were retrieved in all mouse NAFLD models, a distinct rounding of these cells concomitant with clear reticular cytoplasm was rarely found in all models.

Based upon the most important overlapping features, we selected the following main criteria for establishing a rodent NAFLD scoring system: 1) steatosis by determining the severity of macrovesicular steatosis, microvesicular steatosis and hypertrophy (as percentage of total area affected) and 2) inflammation by counting the number of inflammatory cell aggregates (as average number of five microscopic fields) (**Figure 2**).

In addition, the different staging of NAFLD was analyzed by identifying whether fibrosis was present and to which extent. In our present study, the most severe fibrosis was observed in the LDLR$^{-/-}$.Leiden mice, followed by the E3L mice. In both models fibrosis was situated in both pericentral and perisinusoidal zone and sometimes bridging fibrosis was observed (**Figure 3**).

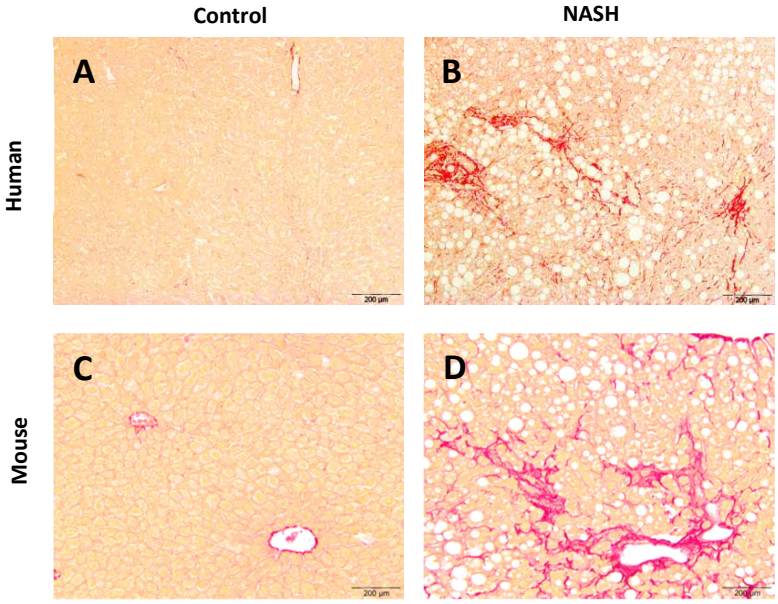

Figure 3: Liver fibrosis. Photomicrograph of cells with collagen staining (Sirius red). Liver histological cross-sections are from a healthy control subject (A) and a NASH patient (B) or a healthy control (C) and a LDLR$^{-/-}$. Leiden mouse fed a high fat diet to induce NASH (D). All photomicrographs: Sirius red; magnification 100x.

Validation of histological NAFLD scoring system in mice

A total of 36 mouse liver samples were used as validation set. This set of histological specimen covered the whole spectrum of NAFLD, from healthy unaffected samples to severe NASH livers with fibrosis (and included livers from various strains of mice). To evaluate the agreement between different observers, ten different observers analyzed the study set blindly. The level of inter-observer variation was subsequently evaluated using the Intraclass Correlation Coefficient (ICC). The ICC indicated a high correlation for the analysis of macrovesicular steatosis and microvesicular steatosis (ICC=0.784 and 0.776, both $p<0.001$, respectively) and a moderate correlation for the analysis of hypertrophy and inflammation (ICC=0.685 and 0.650, both $p<0.001$) between the different observers (**Table 5**). In conjunction with ICC, the Bland-Altman plots for two observers were also reported to visualize the correlation (**Figure 4**). In addition, the agreement between two pathologists was examined. The ICC indicated a very good correlation for the analysis of microvesicular steatosis (ICC=0.919, $p<0.001$), high for macrovesicular steatosis and

Table 5: Inter-observer reproducibility of NASH histological features according to the mouse NAFLD/NASH scoring system.

Histological feature	ICC	CI	P
Macrovesicular steatosis	0.784	0.681–0.869	<0.001
Microvesicular steatosis	0.776	0.679–0.860	<0.001
Hypertrophy	0.685	0.565–0.796	<0.001
Inflammation	0.650	0.517–0.779	<0.001

ICC: intraclass correlation coefficient (two-way random effects model, with absolute agreement); CI: 95% confidence interval; P: level of significance.

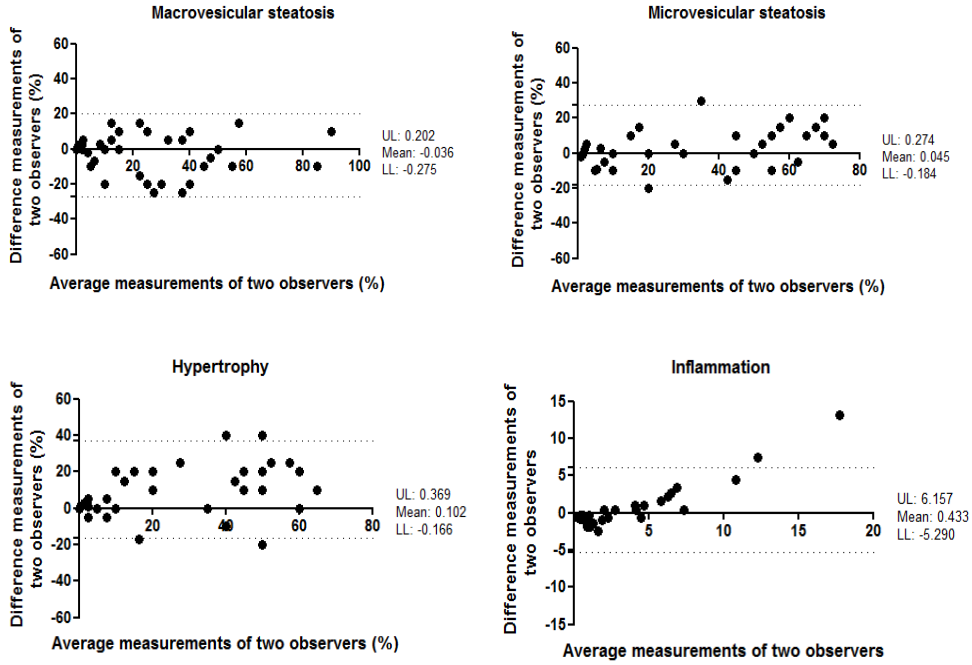

Figure 4: Bland-Altman plot for correlation analysis between two observers for measurement of macrovesicular steatosis, microvesicular steatosis, hypertrophy and inflammation. X-axis: average measurements of two observers. Y-axis: Difference between measurements of two observers. UL: Upper 95% limits of agreement. LL: Lower 95% limits of agreement.

hypertrophy (ICC=0.814 and 0.784, both p<0.001, respectively) but low correlation for the analysis of inflammation (ICC=0.471, p<0.01) between the two pathologists (**Supplemental Table 2**).

The agreement between different observations of one observer was evaluated by analysis of the study set during two separate scoring assessments that were separated by an interval of more than 3 months. In the analysis of intra-observer reproducibility, the ICC indicated a high correlation for the analysis of macrovesicular steatosis, microvesicular

steatosis and hypertrophy (ICC=0.871, 0.871 and 0.896, all p<0.001, respectively) and a very high correlation for the analysis of inflammation (ICC=0.931, p<0.001) between the different time points of analysis (**Table 6**). The Bland-Altman plots confirmed that a correlation was observed between the first and second scoring assessments (**Figure 5**).

Table 6: Intra-observer reproducibility of NASH histological features according to the mouse NAFLD/NASH scoring system.

Histological feature	ICC	CI	P
Macrovesicular steatosis	0.871	0.729–0.937	<0.001
Microvesicular steatosis	0.871	0.740–0.935	<0.001
Hypertrophy	0.896	0.805–0.945	<0.001
Inflammation	0.931	0.802–0.971	<0.001

ICC: intraclass correlation coefficient (two-way random effects model, with absolute agreement); CI: 95% confidence interval; P: level of significance.

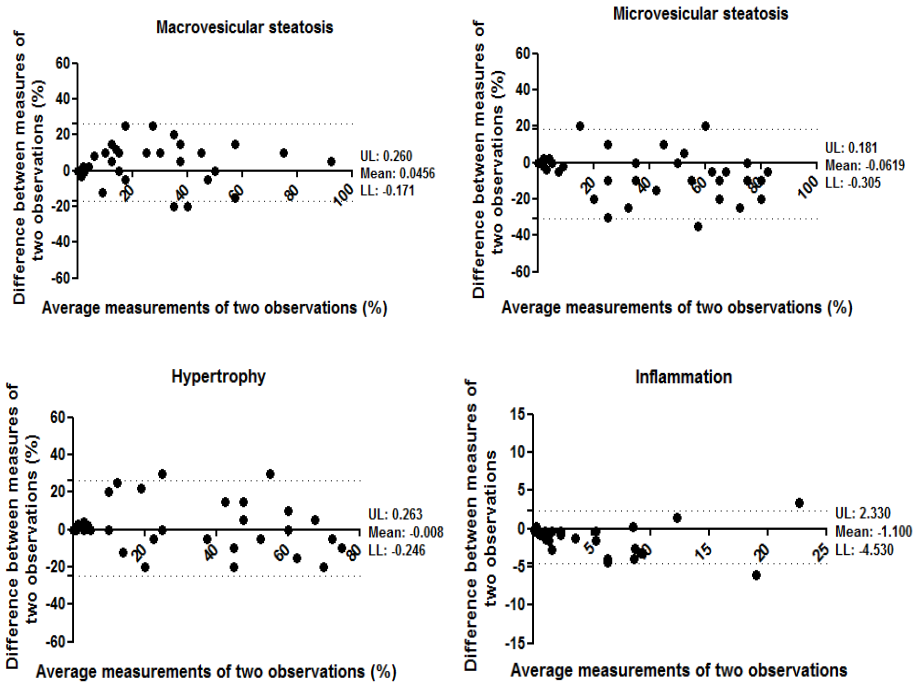

Figure 5: Bland-Altman plot for correlation analysis between two observations of one observer for measurement of macrovesicular steatosis, microvesicular steatosis, hypertrophy and inflammation. X-axis: average measurements of two observations. Y-axis: Difference between measurements of two observations. UL: Upper 95% limits of agreement. LL: Lower 95% limits of agreement.

DISCUSSION

A uniform, well-defined grading system that accurately defines the severity of NAFLD is a prerequisite for diagnosis and treatment of NASH, but also for preclinical research and development of novel pharmaceutical treatments. This study systematically compared human NAFLD liver pathology with the experimental liver pathology of several NAFLD mouse models (with emphasis on diet-inducible NAFLD models with obese phenotype). We found that specific features of human NASH, like (macro- or microvesicular) steatosis, lobular and portal inflammation, microgranulomas, large lipogranulomas and fibrosis were present in the rodent models as well, but other features were absent (apoptosis, pigmented macrophages, megamitochondria, Mallory-Denk bodies and nuclear glycogenation) in the mouse NAFLD models or only occasionally retrieved (ballooning). In general, the NASH pathology of the mouse models was slightly less severe than the human NASH pathology, and many models mainly display early disease stages which make them particularly suitable for the development of novel treatments that target the early processes of NASH or try to prevent fibrosis.

Our proposed scoring system (Table 4) is based on the features pertaining to mouse NAFLD and differs from the NAS scoring method for humans in that we omitted the assessment of ballooning and added the measurement of hepatocellular hypertrophy. Clinically, hepatic ballooning is a structural manifestation of microtubular disruption and hepatocyte injury [15]. Hepatic ballooning can be histopathologically identified as cells, which have rounded contours, a central and (small) pyknotic nucleus and two to three times the size of adjacent normal hepatocytes and that are characterized by a clear or wispy cytoplasm on H&E stained sections [15-17]. The underlying source of the swelling cannot be determined on H&E staining and therefore consensus on the underlying mechanism has remained elusive. The grading of ballooning into different scores has been difficult to perform and the definition has remained largely descriptive for the less advanced ballooning cells (grade 1) [18, 19]. As a consequence, ballooning is subject to significant inter-observer variation: there is often disagreement even among experts about the presence or absence of cellular ballooning in NASH [5, 6]. Although enlarged hepatocytes were retrieved in all mouse NAFLD models, distinct ballooning was occasionally found in the models studied and under the conditions employed. The enlargement of the cells was primarily due to lipid accumulation, as confirmed via Oil-red-O staining (data not shown). Since ballooning can be detected by the loss of K8/18 in the cytoplasm, we performed a CK-18 staining. In some hypertrophic cells a reduction, but not complete loss, in CK-18 staining in the cytoplasm could be observed (**Supplemental Figure 2**). We cannot rule out that either in other animal models or in the models at a more advanced stage of NASH, ballooning can occur more prominently. In order to define quantitatively measures we decided to omit ballooning from the proposed non-human, rodent NAFLD scoring system and to add hepatocellular hypertrophy. Importantly, hepatocellular hypertrophy is not a substitute of ballooning because, in contrast to ballooning, hypertrophy is not a sign of cellular injury, and merely refers to an abnormal enlargement of the cells without acknowledging the source of this enlargement.

In order to enhance the reproducibility of the scoring system, between different observers and between different observations of one observer, we kept our scoring

system simple and did not take into account the zonal distribution pattern of the vesicular steatosis, hypertrophy and fibrosis nor with regards to inflammation, i.e. the type of inflammatory cells. Nevertheless, we do acknowledge the importance of this additional information and although not quantitatively embedded in our scoring system, we did evaluate the zonal patterns of the scored features and types of inflammatory cells in our models and found for C57BL6 on HFD, E3L, E3L.CETP, $LDLR^{-/-}$ and KKA^{y} mice that the pericentral zone was most prominently affected thereby resembling the pathology in humans, whereas for C57BL6 on MCD diet predominantly macrovesicular steatosis around the periportal zone was observed. Furthermore, in all models with hepatic inflammation we found a mixture of inflammatory cells consisting of monocytes, Kupffer cells and polymorphic nuclear cells. Based on time course analyses in the models studied herein, MPO-positive immune cells (neutrophils) are typically found in the inflammatory cell aggregates, which resembles the situation in humans [20], and indicates that tissue damage has occurred.

The NASH CRN scoring system is not including fibrosis in the activity score, but is using a separate grading system for fibrosis, based on perisinusoidal, periportal and bridging fibrosis or cirrhosis. Although fibrosis is not a requirement for the diagnosis of NASH, fibrosis is often present in NASH patients. Until recently, NASH was the only pattern within NAFLD that was recognized to be associated with the development of advanced fibrosis [21]. Fibrosis however can be unequally distributed throughout the liver and therefore sampling variability plays an important role in the diagnosis of clinical samples [22]. As expected, small biopsies (<1.6 cm) present higher variability for NAFLD fibrosis stage than larger biopsies [23]. Fortunately with (rodent) animal studies the whole liver can be analyzed, facilitating a proper pathological classification.

In our analysis, the rodent scoring system appears to be reproducible since concordance in the inter-observer and intra-observer scoring of macrovesicular steatosis and microvesicular steatosis were both high and moderate for hepatocellular hypertrophy, with better intra-observer scores than inter-observer scores for all features. In rodents the best measure of steatosis is biochemical quantification of hepatic triglycerides. True validation of the scoring system of steatosis would therefore be a correlation with biochemical triglyceride analysis. In several experiments, using different mouse strain and diet combinations, we correlated the scores of macrovesicular steatosis, microvesicular steatosis and hypertrophy with the biochemically measured hepatic triglycerides. In all experiments, we found a correlation, although interestingly in some mouse strain-diet combinations the correlation was better with microvesicular steatosis and in other mouse strain-diet combinations the correlation was better with macrovesicular steatosis. As an example the correlation of the samples used in the validation set (consisting of different mouse strains and different diets) for biochemical triglyceride measurement and microvesicular steatotis is shown in **Supplemental Figure 3**). The inter-observer scoring of inflammation had the lowest concordance, while remarkably for the intra-observer scoring of inflammation the highest concordance was observed, suggesting that the scoring of this feature is the most subjective. These results corroborate the findings of several previous reproducibility studies that consistently report less agreement for scoring of inflammation [24-28]. The studies that also evaluated the inter-observer agreement all show better intra-observer scores than inter-observer scores [24, 25, 28].

One limitation of our study is that we based the rodent scoring system on the evaluation of five mouse strains and their comparison with the human features of steatosis and steatohepatitis. It remains to be seen whether the proposed rodent scoring system is applicable to other rodent models and whether the models used herein are representative for other models. However, since the basic features of NASH, namely steatosis and inflammation are displayed correctly in our scoring system, we expect the scoring system will be applicable for other animal models as well.

In conclusion, we established a simple, robust and generic NAFLD scoring system for rodents that is reliable and reproducible among observers. This study demonstrates its use in preclinical research using several rodent models which display different stages of the etiology of NAFLD.

ACKNOWLEDGEMENTS

The authors gratefully acknowledge Joline Attema, Mark Boer, Frits van der Ham, Sabine Mourits, Carla Persoon, Herma van Roestenburg, Christa de Ruiter and Marijke Voskuilen for their help in scoring the liver samples and Dr. Ron Wolterbeek for statistical advice.

REFERENCES

1. Lazo M, Clark JM. (2008) The epidemiology of nonalcoholic fatty liver disease: A global perspective. Semin Liver Dis 28: 339-350.

2. Williams CD, Stengel J, Asike MI, Torres DM, Shaw J, et al. (2011) Prevalence of nonalcoholic fatty liver disease and nonalcoholic steatohepatitis among a largely middle-aged population utilizing ultrasound and liver biopsy: A prospective study. Gastroenterology 140: 124-131.

3. Tiniakos DG, Vos MB, Brunt EM. (2010) Nonalcoholic fatty liver disease: Pathology and pathogenesis. Annu Rev Pathol 5: 145-171.

4. Younossi ZM. (2008) Review article: Current management of non-alcoholic fatty liver disease and non-alcoholic steatohepatitis. Aliment Pharmacol Ther 28: 2-12.

5. Kleiner DE, Brunt EM, Van Natta M, Behling C, Contos MJ, et al. (2005) Design and validation of a histological scoring system for nonalcoholic fatty liver disease. Hepatology 41: 1313-1321.

6. Brunt EM, Janney CG, Di Bisceglie AM, Neuschwander-Tetri BA, Bacon BR. (1999) Nonalcoholic steatohepatitis: A proposal for grading and staging the histological lesions. Am J Gastroenterol 94: 2467-2474.

7. van den Maagdenberg AM, Hofker MH, Krimpenfort PJ, de Bruijn I, van Vlijmen B, et al. (1993) Transgenic mice carrying the apolipoprotein E3-leiden gene exhibit hyperlipoproteinemia. J Biol Chem 268: 10540-10545.

8. Nishina PM, Verstuyft J, Paigen B. (1990) Synthetic low and high fat diets for the study of atherosclerosis in the mouse. J Lipid Res 31: 859-869.

9. Jiang XC, Agellon LB, Walsh A, Breslow JL, Tall A. (1992) Dietary cholesterol increases transcription of the human cholesteryl ester transfer protein gene in transgenic mice. dependence on natural flanking sequences. J Clin Invest 90: 1290-1295.

10. van den Hoek AM, van der Hoorn JW, Maas AC, van den Hoogen RM, van Nieuwkoop A, et al. (2014) APOE*3Leiden.CETP transgenic mice as model for pharmaceutical treatment of the metabolic syndrome. Diabetes Obes Metab 16: 537-544.

11. Westerterp M, van der Hoogt CC, de Haan W, Offerman EH, Dallinga-Thie GM, et al. (2006) Cholesteryl ester transfer protein decreases high-density lipoprotein and severely aggravates atherosclerosis in APOE*3-leiden mice. Arterioscler Thromb Vasc Biol 26: 2552-2559.
12. Verschuren L, Kooistra T, Bernhagen J, Voshol PJ, Ouwens DM, et al. (2009) MIF deficiency reduces chronic inflammation in white adipose tissue and impairs the development of insulin resistance, glucose intolerance, and associated atherosclerotic disease. Circ Res 105: 99-107.
13. Munro B. (1997) Statistical methods for health care research. New York: Lippincott Williams & Willkins.
14. Bland JM, Altman DG. (1986) Statistical methods for assessing agreement between two methods of clinical measurement. Lancet 1: 307-310.
15. Brunt EM. (2010) Pathology of nonalcoholic fatty liver disease. Nat Rev Gastroenterol Hepatol 7: 195-203.
16. Brunt EM. (2001) Nonalcoholic steatohepatitis: Definition and pathology. Semin Liver Dis 21: 3-16.
17. Bedossa P, Poitou C, Veyrie N, Bouillot JL, Basdevant A, et al. (2012) Histopathological algorithm and scoring system for evaluation of liver lesions in morbidly obese patients. Hepatology 56: 1751-1759.
18. Lackner C. (2011) Hepatocellular ballooning in nonalcoholic steatohepatitis: The pathologist's perspective. Expert Rev Gastroenterol Hepatol 5: 223-231.
19. Caldwell S, Ikura Y, Dias D, Isomoto K, Yabu A, et al. (2010) Hepatocellular ballooning in NASH. J Hepatol 53: 719-723.
20. Liang W, Lindeman JH, Menke AL, Koonen DP, Morrison M, et al. (2014) Metabolically induced liver inflammation leads to NASH and differs from LPS- or IL-1beta-induced chronic inflammation. Lab Invest 94: 491-502.
21. Kleiner DE, Brunt EM. (2012) Nonalcoholic fatty liver disease: Pathologic patterns and biopsy evaluation in clinical research. Semin Liver Dis 32: 3-13.
22. Ratziu V, Charlotte F, Heurtier A, Gombert S, Giral P, et al. (2005) Sampling variability of liver biopsy in nonalcoholic fatty liver disease. Gastroenterology 128: 1898-1906.
23. Goldstein NS, Hastah F, Galan MV, Gordon SC. (2005) Fibrosis heterogeneity in nonalcoholic steatohepatitis and hepatitis C virus needle core biopsy specimens. Am J Clin Pathol 123: 382-387.
24. Younossi ZM, Gramlich T, Liu YC, Matteoni C, Petrelli M, et al. (1998) Nonalcoholic fatty liver disease: Assessment of variability in pathologic interpretations. Mod Pathol 11: 560-565.
25. Fukusato T, Fukushima J, Shiga J, Takahashi Y, Nakano T, et al. (2005) Interobserver variation in the histopathological assessment of nonalcoholic steatohepatitis. Hepatol Res 33: 122-127.
26. Merriman RB, Ferrell LD, Patti MG, Weston SR, Pabst MS, et al. (2006) Correlation of paired liver biopsies in morbidly obese patients with suspected nonalcoholic fatty liver disease. Hepatology 44: 874-880.
27. Vuppalanchi R, Unalp A, Van Natta ML, Cummings OW, Sandrasegaran KE, et al. (2009) Effects of liver biopsy sample length and number of readings on sampling variability in nonalcoholic fatty liver disease. Clin Gastroenterol Hepatol 7: 481-486.
28. Juluri R, Vuppalanchi R, Olson J, Unalp A, Van Natta ML, et al. (2011) Generalizability of the nonalcoholic steatohepatitis clinical research network histologic scoring system for nonalcoholic fatty liver disease. J Clin Gastroenterol 45: 55-58.

SUPPLEMENTARY DATA

Supplemental Table 1: Additional histological features of human samples per diagnosed category.

Histological feature	Score/code	Healthy (n=9)	NAFLD (n=11)	NASH (n=10)
Microgranulomas	0	9	11	10
	1	0	0	0
Large lipogranulomas	0	9	11	8
	1	0	0	2
Portal inflammation	0	9	11	9
	1	0	0	1
Acidophil bodies	0	9	11	10
	1	0	0	0
Pigmented macrophages	0	9	11	7
	1	0	0	3
Megamitochondria	0	9	11	8
	1	0	0	2
Mallory-Denk bodies	0	9	11	10
	1	0	0	0
Glycogenated nuclei	0	9	8	6
	1	0	3	4

Number of subjects per score/code are shown for the indicated histological features.

Supplemental Table 2: Inter-pathologist reproducibility of NASH histological features according to the mouse NAFLD/NASH scoring system.

Histological feature	ICC	CI	P
Macrovesicular steatosis	0.814	0.667–0.900	<0.001
Microvesicular steatosis	0.919	0.848–0.957	<0.001
Hypertrophy	0.784	0.619–0.883	<0.001
Inflammation	0.471	0.145–0.704	0.003

ICC: intraclass correlation coefficient (two-way random effects model, with absolute agreement); CI: 95% confidence interval; P: level of significance.

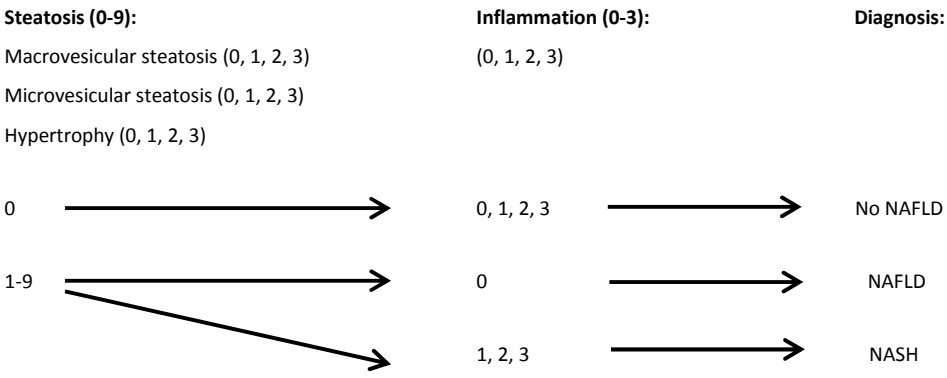

Supplemental Figure 1: Diagnosis diagram for NAFLD.

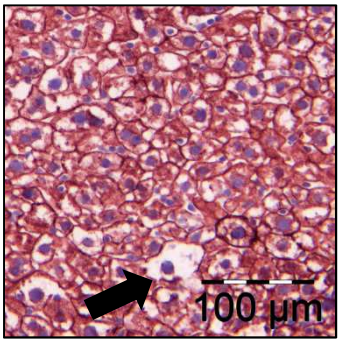

Supplemental Figure 2: CK-18 staining. Loss of CK18 staining in the cytoplasm could be observed in a few hypertrophic cells (arrow).

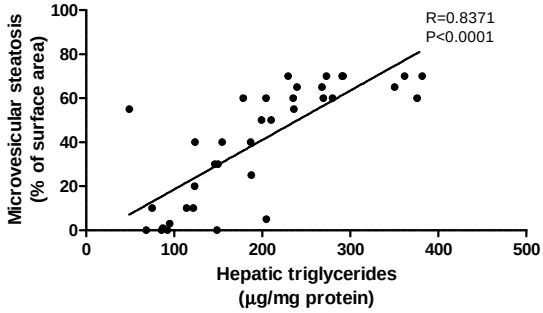

Supplemental Figure 3: Correlation analysis. Correlation of the samples used in the validation set for biochemical triglyceride measurement and microvesicular steatotis.

METABOLICALLY INDUCED LIVER INFLAMMATION LEADS TO NASH AND DIFFERS FROM LPS or IL-1β-INDUCED CHRONIC INFLAMMATION

Wen Liang
Jan H. Lindeman
Aswin Menke
Debby Koonen
Martine Morrison
Louis M. Havekes
Anita M. van den Hoek
Robert Kleemann

Lab Invest. 2014; 94(5):491-502

ABSTRACT

Background & aims: The nature of the chronic inflammatory component that drives the development of non-alcoholic hepatosteatitis (NASH) is unclear and potential inflammatory triggers have not been compared to date. We tested the influence/effect of non-metabolic triggers (LPS, IL-1β, administered by slow-release minipumps) and metabolic dietary triggers (carbohydrate, cholesterol) of inflammation on the progression of bland liver steatosis (BS) to NASH.
Methods: ApoE3L.CETP mice fed a high-fat diet (HFD) developed BS after 10 weeks. Then, inflammatory triggers were superimposed or not (control) for 6 more weeks. Mouse livers were analyzed with particular emphasis on hallmarks of inflammation in human NASH. These hallmarks were defined in human liver biopsies with and without NASH.
Results: Livers of HFD-treated control mice remained steatotic and did not progress to NASH. All 4 inflammatory triggers applied activated hepatic NFκB significantly and comparably (⩾5-fold). However, HFD+LPS or HFD+IL1β did not induce a NASH-like phenotype and caused intrahepatic accumulation of almost exclusively mononuclear cells. By contrast, mice treated with metabolic triggers developed NASH, characterized by enhanced steatosis, hepatocellular hypertrophy and formation of mixed-type inflammatory foci containing MPO-positive granulocytes (neutrophils) as well as mononuclear cells, essentially as observed in human NASH. Specific for the metabolic inducers was an activation of the pro-inflammatory transcription factor AP-1, neutrophil infiltration, and induction of risk factors associated with human NASH, i.e. dyslipidemia (by cholesterol) and insulin resistance (by carbohydrate).
Conclusion: HFD feeding followed by NFκB activation per se (LPS, IL-1β) does not promote the transition from BS to NASH. HFD feeding followed by metabolically-evoked inflammation induces additional inflammatory components (neutrophils, AP-1 pathway) and causes NASH.

INTRODUCTION

Nonalcoholic fatty liver disease (NAFLD) is emerging as one of the most common liver disorders in modern societies (1). Its prevalence in the general population is strongly increasing together with obesity, dyslipidemia and the metabolic syndrome (2). NAFLD encompasses a range of conditions associated with accumulation of fat within liver cells. The most benign form of NAFLD is bland steatosis (BS), which is characterized by the accumulation of lipid droplets. BS can remain stable for many years and will never progress in many cases (1). In other cases BS does progress, leading to development of non-alcoholic steatohepatitis (NASH), which is characterized by fat accumulation and inflammation. This condition is not benign and can further progress to liver fibrosis and cirrhosis with high rates of morbidity and mortality (3, 4). The factors that trigger this transition from BS to NASH are unknown.

The pathogenesis of NASH is thought to be driven by a lipid component and an inflammatory component (2, 5). Excessive intrahepatic fat accumulation may sensitize the liver to subsequent inflammatory insults that promote the development of NASH. The exact nature of these inflammatory insults or 'second hits', viz. the mechanism inducing the inflammatory component of the disease, is largely unclear (6). The pro-inflammatory transcription factor NFκB may critically influence this process and chronic activation of NFκB is associated with many pathogenic liver conditions (7). A causal role for hepatic NFκB in the progression of BS to NASH has been proposed recently in transgenic mice selectively expressing constitutively active IKKβ in hepatocytes (8). Among the inflammatory triggers that may be responsible for chronic activation of NFκB in liver cells are circulating endotoxins (LPS) or pro-inflammatory cytokines such as interleukin-1beta (IL-1β) (9, 10). However, low-grade hepatic inflammation may also be evoked by other types of stimuli such as unhealthy diets or excess eating, which represent metabolic triggers of inflammation that may activate multiple pathways simultaneously (11, 12). For instance, diets with a high content of metabolizable energy from carbohydrate or diets rich in cholesterol can cause chronic activation of NFκB in the liver (6, 12-15).

In this study we tested the influence of different inflammatory triggers with NFκB-activating properties on the transition of BS to NASH and analyzed whether disease progression depends on the type of trigger employed. More specifically, we compared the effects of non-dietary inflammatory stimuli (LPS, IL-1β) and diet-related metabolic inflammatory stimuli (carbohydrate, cholesterol) all of which were superimposed on a high-fat diet (HFD) in separate groups of mice. Transgenic ApoE3*Leiden.huCETP (E3L.CETP) mice were used because their lipoprotein metabolism is translational to the human situation and these animals are prone to develop obesity, dyslipidemia and NAFLD on HFD (16, 17). Chronic exposure to low concentrations of LPS and IL-1β was achieved by minipump technology, and metabolically evoked inflammation was induced by feeding diets rich in carbohydrates or cholesterol. Prior to analysis of experimental NASH, human liver biopsies with and without NASH were analyzed to define hallmarks of inflammation of human NASH. Combined histological and biochemical analysis of mouse livers resulted in identification of cellular and molecular determinants that are crucial for the transition of BS to NASH.

MATERIALS AND METHODS

Human liver biopsies

Human liver biopsies were obtained at autopsy for postmortem histological analysis by pathologists (Department of Pathology; Leiden University Medical Center/LUMC, Leiden, The Netherlands). N=21 specimens with NASH and n=12 control subjects without NASH were used for this study (diagnosed by pathologist). Tissue was obtained and handled in accordance with the guidelines set by the LUMC medical ethical committee. Cardiovascular disease was the predominant cause of death. In all, 40% of the subjects were female and 60% male. The average age was 62 years. Cross-sections were stained with anti-MPO (A0398, Dako, Glostrup, Denmark) and phospho-p65-NFκB (#3037, Cell Signaling, Danvers MA, USA) as described (18).

Animals and diets

Male ApoE*3-Leiden.huCETP transgenic mice (E3L.CETP) were 10-14 weeks old and obtained from an in-house breeding colony (TNO Metabolic Health Research) (18). Briefly, ApoE*3-Leiden were crossed with hemizygous human CETP transgenic mice and offspring was genotyped using the primers CETP-F sequence: GAATGTCTCAGAGGACCTCCC, CETP-R sequence: CTTGAACTCGTCTCCCATCAG; ApoC1-L sequence: GGTCCCGGGCACTTCCC TTAGCCCCA; ApoC1-R sequence: TTTGAGCTCGGCTCTTGAGACAGGAA. Furthermore, presence of human ApoE3 protein and human CETP protein in plasma was confirmed by ELISA.

Experiments were approved by an ethical committee on 'Animal care and Experimentation', Zeist, The Netherlands. Mice were kept on chow diet (Ssniff R/M-H, Ssniff Spezialdiäten, Soest, Germany) until the start of the experiment. Animals had free access to water and diet during the study period of 16 weeks. The group size was n=9-10. One group remained on chow and served as aging control. The other animals received a high-fat diet (HFD; 24% w/w lard, Research Diets, New Brunswick NJ, USA) for 10 weeks (run-in) and were then matched into groups based on total plasma cholesterol, triglycerides and body weight. HFD feeding was continued in all groups. Groups were additionally treated with one of the following treatments until week 16: LPS from Salmonella minnesota R595 (Lot#30446A1, List-Biological Laboratories, Campbell CA, USA) by minipump at 5 µg/day; recombinant murine IL-1β (Lot#030447, PeproTech, Rocky-Hill NJ, USA) by minipump at 100 ng/day; dietary carbohydrate (Ensure® Plus in drinking water, Abbott Laboratories, Hoofddorp, The Netherlands); dietary cholesterol (1% w/w mixed into HFD) (Sigma-Aldrich, Zwijndrecht, The Netherlands). Osmotic minipumps (Alzet, Lot#10194-08, Maastricht, The Netherlands) were placed subcutaneously in the back region (flow-rate: 0.10 µL/hour, 101 µL total volume) under isoflurane anesthesia. Two controls groups were included; they were treated with either HFD+PBS (minipump) or HFD only. These groups were comparable in all histological scores and were therefore analyzed as one.

Histological and biochemical analysis

The right median liver lobe (lobus dexter medialis hepatis) was carefully isolated, fixed in 4% paraformaldehyde (2 days), embedded in paraffin and cross-sectioned (5 µm). The other

liver lobes were snap-frozen and stored at -80°C. Hematoxylin-eosin (HE)-stained cross-sections were scored blindly by a pathologist using an adapted grading method for human NASH (19) with specific emphasis on hallmarks of steatosis and inflammation. Briefly, two cross-sections were examined per mouse and the level of vacuolization was determined relative to the total liver area analyzed, i.e. expressed as a percentage. The extent of vacuolization was scored as 'Slight' (<5%), 'Moderate' (5-33%), 'Severe' (34-66%) and 'Very Severe' (>66%). Of note, hepatocellular ballooning (central nucleus, web-like structure in cytoplasm) is a hallmark of human NASH but mouse livers merely show enlarged hepatocytes containing small intracellular lipid droplets, herein referred to as 'hepatocellular hypertrophy'. The extent of enlarged hepatocytes (diameter >1.5 normal) was analyzed using the same percentage categories as for vacuolization to provide quantitative information about abnormally enlarged cells. Inflammation was scored by counting and analyzing the type of inflammatory cells (mononuclear and/or polymorph nuclear) in a defined area of five random microscopic fields per animal. Inflammation was graded as 'Normal' (<0.5 foci), 'Slight' (0.5-1.0 foci), 'Moderate' (1.0-2.0 foci), 'Severe' (>2.0 foci). Collagen was stained using Picro-Sirius red staining (Sigma-Aldrich).

Liver lipids

The intrahepatic concentration of free cholesterol, triglycerides and cholesteryl esters was analyzed as described (20). Briefly, 200 µg of frozen liver biopsies were homogenized in MilliQ H_2O and the protein content was determined. Two µg of cholesterol acetate was added to each sample as an internal standard. Lipids were extracted using methanol and chloroform. Extracted lipids were then separated by thin layer chromatography using a silica-gel-60 pre-coated plate. Plates were incubated at 130°C for 30 min and band densities were then quantified (20). In addition, cryostat-sections were stained with Oil-Red O (Sigma-Aldrich) to identify lipids, and counterstained with hematoxylin (Sigma-Aldrich) to visualize nuclei.

Immunohistochemical staining

Paraffin-embedded liver cross-sections were used for analysis of MPO-positive cells (neutrophils) using anti-MPO (ab9535-Abcam, Cambridge, UK). After pre-treatment with target retrieval solution (3-in-1; Dako) at pH 9.0, cross-sections were incubated with primary anti-MPO overnight. Sections were peroxidase blocked in 3% H_2O_2 in methanol for 10 minutes and detected with Dako Envision-Flex amplification kit (Product#K800021). For analysis of CD11b, frozen liver samples were used. After fixation with acetone, cross-sections were incubated with anti-CD11b (Lot#ab8878, Abcam) for one hour followed by incubation with biotinylated rabbit anti-rat antibody (Lot#00065538, Dako). Immunoreactivity was visualized with streptavidin/HRP (Lot#00057815, Dako) and AEC (Lot#10043262, Dako). For all IHC analyses, negative controls were performed by omitting the primary antibody.

Analysis of transcription factor activity in liver homogenates

To determine the amount of activated p65-NFκB, AP-1, STAT3 and C/EBP-β protein in livers, protein extracts were prepared using a Nuclear Extract Kit (Cat.#40010, ActiveMotif, Rixensart, Belgium). The protein content of the extracts was determined with Bio-Rad dye

reagent (Cat#500-0006, Bio-Rad Laboratories-GmbH, Munich, Germany). Six µg of protein was used for transcription factor activity analysis using TransAM® kits for NFκB-p65 Chemi, c-Jun, STAT3 and C/EBP-β kits (Cat.#40097, 46096, 45196, 44196, ActiveMotif) as reported (11, 20). Briefly, the amount of active transcription factor was determined by measuring its binding capacity to a consensus binding sequence in presence of a competitor oligonucleotide or a mutant (non-competitor) oligonucleotide to control for the specificity of DNA binding. Data are provided as relative units.

Plasma parameters, lipoproteins and plasma inflammatory markers

EDTA (Sarstedt, Numbrecht, Germany) plasma was collected after a 5-hour fast (8 am to 1 pm). Plasma levels of glucose (Instruchemie, Delfzijl, The Netherlands), insulin (Mercodia, Uppsala, Sweden), total cholesterol and triglycerides (Roche Diagnostics, Almere, The Netherlands) were measured with commercial kits. HOMA index was calculated according to the formula HOMA = fasting plasma glucose (mM) x fasting plasma insulin (ng/mL)/22.5. Lipoprotein profile analysis was performed with AKTA-FPLC (18). The plasma levels of E-selectin and SAA were determined by ELISA (R&D-Systems, Abington, UK for E-selectin, Life Technologies, Bleiswijk, the Netherlands for SAA). Plasma ALAT activity was measured using a Reflotron® kit (Roche Diagnostics).

Statistics Analysis

Statistical analyses were performed with StatView software (SAS-Institute, Cary, NL), and a P-value <0.05 was considered statistically significant. Differences between groups were analyzed using Mann-Whitney non-parametric test for two independent samples. The data obtained from histological scoring of livers were analyzed using 2-sided Fisher's exact test. All values shown represent means ± SEM.

RESULTS

Characterization of the inflammatory component in human NASH

HE-stained human tissue biopsies were analyzed for steatosis and inflammation. Livers of patients with NASH showed pronounced vacuolization compared with controls (**Figure 1A/B**). Quantitative analysis revealed that about 40% of the surface area was steatotic (P<0.001 versus control; **Supplementary Material-A**) of which 35% was macrovesicular steatosis and 5% microvesicular steatosis. Hepatocellular ballooning was observed in NASH livers but not in controls (**Figure 1A/B**). Also, enlarged hepatocytes containing small lipid droplets were observed in NASH specimens only (**Supplementary Material-B**). NASH livers were characterized by lobular inflammation, i.e. an abundant presence of mononuclear cells and polymorph-nuclear leukocytes (granulocytes) which formed foci (**Figure 1A/B**). Inflammatory cell foci contained CD68-positive cells of the monocytes/macrophage lineage (not shown) as well as granulocytes with MPO-positive immunoreactivity (neutrophils), a hallmark of human NASH (**Figure 1C/D**). NASH livers also showed a pronounced expression of p65-NFκB (in inflammatory foci and steatotic areas), while only a few p65-NFκB-positive cells were observed in healthy control livers

(**Figure 1E/F**). Fibrosis was present in most (73%) human NASH specimens, and in none of the controls (**Figure 1G/H**).

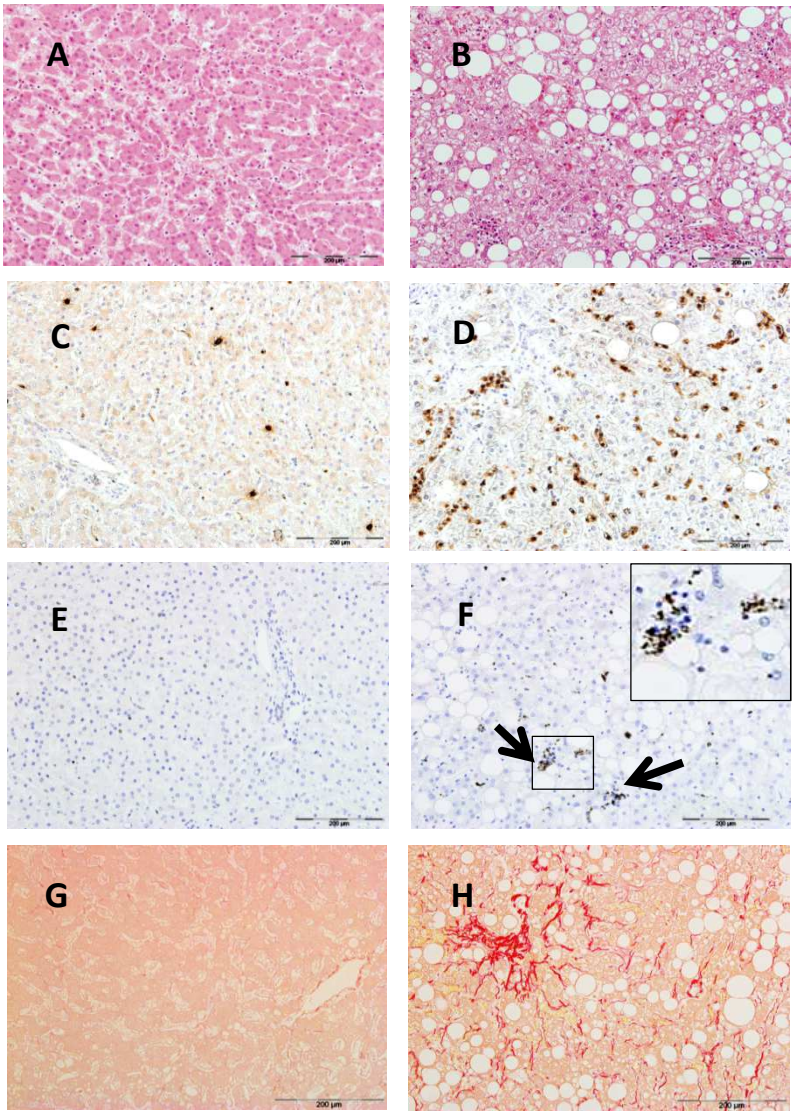

Figure 1: Analysis of inflammation in human NASH. Representative photographs of control livers (n=12, panels left) were compared to NASH specimens (n=21, panels right). (A/B) HE staining showed pronounced vacuolization in NASH livers which was associated with inflammatory cell aggregates (solid arrow) and hepatocellular ballooning (magnified in insert). (C/D) Immunostaining showed inflammatory cell foci (arrows) containing myeloperoxidase (MPO)-positive cells in NASH. (E/F) Immunostaining of p65-NFκB-positive cell clusters (arrows) in NASH (magnified in insert). (G/H) Picro Sirius red staining demonstrated NASH with fibrosis in 15 out 21 specimens.

Effects of HFD feeding and addition of inflammatory triggers on the development of experimental NASH

To gain insight into the nature of the inflammatory trigger that may underlie the development of BS into NASH, we evaluated the effects of different inflammatory stimuli superimposed on HFD feeding. Treatment with inflammatory stimuli was started after a 10-week run-in period on HFD, which resulted in BS and moderate pericentral hepatocellular vacuolization (**Supplementary Material-C**). Lobular inflammation was not observed after 10 weeks of HFD run-in.

HFD feeding was continued for six more weeks and experimental groups additionally received either PBS (minipump control), LPS (minipump), IL-1β (minipump), dietary carbohydrate (Ensure®) or dietary cholesterol. A second control group was continued on HFD only. A separate group was fed chow during the complete experimental period (16 weeks) and served as a reference. All interventions were well-tolerated and the superimposed inflammatory triggers did not affect the daily food intake relative to HFD control, i.e. calorie intake was comparable between the groups (on average 12 kcal/day per animal) except for the HFD+carbohydrate group (16 kcal/day per animal). At sacrifice, livers were immediately prepared for histological examination and biochemical analysis of active p65-NFκB. Representative photomicrographs of livers are shown in **Figure 2A-F**. Reference mice on chow had normal livers without steatosis or inflammation (**Figure 2A**). The two control groups, i.e. HFD feeding alone and HFD+PBS-minipump treatment, were comparable and showed moderate steatosis with vacuolization of the pericentral zone and the midzone as well as hepatocellular hypertrophy (individual data provided in **Supplementary Material-D**). Livers of these groups hardly contained inflammatory foci, demonstrating that HFD feeding *per se* is not sufficient to induce a NASH-like phenotype within a period of 16 weeks (**Figure 2B**).

Consistent with the low abundance of cellular inflammation in HFD-treated mice, the level of transcriptionally active p65-NFκB protein measured by TransAM® was very low (1.1×10^5 relative units, RLU) (**Figure 3A**). Treatment with the inflammatory triggers LPS, IL-1β, carbohydrate and cholesterol resulted in significantly higher levels of activated p65-NFκB protein in mouse livers. The p65-NFκB activating effects of the different inflammatory stimuli were statistically comparable. This demonstrates that p65-NFκB was activated at least 5-fold or more in liver at the end of the study relative to HFD alone.

Histological analysis of experimental NASH allowed quantification of the effects of the different inflammatory triggers on vacuolization, hypertrophy and inflammation compared with HFD alone (**Figure 3A-C**; individual histological scores see **Supplementary Material-D/E**). Chronic exposure to LPS did not further aggravate vacuolization and hypertrophy relative to HFD control (**Figures 2C** and **3B/C**). The inflammatory cell content of LPS-treated animals was higher than in controls treated with HFD only. Inflammatory cells were mainly mononuclear and diffusely distributed, and polymorph nuclear cells were hardly observed. Surprisingly, livers of mice treated with IL-1β showed even less

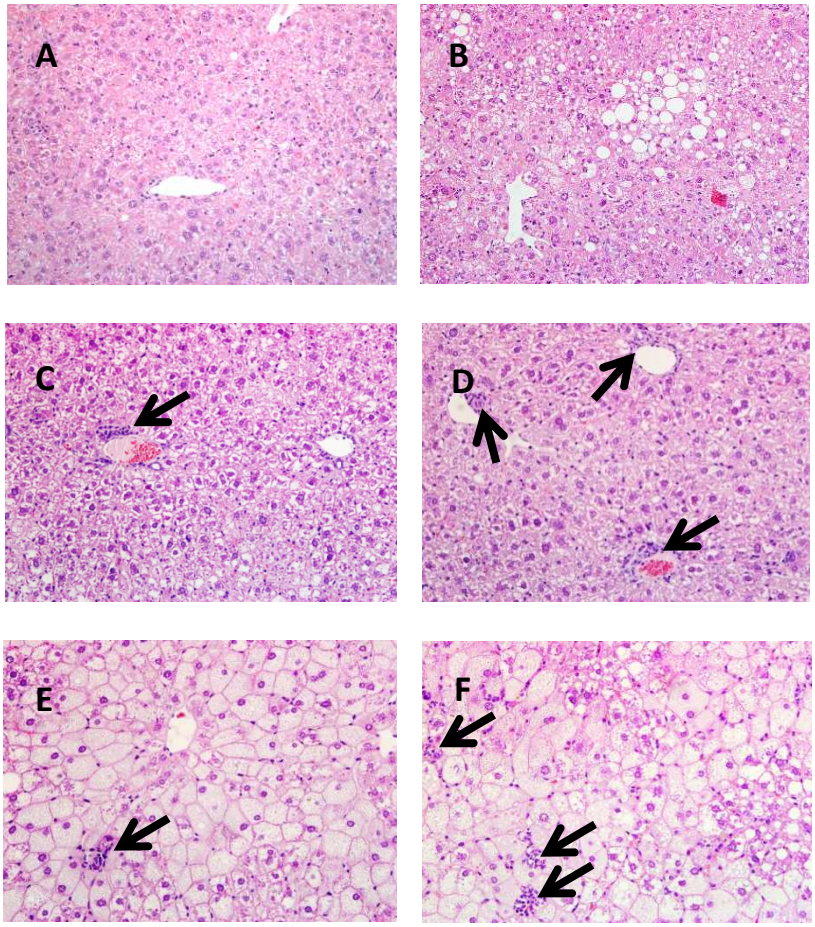

Figure 2: Histological presentation of experimental NASH. Representative photomicrographs are shown at 200-fold magnification. Mice were treated with (A) chow (reference group), (B) HFD (control group) and HFD plus additional inflammatory stimuli (C) LPS, (D) IL-1β, (E) dietary carbohydrate and (F) dietary cholesterol. Inflammatory infiltrates are indicated with arrows.

vacuolization than HFD control mice (**Figure 2D** and **3B**). Hepatocellular hypertrophy was not observed with IL-1β. Similar to LPS, the inflammatory cell content was higher than in HFD controls, but again inflammatory cells were predominately of the mononuclear type and diffusely distributed across the liver. Inflammatory cell foci were frequently found in close proximity to vascular structures.

In contrast to LPS and IL-1β, the metabolic stimuli (carbohydrate and cholesterol) clearly promoted the development of a NASH-like phenotype and resulted in pronounced changes in shape and size of hepatocytes: Carbohydrate-treated animals showed

pronounced micro-vacuolization and enlarged hepatocytes containing small lipid droplets, also in the periportal zone, which was not affected in HFD control livers (**Figure 2E** and

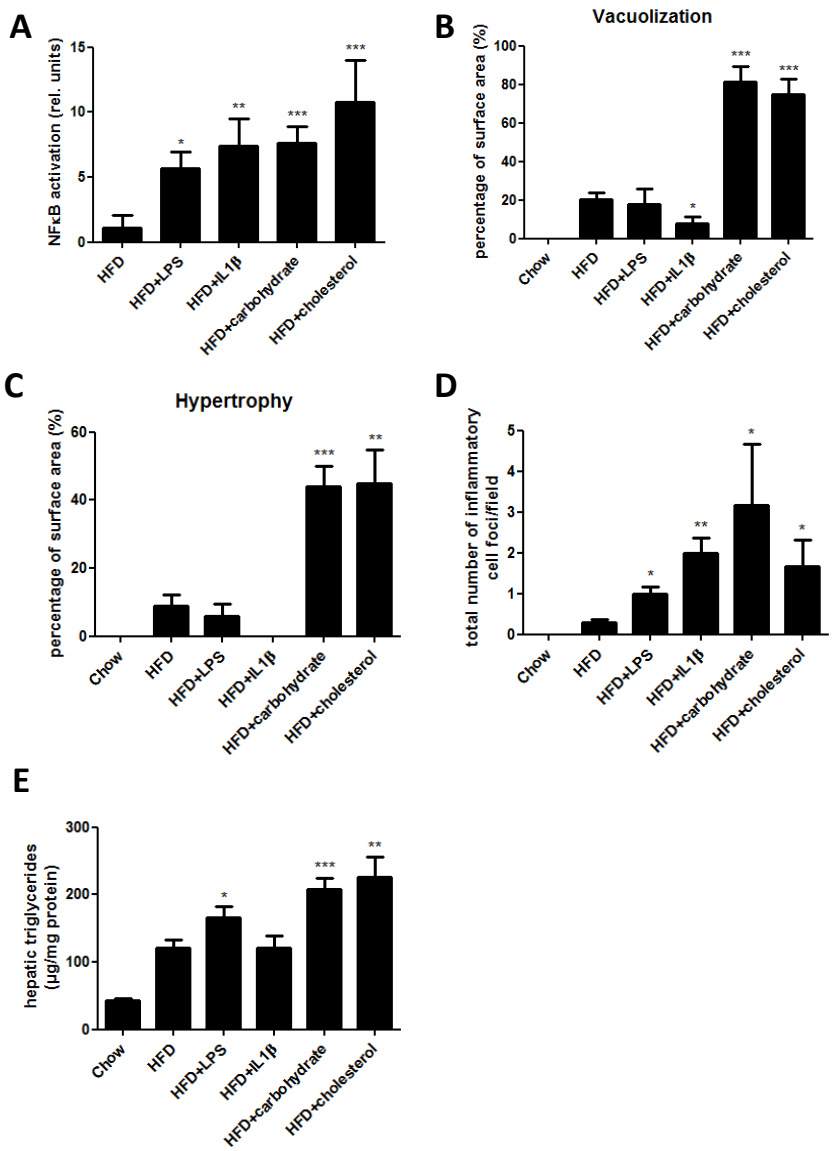

Figure 3: Quantitative analysis of experimental NASH. Quantification of (A) activated p65-NFkB measured by TransAM® in liver homogenates, (B) vacuolization and (C) hepatocellular hypertrophy as percentage of the total liver area analyzed (%). (D) Number of inflammatory foci per microscopic field. (E) Quantitative analysis of the intrahepatic triglycerides. Groups treated with inflammatory stimuli are compared to HFD control. *P<0.05, **P<0.01, ***P<0.001.

Supplementary Material-D). Quantification of hepatocellular vacuolization and hypertrophy revealed that carbohydrate feeding increased these parameters significantly and about 4-fold ($P<0.05$) relative to HFD (**Figure 3B/C**). Mixed-type inflammatory cells (i.e. mononuclear and polymorph nuclear cells) were present and inflammatory cell foci were observed.

Cholesterol-treated livers resembled carbohydrate-treated livers and also showed extensive micro and macro-vacuolization with large vacuoles in pericentral and periportal zones. Livers had a significantly increased content of inflammatory cell foci (**Figure 2F**). The effects of cholesterol on vacuolization, hypertrophy and inflammation were all significant (**Figure 3B-D**) and statistically comparable to the effect of the other metabolic trigger, carbohydrate.

Biochemical analysis of the intrahepatic triglyceride concentrations (**Figure 3E**) and parallel Oil Red O staining (not shown) were in line with the histological analyses and confirmed that only the metabolic triggers, carbohydrate and cholesterol, promoted a transition of BS to NASH. Most of the mice did not develop fibrosis within the study period: only one mouse (cholesterol treated group) did develop NASH with fibrosis (Sirius red collagen staining, not shown).

Effect of non-metabolic and metabolic inflammatory triggers on inflammatory cells and inflammatory pathways

Experimental livers were further analyzed histologically and biochemically to identify determinants that distinguish the metabolic triggers from LPS and IL-1β. A more refined histological analysis of inflammatory cells present in liver revealed that LPS and IL-1β treatment led to an almost exclusive recruitment of mononuclear cells; whereas carbohydrate and cholesterol treated livers contained mixed-type inflammatory cells including polymorph nuclear cells (**Figure 4G**). Consistent with this observation, more MPO-positive cells (neutrophils) were observed in the groups exposed to carbohydrate or cholesterol but not in those treated with LPS or IL-1β (**Figure 4A-F**). Immunohistochemical analysis of the monocyte/macrophage marker CD68 revealed no difference among the experimental groups, except a slight increase in the IL-1β-treated (1.5-fold) and cholesterol-treated (2-fold) groups (not shown). Furthermore, the number of Mac1/CD11b-positive cells did not differ between the groups (not shown). Together, this shows that an abundant presence of neutrophils, a hallmark of human NASH, discriminates the two metabolic inflammatory triggers from the two non-dietary triggers (LPS and IL-1β).

To gain more insight into the molecular effects of the different triggers we analyzed transcription factor activity downstream of specific inflammatory pathways by TransAM® technology. Independent of the type of inflammatory trigger, the activity of C/EBP-β tended to be lower than in HFD controls (**Supplementary Material-F**). The transcriptional activity of STAT3 was slightly increased in the LPS- and IL-1β-treated groups but the effects did not reach statistical significance (**Supplementary Material-G**). Treatment with carbohydrate and cholesterol significantly increased the transcriptional activity of AP-1, an effect that differentiated the metabolic triggers from LPS and IL-1β (**Figure 4H**). With respect to systemic markers of inflammation, plasma E-selectin levels were increased by

IL-1β and plasma SAA levels were increased by IL-1β, carbohydrate and cholesterol treatment (**Table 1**).

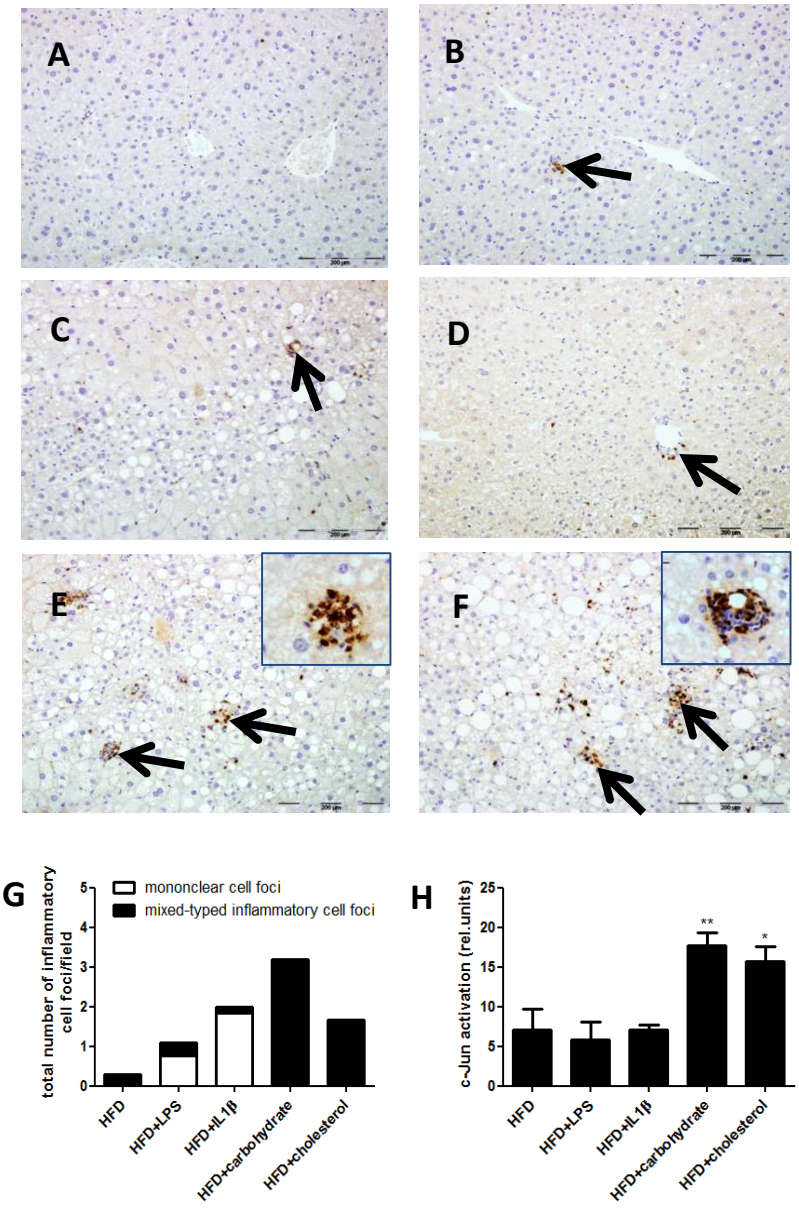

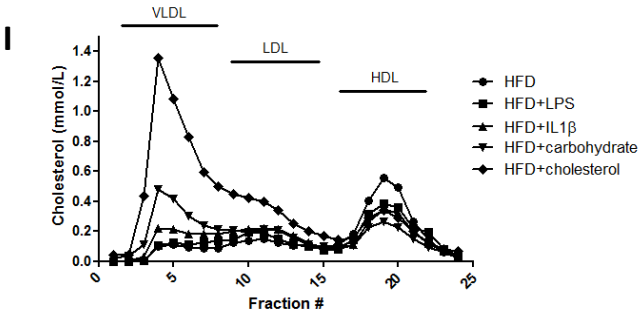

Figure 4: Characterization of inflammation in experimental NASH. Immunohistochemical staining of MPO in (A) chow reference, (B) HFD control and HFD plus (C) LPS, (D) IL-1β, (E) carbohydrate or (F) cholesterol. Inflammatory cell foci (arrows) containing MPO-positive cells. (G) Relative contribution of mononuclear cell foci and mixed-type inflammatory cell foci to the overall content of inflammatory cells for each group (H) Transcriptional activity of c-Jun (a subunit of AP-1) protein by TransAM® analysis. (I) Lipoprotein profile at t=16 weeks. *P<0.05, **P<0.01.

Table 1: Experimental treatments have a differential effect on risk factors of NASH. Parameters shown were determined in fasting plasma at the end of the experimental period (week 16). Intrahepatic lipids were determined in freshly prepared tissue homogenates. Values are means ± SEM. Significance is indicated *P<0.05, **P<0.01, ***P<0.001 versus HFD control (Mann-Whitney test).

	HFD	**HFD + LPS**	**HFD + IL1β**	**HFD + carbohydrate**	**HFD + cholesterol**
Body weight [g]	**39.9**±0.9	**39.9**±1.5	**37.3**±2.0	**47.6**±1.2***	**42.1**±2.0
Visceral fat [g]	**0.7**±0.1	**0.7**±0.1	**0.7**± 0.1	**1.1**±0.1**	**0.7**±0.1
Cholesterol [mM]	**4.7**±0.3	**4.2**±0.3	**4.8**±0.4	**6.5**±0.6*	**16.2**±2.0***
Triglycerides [mM]	**1.4**±0.3	**1.6**±0.2	**2.1**±0.3*	**4.3**±0.6***	**3.4**±0.7**
Fasting glucose [mM]	**13.5**±0.9	**13.3**±0.6	**10.9**±0.9*	**17.2**±0.8**	**14.4**±0.7
Insulin [ng/mL]	**1.15**±0.3	**1.37**±0.3	**2.41**±0.6	**4.28**±0.9**	**1.15**±0.3
Intrahepatic free cholesterol [µg/mg protein]	**14.1**±0.7	**16.6**±0.9*	**14.5**±0.7	**17.2**±0.9*	**20.1**±1.6**
Intrahepatic cholesterol ester [µg/mg protein]	**12.8**±0.8	**14.5**±1.5	**12.4**±1.4	**20.4**±2.9*	**48.0**±4.0***
ALAT [U/L]	**76**±16	**76**±22	**59**±15	**176**±66*	**151**±41
E-selectin [ng/mol]	**30**±7	**33**±1	**66**±2***	**31**±1	**31**±1
SAA [µg/mL]	**5.03**±1.30	**5.30**±1.67	**37.8**±14.2**	**6.7**±2.2*	**14.5**±4.6**

Effect of non-metabolic and metabolic inflammatory triggers on risk factors associated with NASH

Table 1 shows data of risk factors that are typically associated with NASH development in humans, e.g. body weight, visceral fat mass, plasma lipids, fasting glucose and insulin, and ALAT. These risk factors were not affected by LPS. IL-1β treatment also did not affect these parameters, except a slight increase in triglycerides and a decrease in glucose. In contrast, the metabolic triggers worsened risk factors that are typically associated with

NASH development in humans. Carbohydrate treatment resulted in an increased body weight (47.6 ± 1.2 g; P<0.001) and visceral fat mass (1.1 ± 0.05 g; P<0.01) beyond that of HFD controls. Also, plasma cholesterol and triglyceride concentrations were significantly higher in carbohydrate-treated animals. Increased fasting plasma glucose (17.2 ± 0.8 mM; P<0.01) and insulin (4.28 ± 0.9 ng/mL; P<0.05) levels indicated insulin resistance ($HOMA_{carbohydrate}$= 3.3 versus $HOMA_{HFD\ control}$= 0.9). Treatment with cholesterol had a marked adverse effect on plasma cholesterol and triglycerides and little effect on the other risk factors. Also, intrahepatic free cholesterol and cholesterylester levels were increased. Lipoprotein profile analysis revealed that the observed increase in plasma cholesterol was confined to VLDL/LDL-sized particles. All treatment groups showed a relative decrease in HDL compared to HFD control animals (**Figure 4I**). Plasma ALAT levels were only elevated in the groups treated with metabolic inflammatory triggers.

DISCUSSION

There is ample evidence that development of NASH is driven by chronic inflammation but the nature of the inflammatory component is not very clear (1-5, 21), and possible inflammatory triggers have not been investigated systematically. The present study examined the influence of metabolically evoked inflammation (carbohydrate, cholesterol) and non-metabolic inflammatory triggers (LPS, IL-1β) on the development of experimental NASH. Herein, we present the first head-to-head comparison of these triggers, revealing that they differ in their potency to stimulate progression of steatosis and induction of NASH. Only the metabolic triggers aggravated steatosis and led to an infiltration of neutrophils as well as activation of AP-1, a hallmark of lipotoxicity (22). Furthermore, they induced metabolic risk factors (insulin resistance, dyslipidemia) associated with NASH development in humans, which were not observed for the non-metabolic triggers.

The HFD control group that remained on HFD during the complete experimental period did not show inflammatory cell infiltrates, had low AP-1 and NFκB levels and did not progress from steatosis to NASH. Treatment with metabolic or non-metabolic inflammatory triggers activated hepatic NFκB significantly and comparably. Despite this clear pro-inflammatory effect in liver, LPS and IL-1β-treated mice did not progress to NASH. Thus, simultaneous HFD feeding and activation of hepatic NFκB *per se* in livers with established steatosis is not sufficient to induce NASH development, indicating that additional inflammatory factors or pathways are involved. Livers of LPS and IL-1β-treated groups exhibited cell infiltrates consisting almost exclusively of mononuclear cells, with hardly any mixed-type infiltrates, a characteristic feature of biopsy-proven human NASH (21). The selective effect of endotoxin on recruitment of mononuclear cells is in line with human and rodent studies in which elevated LPS activity in serum was associated with macrophage-mediated chronic inflammation and increased levels of monocyte chemoattractant protein-1 (23, 24). Thus, chronic LPS and IL-1β exposure may merely activate and recruit specific populations of inflammatory cells to liver and the absence of neutrophil infiltrates indicates these triggers by themselves do not cause hepatocellular damage. Consistent with this notion we observed no increase in ALAT when mice were treated with LPS or IL-1β. Hence, administration of LPS and IL-1β by minipump constitutes

an ‘exogenous’ form of inflammation while the two metabolic triggers employed herein affect liver metabolism (20) and ‘endogenous’ inflammatory processes related to it (12, 14), possibly causing liver damage. Lipotoxicity and/or the relatively high levels of free cholesterol observed in these groups may constitute causes of liver damage.

Neutrophil infiltration is an important hallmark of biopsy-proven NASH in humans (21) that distinguishes subjects with NASH from those without, independent of obesity (25). It is not clear whether neutrophils are innocent bystanders or causally involved in the pathogenesis, and investigators have only recently begun to characterize the role of neutrophils in NAFLD. The molecular mechanisms that allow neutrophils to home to the liver are also not well understood (26). We observed a marked infiltration of neutrophils with metabolic triggers despite low E-selectin levels. In accordance with our observations, adhesion of neutrophils within liver sinusoids is thought to be independent of selectins and differs fundamentally from other tissues (26). The activation of AP-1 may explain why metabolic inflammatory triggers stimulate neutrophil recruitment: the main chemoattractants for neutrophils in mice, keratinocyte cytokine (KC)(CXCL-8/IL-8 in humans) and macrophage inflammatory protein-2 (MIP-2), are transcriptionally regulated by NFκB *and* AP-1 (27). Transcription of MIP-2 depends on a simultaneous activation of both transcription factors, i.e. a condition that was achieved with two metabolic triggers in the present study but was absent in the case of the two non-metabolic triggers. Further support for a crucial role of the AP-1 signaling pathway in NASH comes from knock-out studies: phosphorylation of the AP-1 subunit c-Jun is diminished in Jnk1-deficient mice and these mice show a reduced development of steatohepatitis (28).

Of note, the two metabolic triggers induced different factors that are known to be risk factors for NASH in humans, i.e. adiposity/insulin resistance (carbohydrate) and dyslipidemia (cholesterol). This suggests that the pathogenic processes leading to liver damage, neutrophil infiltration and AP-1 activation may differ between these triggers. Because plasma levels of HDL were reduced by both metabolic as well as non-metabolic triggers, it is unlikely that HDL has a major role in the pathogenic processes mediating the transition from steatosis to NASH. Our data also do not indicate a major role for the inflammatory pathways leading to activation of STAT3 or C/EBP-β.

Treatment with inflammatory stimuli was started once steatosis was already manifest (after 10 weeks of HFD feeding) and reportedly still reversible (29), in order to mimic a risk population with established steatosis (21, 30). HFD feeding alone causes metabolic stress and renders livers susceptible to injury (13, 20) and the superimposed insults represent ‘second hits’. Importantly, feeding of a HFD alone only resulted in a steatotic liver within the study period and did not cause NASH or cellular inflammation. This has also been observed in other HFD-feeding studies of comparable lengths of time using diets with similar content of fat, i.e. ≤25% w/w. This equals about 45% energy from fat (20) which is reached in human diets in Finland and Crete (31). Of note, experimental diets that contain very high, supraphysiological quantities of fat (e.g. >50% energy) as well as experimental diets deficient in methionine and choline (MCD diets) may develop a more severe and different liver pathology. The translational character of such studies is debated because MCD-fed mice lose weight due to a vastly lower caloric intake and do not become insulin resistant while most humans with NASH are obese and insulin resistant (1-3).

It is generally assumed that chronic activation of NFκB in the liver is a main driver of the transition from BS to NASH. In the present study we compared different NFκB-inducing inflammatory triggers (head-to-head and superimposed on HFD) regarding their ability to induce this transition to NASH. We observed that activation of NFκB in the liver *per se* (upon stimulation with LPS or IL-1β) does not promote a transition from BS to NASH. By contrast, metabolic inducers of inflammation like cholesterol and carbohydrate had a greater ability to induce a human NASH-like phenotype. This suggests that chronic inflammation caused by metabolic triggers activates additional inflammatory pathways and biological processes than LPS or IL-1β. To our knowledge, this is the first study that compares metabolic inflammatory triggers (high carbohydrate, cholesterol) to non-metabolic (classical) inflammatory chronic triggers (LPS, IL-1β) in a head-to-head approach, and that defines molecular differences between 'metabolic' and 'non-metabolic' inflammatory triggers. More specifically, we show that metabolic triggers activate AP-1 in the liver and lead to neutrophil infiltration, both of which could be causative factors in the development of NASH. These mechanistic insights as well as the experimental conditions defined herein may help to further elucidate the etiology of NASH and contribute to development of therapeutic strategies directed at attenuating metabolic overload and associated pathologic conditions.

ACKNOWLEDGEMENTS

The authors thank Erik H. Offerman, Niels Kloosterhuis, José van der Hoorn, Adri Mulder, Karin Toet and Simone van der Drift-Droog for technical assistance. This research was performed within the framework of CTMM, the Center for Translational Molecular Medicine (www.ctmm.nl), project PREDICCt (grant 01C-104), and supported by the Dutch Heart Foundation, Dutch Diabetes Research Foundation and Dutch Kidney Foundation.

REFERENCES

1. Bellentani S, Marino M. Epidemiology and natural history of non-alcoholic fatty liver disease (NAFLD). Ann Hepatol 2009;8 Suppl 1:S4-8.

2. Edmison J, McCullough AJ. Pathogenesis of non-alcoholic steatohepatitis: Human data. Clin Liver Dis 2007;11(1):75,104, ix.

3. Lazo M, Clark JM. The epidemiology of nonalcoholic fatty liver disease: A global perspective. Semin Liver Dis 2008;28(4):339-50.

4. Fujii H, Kawada N. Inflammation and fibrogenesis in steatohepatitis. J Gastroenterol 2012;47(3):215-25.

5. Harmon RC, Tiniakos DG, Argo CK. Inflammation in nonalcoholic steatohepatitis. Expert Rev Gastroenterol Hepatol 2011;5(2):189-200.

6. Nomura K, Yamanouchi T. The role of fructose-enriched diets in mechanisms of nonalcoholic fatty liver disease. J Nutr Biochem 2012;23(3):203-8.

7. Wieckowska A, Feldstein AE. Diagnosis of nonalcoholic fatty liver disease: Invasive versus noninvasive. Semin Liver Dis 2008;28(4):386-95.

8. Cai D, Yuan M, Frantz DF, et al. Local and systemic insulin resistance resulting from hepatic activation of IKK-beta and NF-kappaB. Nat Med 2005;11(2):183-90.

9. Ruiz AG, Casafont F, Crespo J, et al. Lipopolysaccharide-binding protein plasma levels and liver TNF-alpha gene expression in obese patients: Evidence for the potential role of endotoxin in the pathogenesis of non-alcoholic steatohepatitis. Obes Surg 2007;17(10):1374-80.
10. Nozaki Y, Saibara T, Nemoto Y, et al. Polymorphisms of interleukin-1 beta and beta 3-adrenergic receptor in japanese patients with nonalcoholic steatohepatitis. Alcohol Clin Exp Res 2004;28(8 Suppl Proceedings):106S-10S.
11. Liang W, Tonini G, Mulder P, et al. Coordinated and interactive expression of genes of lipid metabolism and inflammation in adipose tissue and liver during metabolic overload. PLoS One 2013;8(9):e75290.
12. Kleemann R, Verschuren L, van Erk MJ, et al. Atherosclerosis and liver inflammation induced by increased dietary cholesterol intake: A combined transcriptomics and metabolomics analysis. Genome Biol 2007;8(9):R200.
13. Wielinga PY, Yakala GK, Heeringa P, et al. Beneficial effects of alternate dietary regimen on liver inflammation, atherosclerosis and renal activation. PLoS One 2011;6(3):e18432.
14. Vergnes L, Phan J, Strauss M, et al. Cholesterol and cholate components of an atherogenic diet induce distinct stages of hepatic inflammatory gene expression. J Biol Chem 2003;278(44):42774-84.
15. Neuschwander-Tetri BA. Hepatic lipotoxicity and the pathogenesis of nonalcoholic steatohepatitis: The central role of nontriglyceride fatty acid metabolites. Hepatology 2010;52(2):774-88.
16. Bijland S, van den Berg SA, Voshol PJ, et al. CETP does not affect triglyceride production or clearance in APOE*3-leiden mice. J Lipid Res 2010;51(1):97-102.
17. Westerterp M, van der Hoogt CC, de Haan W, et al. Cholesteryl ester transfer protein decreases high-density lipoprotein and severely aggravates atherosclerosis in APOE*3-leiden mice. Arterioscler Thromb Vasc Biol 2006;26(11):2552-9.
18. Lindeman JH, Abdul-Hussien H, van Bockel JH, et al. Clinical trial of doxycycline for matrix metalloproteinase-9 inhibition in patients with an abdominal aneurysm: Doxycycline selectively depletes aortic wall neutrophils and cytotoxic T cells. Circulation 2009;119(16):2209-16.
19. Kleiner DE, Brunt EM, Van Natta M, et al. Design and validation of a histological scoring system for nonalcoholic fatty liver disease. Hepatology 2005;41(6):1313-21.
20. Kleemann R, van Erk M, Verschuren L, et al. Time-resolved and tissue-specific systems analysis of the pathogenesis of insulin resistance. PLoS One 2010;5(1):e8817.
21. Hubscher SG. Histological assessment of non-alcoholic fatty liver disease. Histopathology 2006;49(5):450-65.
22. Van Rooyen DM, Gan LT, Yeh MM, et al. Pharmacological cholesterol lowering reverses fibrotic NASH in obese, diabetic mice with metabolic syndrome. J Hepatol 2013.
23. Lassenius MI, Pietilainen KH, Kaartinen K, et al. Bacterial endotoxin activity in human serum is associated with dyslipidemia, insulin resistance, obesity, and chronic inflammation. Diabetes Care 2011;34(8):1809-15.
24. Westerterp M, Berbee JF, Pires NM, et al. Apolipoprotein C-I is crucially involved in lipopolysaccharide-induced atherosclerosis development in apolipoprotein E-knockout mice. Circulation 2007;116(19):2173-81.
25. Rensen SS, Slaats Y, Nijhuis J, et al. Increased hepatic myeloperoxidase activity in obese subjects with nonalcoholic steatohepatitis. Am J Pathol 2009;175(4):1473-82.
26. Kubes P, Mehal WZ. Sterile inflammation in the liver. Gastroenterology 2012;143(5):1158-72.
27. Orlichenko LS, Behari J, Yeh TH, et al. Transcriptional regulation of CXC-ELR chemokines KC and MIP-2 in mouse pancreatic acini. Am J Physiol Gastrointest Liver Physiol 2010;299(4):G867-76.
28. Singh R, Wang Y, Xiang Y, et al. Differential effects of JNK1 and JNK2 inhibition on murine

steatohepatitis and insulin resistance. Hepatology 2009;49(1):87-96.
29. Radonjic M, Wielinga PY, Wopereis S, et al. Differential effects of drug interventions and dietary lifestyle in developing type 2 diabetes and complications: A systems biology analysis in LDLr-/- mice. PLoS One 2013;8(2):e56122.
30. Brunt EM. Pathology of nonalcoholic fatty liver disease. Nat Rev Gastroenterol Hepatol 2010;7(4):195-203.
31. Hu FB, Manson JE, Willett WC. Types of dietary fat and risk of coronary heart disease: A critical review. J Am Coll Nutr 2001;20(1):5-19.

SUPPLEMENTARY DATA

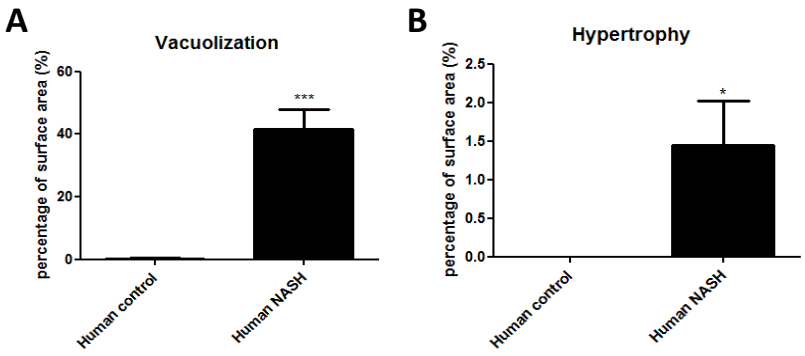

Supplemental Figure A/B: Histological quantification of vacuolization (A) and hepatocellular hypertrophy (B). The percentage of A) vacuolization (micro- and macrovacuolization) and B) hypertrophic cells was analyzed in human liver sections. Hepatocellular hypertrophy is defined as enlargement of hepatocytes (>1.5 normal diameter) and characterized by small lipid droplets in the cytoplasm of the hepatocytes.
Values are means ± SEM. ***P≤0.001 indicates statistical significance between human control livers and NASH livers tested by Mann-Whitney test. *P≤0.05 indicates statistical significance between human control livers and NASH livers tested by Wilcoxon matched-pairs signed rank test. Wilcoxon testing was used because hypertrophy was absent in all control livers.

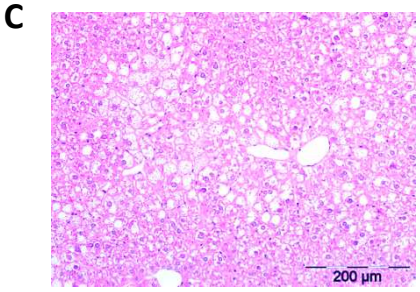

Supplemental Figure C: Histological presentation of steatosis in ApoE*3L.CETP mice after 10 weeks of HFD feeding (end of run-in). Animals developed simple steatosis during the run-in period on HFD. This condition defines the start of the intervention with inflammatory triggers.

D

Supplemental Figure D: Histological analysis of individual mice and their NASH pathology. The first column specifies the experimental groups and rows represent individual mice. Livers (two cross-sections per animal) were analyzed for centrilobular vacuolization (CHV), midzonal vacuolization (MHV), periportal vacuolization (PHV), hepatocellular hypertrophy (HHP) and inflammatory cell clusters (foci). Depending on the type of inflammatory cells in a cluster, a distinction was made between mononuclear inflammatory cell clusters (MNC) and mixed-type (mononuclear and polymorph) nuclear cell clusters (MIC). The color code (from green to red) represents the severity of a parameter as indicated in the columns at the right.

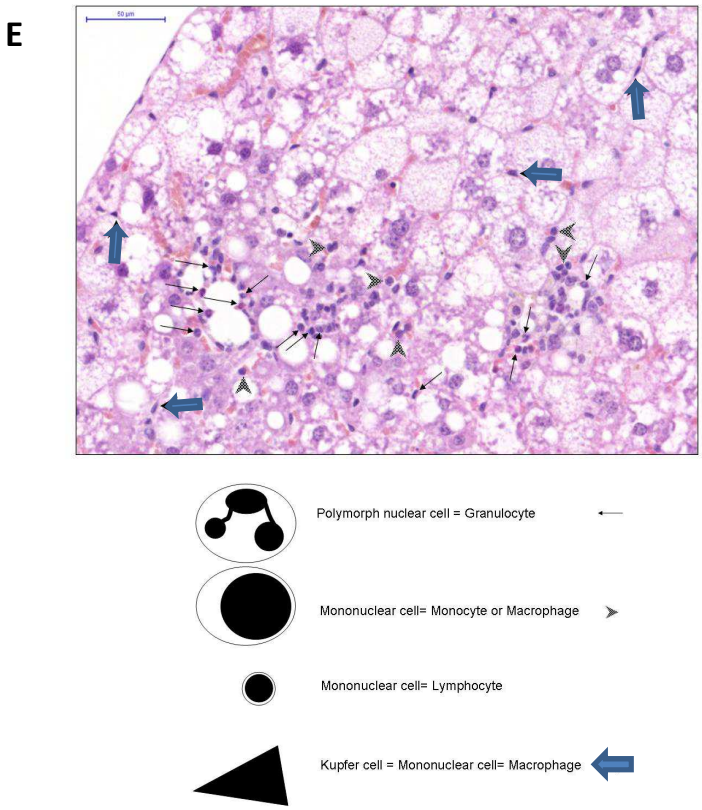

Supplemental Figure E: Histological presentation of a mouse liver with NASH (as a reference). The different inflammatory cells present in NASH (polymorph nuclear cell; monocyte/macrophage; lymphocyte and Kupfer cells) are indicated with arrows as specified above. These hallmarks of inflammation were not found after 10 weeks of HFD feeding in ApoE*3L.CETP mice (end of run-in).

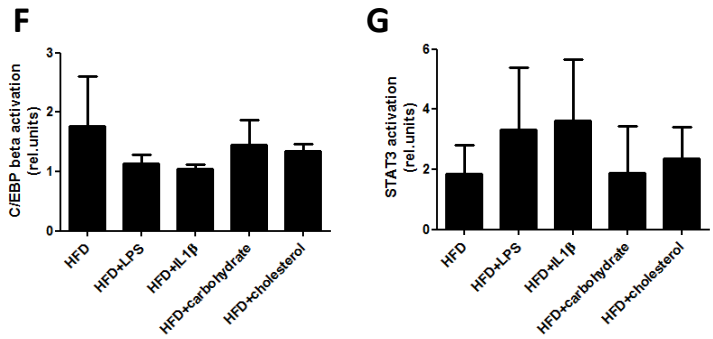

Supplemental Figure F/G: Activity of transcription factors C/EBP-β and STAT3 using TransAM® analysis. There were no significant differences between the experimental groups. Values are means ± SEM.

DEVELOPMENT OF MICROVESICULAR AND MACROVESICULAR STEATOSIS IS ASSOCIATED WITH DISTINCT INFLAMMATORY EVENTS IN LIVERS: A TIME-COURSE STUDY OF CHOLESTEROL-INDUCED NASH

Wen Liang
Lars Verschuren
Karin Toet
Louis M. Havekes
Anita M. van den Hoek
Robert Kleemann

Submitted

ABSTRACT

Background: The pathogenesis of NASH involves a lipid component (steatosis) and an inflammatory component but it is unclear how they are related with each other. The present time-course study aims at defining the time points at which microvesicular and macrovesicular steatosis emerge during NASH development and how these forms of steatosis are linked to critical events of inflammation, that is formation of inflammatory cell aggregates, activation of NFκB and AP-1 pathways, and liver fibrosis.
Method: ApoE3Leiden.CETP transgenic mice were fed a NASH-inducing high-fat diet containing 1% (w/w) cholesterol (HFC) for 12 weeks. Groups of mice were sacrificed in monthly intervals and compared to groups of control mice. The pathogenesis was analyzed by histological and biochemical methods, and microarray pathway analysis.
Results: Steatosis development started in the pericentral zone and microvesicular steatosis preceded macrovesicular steatosis. While microvesicular steatosis reached a plateau after 4 weeks, macrovesicular steatosis intensified gradually and continuously over time. Microvesicular steatosis significantly correlated with activation of NFκB, which represents an early inflammatory event in the pathogenesis, whereas macrovesicular steatosis correlated with the number of lobular inflammatory cell aggregates, which constitutes a late inflammatory event. The pro-inflammatory regulator AP-1 was activated later in time (t=12 weeks) and this activation was accompanied by a strong increase in transaminases (ALT, AST) and onset of liver fibrosis.
Conclusion: Microvesicular steatosis precedes macrovesicular steatosis and is related to NFκB activation. The two forms of steatosis differ in their distinct time pattern and correlates with specific features of inflammation. A link exists between development of macrovesicular steatosis, formation of lobular inflammatory cell aggregates and onset of liver fibrosis.

INTRODUCTION

Nonalcoholic fatty liver disease (NAFLD) is associated with visceral obesity and has become a global pandemic with an estimated prevalence of more than 25% in many countries (1). NAFLD covers a spectrum of liver damage ranging from simple steatosis (NAFL) to nonalcoholic steatohepatitis (NASH) and liver fibrosis (2). The disease frequently coexists with dyslipidemia and insulin resistance but the exact processes underlying the pathogenesis of NAFLD are not well understood.

Typically, patients remain asymptomatic during the early stages of the disease and NAFLD is often diagnosed at a late stage, when the liver is already severely and irreversibly damaged (liver fibrosis, cirrhosis). Hence, little is known about the early, potentially reversible, disease processes and their relationship over time. This study concentrates on the early events of NAFLD development and the processes which have a role in the transition of NAFL to NASH, with particular emphasis on the time sequence of these events over time.

An important early histological hallmark of NAFL is the accumulation of lipids in liver cells, referred to as microvesicular and macrovesicular steatosis. In addition to this lipid component, an inflammatory component is evoked which drives the pathogenesis towards NASH and liver fibrosis (3, 4). A defining characteristic of this inflammatory component in NASH is the formation of immune cell aggregates in liver, i.e. lobular inflammatory clusters composed of neutrophils and macrophages (5), as well as the stimulation of specific inflammatory pathways that result in activation of NFκB and AP-1, two transcriptional master regulators of inflammatory genes contributing to liver fibrosis (6). Based on clinical observations and experimental models in animals, it has long been thought that steatosis precedes inflammation (reviewed in the reference (7)), but it is still unclear how they are linked and whether microvesicular or macrovesicular steatosis (or both) are related to the onset of the inflammatory component of the disease. To explore a putative interrelationship, the present longitudinal study aimed at defining the time points at which microvesicular and macrovesicular steatosis emerge during NAFLD relative to the onset of inflammation. In subsequent biochemical and histological analyses we examined possible correlations between a specific form of steatosis and the specific hallmarks of liver inflammation, i.e. formation of inflammatory cell aggregates, NFκB and AP-1 activation, liver fibrosis.

To study the relationship between steatosis and inflammation, a diet-inducible model of NAFLD was used, ApoE3Leiden.CETP transgenic mice (E3L.CETP) (8). E3L.CETP mice express human transgenes the gene products of which are involved in lipid transport (APOE*3, APOC1, CETP). The model mimics human lipoprotein metabolism and animals develop human-like dyslipidemia when treated with a high fat diet (9). E3L.CETP mice were fed an established NASH-inducing HFD containing 1% cholesterol (HFC) (8) for 12 weeks and compared to littermates fed the same diet without cholesterol (HFD) which merely induces a stage of NAFL in this period. Factors that potentially contribute to the transition from NAFL to NASH can thus be defined by comparing the effects of HFC and HFD. Groups of mice were sacrificed in monthly intervals up to the stage at which NASH and fibrosis had developed in the HFC group. The pathology was scored using an adapted

grading system for human NAFLD (8). Histological analyses and biochemical measurements in conjunction with microarray data of this time course enabled us to demonstrate that specific links exist between microvesicular and macrovesicular steatosis and liver inflammation.

MATERIALS AND METHODS

Animals and diets

Experiments were approved by an independent Animal Care and Use Committee and were in compliance with European Community specifications regarding the use of laboratory animals. Human CETP transgenic mice that express cholesteryl ester transfer protein (CETP) under control of its natural flanking regions (strain 5203) (10) were obtained from Jackson Laboratories (Bar Harbor, MC) and cross-bred with APOE*3Leiden mice to obtain heterozygous E3L.CETP mice (9, 11). All animals were housed in a temperature-controlled room on a 12 hour light-dark cycle and had free access to food and water. Male E3L.CETP mice (16-19 weeks of age) received a low fat diet (LFD; 10 kcal% lard, Research Diets, New Brunswick, NJ, USA) for a 4-week run-in period, after which they were matched for body weight, plasma cholesterol and triglycerides into two experimental groups and dietary treated for 12 weeks. Control animals (HFD, n=40) received a high fat diet (HFD; 45 kcal % lard, Research Diets, New Brunswick, NJ, USA) for 12 weeks. To induce NASH, another group of mice (HFC, n=30) were fed a HFD supplemented with 1% (w/w) cholesterol (Research Diets, USA) for 12 weeks. In addition, a reference group (REF, n=5) remained on LFD until the end of the study and served as aging control group. Food intake and body weight were monitored throughout the study. Every 4 weeks, EDTA plasma samples were collected from the tail vein after 5h of fasting. At the time points t=0, 4, 8 and 12 weeks n=10 HFD mice and n=10 HFC mice were sacrificed by CO_2 asphyxiation. The medial liver lobe was fixed in formalin and embedded in paraffin for histological analysis of NASH and the left lobe was snap frozen in liquid nitrogen and stored at -80°C for liver lipid and biochemical analyses. The adipose tissue was collected, weighed and also stored at -80°C.

Histological assessment of NASH

NASH development was assessed in haematoxylin and eosin-stained (Sigma-Aldrich) liver sections (3 μM) by analysis of steatosis, inflammation and fibrosis, the key features of NASH. Steatosis was determined at a 40 × magnification by analysis of macrovesicular and microvesicular steatosis (8), expressed as the percentage of the total liver slice area affected. Hepatic inflammation was analyzed by counting the number of inflammatory foci per field at a 100 × magnification (view size 3.1 mm^2) in five different fields per specimen in a random way, and was expressed as the average number of foci per field. Hepatic collagen content was stained histochemically using Picro-Sirius Red staining (Chroma, WALDECK-Gmbh, Münster, Germany). Hepatic fibrosis was identified at 40 x magnification and analyzed by scoring whether pathologic collagen staining was absent (grade 0; only in vessels) or collagen staining observed within perisinusoidal or periportal area (grade 1), within perisinusoidal and periportal area (grade 2) or bridging fibrosis (grade 3).

Liver lipid analysis

The intrahepatic concentration of free cholesterol, triglycerides, and cholesteryl esters was analysed as described (8). Briefly, lipids were extracted from liver homogenates using the Bligh and Dyer method and separated by high performance thin layer chromatography (HPTLC) on silica gel plates. Lipid spots were stained with colour reagent (5 g of $MnCl_{24}H_2O$, 32 ml of 95–97% H_2SO_4 added to 960 ml of CH_3OH:H2O 1:1 v/v) and triglycerides, cholesteryl esters and free cholesterol were quantified using TINA version 2.09 software (Raytest, Straubenhardt, Germany).

Analysis of transcription factor activity in liver homogenates

To determine the amount of activated p65-NFκB and AP-1 in livers, protein extracts were prepared using a Nuclear Extract Kit (cat. no. 40010; ActiveMotif, Rixensart, Belgium) as reported (12). The protein content of the extracts was determined with Bio-Rad dye reagent (cat. no. 500-0006; Bio-Rad Laboratories GmbH, Munich, Germany). Six micrograms of protein was used for transcription factor activity analysis using TransAM® kits for NFκB-p65 Chemi, c-Jun (AP-1) kits (cat. no. 40097 and 46096; ActiveMotif) as reported (13). Briefly, the amount of active transcription factor was determined by measuring its binding capacity to a consensus binding sequence in the presence of a competitor oligonucleotide or a mutant (non-competitor) oligonucleotide to control for the specificity of DNA binding.

Analysis of plasma parameters

EDTA (Sarstedt, Numbrecht, Germany) plasma was collected after a 5h fast (0800–1300 hours). Plasma levels of total cholesterol, triglycerides (Roche Diagnostics, Almere, The Netherlands), and insulin (Mercodia, Uppsala, Sweden) were measured with commercial kits. Plasma glucose was determined using the 'Freestyle glucose measurement system' from Abbott (Heerlen, The Netherlands). Homeostasis model assessment (HOMA) index was calculated according to the formula: HOMA=fasting plasma glucose (mM) × fasting plasma insulin (ng/ml)/22.5. Plasma alanine transaminase (ALT) (GPT, cat. no. 10745138) and aspartate aminotransferase (AST) (GOT, cat. no. 10745120) activities were measured using Reflotron® kits (Roche Diagnostics).

Microarray hybridisation and data analysis

Microarray gene expression analysis was performed essentially as reported in (14, 15). Briefly, total RNA was extracted from individual livers using glass beads and RNAzol (Campro Scientific, Veenendaal, The Netherlands). After quality control of RNA integrity using RNA 6000 Nano Lab-on-a-Chip kit and a bioanalyzer 2100 (Agilent Technologies), biotinylated cRNA was prepared with an Illumina® TotalPrep™ RNA Amplification Kit (Ambion, art. no. AM-IL1791. Biotinylated cRNA was hybridized onto the MouseRef-8 Expression BeadChip (Illumina) by a service provider (Service XS, Leiden, the Netherlands). Genomestudio v1.1.1 software (Illumina) was used for subsequent gene expression analysis as described (15). Differentially expressed probes were identified using the limma package of R/Bioconductor. Differentially expressed probes were selected based on the cut-off value False discovery rate (FDR) <0.05. Selected differentially expressed probes were used as an input for pathway analysis using Ingenuity Pathway Analysis suite

(http://www.ingenuity.com). Upstream regulator analysis was performed as reported (12, 15) to determine the activation state of transcription factors based on the observed differential gene expression. A positive (negative) activation Z-score indicates activation (inhibition) of a particular transcription factor. An activation Z-score <-2 or >2 indicates significant activation or inhibition of a pathway or process.

Statistics Analysis

Statistical analyses were performed with Graphpad Prism software (version 5.03, Graphpad Software Inc., La Jolla, USA). Changes over time (versus baseline t=0) or different between groups of HFD versus HFC at each time point) were statistically analysed using Mann-Whitney non-parametric test. Association between two parameters were analysed by Spearman's rank correlation coefficient. A P-value <0.05 was considered statistically significant. All data are presented as mean ± SEM.

RESULTS

HFC induces adiposity and circulating risk factors of NAFLD

Table 1 shows the development of body weight and visceral fat over time in groups of mice treated with HFD and HFD supplemented with cholesterol (HFC). Body weight increased strongly during HFD from 29.8 g at the start to 46.5 g in week 12 and this increase was comparable for HFC (47.6 g at end of study). Body weight gain was paralleled by a marked increase in ectopic visceral fat: compared with t=0, the mass of the major visceral fat depots (i.e. epididymal and mesenteric fat together) increased more than 3-fold, from 0.27 g to 1.02 g in the HFD group, and the HFC group showed a comparable increase.

Plasma cholesterol levels were 5.5 mM at t=0 and remained stable during HFD feeding (5.9 mM at endpoint), but HFC feeding strongly increased plasma cholesterol reaching a level of 25.9 mM in week 12 (**Table 1**). Plasma triglycerides were 3.3 mM at t=0 and decreased during HFD feeding to 2.1 mM (in week 12) while HFC-treated animals exhibited pronounced hypertriglyceridemia of 6.7 mM at the end of the study.

Fasting plasma glucose and fasting plasma insulin increased comparably in HFD and HFC treated groups: fasting glucose was 10.7 mM at t=0 and reached 17.0 mM in HFD and 16.0 mM in HFC after 12 weeks of diet feeding. Fasting insulin increased from 0.7 mM to 5.8 mM in HFD and to 4.4 mM in HFC. The HOMA increased in HFD and HFC treated groups significantly, indicating that both diets induced insulin resistance.

Subsequent analysis of liver enzymes showed a significant decrease in AST and ALT during HFD treatment, while HFC had an opposite effect and increased AST significantly, particularly between week 8 and 12 (**Table 1**). Also, ALT significantly increased by HFC in week 12, which indicated that long-term HFC diet feeding causes liver damage.

Collectively, these data demonstrated that the HFC diet induced experimental hypercholesterolemia and hypertriglyceridemia in the context of obesity and insulin resistance within 12 weeks.

Table 1: Body weight, plasma and liver lipids and liver injury marker over time. Parameters shown were determined in fasting plasma over time. Intrahepatic lipids were determined in freshly prepared tissue homogenates. Values are means±SEM. Significance is indicated *P<0.05, versus t=0 control, #P<0.05 versus HFD control in the same time point. (Mann-Whitney test).

	t=0	t=4		t=8		t=12	
		HFD	HFC	HFD	HFC	HFD	HFC
Body weight [g]	29.8 ± 0.6	38.5 ± 1.1*	37.2 ± 0.7*	43.8 ± 1.4*	43.3 ± 1.1*	46.5 ± 1.7*	47.6 ± 2.0*
Liver [g]	1.76 ± 0.10	1.51 ± 0.08	1.83 ± 0.09#	1.87 ± 0.23	2.41 ± 0.20*#	2.06 ± 0.16	3.12 ± 0.20*#
Visceral fat [g]	0.27 ± 0.02	0.51 ± 0.06*	0.50 ± 0.08*	0.85 ± 0.11*	0.79 ± 0.11*	1.02 ± 0.12*	0.82 ± 0.11*
Cholesterol [mM]	5.52 ± 0.30	4.95 ± 0.18	13.09 ± 0.88*#	5.69 ± 0.33	17.88 ± 1.98*#	5.86 ± 0.32	25.91 ± 2.03*#
Triglycerides [mM]	3.28 ± 0.20	1.76 ± 0.10	2.89 ± 0.24#	1.61 ± 0.16	2.77 ± 0.42	2.11 ± 0.26	6.65 ± 1.09*
Fasting glucose [mM]	10.74 ± 0.41	13.76 ± 0.53*	13.62 ± 0.48*	14.74 ± 0.53*	15.17 ± 0.51*	16.99 ± 0.50*	15.99 ± 0.71*
Insulin [ng/mL]	0.72 ± 0.11	2.84 ± 0.39*	1.98 ± 0.30*	4.62 ± 0.66*	2.25 ± 0.42*#	5.83 ± 0.75*	4.37 ± 0.75*
HOMA	0.4 ± 0.1	3.1 ± 0.2*	1.3 ± 0.2*#	2.9 ± 0.5*	1.9 ± 0.3*	4.5 ± 0.6*	3.2 ± 0.6*
ALT [U/L]	122 ± 10	96 ± 8	151 ± 40	94 ± 23	101 ± 22	86 ± 11*	305 ± 54*#
AST [U/L]	270 ± 21	199 ± 28*	341 ± 112	184 ± 34*	172 ± 21*	141 ± 9*	520 ± 81*#

Time course analysis of microvesicular and macrovesicular steatosis

HE-stained liver cross-sections were used for histological evaluation and quantification of microvesicular and macrovesicular steatosis over time. HFD treatment merely resulted in bland steatosis (mild NAFL) while HFC induced pronounced steatosis. Independent of the type of diet, steatosis started in the pericentral area, and the diets generally induced more microvesicular steatosis than macrovesicular steatosis. Steatosis development was accompanied with formation of inflammatory cell aggregates (from 8 weeks onwards) in the HFC group specifically (**Figure 1 A**), which is a defining characteristic of NASH in humans. HFC but not HFD induced onset of fibrosis at week 12 as shown by the development of perihepatocellular patches of collagen (Sirius Red staining; **Figure 1B**).

Refined and quantitative analysis of steatosis development over time revealed that microvesicular and macrovesicular steatosis developed simultaneously in control mice on HFD: both forms of steatosis were induced by HFD at week 8 and remained at a stably elevated until week 12 (microvesicular steatosis: 21% of the surface area; and macrovesicular steatosis: 10%,) (**Figure 2A/B**). By contrast, HFC rapidly induced microvesicular steatosis (already after 4 weeks) which covered about 51% of the surface area, i.e. about twice as much than observed with HFD. Notably, HFC-induced microvesicular steatosis did not further progress after week 8, while HFC-induced macrovesicular steatosis showed a continuous increase until the end of the study. For instance, between week 8 and 12, HFC-induced macrovesicular steatosis almost doubled (from 14% to 24% of the surface area), while it remained unchanged in the same period with HFD treatment (**Figure 2B**).

Collectively, the comparative analysis of steatosis development by HFD and HFC revealed two differences which characterize the NASH-inducing diet HFC: 1) Microvesicular steatosis developed more rapidly (week 4) and stabilized at a higher (2-fold) absolute level. 2) Macrovesicular steatosis increased gradually throughout study. The

time course also showed that HFC-induced microvesicular steatosis (week 4) preceded the development of macrovesicular steatosis (week 8).

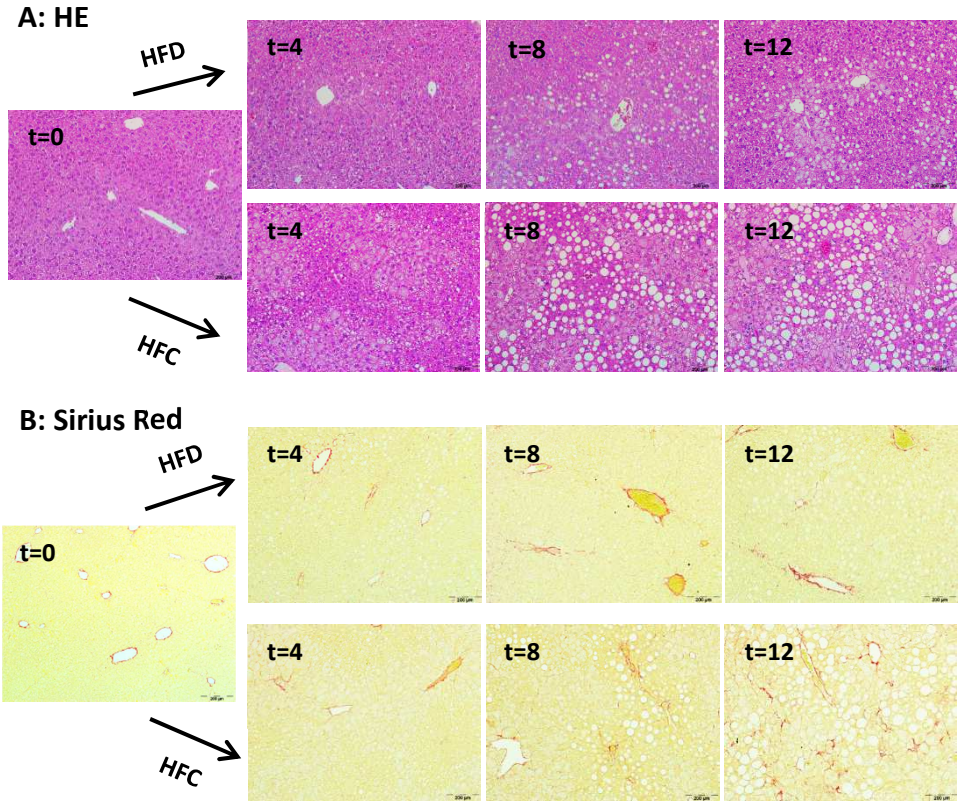

Figure 1: Histological analysis of liver cross-sections over time. Paraffin-embedded livers from the HFC group (upper rows) and the HFD group (lower rows) were stained with HE (A) for general histological analysis or with Sirius Red (B) for analysis of collagen. For each diet and time point n=10 livers were analyzed. The figure shows representative photomicrographs for each time point (t=0, 4 weeks, 8 weeks, 12 weeks). LFD=low fat control diet; HFD=high fat diet; HFC=high fat diet containing 1% cholesterol.

Time course analysis of intrahepatic liver lipids

Changes in major liver lipids (triglycerides, TG; cholesterol esters, CE; free cholesterol, FC) were analyzed next. TG were the most abundant form of liver lipids with baseline levels of 83 µg/mg protein, followed by CE (18 µg/mg protein) and FC (17 µg/mg protein). HFD feeding resulted in slight increase of liver TG (not significant effect) at week 8 and 12. HFD did not affect the concentrations of CE and FC, indicating that the steatosis in HFD group is mainly attributable to an accumulation of TG (**Figure 2C**).

By contrast, HFC strongly induced TG, CE and FC with significant effects already after 4 weeks (for TG and CE) indicating that steatosis induced by HFC is more complex than with HFD because it also involves accumulation of CE and FC. The increase in liver CE in particular paralleled the time profile of microvesicular steatosis (**Figure 2D**). FC were stable levels until week 4 followed by a marked increase between week 8 and 12 (**Figure 2E**).

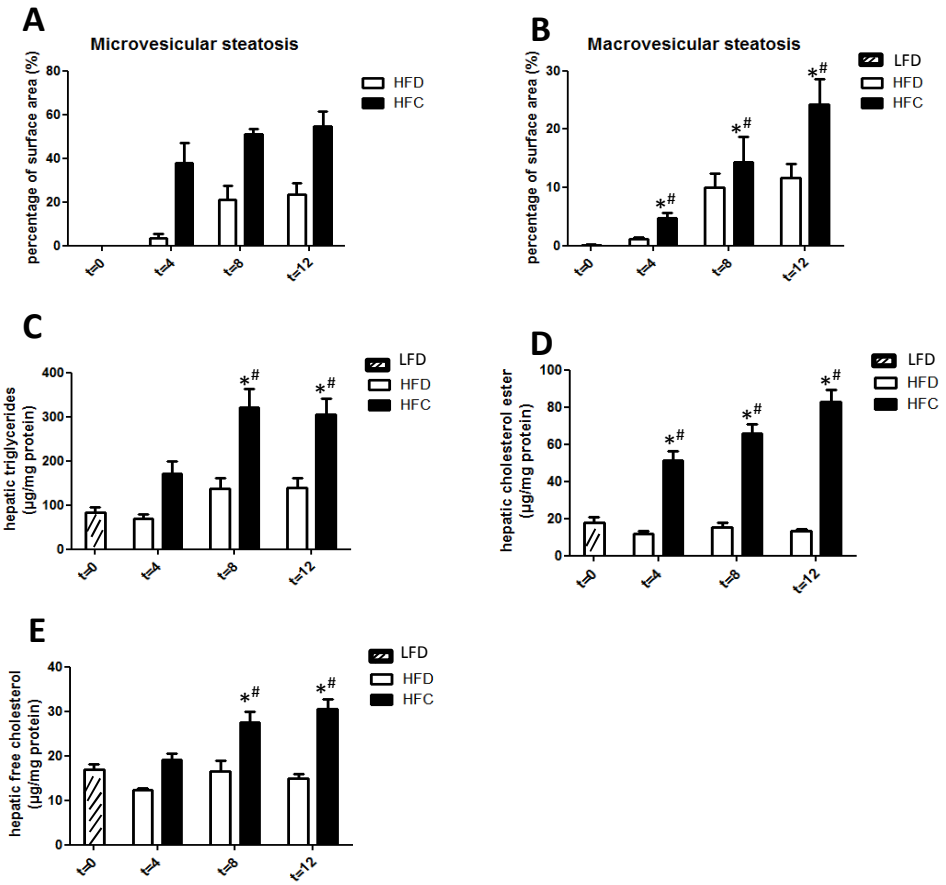

Figure 2: Quantitative histological analysis of steatosis and liver lipids. HE-stained liver cross-sections of the time course were analyzed histologically to determine the level of microvesicular steatosis (A), macrovesicular steatosis (B) during HFC and HFD diet feeding at the time points indicated. Liver lipids were analyzed biochemically in homogenates prepared from frozen livers. The concentration of triglycerides (C), cholesterylesters (D) and free cholesterol (E) were determined during the time course. LFD=low fat control diet; HFD=high fat diet; HFC=high fat diet containing 1% cholesterol. Data represent means ± SEM; *P<0.05 HFC compared to t=0; #P<0.05 between HFC and HFD at a particular time point.

Time course analysis of cellular and molecular inflammation in relation to steatosis

As specifically the HFC diet caused inflammation and NASH, we next evaluated the development of cellular and molecular inflammation in the HFC group in order to define a possible relationship with specific forms of steatosis.

Quantification of inflammatory cell aggregates in liver cross-sections demonstrated that HFD treated mice hardly developed lobular cellular inflammatory aggregates throughout the study while HFC strongly induced lobular inflammation already after 4 weeks, showing a marked further increase between 8 and 12 weeks (**Figure 3A**). To analyze whether an association exists between the level of micro-/macrovesicular steatosis and the hepatic content of inflammatory cells, the individual steatosis data were correlated to the corresponding inflammatory cell counts. This analysis revealed a significant positive correlation between inflammatory cell aggregates induced by HFC and macrovesciular steatosis (r=0.4489; p=0.0128) (**Figure 3B**). The association between steatosis and inflammatory cell aggregates was specific for macrovesicular steatosis because there was no correlation with microvesicular steatosis (not shown).

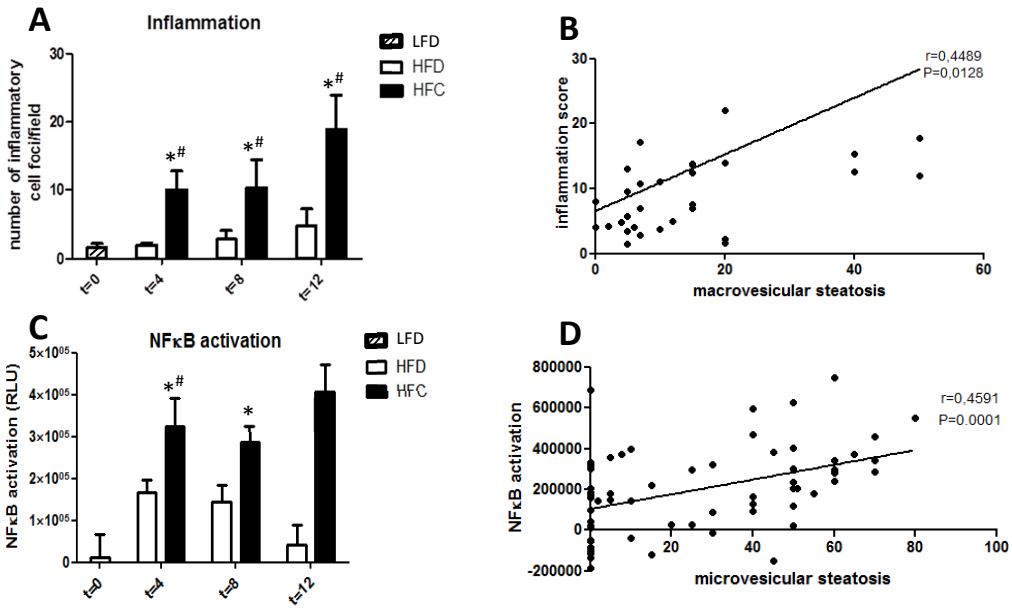

Figure 3: Quantitative histological analysis of steatosis and liver lipids. Inflammatory cell aggregates (A) were counted in HE-stained liver cross-sections. (B) Spearman's rank correlation analysis of macrovesicular steatosis and inflammatory cell aggregates (data from HFC treated animals). (C) Transcriptional activity of p65-NFκB determined by TransAM® assay in freshly prepared liver homogenates. (D) Spearman's rank correlation analysis of microvesicular steatosis and p65-NFκB activity (data from all HFD and HFC animals). Data represent means ± SEM; *P<0.05 HFC compared to t=0; #P<0.05 between HFC and HFD at a particular time point.

To analyze molecular inflammation, the transcriptional activity of NFκB and AP-1, two important regulators of inflammatory gene expression, was quantified in freshly prepared liver homogenates using TransAM® assay. HFD activated NFκB transiently (only in week 4) whereas HFC-stimulated NFκB activation was much stronger and persisted until the end of the study (**Figure 3C**). The time pattern of HFC-induced NFκB activation resembled those of microvesicular hepatocellular steatosis suggesting a relationship between microvesicular steatosis and NFκB activation. Indeed, the individual microvesicular steatosis scores were positively correlated with NFκB activity data of corresponding mice (**Figure 3D**). This correlation was highly significant (P=0.0001) and specific for microvesicular steatosis (no correlation existed between macrovesicular steatosis and NFκB activity).

Subsequent analysis of the transcriptional activity of AP-1 in HFD and HFC treated livers showed that AP-1 activity was below the detection limit of the assay until week 8. Thereafter, a modest AP-1 activation was observed in some animals of the HFC group at week 12 (not shown). Altogether, these data demonstrate that macrovesicular steatosis is positively correlated to cellular inflammation in developing NAFLD and that microvesicular steatosis has a positive correlation with NFκB activity.

HFC feeding results in AP-1 activation and fibrosis at the end of the study

For a more refined analysis of liver inflammation microarray gene expression analysis was performed in corresponding livers of the time course. Gene enrichment analysis confirmed a marked increase in inflammatory processes between week 8 and 12 and the number of differentially expressed genes associated to the 'inflammatory response pathway' increased strongly over time (i.e. 74 genes at t=4 weeks, 160 genes at t=8 weeks and 546 at t=12 weeks) (not shown). Consistent with this, AP-1 was significantly activated at the last time point (t=12 weeks; Z=3.499; P-value=1.40E-08) (**Table 2**) and transcriptionally active based on the expression changes of 87 target genes (**Figure 4A**). Also between t=8 weeks and t=12 weeks, the process of hepatic fibrosis was significantly activated including 'hepatic stellate cell activation' and 'myofibroblast activation' shown in **Figure 4B**. Among the genes upregulated in these pathways were 16 pro-fibrotic genes controlled by AP-1. The gene expression changes were confirmed histologically by grading of collagen deposition upon Sirius Red staining) (**Figure 1B**). There was no difference between HFD and HFC until week 8, but at the end of the study, in week 12, HFC significantly induced fibrosis (**Figure 4C**). This induction paralleled the observed marked increase in macrovesicular steatosis and the elevation of ALT and AST in the circulation at this time point. The two liver damage markers correlated significantly with the individual fibrosis scores, i.e. ALT (r=0.6991; P<0.001) and AST (r=0.6921; P<0.001) further supporting the association between liver damage and collagen deposition.

Table 2: Transcription factor activation analysis. Analysis of the activity of upstream regulators based on expression of their target genes using microarray gene expression data. A positive Z-score indicates activation of a transcription factor by HFC relative to HFD. A Z-score ≥2 indicates significant activation. The gene expression levels of some of these transcription factors (Nfκb1, Rel A, c-jun,) was significantly upregulated (FDR<0.05).

Upstream regulator	Predicted state	Activation Z-score	P-value of overlap
NFκB (complex)	activated	5.833	5.49E-12
NFκB1	activated	3.077	6.50E-05
RelA	activated	3.921	6.97E-04
AP-1 (complex)	activated	3.910	2.36E-04
c-Jun	activated	3.499	1.48E-10
JunB	activated	1.883	4.54E-06
c-Fos	activated	1.747	3.77E-11
FosB	activated	1.387	2.00E-02

A

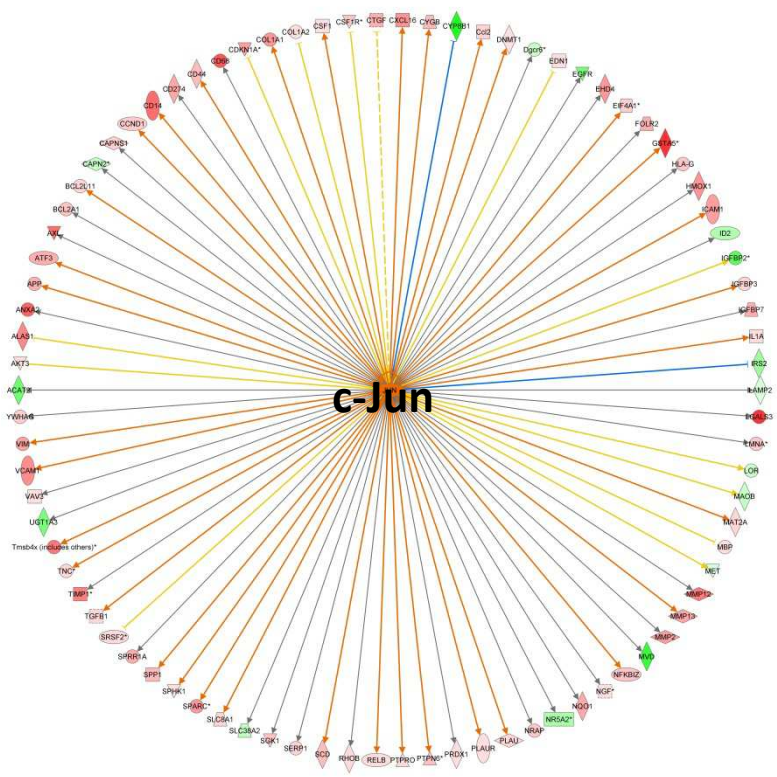

B

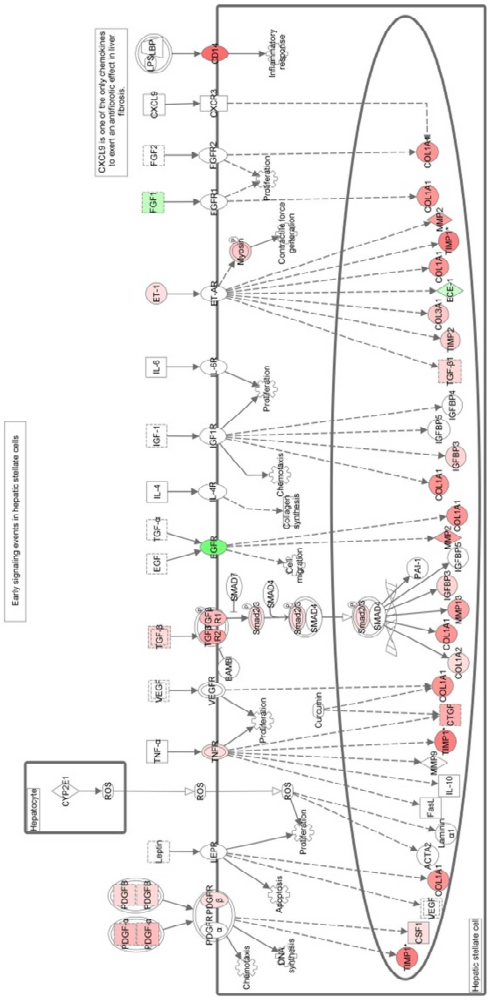

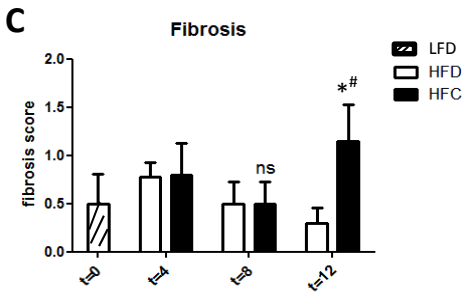

Figure 4: Onset of fibrotic gene expression and liver fibrosis after 12 weeks of HFC feeding. (A) Gene set enrichment analysis of microarray data showing 87 significantly differentially expressed target genes of c-jun at t=12 weeks. Upregulation is indicated in red and downregulation in green. (B) Activation of the process 'Early signaling events in hepatic stellate cells' showing upregulation of many profibrotic genes (in red). These induction was observed at t=12 weeks but not earlier time points. Other profibrotic processes were also activated (see supplementary information). (C) Histological grading of liver fibrosis based on Sirius Red-stained liver cross-sections over time.

DISCUSSION

This longitudinal study analyzed the relationship between development of micro- and marcovesicular steatosis and inflammation in the pathogenesis of NAFLD using a diet-inducible model of disease. We observed that steatosis started in the pericentral zone and that microvesicular steatosis and macrovesicular steatosis developed in a different way over time: Microvesicular steatosis was induced rapidly (already after 4 weeks) and preceded macrovesicular steatosis which developed more slowly. While microvesicular steatosis remained at a high elevated level throughout the study, macrovesicular steatosis developed gradually and continuously over time. The amount of microvesicular steatosis correlated with activation of NFκB, which represents an early inflammatory event in liver tissue, whereas macrovesicular steatosis correlated with the number of inflammatory cell aggregates in the liver, which constitutes a late inflammatory event of lobular inflammation. The activation of the pro-inflammatory regulator AP-1 also occurred at a late time point (t=12 weeks) and was accompanied by a marked increase in transaminases (ALT, AST) as well as an onset of liver fibrosis.

The development of liver steatosis (NAFL) in the control group was comparable to other studies in which mice were treated with high fat diets for 12 weeks (12, 16). Supplementation of 1% cholesterol to this diet (HFC) resulted in disease progression towards a fatty inflamed liver (NASH) with early fibrosis. This was achieved in the presence of combined obesity, insulin resistance and dyslipidemia (mainly (VLDL and LDL) which are documented risk factors of NASH in humans (1, 17). While obesity and insulin resistance were comparable in HFD and HFC groups, total plasma cholesterol was significantly higher (> 4-fold) in HFC which provides an indication that this risk factor may have contributed predominantly to disease progression towards NASH under the conditions employed. Consistent with this, Wouters and coworkers have shown that dietary cholesterol can be an important risk factor for the progression to hepatic inflammation, possibly in the form of modified plasma lipoproteins (18). It is also possible that dietary cholesterol exerts a direct effect on hepatic lipid and cholesterol metabolism thereby promoting lipid accumulation, lipotoxicity and local hepatic inflammation (19-21).

A systematic time-resolved analysis of the development of distinct forms of steatosis (microvesicular and macrovesicular steatosis) in relation to inflammation has not been documented so far. It has long been thought that liver steatosis and inflammation develop sequentially (e.g. ‘two hit’ hypothesis), but more recently a simultaneous development of steatosis and inflammation is also proposed (3, 17, 22). The present study shows that a more refined description of steatosis and inflammation is more accurate, because microvesicular steatosis and macrovesicular steatosis develop sequentially. In the case of inflammation, the early event of NFκB activation clearly precedes the formation of inflammatory cell aggregates and activation of AP-1. Notably, the level of microvesicular and macrovesicular steatosis correlates with NFκB activation and cellular inflammation, respectively, which supports the view that specific forms of steatosis are paralleled by specific inflammatory events.

We observed that microvesicular steatosis precedes macrovesicular steatosis, the latter of which is a hallmark of NASH pathology in humans (1). The exact role of microvesicular steatosis in NAFLD however is uncertain. It is assumed that microvesicular steatosis is

associated with mitochondrial stress, dysfunction or injury and this form of steatosis is observed in pediatric Reye syndrome and genetic diseases such as carnitine deficiency (23). It is possible that this mitochondrial impairment represents an early event of metabolic incompetence of the liver and mitochondrial dysfunction is associated with a pro-oxidative and pro-inflammatory state of organs and activation of NFκB (19, 24) which is consistent with our observations. The exact processes underlying the activation of inflammatory cascades under this condition and the molecules which operate at the interface between metabolism and inflammation are unknown. One of the possible mediators is the inflammasome which can sense specific lipids that accumulate in steatotic livers (e.g. palmitic acid as well as small cholesterol crystals) (21, 25) and which evokes local tissue inflammation through the production of IL-1β and IL-18 via a caspase-1-dependent enzymatic process.

The animal model used herein, E3L.CETP mice, develops about two times more microvesicular steatosis than macrovesicular steatosis when fed the HFC diet. Microvesicular steatosis already developed with HFD under conditions of NAFL, and macrovesciular steatosis developed only when cholesterol was supplemented to the diet to induce progression of the pathogenesis towards NASH. Other diet-inducible transgenic models of NAFLD such as $LDLR^{-/-}$ mice develop more macrovesicular steatosis, resembling the pathology of human NASH (26, 27). Since all these models share the same C57BL.6 background, it is amenable that the transgenes present in E3L.CETP mice are responsible for extensive development of microvesicular steatosis. Because E3L mice which lack CETP do also predominantly develop microvesicular steatosis (12), it is likely that other human transgenes, i.e. APOE3 and human APOC1 which are expressed by E3L and E3L.CETP mice, are responsible for the susceptibility to develop microvesicular steatosis. It is unclear whether small lipid droplets that characterize microvesicular steatosis can fuse to form larger lipid droplets as seen in livers with macrovesicular steatosis, or whether macrovesicular and microvesicular steatosis develop independently from each other (4). Little is known about the pathological implications of microvesicular and macrovesicular steatosis, and a more recent experimental evidence provides an indication for a tight relationship between macrovesicular steatosis and fibrosis: A comparison of different strains of rats with either solely microvesicular steatosis (Lewis rats), pure macrovesicular steatosis (Sprague Dawley rats) and mixed-type steatosis (Wistar rats) showed that Sprague Dawley rats had the highest degree of hepatocyte damage and fibrosis (28). This is consistent with our observation that HFC induced macrovesicular steatosis between 8 and 12 weeks which is accompanied by a marked increase of the injury markers ALT and AST, activation of AP-1 and formation of liver fibrosis in this period.

In all, the dietary conditions employed herein allowed a time-resolved study of NAFLD in the context of combined visceral obesity, insulin resistance and dyslipidemia i.e. hallmarks of the disease in humans that are not or only inadequately mimicked in models using diets deficient in methionine and choline or in chemically-induced fibrosis models (e.g. CCL4 model). The study demonstrates that steatosis itself develops sequentially (first microvesicular, then macrovesicular) and so does inflammation (first NFκB, then inflammatory aggregates, then AP-1 and fibrosis). Better insight into the sequence of these events is important for our understanding of the associations between lipid

accumulation and hepatic inflammation, as well as for the development of (drug) interventions.

ACKNOWLEDGEMENTS

The authors gratefully acknowledge Erik Offerman and Wim van Duyvenvoorde for their help and technical assistance. This research was performed within the framework of CTMM, the Center for Translational Molecular Medicine (www.ctmm.nl), project PREDICCT. The authors thank the TNO research programs 'Personalized Prevention and Therapy - Op Maat' and 'Enabling Technology Systems Biology' for supporting this study.

REFERENCES

1. Loomba R, Sanyal AJ. The global NAFLD epidemic. Nat Rev Gastroenterol Hepatol 2013;10(11):686-90.
2. Bellentani S, Marino M. Epidemiology and natural history of non-alcoholic fatty liver disease (NAFLD). Ann Hepatol 2009;8 Suppl 1:S4-8.
3. Tiniakos DG, Vos MB, Brunt EM. Nonalcoholic fatty liver disease: Pathology and pathogenesis. Annu Rev Pathol 2010;5:145-71.
4. Sahini N, Borlak J. Recent insights into the molecular pathophysiology of lipid droplet formation in hepatocytes. Prog Lipid Res 2014;54:86-112.
5. Hubscher SG. Histological assessment of non-alcoholic fatty liver disease. Histopathology 2006;49(5):450-65.
6. Harmon RC, Tiniakos DG, Argo CK. Inflammation in nonalcoholic steatohepatitis. Expert Rev Gastroenterol Hepatol 2011;5(2):189-200.
7. Jou J, Choi SS, Diehl AM. Mechanisms of disease progression in nonalcoholic fatty liver disease. Semin Liver Dis 2008;28(4):370-9.
8. Liang W, Lindeman JH, Menke AL, et al. Metabolically induced liver inflammation leads to NASH and differs from LPS- or IL-1beta-induced chronic inflammation. Lab Invest 2014;94(5):491-502.
9. van den Hoek AM, van der Hoorn JW, Maas AC, et al. APOE*3Leiden.CETP transgenic mice as model for pharmaceutical treatment of the metabolic syndrome. Diabetes Obes Metab 2014;16(6):537-44.
10. Jiang XC, Agellon LB, Walsh A, et al. Dietary cholesterol increases transcription of the human cholesteryl ester transfer protein gene in transgenic mice. dependence on natural flanking sequences. J Clin Invest 1992;90(4):1290-5.
11. Westerterp M, van der Hoogt CC, de Haan W, et al. Cholesteryl ester transfer protein decreases high-density lipoprotein and severely aggravates atherosclerosis in APOE*3-leiden mice. Arterioscler Thromb Vasc Biol 2006;26(11):2552-9.
12. Liang W, Tonini G, Mulder P, et al. Coordinated and interactive expression of genes of lipid metabolism and inflammation in adipose tissue and liver during metabolic overload. PLoS One 2013;8(9):e75290.
13. Kleemann R, Bureeva S, Perlina A, et al. A systems biology strategy for predicting similarities and differences of drug effects: Evidence for drug-specific modulation of inflammation in atherosclerosis. BMC Syst Biol 2011;5:125,0509-5-125.
14. Radonjic M, Wielinga PY, Wopereis S, et al. Differential effects of drug interventions and dietary lifestyle in developing type 2 diabetes and complications: A systems biology analysis in LDLr-/- mice. PLoS One 2013;8(2):e56122.
15. Verschuren L, Wielinga PY, Kelder T, et al. A systems biology approach to understand the

pathophysiological mechanisms of cardiac pathological hypertrophy associated with rosiglitazone. BMC Med Genomics 2014;7:35,8794-7-35.
16. Gaemers IC, Stallen JM, Kunne C, et al. Lipotoxicity and steatohepatitis in an overfed mouse model for non-alcoholic fatty liver disease. Biochim Biophys Acta 2011;1812(4):447-58.
17. Trauner M, Arrese M, Wagner M. Fatty liver and lipotoxicity. Biochim Biophys Acta 2010;1801(3):299-310.
18. Wouters K, van Gorp PJ, Bieghs V, et al. Dietary cholesterol, rather than liver steatosis, leads to hepatic inflammation in hyperlipidemic mouse models of nonalcoholic steatohepatitis. Hepatology 2008;48(2):474-86.
19. Bechmann LP, Hannivoort RA, Gerken G, et al. The interaction of hepatic lipid and glucose metabolism in liver diseases. J Hepatol 2012;56(4):952-64.
20. Malhi H, Gores GJ. Molecular mechanisms of lipotoxicity in nonalcoholic fatty liver disease. Semin Liver Dis 2008;28(4):360-9.
21. Ioannou GN, Haigh WG, Thorning D, et al. Hepatic cholesterol crystals and crown-like structures distinguish NASH from simple steatosis. J Lipid Res 2013;54(5):1326-34.
22. Tessari P, Coracina A, Cosma A, et al. Hepatic lipid metabolism and non-alcoholic fatty liver disease. Nutr Metab Cardiovasc Dis 2009;19(4):291-302.
23. Ramachandran R, Kakar S. Histological patterns in drug-induced liver disease. J Clin Pathol 2009;62(6):481-92.
24. Hotamisligil GS. Inflammation and metabolic disorders. Nature 2006;444(7121):860-7.
25. Wen H, Gris D, Lei Y, et al. Fatty acid-induced NLRP3-ASC inflammasome activation interferes with insulin signaling. Nat Immunol 2011;12(5):408-15.
26. Gupte AA, Liu JZ, Ren Y, et al. Rosiglitazone attenuates age- and diet-associated nonalcoholic steatohepatitis in male low-density lipoprotein receptor knockout mice. Hepatology 2010;52(6):2001-11.
27. Subramanian S, Goodspeed L, Wang S, et al. Dietary cholesterol exacerbates hepatic steatosis and inflammation in obese LDL receptor-deficient mice. J Lipid Res 2011;52(9):1626-35.
28. Rosenstengel S, Stoeppeler S, Bahde R, et al. Type of steatosis influences microcirculation and fibrogenesis in different rat strains. J Invest Surg 2011;24(6):273-82.

MIRTOSELECT, AN ANTHOCYANIN-RICH BILBERRY EXTRACT, ATTENUATES NON-ALCOHOLIC STEATOHEPATITIS AND ASSOCIATED FIBROSIS IN APOE*3LEIDEN MICE

Martine Morrison
Wen Liang
Petra Mulder
Lars Verschuren
Elsbet Pieterman
Karin Toet
Peter Heeringa
Peter Y. Wielinga
Teake Kooistra
Robert Kleemann

J Hepatol. 2014; S0168-8278(14): 00929-5

ABSTRACT

Background & Aims: Anthocyanins may have beneficial effects on lipid metabolism and inflammation and are demonstrated to have hepatoprotective properties in models of restraint-stress- and chemically-induced liver damage. However, their potential to protect against non-alcoholic steatohepatitis (NASH) under conditions relevant for human pathogenesis remains unclear. Therefore, we studied the effects of the standardized anthocyanin-rich extract Mirtoselect on diet-induced NASH in a translational model of disease.

Methods: ApoE*3Leiden mice were fed a Western-type cholesterol-containing diet without (HC) or with 0.1% (w/w) Mirtoselect (HCM) for 20 weeks to study effects on diet-induced NASH.

Results: Mirtoselect attenuated HC-induced hepatic steatosis, as observed by decreased macro- and microvesicular hepatocellular lipid accumulation and reduced hepatic cholesteryl-ester content. This anti-steatotic effect was accompanied by local anti-inflammatory effects in liver, as demonstrated by reduced inflammatory cell clusters and reduced neutrophil infiltration in HCM. On a molecular level, HC-diet significantly induced hepatic expression of pro-inflammatory genes Tnf, Emr1, Ccl2, Mpo, Cxcl1 and Cxcl2 while this induction was less pronounced or significantly decreased in HCM. A similar quenching effect was observed for HC-induced pro-fibrotic genes, Acta2 and Col1a1 and this anti-fibrotic effect of Mirtoselect was confirmed histologically. Many of the pro-inflammatory and pro-fibrotic parameters positively correlated with intrahepatic free cholesterol levels. Mirtoselect significantly reduced accumulation and crystallisation of intrahepatic free cholesterol, providing a possible mechanism for the observed hepatoprotective effects.

Conclusions: Mirtoselect attenuates development of NASH, reducing hepatic lipid accumulation, inflammation and fibrosis, possibly mediated by local anti-inflammatory effects associated with reduced accumulation and crystallisation of intrahepatic free cholesterol.

INTRODUCTION

Non-alcoholic fatty liver disease (NAFLD) is the most common cause of chronic liver disease in Western countries [1, 2]. It constitutes a spectrum of liver injury, ranging from the clinically benign intrahepatic accumulation of lipids (steatosis), to the more progressive non-alcoholic steatohepatitis (NASH). In addition to hepatic lipid accumulation, NASH is characterised by hepatic inflammation, i.e. infiltration of immune cells [3] and can further progress to fibrosis, cirrhosis and hepatocellular carcinoma. Although the mechanisms by which NASH progresses are not completely understood, it is thought that dysregulation of cholesterol homeostasis and subsequent accumulation of free (unesterified) cholesterol are linked to the pathogenesis of NASH in humans (reviewed in reference [4]). In line with this notion, emerging experimental evidence implicates free cholesterol as a potential trigger of inflammation [5] as well as a possible driving factor in the development of fibrosis [6, 7]. A recent study in experimental and human NASH revealed that intrahepatic accumulation of free cholesterol can lead to the formation of cholesterol crystals in hepatocyte lipid droplets, which may form an important trigger for the progression of simple steatosis to NASH [8].

The anthocyanins, a subclass of the polyphenols, comprise a large group of bioactive compounds that are considered to have many health-promoting effects [9], including cholesterol-lowering [10, 11] and anti-inflammatory effects [12] which may mediate potential hepatoprotective properties [13]. Here we studied the effects of the standardised anthocyanin-rich bilberry (*Vaccinium myrtillus L.*) extract Mirtoselect on the development of NASH. This extract has been demonstrated to reduce circulating makers of inflammation in humans [14, 15] and has beneficial effects in restraint-stress- [16, 17] and chemically-induced [18] models of liver damage. However, its hepatoprotective potential in diet-induced metabolic inflammation and liver disease is unclear. Therefore we studied effects of Mirtoselect on NASH in ApoE*3Leiden (E3L) mice, a translational model of disease [19]. These mice develop diet-induced dyslipidaemia and inflammation on a high-fat/high-cholesterol diet [20], and ultimately develop NASH with fibrosis. Earlier studies have shown that E3L mice are sensitive to nutritional [21] and pharmacological [19] interventions, and show human-like responses to hypolipidaemic compounds [19, 22].

Combined histological, biochemical, and gene expression analyses revealed that Mirtoselect reduces development of NASH, attenuating both steatosis and inflammation as well as the development of hepatic fibrosis. These effects were associated with a reduction in hepatic free cholesterol accumulation and cholesterol crystal formation.

MATERIALS AND METHODS

Animal experiments

Experiments were approved by an independent Animal Care and Use Committee and were in compliance with European Community specifications regarding the use of laboratory animals. ApoE*3Leiden mice (E3L) were used because they allow study of diets and nutrients on lipids (including cholesterol) and liver inflammation [19, 23, 24].

Female E3L mice were fed a Western-type diet (15% cocoa butter, 1% corn oil, 40.5% sucrose, 20% acid casein, 10% corn starch and 6.2% cellulose; diet-T; AB-Diets, Woerden, the Netherlands), supplemented with 1% (w/w) cholesterol (Sigma-Aldrich, Zwijndrecht, the Netherlands) for 20 weeks. The study included a 4-week run-in during which all mice received this diet, after which they were matched for plasma cholesterol and triglycerides into 3 experimental groups (n=15/group). Control animals (HC) continued to receive the Western-type diet for the remainder of the study, while Mirtoselect-treated animals (HCM) received the HC diet with addition of 0.1% (w/w) Mirtoselect (Indena S.A.S., Paris, France). This standardised bilberry (*Vaccinium myrtillus* L.) extract contains 36% anthocyanins. An ageing reference group (REF) received the same Western-type diet mentioned above, but without cholesterol supplementation. Food intake and body weight were monitored throughout the study. Every 4 weeks, blood samples were collected via tail vein bleeding after a 4h fast, for isolation of EDTA plasma. Animals were sacrificed by CO_2 asphyxiation after 16 weeks of dietary treatment to collect livers. The medial lobe was fixed in formalin and embedded in paraffin for histological analysis of NASH and the left lobe was snap frozen in liquid nitrogen and stored at -80°C for cryosectioning, liver lipid- and mRNA-expression analyses.

Histological, biochemical and hepatic gene expression analyses

A detailed description of (immuno)histological, biochemical, and gene expression analyses is provided in (supplement 1). Briefly, development of NASH was assessed histologically using an adapted grading method for human NASH [25, 26]. Plasma lipids were determined with commercially available enzymatic assays and liver lipids were analysed by HPTLC, as described previously [27]. Hepatic gene expression analyses were performed by RT-PCR, using TaqMan® Gene Expression Assays (Life Technologies, Bleiswijk, the Netherlands) and changes in gene expression were calculated using the comparative Ct (ΔΔCt) method, expressed as fold-change relative to REF. Illumina microarray analysis of hepatic gene expression was performed following established normalisation and quality control protocols followed by gene enrichment analysis across pathways and biological processes as described [23]. p65-NFκB activity was determined in liver homogenates by DNA-binding ELISA (TransAM® p65-NFκB Chemi Kit, Active Motif, La Hulpe, Belgium) according to manufacturer's instructions and as described [26].

Statistical analyses

All data are presented as mean ± SD. Statistical analyses were performed using SPSS software (version 22, IBM, Armonk, USA). For normally distributed variables, significance of differences between groups was tested by one-way ANOVA, with Dunnett's Multiple Comparison Post-Hoc Test to compare HC vs REF and HC vs HCM. In case of heterogeneity between groups, variables were analysed by ANOVA using Brown-Forsythe for differences between groups with Dunnett's T3 Post-Hoc Test. Non-normally distributed variables were tested by non-parametric Kruskall-Wallis test followed by Mann-Whitney U. A p-value<0.05 was considered statistically significant.

RESULTS

Mirtoselect attenuates hepatic steatosis and hepatocellular damage

Treatments were well tolerated and there was no effect of Mirtoselect on food intake or body weight (supplement 2a-b). HC-feeding induced hepatosteatosis relative to REF, as observed histologically by a non-zonal accumulation of lipid macrovesicles and microvesicles in hepatocytes (**Figure 1a**). Mirtoselect attenuated the development of hepatic steatosis (**Figure 1a**), completely preventing the HC-induced increase in macrovesicular steatosis ($p<0.001$, **Figure 1b**) and strongly decreasing microvesicular steatosis ($p=0.027$, figure 1c). Analysis of intrahepatic lipid composition revealed that this increase in hepatic steatosis in HC was mainly attributable to an accumulation of lipids esterified to cholesterol (cholesteryl esters), the concentration of which was significantly lower in HCM ($p=0.008$, **Figure 1d**). Comparably, hepatic triglyceride levels (i.e. lipids esterified to glycerol) tended to build up in HC, but no increase was observed in HCM (**Figure 1e**). In association with steatosis, HC-feeding resulted in a pronounced induction of hepatocellular hypertrophy, the development of which was markedly reduced in HCM ($p=0.034$, supplement 3). In HC-fed animals, some of these hypertrophic cells were deficient in cytokeratin 18 (CK-18) compared with neighbouring cells (**Figure 1f**), indicating loss of cytoskeletal function and hepatocellular damage as seen in ballooning cells in human NASH [28, 29]. In Mirtoselect-treated mice, only very few enlarged CK-18 deficient cells were observed (**Figure 1f**), indicating a reduction in hepatocellular damage.

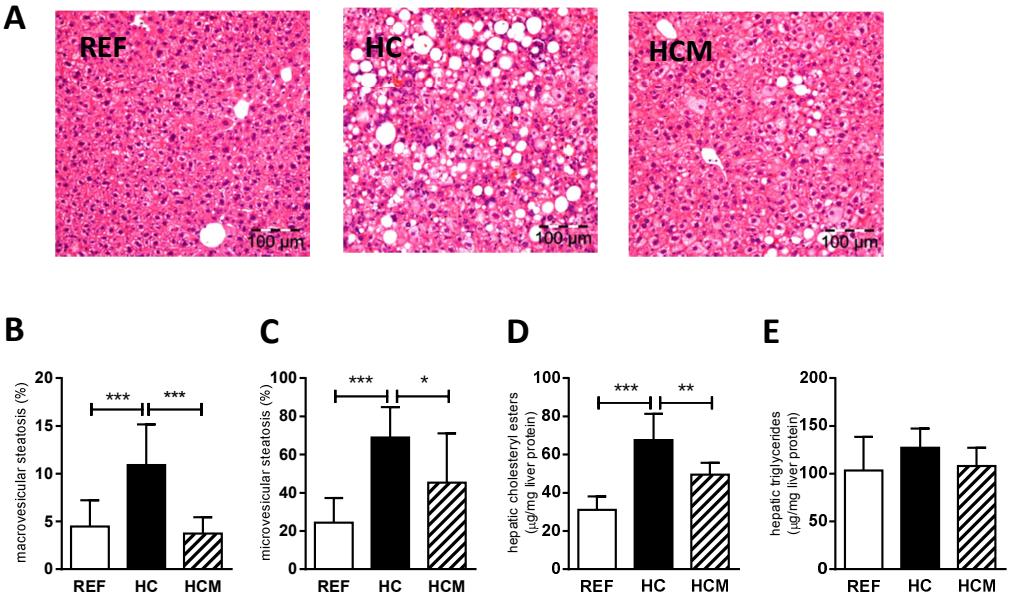

F

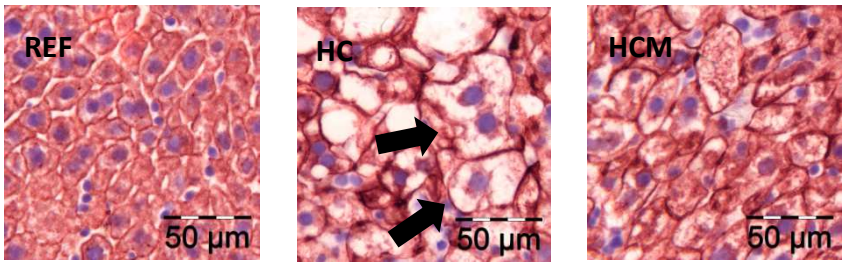

Figure 1: Mirtoselect attenuates hepatic steatosis in cholesterol-fed E3L-mice. Representative photomicrographs of liver sections of reference, high-cholesterol control and Mirtoselect-treated mice (A). Mirtoselect attenuated HC-diet-induced macrovesicular (B) and microvesicular (C) steatosis. Hepatic steatosis in HC-mice was mainly attributable to accumulation of cholesteryl-esters, the build-up of which was decreased by Mirtoselect (D). Hepatic triglycerides tended to accumulate in HC, which was not observed in HCM (E). In HC-fed animals, some hypertrophic cells were CK18-deficient compared with neighbouring cells (arrows); presence of these cells was reduced in HCM (F). REF: non-cholesterol-fed reference, HC: high-cholesterol control, HCM: high-cholesterol+Mirtoselect. Data are mean ± SD. *p<0.05, **p<0.01, ***p<0.001 compared with HC.

Mirtoselect reduces hepatic inflammation

In addition to hepatosteatosis, a defining characteristic of NASH is the presence of hepatic inflammation, which can be observed histologically as the lobular infiltration of inflammatory cells, i.e. inflammatory aggregates containing mononuclear cells (F4/80-positive cells of the monocyte/macrophage lineage) and polymorph nuclear cells (MPO-positive granulocytes, i.e. neutrophils). In comparison with REF, the number of inflammatory cell aggregates increased strongly in HC, and this HC-induced hepatic inflammatory response was fully blunted with Mirtoselect (p<0.001, **Figure 2a**). Investigation of hepatic *Emr1* (F4/80) gene expression revealed that the influx of inflammatory cells was partly attributable to macrophages, which was supported by increased gene expression levels of *Ccl2* (MCP-1), a mediator of monocyte recruitment (**Figure 2b-c**). Mirtoselect did not affect expression of *Emr1*or *Ccl2* (**Figure 2b-c**), indicating that its anti-inflammatory effect may impair the influx of another immune cell type. Hepatic gene expression analysis of the neutrophil marker *Mpo* showed that *Mpo* expression was increased in HC animals and this induction was completely prevented in HCM animals (p=0.034, **Figure 2d**). Immunohistochemical staining of MPO-positive cells confirmed the mRNA expression data and showed that HC induced neutrophil infiltration, which was attenuated by HCM (**Figure 2e**). In line with these findings, the expression of two neutrophil chemoattractants – *Cxcl1* and *Cxcl2* – was upregulated strongly and significantly by HC feeding while induction of these chemokines was less pronounced in HCM animals (*Cxcl1*: p=0.327, *Cxcl2*: p=0.131, **Figure 2f-g**).

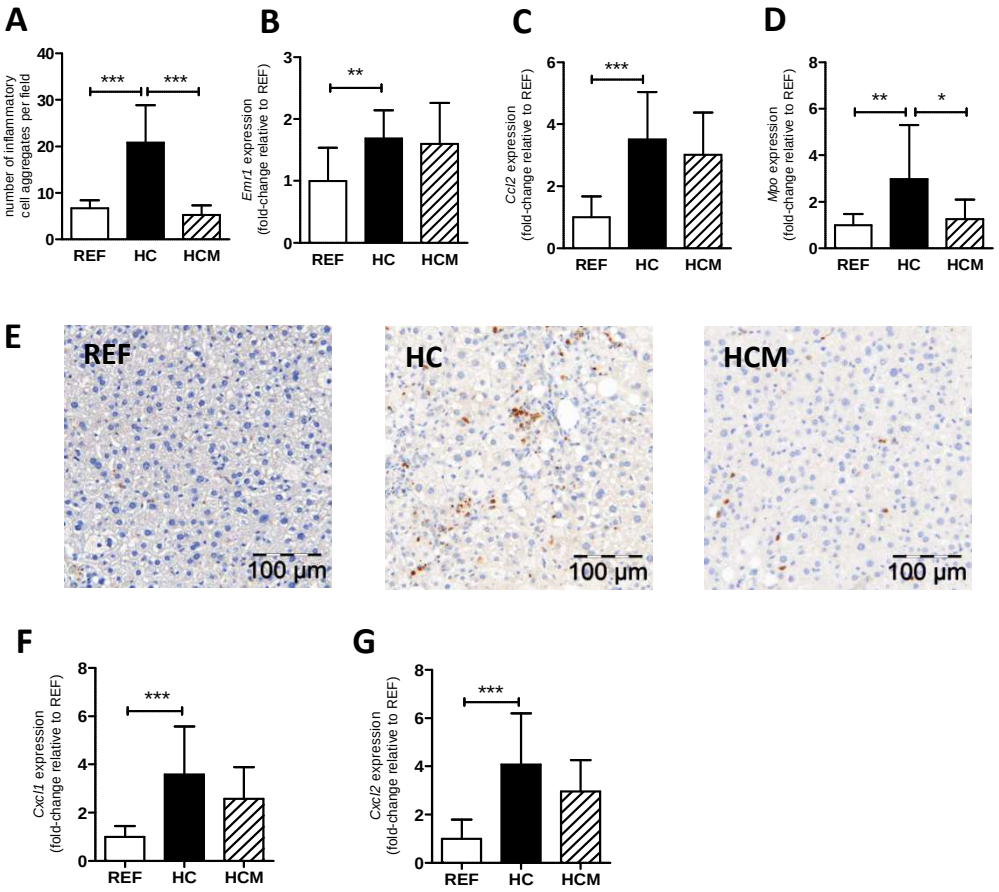

Figure 2: Mirtoselect reduces hepatic inflammation in cholesterol-fed E3L-mice. Number of HC-induced inflammatory cell aggregates was reduced by Mirtoselect (A). HC-diet induced Emr1 (B) and Ccl2 (C) gene expression was not affected by Mirtoselect. Mirtoselect reduced HC-induced Mpo gene expression (D) and number of MPO-positive cells as determined immunohistochemically (E). HC-induced gene expression of neutrophil chemoattractants Cxcl1 (F) and Cxcl2 (G) was less pronounced in HCM. REF: non-cholesterol-fed reference, HC: high-cholesterol control, HCM: high-cholesterol+Mirtoselect. Data are mean ± SD. *p<0.05, **p<0.01, ***p<0.001 compared with HC.

Mirtoselect attenuates hepatic fibrosis

Continued hepatic inflammation is thought to drive the progression of NASH, ultimately resulting in the development of hepatic fibrosis. Histochemical staining of hepatic collagen content by Picro-Sirius Red staining demonstrated that the HC diet caused liver fibrosis,

characterised by periportal, pericentral and perisinusoidal deposition of collagen. This HC-induced fibrosis was much less pronounced in HCM (**Figure 3a**).

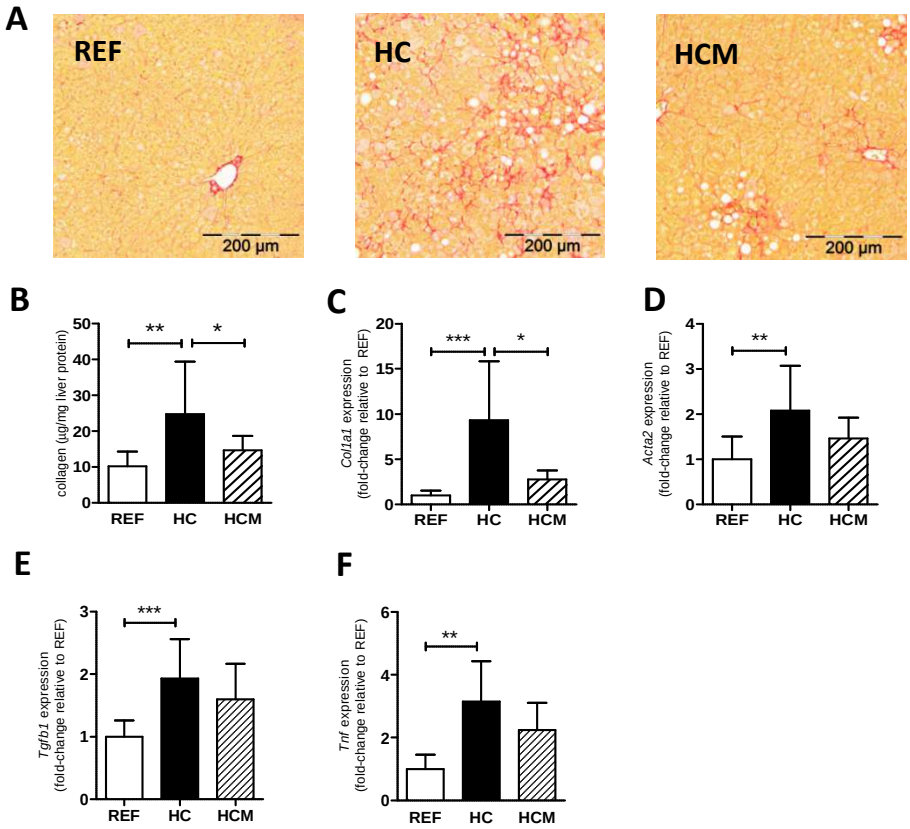

Figure 3: Development of hepatic fibrosis in cholesterol-fed E3L-mice reduced by Mirtoselect. Representative photomicrographs of picro-sirius red-stained liver sections show reduction of HC-induced collagen content in Mirtoselect-treated mice (A), which was confirmed by biochemical analysis of hepatic collagen content (B). Induction of Col1a1 gene expression is prevented by Mirtoselect (C). Gene expression of hepatic stellate cell activation marker Acta2 (D) as well as pro-fibrotic cytokines Tgfb1 (E) and Tnf (F) was induced by HC, while this induction was less pronounced in HCM. REF: non-cholesterol-fed reference, HC: high-cholesterol control, HCM: high-cholesterol+Mirtoselect. Data are mean ± SD. *p<0.05, **p<0.01, ***p<0.001 compared with HC.

In line with these histological observations, biochemical analysis of hepatic collagen content revealed a pronounced increase in collagen content in HC compared with REF, which was significantly reduced in HCM (p=0.034, **Figure 3b**) and hepatic gene expression analysis of *Col1a1* showed significantly increased expression in HC compared with REF, while Mirtoselect quenched this effect and significantly reduced *Col1a1* expression compared with HC (p=0.011, **Figure 3c**). Additionally, HC diet significantly induced expression of the hepatic stellate cell activation marker *Acta2* (α-SMA) (**Figure 3d**), as well

as the pro-fibrotic cytokines *Tgfb1* (TGF-β) and *Tnf* (TNF-α) (**Figure 3e-f**). In line with the attenuating effect of Mirtoselect on hepatic fibrosis development, the induction of these genes was less pronounced, although non-significantly, in HCM (*Acta2:* p=0.173, *Tgfb1:* p=0.174, *Tnf:* p=0.096, **Figure 3d-f**). Subsequent microarray pathway analysis revealed that many genes downstream of TGF-β were affected, indicating strongly and significantly activated TGF-β signalling in HC compared with REF (z=7.539, p=2.5E-51). Mirtoselect strongly inhibited activation of this pathway (z=-4.862, p=3.3E-20 compared with HC). Consistent with this, the process 'Hepatic fibrosis/hepatic stellate cell activation', was strongly activated in HC compared with REF and Mirtoselect suppressed this activation (supplement 4). Together, our data demonstrate that HC-feeding induced histopathological and molecular hallmarks of NASH and fibrosis and that Mirtoselect significantly attenuated disease development.

Intrahepatic free cholesterol correlates with development of NASH and is reduced by Mirtoselect

To gain more insight into the metabolic-inflammatory processes that drive the development of NASH and hepatic fibrosis and the effects of Mirtoselect thereupon, we next analysed a possible metabolic trigger of inflammation: cholesterol. HC-feeding induced dyslipidaemia with increased plasma total cholesterol compared with REF, specifically in the VLDL- and LDL-sized particles. Mirtoselect did not affect circulating cholesterol levels or lipoprotein profile (supplement 5) pointing to a hepatoprotective effect within the liver tissue. As intrahepatic free cholesterol is a very potent inducer of liver inflammation [23] and is elevated intrahepatically in human NASH [30, 31], we determined free cholesterol concentrations in freshly prepared liver homogenates and correlated them with histology scores and gene expression data. Both hepatic inflammation (number of inflammatory clusters observed histologically, p<0.001), and hepatic fibrosis (hepatic *Col1a1* expression, p=0.007) were positively correlated with hepatic free cholesterol levels (**Figure 4a-b**). Further strengthening this notion, we also observed positive significant correlations of hepatic free cholesterol levels with the expression level of many of the investigated pro-inflammatory and pro-fibrotic parameters (i.e. *Ccl2, Cxcl1, Cxcl2, Acta2, Tgfb1* and *Tnf,* shown in supplement 6). Importantly, Mirtoselect fully blunted the disease-associated increase in hepatic free cholesterol, the concentrations of which were comparable to REF and significantly lower than in HC (p=0.008, **Figure 4c**). To further examine the link between cholesterol and inflammation and the effects of Mirtoselect thereupon we analysed activation of inflammatory pathways by microarray as well as biochemically. HC diet significantly induced TNF-α and IL-1β signalling (TNF-α: z=7.539, p=2.5E-51; IL-1β: z=6.516, p=4.70E-30; vs REF) and activated the downstream pro-inflammatory transcription factor NFκB (z=6.245, p=4.82E-14 vs REF). Consistent with this, hepatic free cholesterol levels were positively correlated with biochemically measured transcriptional activation of p65-NFκB (R^2=0.51, p=0.021), providing a link between cholesterol and inflammation. Mirtoselect significantly reduced p65-NFκB activity relative to HC (fold-change relative to REF: 1.15 ± 0.11 in HC vs 0.98 ± 0.05 in HCM, p=0.032).

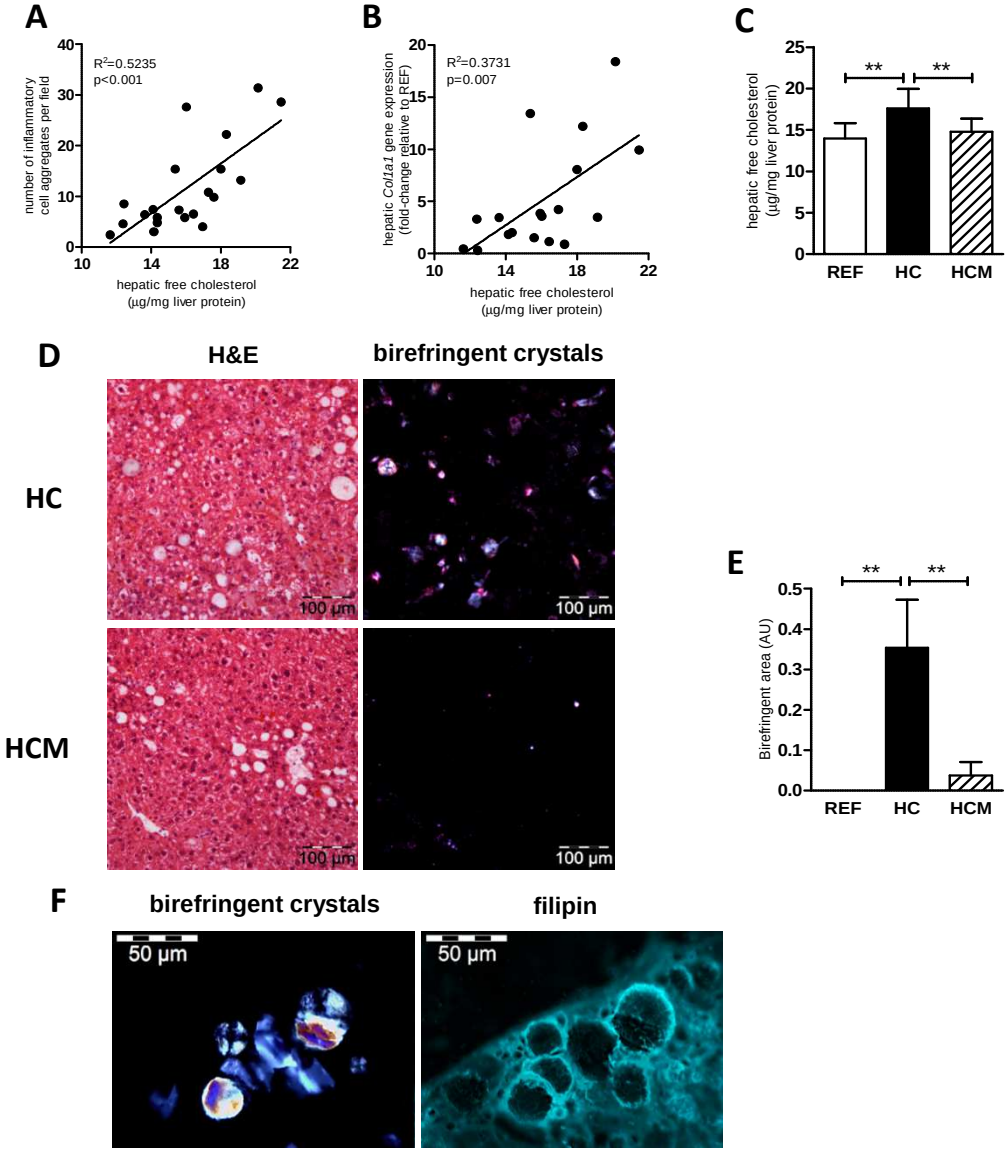

Figure 4: Mirtoselect reduces intrahepatic free cholesterol accumulation and crystallisation in cholesterol-fed E3L-mice. Intrahepatic free cholesterol levels correlated with hepatic inflammation (inflammatory aggregates per field; A) and hepatic fibrosis (Col1a1 expression; B). HC-induced hepatic free cholesterol accumulation was not observed in HCM (C). Representative photomicrographs of liver cryosections (same field under bright-field and polarised-light microscopy) reveal presence of birefringent crystals in HC that were hardly observed in HCM (D). Quantification of birefringent area shows strong HC-induced increase that is not observed in HCM (E). Birefringent crystals stained prominently with free-cholesterol staining filipin (same field under polarised-light and fluorescent microscopy; F). REF: non-cholesterol-fed reference, HC: high-cholesterol control, HCM: high-cholesterol+Mirtoselect. Data are mean ± SD. **p<0.01 compared with HC.

More detailed analysis of processes that may underlie observed effects of Mirtoselect on hepatic cholesterol accumulation showed that plasma markers of cholesterol uptake (plant sterols to cholesterol ratio and cholestanol to cholesterol ratio) or cholesterol biosynthesis (lathosterol to cholesterol ratio) were not affected in HCM (supplement 7). Also, microarray analysis confirmed absence of an effect of Mirtoselect on cholesterol biosynthesis but revealed a significant activation of FXR in HCM (z=2.190, p=7.64E-03) and showed that genes involved in bile acid synthesis, bile acid conjugation and bile salt secretion (e.g. Bsep, Cyp27a1) were upregulated in HCM.

Refined microscopic analysis of liver cross-sections under polarised light revealed that HC-feeding caused pronounced formation of large birefringent crystals within a considerable amount of the macrovesicular lipid droplets, while these crystals were hardly observed in Mirtoselect-treated animals (even in the few regions containing macrovesicles, **Figure 4d-e**). These birefringent crystals stained positively with filipin (**Figure 4f**), which forms a fluorescent complex with free cholesterol specifically, indicating that the observed birefringence is attributable to crystallised free cholesterol. Detailed examination of the liver cross-sections under bright field and polarised light microscopy revealed that many of the hepatocytes containing these crystals were devoid of normal cellular morphology and organisation. The prevention of this intrahepatic cholesterol crystal formation by Mirtoselect provides a possible rationale for its observed hepatoprotective properties.

DISCUSSION

We investigated the potential hepatoprotective properties of a standardised anthocyanin-rich extract (Mirtoselect) in a diet-induced, translational model of NASH with fibrosis. We show that Mirtoselect protects against the development of NASH, reducing hepatic steatosis, hepatic inflammation and hepatic fibrosis, associated with decreased accumulation and crystallisation of intrahepatic free cholesterol. The observed hepatoprotective effects of Mirtoselect were achieved at a dosage that translates to an anthocyanin intake of around 300 mg/day in humans, an intake that is achievable by diet [12, 32, 33].

HC diet-feeding induced intrahepatic lipid accumulation characterised by macro- and microvesicular steatosis, which was mainly attributable to an increase in lipids esterified to cholesterol. Mirtoselect strongly reduced this intrahepatic accumulation of lipids. Experimental support for these observed anti-steatotic effects is provided by results from earlier studies that report improved hepatic cholesterol homeostasis in rodents treated with similar concentrations of anthocyanin-rich extracts [11, 34] or individual anthocyanins [35]. Although these studies were not performed under conditions leading to NAFLD/NASH, they do provide a possible mechanism for the observed reduction in intrahepatic cholesterol: intervention with anthocyanins was found to increase bile acid synthesis [34, 35] and faecal sterol excretion [11, 35], thereby decreasing intrahepatic cholesterol accumulation [11, 35] which is consistent with our observations of FXR activation by Mirtoselect. Although it is the anthocyanin fraction of Mirtoselect that is considered to be the principal bioactive fraction of the extract, it is unknown which of

these anthocyanins or other possibly bioactive constituents (alone or in combination), may be responsible for the observed effects.

In addition to reducing hepatic steatosis Mirtoselect also attenuated hepatic inflammation, completely preventing the HC-induced increase in inflammatory cell aggregates. This anti-inflammatory effect was largely attributable to an effect specifically on the influx of MPO-positive neutrophils, the infiltration of which is recognised as a defining characteristic of inflammation in human NASH [36]. The exact role of neutrophils in the pathogenesis of NASH remains to be elucidated [37], but their ability to release a potent cocktail of reactive oxygen species and proteases implicates them as potential cause of extensive tissue damage [38] that may contribute to amplification of the inflammatory response as well as development of fibrosis. We observed a marked reduction of neutrophils in livers of Mirtoselect-treated mice, but only a modest effect on the hepatic expression of neutrophil chemoattractants *Cxcl1* and *Cxcl2,* suggesting additional mechanisms outside the liver. Indeed, it has been demonstrated that anthocyanins can attenuate the induction of chemokine receptors such as CXCR2 [39], which is required for neutrophil chemotaxis.

Although inflammation is recognised to play an important role in the development of NASH, the nature of the trigger for this inflammatory component remains unclear. Lipotoxicity caused by the build-up of toxic lipid species is thought to play an important role, but the specific lipid species that mediate hepatic lipotoxicity have not been identified with certainty [40]. While triglycerides are the main accumulating lipid species in human NASH, recent studies have implicated free cholesterol as a potential trigger for disease progression [4]. The experimental conditions chosen for the present study emphasize the role of cholesterol in NASH, and limit the study of hepatic triglyceride accumulation. Results from epidemiological studies that link dietary cholesterol intake to increased risk and severity of NAFLD [41, 42] and cirrhosis [43] provide indications that cholesterol may play a causal role in NASH development. In support of this notion, free cholesterol is increased intrahepatically in human [30, 31] and experimental NASH [44] and modulation of hepatic free cholesterol levels by diet [44] or pharmacological intervention [45] is closely linked to the severity of experimental NASH. Furthermore, there are indications that cholesterol-lowering agents (e.g. statins, ezetimibe) may improve NASH in patients with hypercholesterolaemia [46, 47]. Mechanistic studies have shown that free cholesterol accumulation in Kupffer cells [48] and hepatic stellate cells (HSC) [6, 7] promotes inflammation and exacerbates fibrosis (e.g. increased TNF-α and CCL2 expression by Kupffer cells and increased COL1A1 expression in HSC). Results from the study described herein show that intrahepatic free cholesterol levels are positively correlated with many factors that contribute to or reflect progressive development of NASH (e.g. *Ccl2, Cxcl1, Cxcl2, Col1a1, Acta2, Tnf,* and *Tgfb1*). The observed activation of inflammatory signalling routes (IL-1β, TNF-α, TGF-β) by HC as well as the positive correlation between free cholesterol and NFκB activity, point to NFκB activation as an effector of cholesterol-induced inflammation, which is in line with previous observations [23, 27]. Mirtoselect decreases the build-up of this cytotoxic lipid species and associated NFκB activation, thereby providing a possible explanation for its beneficial effects on NAFLD development.

A recently emerging mechanism of cellular toxicity associated with free cholesterol accumulation is intracellular cholesterol crystallisation, which can happen when the concentration of free cholesterol reaches a very high level [49]. Cholesterol crystals, particularly when they are very small (nm range), can trigger inflammation through inflammasome activation [5, 50]. Besides putative pro-inflammatory effects of cholesterol crystals [5, 50], it is plausible that the sheer size of the intrahepatocellular cholesterol crystals observed in the present study (with diameters ranging up to 50 µm) would also cause extensive physical damage to the cells containing them. Indeed, the formed cholesterol crystals may damage cells by physically disrupting the integrity of intracellular structures [49], in line with observations in the present study. Furthermore, cellular damage can result in the release of damage associated molecular patterns (DAMPs), which leads to neutrophil recruitment [37] further enhancing the inflammatory response. Additional support for this mechanism is provided by results from human studies that demonstrate that cholesterol crystals distinguish NASH from simple steatosis [8] and that this accumulation and crystallisation of free cholesterol within steatotic hepatocytes may be an important trigger for disease progression.

Overall, we show that Mirtoselect has beneficial effects in NASH, improving hepatic steatosis, inflammation and fibrosis. Furthermore, we demonstrate the presence of cholesterol crystals and associated tissue damage in NASH and show that dietary intervention with Mirtoselect prevents this accumulation and crystallisation of free cholesterol, providing a possible rationale for its hepatoprotective effects. Given the moderate dose of Mirtoselect used, this study suggests that intervention with naturally occurring, well-tolerated polyphenols may constitute a powerful approach to retard NASH development.

ACKNOWLEDGEMENTS

We would like to thank Wim van Duyvenvoorde and Erik Offerman for their excellent technical assistance.

REFERENCES

[1] Browning J D, Szczepaniak LS, Dobbins R, Nuremberg P, Horton JD, Cohen JC et al. Prevalence of hepatic steatosis in an urban population in the United States: impact of ethnicity. Hepatology 2004; 40:1387-1395.

[2] Clark J M. The epidemiology of nonalcoholic fatty liver disease in adults. J Clin Gastroenterol 2006; 40 Suppl 1:S5-10.

[3] Fujii H, Kawada N. Inflammation and fibrogenesis in steatohepatitis. J Gastroenterol 2012; 47:215-225.

[4] Musso G, Gambino R, Cassader M. Cholesterol metabolism and the pathogenesis of non-alcoholic steatohepatitis. Prog Lipid Res 2013; 52:175-191.

[5] Duewell P, Kono H, Rayner KJ, Sirois CM, Vladimer G, Bauernfeind FG et al. NLRP3 inflammasomes are required for atherogenesis and activated by cholesterol crystals. Nature 2010; 464:1357-1361.

[6] Teratani T, Tomita K, Suzuki T, Oshikawa T, Yokoyama H, Shimamura K et al. A high-cholesterol diet exacerbates liver fibrosis in mice via

accumulation of free cholesterol in hepatic stellate cells. Gastroenterology 2012; 142:152-164.e10.
[7] Tomita K, Teratani T, Suzuki T, Shimizu M, Sato H, Narimatsu K et al. Free cholesterol accumulation in hepatic stellate cells: mechanism of liver fibrosis aggravation in nonalcoholic steatohepatitis in mice. Hepatology 2014; 59:154-169.
[8] Ioannou G N, Haigh WG, Thorning D, Savard C. Hepatic cholesterol crystals and crown-like structures distinguish NASH from simple steatosis. J Lipid Res 2013; 54:1326-1334.
[9] He J, Giusti MM. Anthocyanins: natural colorants with health-promoting properties. Annu Rev Food Sci Technol 2010; 1:163-187.
[10] Qin Y, Xia M, Ma J, Hao Y, Liu J, Mou H et al. Anthocyanin supplementation improves serum LDL- and HDL-cholesterol concentrations associated with the inhibition of cholesteryl ester transfer protein in dyslipidemic subjects. Am J Clin Nutr 2009; 90:485-492.
[11] Liang Y, Chen J, Zuo Y, Ma KY, Jiang Y, Huang Y et al. Blueberry anthocyanins at doses of 0.5 and 1 % lowered plasma cholesterol by increasing fecal excretion of acidic and neutral sterols in hamsters fed a cholesterol-enriched diet. Eur J Nutr 2013; 52:869-875.
[12] Jennings A, Welch AA, Spector T, Macgregor A, Cassidy A. Intakes of anthocyanins and flavones are associated with biomarkers of insulin resistance and inflammation in women. J Nutr 2014; 144:202-208.
[13] Valenti L, Riso P, Mazzocchi A, Porrini M, Fargion S, Agostoni C. Dietary anthocyanins as nutritional therapy for nonalcoholic fatty liver disease. Oxid Med Cell Longev 2013; 2013:145421.
[14] Karlsen A, Paur I, Bohn SK, Sakhi AK, Borge GI, Serafini M et al. Bilberry juice modulates plasma concentration of NF-kappaB related inflammatory markers in subjects at increased risk of CVD. Eur J Nutr 2010; 49:345-355.
[15] Kolehmainen M, Mykkanen O, Kirjavainen PV, Leppanen T, Moilanen E, Adriaens M et al. Bilberries reduce low-grade inflammation in individuals with features of metabolic syndrome. Mol Nutr Food Res 2012; 56:1501-1510.
[16] Bao L, Yao XS, Yau CC, Tsi D, Chia CS, Nagai H et al. Protective effects of bilberry (Vaccinium myrtillus L.) extract on restraint stress-induced liver damage in mice. J Agric Food Chem 2008; 56:7803-7807.
[17] Bao L, Abe K, Tsang P, Xu JK, Yao XS, Liu HW et al. Bilberry extract protect restraint stress-induced liver damage through attenuating mitochondrial dysfunction. Fitoterapia 2010; 81:1094-1101.
[18] Domitrovic R, Jakovac H. Effects of standardized bilberry fruit extract (Mirtoselect(R)) on resolution of CCl4-induced liver fibrosis in mice. Food Chem Toxicol 2011; 49:848-854.
[19] Zadelaar S, Kleemann R, Verschuren L, de Vries-Van der Weij J, van der Hoorn J, Princen HM et al. Mouse models for atherosclerosis and pharmaceutical modifiers. Arterioscler Thromb Vasc Biol 2007; 27:1706-1721.
[20] Duivenvoorden I, Voshol PJ, Rensen PC, van Duyvenvoorde W, Romijn JA, Emeis JJ et al. Dietary sphingolipids lower plasma cholesterol and triacylglycerol and prevent liver steatosis in APOE*3Leiden mice. Am J Clin Nutr 2006; 84:312-321.
[21] Morrison M, van der Heijden R, Heeringa P, Kaijzel E, Verschuren L, Blomhoff R et al. Epicatechin attenuates atherosclerosis and exerts anti-inflammatory effects on diet-induced human-CRP and NFkappaB in vivo. Atherosclerosis 2014; 233:149-156.
[22] van de Steeg E, Kleemann R, Jansen HT, van Duyvenvoorde W, Offerman EH, Wortelboer HM et al. Combined analysis of pharmacokinetic and efficacy data of preclinical studies with statins markedly improves translation of drug efficacy to human trials. J Pharmacol Exp Ther 2013; 347:635-644.
[23] Kleemann R, Verschuren L, van Erk MJ, Nikolsky Y, Cnubben NH, Verheij ER et al. Atherosclerosis and liver inflammation induced by increased dietary cholesterol intake: a combined transcriptomics and metabolomics analysis. Genome Biol 2007; 8:R200.

[24] Verschuren L, Wielinga PY, van Duyvenvoorde W, Tijani S, Toet K, van Ommen B et al. A dietary mixture containing fish oil, resveratrol, lycopene, catechins, and vitamins E and C reduces atherosclerosis in transgenic mice. J Nutr 2011; 141:863-869.

[25] Kleiner D E, Brunt EM, Van Natta M, Behling C, Contos MJ, Cummings OW et al. Design and validation of a histological scoring system for nonalcoholic fatty liver disease. Hepatology 2005; 41:1313-1321.

[26] Liang W, Lindeman JH, Menke AL, Koonen DP, Morrison M, Havekes LM et al. Metabolically induced liver inflammation leads to NASH and differs from LPS- or IL-1beta-induced chronic inflammation. Lab Invest 2014; 94:491-502.

[27] Wielinga P Y, Yakala GK, Heeringa P, Kleemann R, Kooistra T. Beneficial effects of alternate dietary regimen on liver inflammation, atherosclerosis and renal activation. PLoS One 2011; 6:e18432.

[28] Caldwell S, Ikura Y, Dias D, Isomoto K, Yabu A, Moskaluk C et al. Hepatocellular ballooning in NASH. J Hepatol 2010; 53:719-723.

[29] Zatloukal K, Stumptner C, Fuchsbichler A, Fickert P, Lackner C, Trauner M et al. The keratin cytoskeleton in liver diseases. J Pathol 2004; 204:367-376.

[30] Puri P, Baillie RA, Wiest MM, Mirshahi F, Choudhury J, Cheung O et al. A lipidomic analysis of nonalcoholic fatty liver disease. Hepatology 2007; 46:1081-1090.

[31] Caballero F, Fernandez A, De Lacy AM, Fernandez-Checa JC, Caballeria J, Garcia-Ruiz C. Enhanced free cholesterol, SREBP-2 and StAR expression in human NASH. J Hepatol 2009; 50:789-796.

[32] Hertog M G, Hollman PC, Katan MB, Kromhout D. Intake of potentially anticarcinogenic flavonoids and their determinants in adults in The Netherlands. Nutr Cancer 1993; 20:21-29.

[33] Cassidy A, Mukamal KJ, Liu L, Franz M, Eliassen AH, Rimm EB. High anthocyanin intake is associated with a reduced risk of myocardial infarction in young and middle-aged women. Circulation 2013; 127:188-196.

[34] Mauray A, Felgines C, Morand C, Mazur A, Scalbert A, Milenkovic D. Bilberry anthocyanin-rich extract alters expression of genes related to atherosclerosis development in aorta of apo E-deficient mice. Nutr Metab Cardiovasc Dis 2012; 22:72-80.

[35] Wang D, Xia M, Gao S, Li D, Zhang Y, Jin T et al. Cyanidin-3-O-beta-glucoside upregulates hepatic cholesterol 7alpha-hydroxylase expression and reduces hypercholesterolemia in mice. Mol Nutr Food Res 2012; 56:610-621.

[36] Brunt E M, Janney CG, Di Bisceglie AM, Neuschwander-Tetri BA, Bacon BR. Nonalcoholic steatohepatitis: a proposal for grading and staging the histological lesions. Am J Gastroenterol 1999; 94:2467-2474.

[37] Xu R, Huang H, Zhang Z, Wang FS. The role of neutrophils in the development of liver diseases. Cell Mol Immunol 2014; 11:224-231.

[38] Kubes P, Mehal WZ. Sterile inflammation in the liver. Gastroenterology 2012; 143:1158-1172.

[39] Kang M K, Li J, Kim JL, Gong JH, Kwak SN, Park JH et al. Purple corn anthocyanins inhibit diabetes-associated glomerular monocyte activation and macrophage infiltration. Am J Physiol Renal Physiol 2012; 303:F1060-9.

[40] Farrell G C, van Rooyen D, Gan L, Chitturi S. NASH is an Inflammatory Disorder: Pathogenic, Prognostic and Therapeutic Implications. Gut Liver 2012; 6:149-171.

[41] Musso G, Gambino R, De Michieli F, Cassader M, Rizzetto M, Durazzo M et al. Dietary habits and their relations to insulin resistance and postprandial lipemia in nonalcoholic steatohepatitis. Hepatology 2003; 37:909-916.

[42] Yasutake K, Nakamuta M, Shima Y, Ohyama A, Masuda K, Haruta N et al. Nutritional investigation of non-obese patients with non-alcoholic fatty liver disease: the significance of dietary cholesterol. Scand J Gastroenterol 2009; 44:471-477.

[43] Ioannou G N, Morrow OB, Connole ML, Lee SP. Association between dietary nutrient composition and the incidence of cirrhosis or liver cancer in the United States population. Hepatology 2009; 50:175-184.

[44] Van Rooyen D M, Larter CZ, Haigh WG, Yeh MM, Ioannou G, Kuver R et al. Hepatic free cholesterol accumulates in obese, diabetic mice and causes nonalcoholic steatohepatitis. Gastroenterology 2011; 141:1393-403, 1403.e1-5.

[45] Van Rooyen D M, Gan LT, Yeh MM, Haigh WG, Larter CZ, Ioannou G et al. Pharmacological cholesterol lowering reverses fibrotic NASH in obese, diabetic mice with metabolic syndrome. J Hepatol 2013; 59:144-152.

[46] Ekstedt M, Franzen LE, Mathiesen UL, Holmqvist M, Bodemar G, Kechagias S. Statins in non-alcoholic fatty liver disease and chronically elevated liver enzymes: a histopathological follow-up study. J Hepatol 2007; 47:135-141.

[47] Yoneda M, Fujita K, Nozaki Y, Endo H, Takahashi H, Hosono K et al. Efficacy of ezetimibe for the treatment of non-alcoholic steatohepatitis: An open-label, pilot study. Hepatol Res 2010; 40:566-573.

[48] Leroux A, Ferrere G, Godie V, Cailleux F, Renoud ML, Gaudin F et al. Toxic lipids stored by Kupffer cells correlates with their pro-inflammatory phenotype at an early stage of steatohepatitis. J Hepatol 2012; 57:141-149.

[49] Tabas I. Consequences of cellular cholesterol accumulation: basic concepts and physiological implications. J Clin Invest 2002; 110:905-911.

[50] Samstad E O, Niyonzima N, Nymo S, Aune MH, Ryan L, Bakke SS et al. Cholesterol Crystals Induce Complement-Dependent Inflammasome Activation and Cytokine Release. J Immunol 2014; 192:2837-45.

SALSALATE ATTENUATES DIET INDUCED NON-ALCOHOLIC STEATOHEPATITIS BY DECREASING LIPOGENIC AND INFLAMMATORY PROCESSES

Wen Liang
Lars Verschuren
José W.A. van der Hoorn
Joanne Verheij
Andrea D. van Dam
Mariette R. Boon
Hans M.G. Princen
Louis M. Havekes
Robert Kleemann
Anita M. van den Hoek

Submitted

ABSTRACT

Background and aims: Salsalate is an anti-inflammatory drug that was recently found to exhibit beneficial metabolic effects on glucose and lipid metabolism. Although its utility in the prevention and management of a wide range of vascular disorders as well as of type 2 diabetes and metabolic syndrome has been suggested before, the potential of salsalate to protect against non-alcoholic steatohepatitis (NASH) remains unclear. The aim of the present study was therefore to ascertain the effects of salsalate in the development of NASH.

Methods: Transgenic APOE*3Leiden.CETP mice were fed a high fat high cholesterol diet with or without salsalate for 12 and 20 weeks. The effects on body weight, plasma parameters, liver histology and hepatic gene expression were assessed.

Results: Salsalate prevented weight gain, improved dyslipidemia and insulin resistance and ameliorated diet-induced non-alcoholic steatohepatitis, as shown by decreased hepatic micro- and macrovesicular steatosis, reduced hepatic inflammation and reduced development of fibrosis. Salsalate affected lipid metabolism by increasing β-oxidation and decreasing lipogenesis, as shown by the activation of PPAR-α, PGC1-β, RXR-α and inhibition of MLXIPL/ChREBP controlled genes, respectively. Inflammation was reduced by down-regulation of the NFκB pathway and fibrosis development was prevented by down-regulation of TGF-β signaling.

Conclusions: Salsalate was shown to exert a preventive effect on the development of NASH and progression to fibrosis. These data suggest a clinical application of salsalate in preventing NASH.

INTRODUCTION

Owing to the worldwide epidemic of obesity, and the abundance of energy-rich diets with high levels of sugars and saturated fat, non-alcoholic fatty liver disease (NAFLD) is increasingly common. In fact, NAFLD is now considered to be the manifestation of the metabolic syndrome in the liver and has become the most prevalent form of chronic liver disease. Non-alcoholic steatohepatitis (NASH) is a severe form of NAFLD, characterized by steatosis in concert with inflammation, which can progress to liver fibrosis and cirrhosis. To date, no single therapy has been approved for the treatment of NASH. Considering that NASH has serious adverse effects on health, including hepatic failure, development of novel therapies that effectively reverse hepatic fat accumulation and inflammation is evidently needed.

Salsalate is an anti-inflammatory agent that has been used in the clinic for several decades to treat rheumatoid arthritis, osteoarthritis, and related rheumatic conditions. The drug is a dimer of two molecules of salicylate that are linked by an ester bond. The anti-inflammatory effects of salsalate and salicylate are both believed to be attributable to inhibition of the activity of cyclooxygenase (COX), a key enzyme in biosynthesis of proinflammatory prostanoids [1, 2]. In contrast to salicylate, salsalate is well tolerated and considered to be relatively safe for long-term use. Recent studies have shown that salsalate exhibits beneficial effects on glucose and lipid metabolism. In clinical studies, administration of salsalate decreased fasting glucose and HbA1c levels in obese non-diabetics as well as type 2 diabetics, and improved insulin sensitivity [3, 4]. Furthermore, decreases in circulating triglyceride and free fatty acids levels have been reported [5, 6]. In aggregate, these data suggest that this particular combination of effects, i.e. anti-inflammatory effects and beneficial effects on glucose and lipid metabolism, renders salsalate an optimal candidate for treatment of NASH.

To test this hypothesis, we investigated the effect of salsalate on NASH development and liver fibrosis using APOE*3Leiden.CETP mice [7-9]. These mice are prone to develop dyslipidemia, obesity and NAFLD on a high fat/high cholesterol diet, and ultimately develop NASH with fibrosis. Earlier studies have shown that these mice demonstrate human-like responses to different anti-diabetic and hypolipidemic drugs [9-13].

MATERIALS AND METHODS

Animals and induction of NASH and liver fibrosis

Homozygous human cholesteryl ester transfer protein (CETP) transgenic mice (strain 5203) [9, 14] were obtained from Jackson Laboratories (Bar Harbor, MC) and cross-bred with APOE*3Leiden mice (E3L) [15] in our local animal facility at TNO to obtain heterozygous E3L.CETP mice. All animals were housed in a temperature-controlled room on a 12 hour light-dark cycle and had free access to food and water. Animal experiments were approved by the Ethical Committee on Animal Care and Experimentation (Zeist, The Netherlands), and were in compliance with European Community specifications regarding the use of laboratory animals. To assess the effect of salsalate on progression of obesity, dyslipidemia, hyperglycemia and NASH development, 16-19 weeks old male E3L.CETP

mice were fed a high fat, high cholesterol diet (HFC: 45 kcal% fat derived from lard supplemented with 1% (w/w) cholesterol, Research Diets, New Brunswick, NJ, USA) with (n=8) or without (HFC control group, n=9) 1% (w/w) salsalate (2-carboxyphenyl salicylate, TCI Europe N.V., Zwijndrecht, Belgium) for 12 weeks. In addition, five age-matched male E3L.CETP mice on a low fat diet (LFD: 10 kcal% lard, Research Diets, New Brunswick, NJ, USA) were also included (LFD control group, n=5). In a second experiment we assessed whether salsalate would still be able to prevent onset of NASH and liver fibrosis, also after a longer induction period of NASH. To do so, 11-18 weeks old male E3L.CETP mice were fed the HFC diet with (n=8) or without (n=12) 0.33% (w/w) salsalate for 20 weeks. Because of the profound effects of salsalate in the first (short-term) study, the drug dose was lowered pharmacologically (by factor 3).

Analysis of plasma parameters

Blood was collected from the tail vein after 5 h fasting (with food withdrawn around 08.00 am) into EDTA-coated tubes (Sarstedt, Nümbrecht, Germany). Plasma glucose was determined using the 'Freestyle glucose measurement system' from Abbott (Abbott Park, IL, USA). Plasma insulin was measured by ELISA (Mercodia AB, Uppsala, Sweden). Homeostasis model assessment (HOMA) was used to calculate relative insulin resistance (IR). Five hours fasting plasma insulin and fasting blood glucose values were used: IR = [insulin (ng/ml) x glucose (mM)] /22.5. Plasma total cholesterol and triglycerides were determined using a commercially available kit (Roche Diagnostics, Basel, Switzerland). The distribution of cholesterol of the various lipoproteins was determined in plasma pooled per group after separation of lipoproteins by fast-performance liquid chromatography (FPLC) using a Superose 6 column [11]. Plasma alanine transaminase (ALT) and aspartate aminotransferase (AST) were measured using a Reflotron® kit (Roche diagnostics, Basel, Switzerland). All measurements were performed according to the manufacturers' instructions.

Histology

Liver samples (of lobus sinister medialis hepatis and lobus dexter medialis hepatis) were collected (in non-fasted mice), fixed in formalin, paraffin embedded and sections were stained with hematoxylin and eosin (H&E) and Sirius Red. H&E stained cross-sections were scored using an adapted grading system of human NASH [16, 17]. In short, the level of macrovesicular and microvesicular steatosis was determined at 40 to 100 x magnification relative to the total liver area analyzed, which is, expressed as a percentage. Inflammation was scored by counting the number of aggregates of inflammatory cells per field using a 100 x magnification (view size of 3.1 mm^2). The average of five random fields was taken. Relative values against the average of the HFC control group were calculated. Hepatic fibrosis was identified using Sirius Red stained slides and evaluated using an adapted grading system of human NASH [16, 18]. In short, the presence of pathologic collagen staining was scored as either absent (0), observed within perisinusoidal/perivenular or periportal area (1), within both perisinusoidal and periportal area (2), bridging fibrosis (3), or cirrhosis (4). Furthermore, the level of collagen deposition in the perisinusoidal area was determined relative to the total perisinusoidal area analyzed, expressed as a percentage. In addition, fibrosis was quantified by measuring the hydroxyproline (as a

measure for collagen) and proline (as a measure for total protein) content of liver tissue using high performance liquid chromatography (HPLC) as previously described [19] and subsequent calculation of the ratio hydroxyproline above proline.

Hepatic lipid analysis

Liver samples of lobus sinister lateralis hepatis were collected and the intrahepatic concentration of triglycerides, free cholesterol and cholesteryl esters was determined as described previously [10]. Approximately 50 mg of tissue was homogenized in phosphate buffered saline and samples of the homogenate were taken for measurement of protein content. Lipids were extracted and separated by high performance thin layer chromatography (HPTLC) on silica gel plates. Lipid spots were stained with color reagent (5 g $MnCl_2.4H_2O$, 32 mL 95-97% H_2SO_4 added to 960 mL of CH_3OH:H_2O 1:1 v/v) and quantified using TINA® version 2.09 software (Raytest, Straubenhardt, Germany).

Gene expression analysis

The probe-level background subtracted expression values were used as input for lumi package [20] of the R/Bioconductor (http://www.bioconductor.org; http://www.r-project.org) to perform quality control and a quantile normalization. Unexpressed probes ($p>0.01$) were removed from further analysis, and 12947 probes remained in the analysis. Differentially expressed probes were identified using the limma package of R/Bioconductor [21, 22] calculated P-values <0.001 were used as threshold for significance. Selected differentially expressed probes (DEPs) were used as an input for pathway analysis through Ingenuity Pathway Analysis suite (www.ingenuity.com, accessed 2014).

Upstream regulator analysis was performed using the Ingenuity Pathway Analysis (IPA) software. This analysis determines the activation state of transcription factors based on the observed differential gene expression. This results in an overlap p-value and activation z-score for each transcription factor in the IPA knowledgebase. The overlap p-value indicates the significance of the overlap between the known target genes of a transcription factor and the differentially expressed genes measured in an experiment. The activation z-score indicates activation (positive z-score) or inhibition (negative z-score) of a particular transcription factor. An activation z-score <-2 or >2 indicates significant inhibition or activation of a pathway or process.

Statistical analysis

Statistical differences between groups were determined by using the non-parametrical Mann-Whitney test for independent samples. A P-value < 0.05 was considered statistically significant. All values shown represent means ± SEM.

RESULTS

Salsalate prevents weight gain and improves glycemic control and hyperlipidemia

To induce obesity, insulin resistance and hyperlipidemia, E3L.CETP mice were fed a HFC diet for 12 weeks. The HFC feeding resulted in an increased body weight (with 45%, $p<0.01$) and elevated plasma insulin (8.0-fold, $p<0.001$), cholesterol (4.1-fold $p<0.001$) and triglyceride levels (2.7-fold, $p<0.01$) when compared with age-matched control E3L.CETP mice on LFD, while plasma glucose levels remained similar (**Table 1**). The HFC diet led to an increased liver weight (2.0-fold, $p<0.01$) and analysis of liver enzymes showed a concomitant increase in plasma ALT (8.9-fold, $p<0.001$) and AST (3.6-fold, $p<0.001$) as compared to the LFD mice, indicating that the HFC diet caused liver damage (**Table 1**).

Salsalate treatment profoundly curtailed weight gain, resulting in a significantly lower body weight after 12 weeks of treatment as compared to the HFC control group (with -41%, $p<0.001$; **Table 1**). This decrease was at least partly due to a lower fat mass as reflected by a decrease in perigonadal fat pad weight with salsalate (with -83%, $p<0.001$, data not shown). Fasting plasma glucose and insulin levels were significantly lower as compared to HFC control group after treatment with salsalate (with -36% and -89%, respectively, both $p<0.01$; **Table 1**). Salsalate significantly decreased insulin resistance as reflected by the homeostasis model assessment (HOMA) index (with -91%, $p<0.01$), normalizing it to similar levels as age matched control mice on LFD. Plasma lipids were also improved by salsalate treatment: more specifically, salsalate significantly decreased plasma cholesterol and triglycerides as compared to the HFC control group (with -72% and -91%, respectively, both $p<0.001$; **Table 1**), mainly due to a reduction in VLDL and LDL, while HDL-cholesterol was slightly increased (**Supplemental Figure 1**). Furthermore, liver weight, plasma ALT and AST were all significantly lower in the salsalate treated groups as compared to the HFC control group (with -37%, -73% and -64%, respectively, all $p<0.001$; **Table 1**).

Salsalate prevents hepatic steatosis and inflammation

NASH development was histologically evaluated using H&E and Sirus Red stained liver cross-sections. HFC feeding induced pronounced steatosis, while treatment with salsalate fully prevented this induction resulting in a similar histological appearance as observed in the LFD group (**Figure 1**). Quantitative analysis revealed that in the HFC group about 85% of the surface area was steatotic, of which 60% consisted of microvesicular steatosis and 25% of macrovesicular steatosis (**Figure 2ab**). Treatment with salsalate completely prevented the development of micro- and macrovesicular steatosis (resulting in an average surface area of 0.1% and 0%, respectively, both $p<0.001$). Biochemical analysis of intrahepatic liver lipids was in line with the histological analysis and revealed that HFC feeding resulted in a significant increase in hepatic triglycerides and cholesterol esters as compared to the LFD control group (5.1-fold and 4.1-fold, respectively, both $p<0.01$) and tended to increase free cholesterol as well (1.6-fold, $p=0.065$; **Figure 2cde**).

Table 1: Plasma parameters.

	LFD	HFC	HFC+S
Body weight (g)	33.8 ± 1.9	49.0 ± 1.4$^{\#}$	28.9 ± 1.1*$^{\#}$
Plasma glucose (mM)	12.6 ± 0.8	13.1 ± 0.7	8.4 ± 0.7*$^{\#}$
Plasma insulin (ng/mL)	0.6 ± 0.2	4.8 ± 0.7$^{\#}$	0.5 ± 0.2*
HOMA	0.4 ± 0.1	2.8 ± 0.4$^{\#}$	0.2 ± 0.1*
Plasma cholesterol (mM)	6.5 ± 1.0	26.9 ± 1.9$^{\#}$	7.5 ± 0.4*
Plasma triglycerides (mM)	2.6 ± 0.3	7.2 ± 1.0$^{\#}$	0.6 ± 0.05*$^{\#}$
Liver weight (g)	1.6 ± 0.1	3.2 ± 0.2$^{\#}$	2.0 ± 0.1*$^{\#}$
Plasma ALT (U/L)	32.2 ± 7.5	286.6 ± 53.5$^{\#}$	77.4 ± 9.2*$^{\#}$
Plasma AST (U/L)	131.8 ± 18.3	473.7 ± 70.5$^{\#}$	173.0 ± 9.3*

*Body weight, liver weight and plasma parameters in APOE*3Leiden.CETP mice fed a low fat diet (LFD), a high fat and high cholesterol diet (HFC) or a high fat and high cholesterol diet supplemented with salsalate (HFC+S). Data are mean ± SEM. * p<0.05 vs. HFC; $^{\#}$ p<0.05 vs. LFD.*

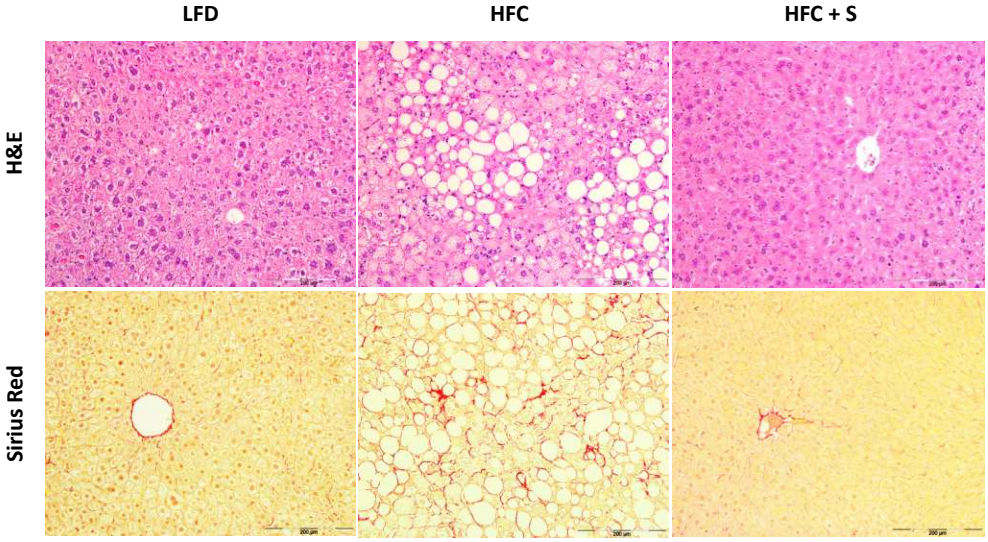

Figure 1: Histological photomicrographs of NASH in mice. Liver histological cross-sections from APOE*3Leiden.CETP mice fed a low fat diet (LFD), a high fat and high cholesterol diet (HFC) or a high fat and high cholesterol diet supplemented with salsalate (HFC+S) for 12 weeks. Upper photomicrographs: Hematoxylin and eosin (H&E); lower photomicrographs: Sirius Red staining; magnification 200x.

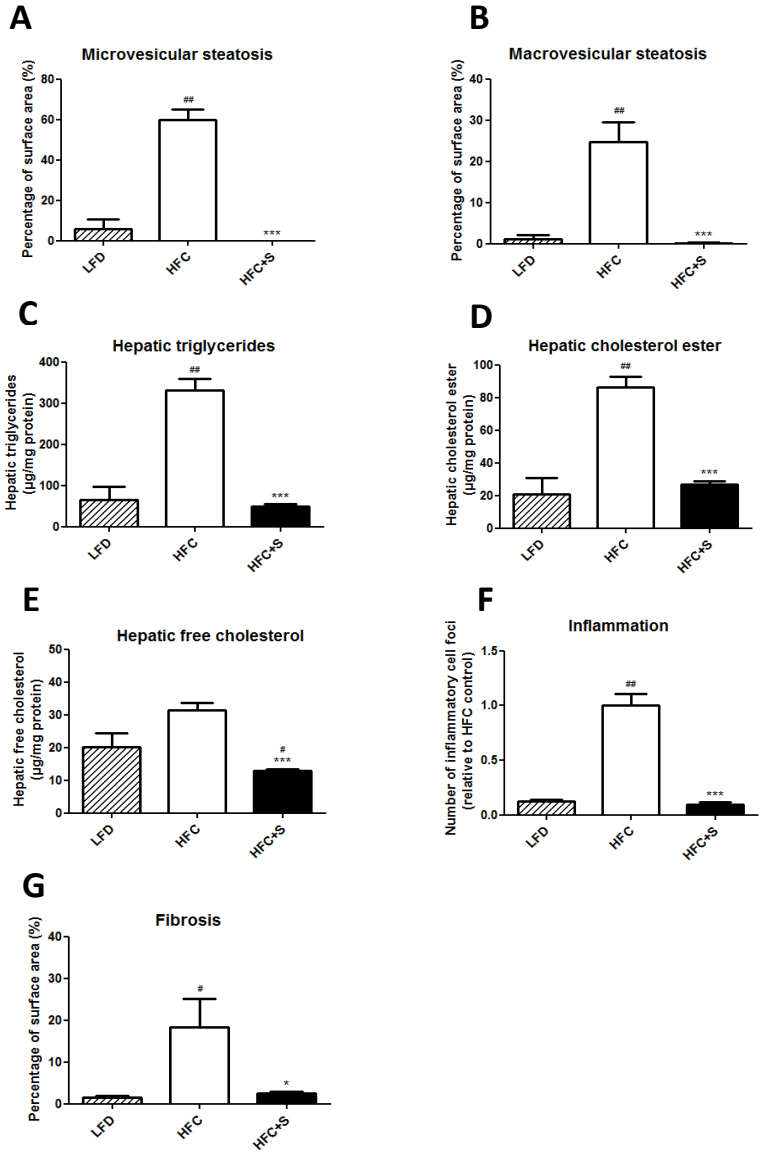

Figure 2: Hepatocellular steatosis and inflammation. Quantitative analysis of non-alcoholic steatohepatitis in APOE*3Leiden.CETP mice fed a low fat diet (LFD), a high fat and high cholesterol diet (HFC) or a high fat and high cholesterol diet supplemented with salsalate (HFC+S) for 12 weeks. Microvesicular (A) and macrovesicular (B) steatosis as percentage of total liver area, intrahepatic triglycerides (C), intrahepatic cholesterol esters (D) and intrahepatic free cholesterol (E), inflammatory foci per microscopic field (F) and fibrosis score (G) were analyzed. Data are mean ± SEM. * $p<0.05$ vs. HFC; $^{\#}$ $p<0.05$ vs. LFD.

Salsalate treatment normalized the intrahepatic lipids, resulting in significantly lower levels of hepatic triglycerides, cholesterol esters and free cholesterol as compared to the HFC group (6.7-fold, 3.2-fold and 2.4-fold decrease, respectively, all $p<0.001$). HFC feeding also induced lobular inflammation, characterized by the presence of mononuclear cells and polymorphonuclear cells that formed aggregates, while the livers of the salsalate treated mice hardly contained inflammatory aggregates (**Figure 1**). Quantification of lobular inflammation showed that the HFC feeding resulted in a significant increase in the number of aggregates as compared to the LFD control group (8.0-fold, $p<0.001$). Salsalate treatment fully blunted this HFC induced inflammation as shown by a significantly lower number of inflammatory aggregates relative to HFC group (10.2-fold decrease, $p<0.001$; **Figure 2f**). Twelve weeks of HFC feeding induced onset of fibrosis, as shown by the patches of collagen deposition (**Figure 1**; Sirius Red staining). Fibrosis evaluation according to human grading scores revealed that some fibrosis was located within perisinusoidal and periportal area for all groups (score F2 for all groups). No bridging fibrosis was seen. However, the amount of perisinusoidal fibrosis (expressed as a percentage) significantly differed between groups and was significantly reduced in the salsalate treated group as compared to HFC group (7.5-fold decrease, $p<0.05$; **Figure 2g**).

Salsalate affects expression of genes involved in lipid metabolism, inflammation and energy metabolism

To further investigate the mechanism by which salsalate affects NASH development, transcriptome analysis of liver tissue was performed. Genes that were differentially expressed in the salsalate treated group relative to the HFC control group were used for analysis of biological processes. Enrichment analysis identified seventy biological process categories that were significantly changed by salsalate. A subset of these biological process categories, including several with relevance to NASH development, is shown in **Figure 3a**. The categories 'Lipid Metabolism', 'Inflammatory Response', 'Energy Production' and 'Connective Tissue Disorders' were found to be predominanty affected by salsalate treatment. We subsequently analyzed these four processes each in more detail by performing an upstream regulator analysis that determines the activation state (z-score) of the transcription factors involved, based on the changes in expression of their target genes. For each category, the transcription factors that significantly affect a pathway and have relevance to NASH development are shown in **Table 2**. The transcriptomics analysis revealed that salsalate affected lipid metabolism by increasing β-oxidation, as shown by the activation of PPAR-α, PGC1-β and RXR-α controlled genes. Especially PPAR-α is one of the most important transcription factors in lipid metabolism and activation promotes uptake and utilization of fatty acids by upregulation of genes involved in fatty acid transport, binding and activation, and peroxisomal and mitochondrial fatty acid β-oxidation. Furthermore, salsalate inhibited lipogenesis as shown by the inhibition of MLXIPL/ChREBP, the major transcription factor for activation of triglyceride synthesis. Inflammation was evidently inhibited by salsalate, since almost all transcription factors in the inflammatory response process were found to be inactive when compared with HFC. The NFκB pathway plays a central role in NASH development and the involved transcriptional regulators were clearly inhibited by salsalate treatment.

Most of the transcription factors in energy production were activated and in general the effects of salsalate were directed at mitochondrial activation and peroxisomal and mitochondrial β-oxidation. We also performed an upstream regulator analysis for the process 'Connective Tissue Disorders', since this might provide more insight in pathways contributing to the development of hepatic fibrosis. Salsalate inhibited most transcription factors in this category, including AP-1, an important regulator of differentiation, proliferation and apoptosis. Moreover, salsalate inhibited TGF-β signaling. TGF-β stimulates the proliferation and activation of fibroblasts, which deposit connective tissue and plays an important role in fibrosis. To investigate the effects of salsalate on expression of genes pertaining to fibrosis in more detail, a pathway analysis was performed (**Figure 3bcd**). The significant expression changes upon salsalate treatment in genes belonging to generic sequence of events from liver injury to fibrogenesis are presented in Figure 3b and demonstrate the cell specific down-regulation of fibrogenic genes in the liver. More specifically, the early signaling events in hepatic stellate cells (**Figure 3c**), containing PDGF, TGF-β, IGF-1 and ET-1 and associated down-stream factors were down-regulated by salsalate. Furthermore, also in already activated stellate cells, salsalate was able to down-regulate genes involved in fibrogenesis (**Figure 3d**). All together, these expression changes unambiguously show a profound down-regulation of the fibrogenesis pathway.

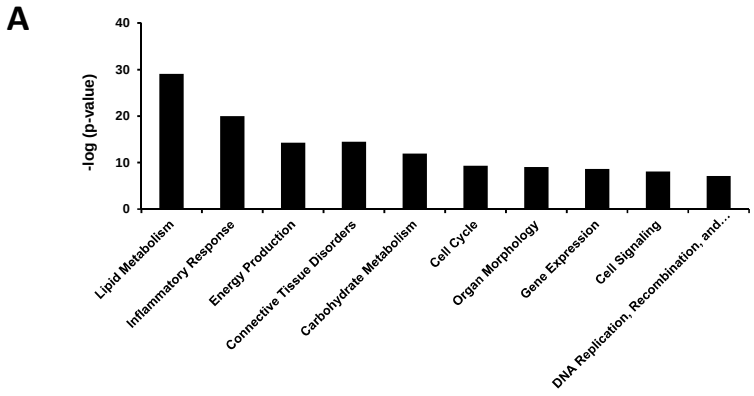

B

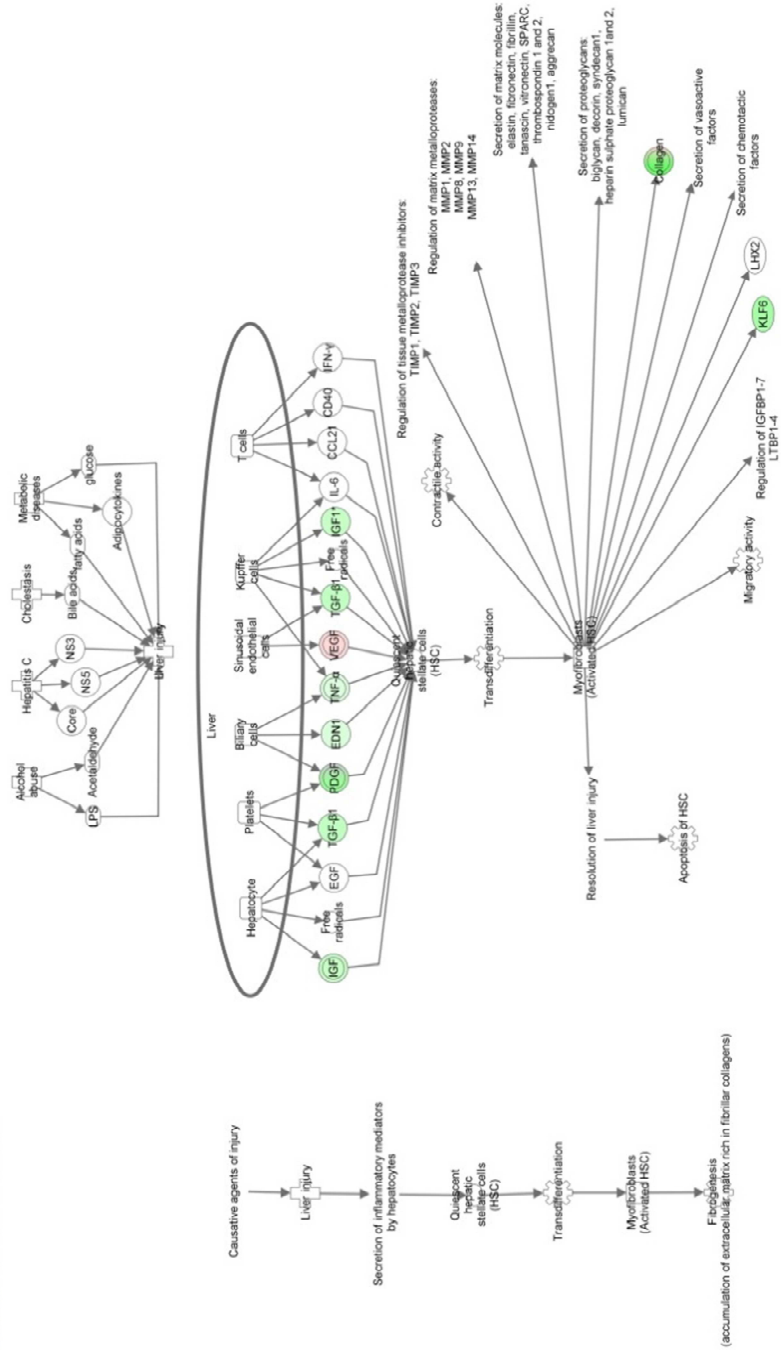
Causative agents of injury
Liver injury
Secretion of inflammatory mediators by hepatocytes
Quiescent hepatic stellate cells (HSC)
Transdifferentiation
Myofibroblasts (Activated HSC)
Fibrogenesis
(accumulation of extracellular matrix rich in fibrillar collagens)
Liver
Hepatocyte
Free radicals
IGF
EGF
Platelets
TGF-β1
Biliary cells
PDGF
EDN1
Sinusoidal endothelial cells
TNF-α
VEGF
Kupffer cells
Free radicals
TGF-β1
IGF1
IL-6
T cells
CCL21
CD40
IFN-γ
Quiescent hepatic stellate cells (HSC)
Transdifferentiation
Myofibroblasts (Activated HSC)
Resolution of liver injury
Apoptosis of HSC
Contractile activity
Migratory activity
Regulation of tissue metalloprotease inhibitors: TIMP1, TIMP2, TIMP3
Regulation of matrix metalloproteases: MMP1, MMP2 MMP8, MMP9 MMP13, MMP14
Secretion of matrix molecules: elastin, fibronectin, fibrillin, tenascin, vitronectin, SPARC, thrombospondin 1 and 2, nidogen1, aggrecan
Secretion of proteoglycans: biglycan, decorin, syndecan1, heparin sulphate proteoglycan 1and 2, lumican
Collagen
Secretion of vasoactive factors
Secretion of chemotactic factors
LHX2
KLF6
Regulation of IGFBP1-7 LTBP1-4
Liver injury
Metabolic diseases
glucose
fatty acids
Adipocytokines
Cholestasis
Bile acids
Hepatitis C
NS3
NS5
Core
Alcohol abuse
Acetaldehyde
LPS

C

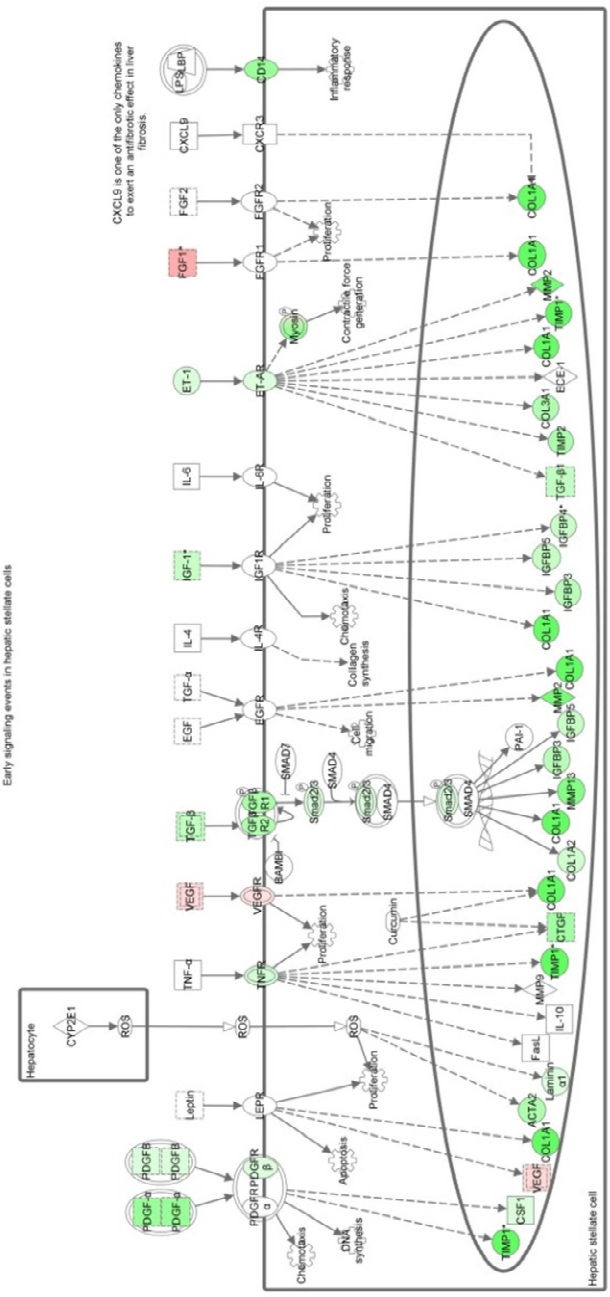
Early signaling events in hepatic stellate cells
CXCL9 is one of the only chemokines to exert an antifibrotic effect in liver fibrosis.
Hepatocyte
CYP2E1
ROS
LPS
LBP
CD14
Inflammatory response
CXCL9
CXCR3
FGF2
FGFR2
FGF1
FGFR1
Proliferation
Myosin
Contractile force generation
ET-1
ET-AR
IL-6
IL-6R
IGF-1
IGF1R
Chemotaxis
IL-4
IL-4R
Collagen synthesis
TGF-β
EGF
EGFR
Cell migration
TGFβ R2
TGFβ R1
SMAD7
Smad2/3
SMAD4
Smad2/3/4
PAI-1
BAMBI
VEGF
VEGFR
Curcumin
TNF-α
TNFR
Lectin
LEPR
Apoptosis
PDGF-A
PDGF-B
PDGFRα
PDGFRβ
PDGFB
DNA synthesis
Hepatic stellate cell
COL14A1
COL1A1
MMP2
TIMP1
COL1A1
ECE1
COL3A1
TIMP2
TGF-β1
IGFBP4
IGFBP5
IGFBP3
COL14A1
MMP2
COL14A1
IGFBP5
IGFBP3
MMP13
COL1A1
COL1A2
COL14A1
CTGF
TIMP1
MMP9
IL-10
Fas
Laminin α1
ACTA2
COL1A1
VEGF
CSF1
TIMP1

D

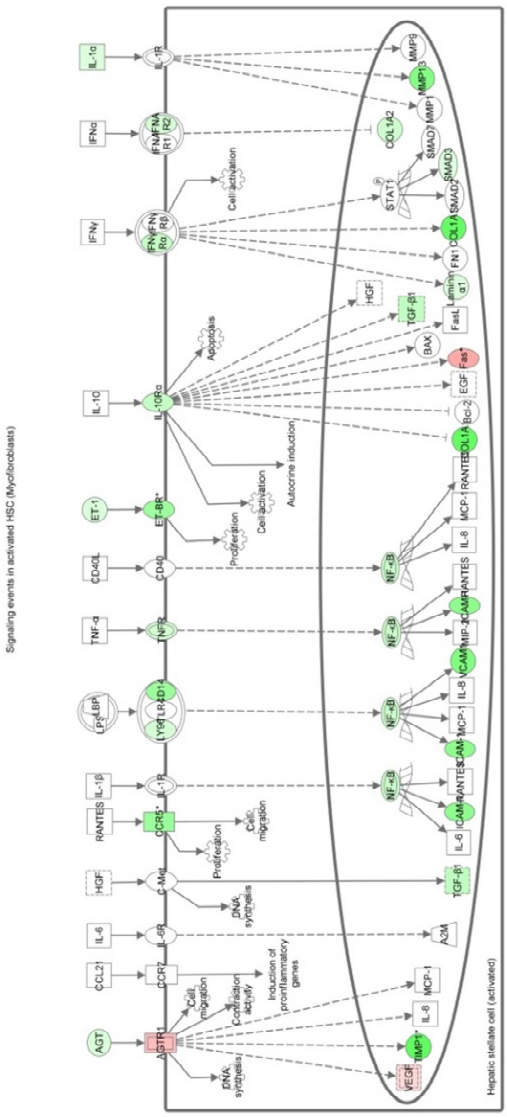

Figure 3: Enriched biological processes and hepatic fibrosis pathway analysis. A selection of significantly enriched biological processes (-log (p-value)) (A) in livers of APOE*3Leiden.CETP mice fed a high fat and high cholesterol diet supplemented with salsalate for 12 weeks relative to high fat and high cholesterol diet fed control group. Pathway analysis (B,C,D) showing statistically significant hepatic gene expression changes in hepatic fibrosis signaling upon 12 weeks of salsalate feeding in APOE*3Leiden.CETP mice fed a high fat and high cholesterol diet.

Table 2: Hepatic gene expression.

Upstream regulator	Activation z-score	p-value of overlap	Function
Lipid metabolism			
PPARA	5.567	2.65E-86	Major regulator of lipid metabolism
PPARGC1B	2.724	7.19E-11	Involved in fat oxidation
RXRA	2.417	1.93E-35	Required for PPARA transcriptional activity on fatty acid oxidation genes
ESRRA	2.215	1.73E-11	Regulator of gluconeogenesis and fatty acid metabolism
NR5A2	2.065	2.34E-08	Regulator of cholesterol and bile acid metabolism
MLXIPL	-2.194	3.82E-05	Activator of triglyceride synthesis
SERTAD2	-2.000	4.43E-04	Modulates fat storage by down-regulating adipocyte lipolysis
Inflammatory response			
NFkB (complex)	-6.676	1.40E-43	Key regulator of immune and inflammatory responses
NFKB1	-3.427	1.46E-29	DNA binding subunit of the NFkB protein complex
NFATC2	-3.313	5.31E-11	Pays a central role in inducing gene transcription during the immune response
IRF1	-3.252	1.33E-15	Regulator of immune response, apoptosis and DNA damage
NFKBIA	-3.186	4.70E-32	Inhibitor of NFkB
REL	-3.064	5.83E-12	Important role in B-cell survival and proliferation
CEBPD	-2.883	1.54E-10	Regulator of immune and inflammatory responses
RELA	-2.862	8.80E-36	Involved in NFκB heterodimer formation, nuclear translocation and activation
Nfat (family)	-2.611	1.09E-03	Family of transcription factors important in immune response
USF2	-2.567	6.67E-05	Binds to a symmetrical DNA sequence that is found in viral and cellular promoters
SQSTM1	-2.566	1.93E-06	Activator of the NFkB signaling pathway
STAT1	-2.175	4.63E-25	Important for cell viability in response to different cell stimuli and pathogens
Energy production			
PPARA	4.788	4.19E-39	Regulates the peroxisomal beta-oxidation pathway of fatty acids
INSR	4.588	1.33E-23	Insulin receptor that plays a key role in the regulation of glucose homeostasis
ESRRA	3.069	9.85E-16	Regulator of mitochondrial biogenesis and oxidative phosphorylation
PPARGC1A	2.729	6.67E-19	Regulator of mitochondrial biogenesis and function.
PPARGC1B	2.592	1.65E-08	Involved in non-oxidative glucose metabolism and energy expenditure
FOXO1	2.400	1.89E-09	Regulator of gluconeogenesis and glycogenolysis by insulin signaling
PCK1	-2.646	2.94E-13	Main control point for the regulation of gluconeogenesis
SERTAD2	-2.000	2.08E-06	Inhibitor of thermogenesis and oxidative metabolism
Connective tissue disorders			
SMAD7	2.054	9.33E-12	Inhibitor of TGF-β signaling
TGFB1	-3.838	2.90E-52	Controls cell growth, cell proliferation, cell differentiation and apoptosis
SMAD3	-2.758	1.12E-11	Regulator of TGF-β mediated transcription
STAT3	-2.558	6.13E-17	Key regulator for cell growth and apoptosis
Ap1	-2.373	2.75E-14	Regulator of differentiation, proliferation, and apoptosis

*Effect of salsalate on hepatic gene expression involved in lipid metabolism, inflammatory response, energy production and connective tissue disorders. APOE*3Leiden.CETP mice received a high fat, high cholesterol diet with or without salsalate for 12 weeks. Data represent predicted activation state (z-score) of the upstream regulators, based on the expression changes of known target genes. The overlap p-value indicates the significance of the overlap between the known target genes of a transcription factor and the differentially expressed genes measured in an experiment. Red color indicates up-regulation and green color indicates down-regulation.*

Salsalate prevents hepatic fibrosis

In a second experiment the HFC induction period of NASH was prolonged (to 20 weeks) to evaluate whether salsalate would still be able to prevent onset of NASH and liver fibrosis, also after a longer metabolic overload. Again salsalate treatment led to a significantly lower body weight, plasma insulin, cholesterol and triglycerides levels as compared the HFC control group (with -26%, -81%, -45% and -76%, respectively, all $p<0.01$; data not shown). Histological evaluation of the liver confirmed the results of the first experiment and demonstrated that salsalate attenuated NASH development in this experiment as well, also after the longer NASH induction period and at the lower dose used (**Figure 4**). Quantitative analysis showed that microvesicular steatosis and macrovesicular steatosis were significantly lower in the salsalate treated group as compared to the HFC group (with 86%, $p<0.05$ and 98%, $p<0.001$, respectively; **Figure 5ab**).

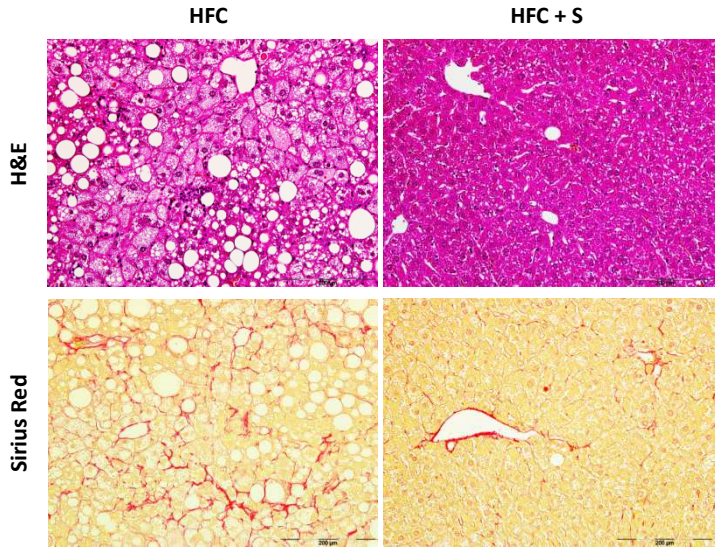

Figure 4: Histological photomicrographs of NASH in mice. Liver histological cross-sections from APOE*3Leiden.CETP mice fed a high fat and high cholesterol diet (HFC) or a high fat and high cholesterol diet supplemented with salsalate (HFC+S) for 20 weeks. Upper photomicrographs: Hematoxylin and eosin (H&E); lower photomicrographs: Sirius Red staining; magnification 200x.

Also lobular inflammation, quantified as the number of inflammatory aggregates, was significantly lower in the salsalate treated group relative to the HFC group (with -87%, $p<0.001$; **Figure 5c**). Twenty weeks of HFC feeding resulted in distinct fibrosis located in perisinusoidal/perivenular and periportal area (**Figure 4**; Sirius Red staining). In all animals at least some periportal and perisinusoidal fibrosis was seen (stage 2), but the extent of perisinusoidal fibrosis was profoundly reduced by salsalate treatment (4.1-fold decrease, $p<0.01$; **Figure 5d**). We also analyzed fibrosis quantitatively by measuring the ratio of hydroxyproline (as a measure for collagen) above proline (as a measure for total protein). The hydroxyproline/proline ratio was significantly lower (with 33%, $p<0.01$) in the salsalate treated group as compared to the HFC group (**Figure 5e**). Collectively, these data demonstrated that salsalate was able to attenuate different aspects of NASH, which are steatosis, inflammation and fibrosis.

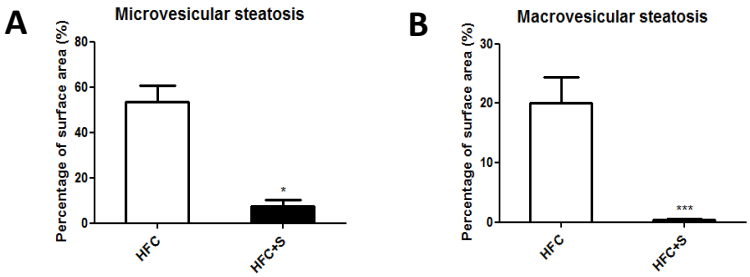

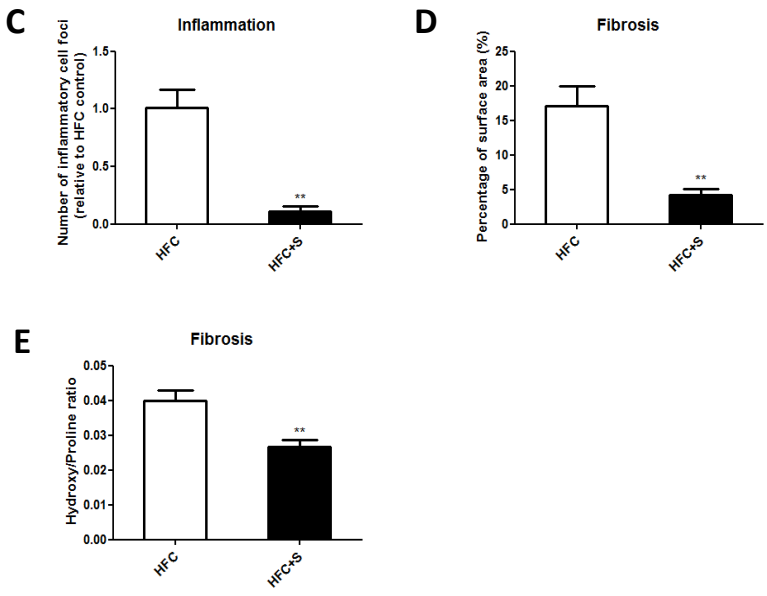

Figure 5: Hepatocellular steatosis, inflammation and fibrosis. Quantitative analysis of non-alcoholic steatohepatitis in APOE*3Leiden.CETP mice fed a high fat and high cholesterol diet (HFC) or a high fat and high cholesterol diet supplemented with salsalate (HFC+S) for 20 weeks. Microvesicular (A) and macrovesicular (B) steatosis as percentage of total liver area, inflammatory foci per microscopic field (C), percentage perisinusoidal fibrosis (D), and the hydroxyproline/proline ratio (E) were analyzed. Data are mean ± SEM. *p<0.05, **p<0.01, ***p<0.001.

DISCUSSION

In this study, we demonstrate for the first time that the treatment of obese, dyslipidemic and insulin-resistant E3L.CETP mice with salsalate markedly ameliorates diet-induced non-alcoholic steatohepatitis and reduces the development of hepatic fibrosis. Bio-informatics analysis of the gene expression data identified regulatory pathways and upstream regulators in the liver that are specifically influenced by salsalate.

Surprisingly, hardly any preclinical or animal studies have been performed to evaluate the potential of salsalate as a treatment for NASH and liver fibrosis, although its utility in the prevention or management of a wide range of vascular disorders as well as of type 2 diabetes and metabolic syndrome and NAFLD has been suggested before [23, 24]. Only one study showed that salsalate can ameliorate hepatic steatosis in rats that were fed a high fat diet [25]. In this study rats received a high fat diet for 8 weeks and the salsalate treated group received salsalate mixed in the high fat diet for an additional 6 weeks. The authors did not report whether inflammation was induced by the diet nor the effects of salsalate there upon, but the duration of the diet was probably too short in this model to induce progression from NAFLD to NASH [26]. Our results corroborate these findings and

confirm the beneficial effects of salsalate on steatosis. In addition, in our mouse model we were able to model not only steatosis, dyslipidemia and insulin resistance, but also hepatic inflammation and the natural progression of NASH to fibrosis, and we demonstrated the beneficial effects of salsalate on all these different aspects of NASH.

The mechanisms responsible for the beneficial metabolic effects of salsalate are not fully defined. The anti-inflammatory effects are believed to be attributable to inhibition of pro-inflammatory mediators such as the prostaglandins [1], but also inhibition of neutrophil activation has been reported as an alternative mechanism [27]. Inhibition of the NFκB inflammatory pathway by salsalate has been shown in several rodent studies [25, 28] as well as in humans [5]. In addition, studies in humans have shown that salsalate can increase resting energy expenditure [5, 29]. Our data support the notion that salsalate inhibits the NFκB pathway and corroborate the increase in energy metabolism. Furthermore, our data revealed an important role for PPAR-α mediated pathways with regard to the beneficial effects of salsalate on lipid metabolism.

Recent clinical studies have shown that salsalate improved inflammatory parameters, glycemica and insulin resistance in pre-diabetic and type 2 diabetic patients [6, 30]. Furthermore, a few clinical trials have been performed that investigated the impact of salsalate on vascular function [31] and currently a clinical trial is being performed that is using salsalate to target inflammation in cardiovascular disease (TINSAL-CVD study). In the latter trial, salsalate will be given for 30 months in participants with cardiovascular disease. This trial is estimated to be completed in 2015 and will provide information of the effects of salsalate in relation to NAFLD/NASH as well, since as a secondary outcome measure, the effects of salsalate on fatty liver via computerized tomography and on levels of AST and ALT will be evaluated. Although the pleiotropic effects of salsalate, i.e. anti-inflammatory effects and recently described beneficial effects on lipid and glucose metabolism, renders salsalate an excellent candidate for treatment of NASH, not many designated clinical studies have been performed that evaluate the potential beneficial effects of salsalate on NASH. To our knowledge, only one clinical study aiming to find effects of salsalate on NASH has been reported [32]. In this study salsalate did not change severity of fatty liver nor ALT and AST levels. However, the treatment period was only one month and salsalate did not affect blood glucose and triglyceride levels, while several other studies have reported significant decreases in plasma glucose and triglyceride levels upon salsalate treatment [6, 31].

In summary, we reproduced NASH development with progression to fibrosis in HFC fed APOE*3Leiden.CETP mice, a model that is characterized by obesity, metabolic anomalies and histopathological features similar to those observed in human NASH. In this model, salsalate exerted a preventive effect on the development of NAFLD and progression to steatohepatitis and fibrosis. We infer that salsalate may be pharmacologically useful for preventing the progression of steatohepatitis and fibrosis, and a promising therapeutic agent for human NASH. Further clinical studies are warranted to investigate the putative beneficial effects of salsalate on NASH in humans.

ACKNOWLEDGEMENTS

The authors gratefully acknowledge Erik Offerman and Frits van der Ham at TNO Metabolic Health Research for their help and technical assistance. This research was performed within the framework of CTMM, the Center for Translational Molecular Medicine (www.ctmm.nl), project PREDICCT. The authors thank the TNO research programs 'Personalized Prevention and Therapy - Op Maat' and 'Enabling Technology Systems Biology' for supporting this study.

REFERENCES

[1]Morris HG, Sherman NA, McQuain C, Goldlust MB, Chang SF, Harrison LI. Effects of salsalate (nonacetylated salicylate) and aspirin on serum prostaglandins in humans. Ther Drug Monit 1985;7(4):435-438.

[2]Xu XM, Sansores-Garcia L, Chen XM, Matijevic-Aleksic N, Du M, Wu KK. Suppression of inducible cyclooxygenase 2 gene transcription by aspirin and sodium salicylate. Proc Natl Acad Sci U S A 1999 Apr 27;96(9):5292-5297.

[3]Koska J, Ortega E, Bunt JC, et al. The effect of salsalate on insulin action and glucose tolerance in obese non-diabetic patients: results of a randomised double-blind placebo-controlled study. Diabetologia 2009 Mar;52(3):385-393.

[4]Goldfine AB, Fonseca V, Jablonski KA, et al. The effects of salsalate on glycemic control in patients with type 2 diabetes: a randomized trial. Ann Intern Med 2010 Mar 16;152(6):346-357.

[5]Goldfine AB, Silver R, Aldhahi W, et al. Use of salsalate to target inflammation in the treatment of insulin resistance and type 2 diabetes. Clin Transl Sci 2008 May;1(1):36-43.

[6]Goldfine AB, Fonseca V, Jablonski KA, et al. Salicylate (salsalate) in patients with type 2 diabetes: a randomized trial. Ann Intern Med 2013 Jul 2;159(1):1-12.

[7]Westerterp M, van der Hoogt CC, de Haan W, et al. Cholesteryl ester transfer protein decreases high-density lipoprotein and severely aggravates atherosclerosis in APOE*3-Leiden mice. Arterioscler Thromb Vasc Biol 2006 Nov;26(11):2552-2559.

[8]Zadelaar S, Kleemann R, Verschuren L, et al. Mouse models for atherosclerosis and pharmaceutical modifiers. Arterioscler Thromb Vasc Biol 2007 Aug;27(8):1706-1721.

[9]van den Hoek AM, van der Hoorn JW, Maas AC, et al. APOE*3Leiden.CETP transgenic mice as model for pharmaceutical treatment of the metabolic syndrome. Diabetes Obes Metab 2014 Jun;16(6):537-544.

[10]van der Hoogt CC, de Haan W, Westerterp M, et al. Fenofibrate increases HDL-cholesterol by reducing cholesteryl ester transfer protein expression. J Lipid Res 2007 Aug;48(8):1763-1771.

[11]van der Hoorn JW, de Haan W, Berbee JF, et al. Niacin increases HDL by reducing hepatic expression and plasma levels of cholesteryl ester transfer protein in APOE*3Leiden.CETP mice. Arterioscler Thromb Vasc Biol 2008 Nov;28(11):2016-2022.

[12]de Haan W, de Vries-van der Weij J, van der Hoorn JW, et al. Torcetrapib does not reduce atherosclerosis beyond atorvastatin and induces more proinflammatory lesions than atorvastatin. Circulation 2008 May 13;117(19):2515-2522.

[13]Kuhnast S, van der Hoorn JW, Pieterman EJ, et al. Alirocumab inhibits atherosclerosis, improves the plaque morphology, and enhances the effects of a statin. J Lipid Res 2014 Aug 19.

[14]Jiang XC, Agellon LB, Walsh A, Breslow JL, Tall A. Dietary cholesterol increases transcription of the human cholesteryl ester transfer protein gene in transgenic mice. Dependence on natural

flanking sequences. J Clin Invest 1992 Oct;90(4):1290-1295.
[15]van den Maagdenberg AM, Hofker MH, Krimpenfort PJ, et al. Transgenic mice carrying the apolipoprotein E3-Leiden gene exhibit hyperlipoproteinemia. J Biol Chem 1993 May 15;268(14):10540-10545.
[16]Kleiner DE, Brunt EM, Van Natta M, et al. Design and validation of a histological scoring system for nonalcoholic fatty liver disease. Hepatology 2005 Jun;41(6):1313-1321.
[17]Liang W, Lindeman JH, Menke AL, et al. Metabolically induced liver inflammation leads to NASH and differs from LPS- or IL-1beta-induced chronic inflammation. Lab Invest 2014 May;94(5):491-502.
[18]Tiniakos DG, Vos MB, Brunt EM. Nonalcoholic fatty liver disease: pathology and pathogenesis. Annu Rev Pathol 2010;5:145-171.
[19]Bank RA, Krikken M, Beekman B, et al. A simplified measurement of degraded collagen in tissues: application in healthy, fibrillated and osteoarthritic cartilage. Matrix Biol 1997 Nov;16(5):233-243.
[20]Du P, Kibbe WA, Lin SM. lumi: a pipeline for processing Illumina microarray. Bioinformatics 2008 Jul 1;24(13):1547-1548.
[21]Smyth GK. Linear models and empirical bayes methods for assessing differential expression in microarray experiments. Stat Appl Genet Mol Biol 2004;3:Article3.
[22]Verschuren L, Wielinga PY, Kelder T, et al. A systems biology approach to understand the pathophysiological mechanisms of cardiac pathological hypertrophy associated with rosiglitazone. BMC Med Genomics 2014 Jun 17;7:35-8794-7-35.
[23]McCarty MF. Salsalate may have broad utility in the prevention and treatment of vascular disorders and the metabolic syndrome. Med Hypotheses 2010 Sep;75(3):276-281.
[24]McCarty MF. Full-spectrum antioxidant therapy featuring astaxanthin coupled with lipoprivic strategies and salsalate for management of non-alcoholic fatty liver disease. Med Hypotheses 2011 Oct;77(4):550-556.
[25]Jung TW, Youn BS, Choi HY, et al. Salsalate and adiponectin ameliorate hepatic steatosis by inhibition of the hepatokine fetuin-A. Biochem Pharmacol 2013 Oct 1;86(7):960-969.
[26]Xu ZJ, Fan JG, Ding XD, Qiao L, Wang GL. Characterization of high-fat, diet-induced, non-alcoholic steatohepatitis with fibrosis in rats. Dig Dis Sci 2010 Apr;55(4):931-940.
[27]Altman RD. Neutrophil activation: an alternative to prostaglandin inhibition as the mechanism of action for NSAIDs. Semin Arthritis Rheum 1990 Feb;19(4 Suppl 2):1-5.
[28]Murthy SN, Desouza CV, Bost NW, et al. Effects of salsalate therapy on recovery from vascular injury in female Zucker fatty rats. Diabetes 2010 Dec;59(12):3240-3246.
[29]Meex RC, Phielix E, Moonen-Kornips E, Schrauwen P, Hesselink MK. Stimulation of human whole-body energy expenditure by salsalate is fueled by higher lipid oxidation under fasting conditions and by higher oxidative glucose disposal under insulin-stimulated conditions. J Clin Endocrinol Metab 2011 May;96(5):1415-1423.
[30]Faghihimani E, Aminorroaya A, Rezvanian H, Adibi P, Ismail-Beigi F, Amini M. Reduction of insulin resistance and plasma glucose level by salsalate treatment in persons with prediabetes. Endocr Pract 2012 Nov-Dec;18(6):826-833.
[31]Goldfine AB, Conlin PR, Halperin F, et al. A randomised trial of salsalate for insulin resistance and cardiovascular risk factors in persons with abnormal glucose tolerance. Diabetologia 2013 Apr;56(4):714-723.
[32]Faghihimani E, Amini M, Adibi A, Naderi Z, Toghiani A, Adibi P. Evaluating the efficacy of Salsalate on prediabetic and diabetic patients with fatty liver: A randomized clinical trial. J Res Pharm Pract 2013 Jan;2(1):40-43.

SUPPLEMENTARY DATA

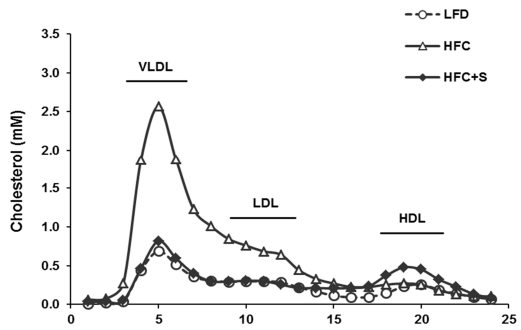

Supplemental Figure 1: Lipoprotein profile. Lipoprotein profiles of APOE*3Leiden.CETP mice a low fat diet (LFD), a high fat and high cholesterol diet (HFC) or a high fat and high cholesterol diet supplemented with salsalate (HFC+S) for 12 weeks. The distribution of cholesterol over the individual lipoprotein profiles in pooled plasma was determined after separation of lipoprotein profiles by FPLC.

COORDINATED AND INTERACTIVE EXPRESSION OF GENES OF LIPID METABOLISM AND INFLAMMATION IN ADIPOSE TISSUE AND LIVER DURING METABOLIC OVERLOAD

Wen Liang*
Giulia Tonini*
Petra Mulder
Thomas Kelder
Marjan van Erk
Anita M. van den Hoek
Rob Mariman
Peter Y. Wielinga
Michela Baccini
Teake Kooistra
Annibale Biggeri
Robert Kleemann

* Both authors contributed equally

PLoS One 2013; 8(9):e75290

ABSTRACT

Background: Chronic metabolic overload results in lipid accumulation and subsequent inflammation in white adipose tissue (WAT), often accompanied by non-alcoholic fatty liver disease (NAFLD). In response to metabolic overload, the expression of genes involved in lipid metabolism and inflammatory processes is adapted. However, it still remains unknown how these adaptations in gene expression in expanding WAT and liver are orchestrated and whether they are interrelated.

Methodoloy/Principal Findings: ApoE*3Leiden mice were fed HFD or chow for different periods up to 12 weeks. Gene expression in WAT and liver over time was evaluated by micro-array analysis. WAT hypertrophy and inflammation were analyzed histologically. Bayesian hierarchical cluster analysis of dynamic WAT gene expression identified groups of genes ('clusters') with comparable expression pattern over time. HFD evoked an immediate response of five clusters of 'lipid metabolism' genes in WAT, which did not further change thereafter. When the storage capacity of WAT became exceeded (>6 weeks), inflammatory clusters were induced. Promoter analysis of clustered genes resulted in specific key regulators which orchestrate the metabolic and inflammatory responses in WAT. Some master regulators played a dual role in control of metabolism and inflammation. When WAT inflammation developed (>6 weeks), genes of lipid metabolism and inflammation became also affected in corresponding livers. These hepatic gene expression changes and, in particular the underlying transcriptional responses, were remarkably similar to those detected in WAT.

Conclusion: In WAT, metabolic overload induced an immediate, stable response on clusters of lipid metabolism genes and induced inflammatory genes later in time. Both processes were controlled and interlinked by specific transcriptional regulators. When WAT inflammation began, the hepatic response to HFD resembled that in WAT. In all, WAT and liver respond to metabolic overload by adaptations in expression of gene clusters controlling lipid metabolism and inflammatory processes in an orchestrated and interrelated manner.

INTRODUCTION

The obesity epidemic has become the most important nutritional problem worldwide. The increasing prevalence of obesity has been ascribed to excessive and unhealthy eating and reduced physical activity [1] and carries with it increased risks for type 2 diabetes (T2DM) and non-alcoholic fatty liver disease (NAFLD) [2-4]. Notably, the existence of metabolic pathways that allow excess energy to be stored as fat suggests that obesity may realistically be viewed as a biological adaptation in times of energy surplus. However, in case of prolonged excess energy supply white adipose tissue (WAT) capacity may exceeded [5, 6] and the liver may serve as an alternative depot for free fatty acids [7, 8]. The resulting metabolic overload of the expanding WAT and subsequently liver is accompanied by local metabolic stress and triggers tissue inflammation [9].

Several studies in mice have demonstrated that the expression of genes of lipid metabolism and inflammation is adjusted in several organs in response to chronic high-fat diet (HFD) feeding [10-12]. These studies are often static and focus on a single organ which is analyzed at one particular time point, typically at a later stage in the disease process when histopathological effects of HFD can be detected (e.g. crown-like structures in WAT, inflammatory gut, hepatic steatosis). Accordingly, many gene expression studies and sophisticated microarray analyses link late stage histological outcomes to gene expression changes of the same (late) time point. However, significant effects on gene expression are likely to start early and change over time. Hence, there is limited understanding of the early events in expanding WAT and in what way lipid metabolism is related to the onset of inflammation during obesity development. Some studies investigated the expression changes of individual inflammatory genes and pathways over time [13-15], but they did not explore whether groups of genes ('gene clusters') change in concert and thus do not provide insight into the global adaptations and possible common transcriptional regulation of clustered genes.

Bayesian hierarchical cluster analysis [16] allows global analysis of dynamic gene expression data of thousands of genes simultaneously to find patterns in the data that are not predicted by the experimenter's current knowledge or preconceptions. For instance, complex gene expression time series can be analyzed to identify genes with similar expression patterns that group into clusters because of common transcriptional regulation. Cluster analysis of the expanding WAT requires dynamic high-quality microarray datasets with multiple early time points, which are scarce [13]. In the present study we investigated two important processes in WAT expansion using cluster analysis: the global adjustment of genes of 'lipid metabolism' and the induction of 'inflammatory genes', and their interrelationship. Because transcriptional control mechanisms are instrumental for adjustment of lipid metabolism as well as inflammatory gene expression [17], we examined whether the genes of the identified clusters share common transcriptional regulation, viz. via key master regulators.

Metabolic overload of WAT upon HFD feeding is, at a later stage, supposed to be accompanied by multiple metabolic and inflammatory effects in the liver [7]. It is presently unknown whether the effects on genes of metabolism and inflammation are similar to WAT and, if so, whether the same master regulators are involved.

WAT and liver tissues and corresponding dynamic genomics datasets from a 12- week HFD feeding experiment [13] in APOE*3Leiden transgenic mice were used. APOE*3Leiden mice have a humanized lipoprotein metabolism and develop obesity, insulin resistance and NAFLD during HFD feeding [18-20]. Bayesian cluster analysis in conjunction with promoter analysis and biochemical measurements showed that adjustment of lipid metabolism and onset of inflammation in WAT occurs sequentially and is orchestrated by specific master regulators that also control comparable changes in lipid metabolism and inflammation in the liver later in time.

MATERIALS AND METHODS

Mouse study and micro-array data

Tissues and micro-array data from a larger time course study in APOE*3Leiden mice in the context of HFD-induced insulin resistance were used [13]. These micro-array datasets (liver and WAT) are freely available on ArrayExpress at the following URL http://www.ebi.ac.uk/arrayexpress/experiments/E-TABM-1039/. Animal experiments were approved by the Institutional Animal Care and Use Committee of The Netherlands Organization for Applied Scientific Research (TNO), and were in compliance with European Community specifications regarding the use of laboratory animals as reported [13]. Briefly, 12 weeks old mice were fed HFD containing (all w/w) 24% fat from beef tallow (of which 12% saturated fatty acids), 24% casein and 20% dextrose (diet number 4031.05; Hope Farms, Woerden, The Netherlands; metabolizable energy: 19.4 MJ/kg; exact diet composition is provided in Table S1) for 12 weeks [13]. Mice were sacrificed at t=0 and after 1, 6, 9 and 12 weeks of HFD feeding (n=15/group). Epididymal adipose tissue and corresponding livers of a subset of animals (n=8) per time point were used for microarray analysis. Our present data are from this subset of animals. A separate control group (n=6) was fed chow (sniff® R/M-H; metabolizable energy: 12.8 MJ/kg; Sniff Spezialdiäten GmbH, Soest, Germany) for the entire study period and served as a reference for the effect of aging.

Histological analysis of tissues

Paraffin-embedded sections of adipose tissue and liver were used for (immuno)histological examination [13]. Liver tissue sections were 5 µm thick and stained with hematoxylin phloxine saffron (HPS). Non-alcoholic fatty liver disease was analyzed as described [21] and vacuolization (micro- and macrovaculolization) and hepatocellular hypertrophy were scored. Sections of epididymal adipose tissue were prepared following a similar procedure [22] and stained with HPS for computer-assisted morphological assessment of adipocyte size and analysis of macrophage accumulation in crown-like structures essentially as reported [20]. CCR2 positive cells were detected using antibody (Abcam ab21667, Cambridge, UK).

Microarray data analysis and Bayesian hierarchical clustering

Quality control analyses and specific protocols for RNA extraction, RNA integrity assessment, and microarray data processing were reported previously [13, 23]. Briefly,

quality control of microarray data was performed using BioConductor packages including simpleaffy and affyplm, through the NuGO pipeline that is available as a Genepattern procedure on http://nbx2.nugo.org [24]. Thirty-eight adipose tissue samples passed the quality control criteria and raw signal intensities (from CEL files) were normalized using the GCRMA algorithm (gc-rma slow). Probesets were remapped and annotated into Entrez gene-ids using the custom MBNI CDF-file, version 9.0.1. The final dataset contained the expression values of 12492 adipose tissue genes represented by unique Entrez gene-ids [25]. Expression data were logtransformed for further analysis of gene expression levels. Microarray gene expression data were confirmed by quantitative real-time PCR for a selection of genes using established protocols and primer/probe sets [13].

For this study, two sets of genes with either lipid metabolism ontology (n=235) or inflammation ontology (n=216) were defined. These genes were differentially expressed at one or more time points ($q<0.05$ ANOVA) and are listed in Table S2. The time course expression data of these genes was subjected to Bayesian hierarchical clustering to structure the data and identify distinct clusters of genes with comparable expression profiles [26].

Gene enrichment analysis

Changes in gene expression were visualized using GeneSpring GX version 10.0 (Agilent Technologies, Santa Clara, CA, USA) and this tool was also used to show the identified gene clusters. An enrichment analysis was performed for the gene lists of each cluster using the DAVID functional enrichment tool [27]. Default settings for enrichment analysis in DAVID were used. The total list of genes was used as input and the most enriched functional gene sets (based on Gene Ontology 'protein domains and pathways') are reported. These functional gene sets contain at least three genes from a particular gene cluster and are more enriched in the cluster than in the input data set (% genes in cluster ≥ 1.3 x % genes in input gene list).

To define the transcription factors that are responsible for control of a particular cluster of genes, the genes of each cluster were subsequently analyzed in Bibliosphere (Genomatix GmbH, Munich, Germany) with respect to a) shared transcription factor binding sites in their promoter regions and b) co-citation analysis (level B2, co-citation restricted to sentences with a function word). Promoters were defined as 500 bp upstream and 100 bp downstream of the Transcription Start Site of the gene transcript. Default settings of the software were used to perform an overall analysis of the promoters of the genes for common transcription factors. The following criteria were used to define the key transcription factors: a) the transcription factor binding sites have to be present in at least three genes of a cluster and b) are more frequently found in the genes belonging to the cluster of interest than in the total list of input genes (%genes in cluster ≥ 1.3 x % genes in input gene list).

Comparison of gene expression changes in adipose tissue and liver

Liver and white adipose tissue (WAT) were compared with respect to differentially expressed genes (DEGs relative to the zero time point) and Venn diagrams were prepared to illustrate overlapping genes. A cutoff of FDR P-value < 0.05 was used to define DEGs in both tissues.

The upstream regulator analysis function of Ingenuity Pathway Analysis (IPA) software and the Ingenuity knowledge base were used to analyze the relationship between upstream transcription factors and expression changes of target genes. To test whether a particular transcription factor identified in WAT was also involved in the liver, we analyzed the hepatic transcriptome for differentially expressed target genes of this transcription factor. A P-value $P<0.05$ indicated that more liver target genes were differentially expressed than expected by chance. Ingenuity Pathway Analysis was also used to test whether a particular transcription factor is activated (positive Z-score >2) or inhibited (negative Z-score <-2) based on the direction of gene expression changes of its target genes.

Transcription factor analysis

Biochemical transcription factor activity was determined in liver homogenates essentially as previously described [13, 28], using TransAM® kit Hnf4α (no. 46296, Active Motif Europe, Rixensart, Belgium). Briefly, liver homogenates were prepared using the Nuclear Extract Kit (no. 40010, Active Motif, Rixensart, Belgium). Equal amounts of protein (10 µg/well) of the liver homogenates were used to determine the amount of active transcription factor. Control tissues of reference mice on chow were used to correct for the effect of aging.

RESULTS

*HFD feeding of APOE*3Leiden mice results in obesity and onset of white adipose tissue inflammation*

APOE*3Leiden mice had an average body weight of 29.2 ± 2.6 g at the start of the experiment (t=0). Animals became obese during HFD feeding and gradually gained 8.30 ± 2.0 g of weight during the experimental period of 12 weeks (**Figure 1A**) while body weight of control mice on chow remained stable (0.23 ± 0.63 g weight gain; not shown). The daily energy intake per mouse was comparable between the groups fed HFD (15.0 ± 0.9 kcal/day) and chow (14.6 ± 3.0 kcal/day). The HFD-evoked increase in body weight was accompanied by an increase in WAT mass as exemplified by epididymal fat mass (**Figure 1B**). Histological analysis of epididymal WAT revealed a significant increase in adipocyte size upon HFD feeding relative to chow-fed controls (4431 ± 140 versus 1665 ± 310 μm^2; $P<0.005$) demonstrating adipocyte hypertrophy during fat accumulation and obesity development (**Figure 1C/1D**). In HFD fed mice, immune cells accumulated in WAT at 12 weeks and first crown-like structures were observed (**Figure 1C/1E**) pointing to an onset of WAT inflammation. Immunochemical analysis demonstrated that accumulating cells in HFD-treated mice were Ccr2-positive (**Figure 1E**) while Ccr2-positive cells were hardly found in age-matched chow control mice. Together, these data demonstrate that 12 weeks of HFD feeding in ApoE*3Leiden mice resulted in metabolic changes (lipid storage and hypertrophy) as well as onset of WAT inflammation.

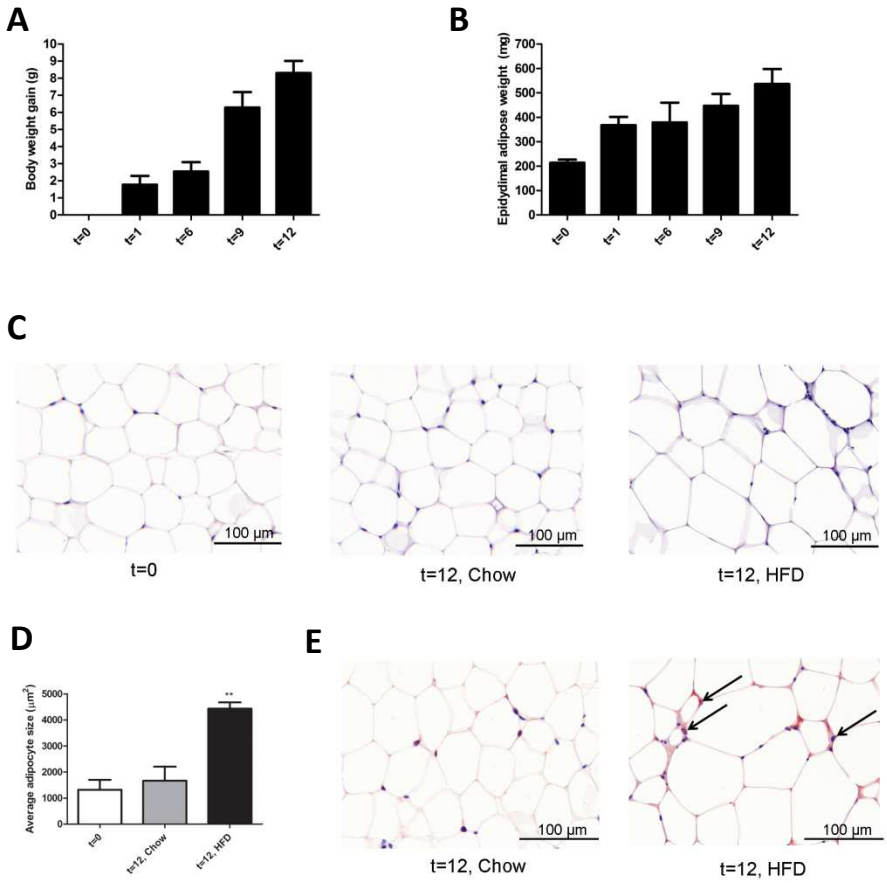

Figure 1: HFD feeding leads to obesity and onset of adipose tissue inflammation. APOE*3Leiden transgenic mice were fed a HFD for 12 weeks and sacrificed at the time points indicated. The average body weight at the start (t=0) of HFD feeding was 29.2 g. A, Body weight gain over time. B, Mass of the epididymal adipose tissue depot during obesity development. Data are presented as mean ± SEM. C, Histological analysis of adipose tissue at start (t=0) and after 12 weeks of HFD or chow feeding (reference for the effect of aging). D, HFD feeding results in adipocyte hypertrophy. Computer-assisted quantification of average adipocytes size ($P<0.05$). E, Marked accumulation of CCR2 positive cells (arrows) in the HFD fed group.

Identification of genes with a similar time profile during HFD feeding

To gain insight into the global effects of HFD feeding on metabolism and inflammation in WAT, two sets of genes (i.e. 235 genes with 'lipid metabolism ontology' and 216 genes with 'inflammation ontology' as defined in Table S2 and Methods) were subjected to Bayesian hierarchical clustering analysis. In this analysis, the individual genes were

grouped into gene clusters based on a concerted dynamical expression over time. Genes with a comparable expression pattern across time grouped into specific clusters: Six clusters of lipid metabolism genes (**Figure 2**) and four clusters of inflammatory genes (**Figure 3**) were defined. Each cluster showed a distinct and specific time profile suggesting that genes within a cluster share common transcriptional regulation.

Overall, HFD feeding had an early effect on the genes of lipid metabolism and most gene expression changes already occurred within the first week. The majority of the genes of 'lipid metabolism' clustered in cluster B and C (165 out of 235). After a slight adjustment in gene expression in week 1, these genes hardly changed over time (**Figure 2**). The expression changes were somewhat more pronounced in other lipid gene clusters (A, D, E and F), but the main effect also occurred in the first week. It is striking that most 'lipid metabolism' genes are rapidly adjusted in the first week and do not adapt to any further extent at the later time points, even when WAT hypertrophy and inflammation are developing. **Table 1** shows that the genes of clusters with somewhat more dynamic expression patterns can be assigned to specific biological processes (gene enrichment analysis). For instance, the genes of cluster A were associated with sphingolipid and ceramide metabolism.

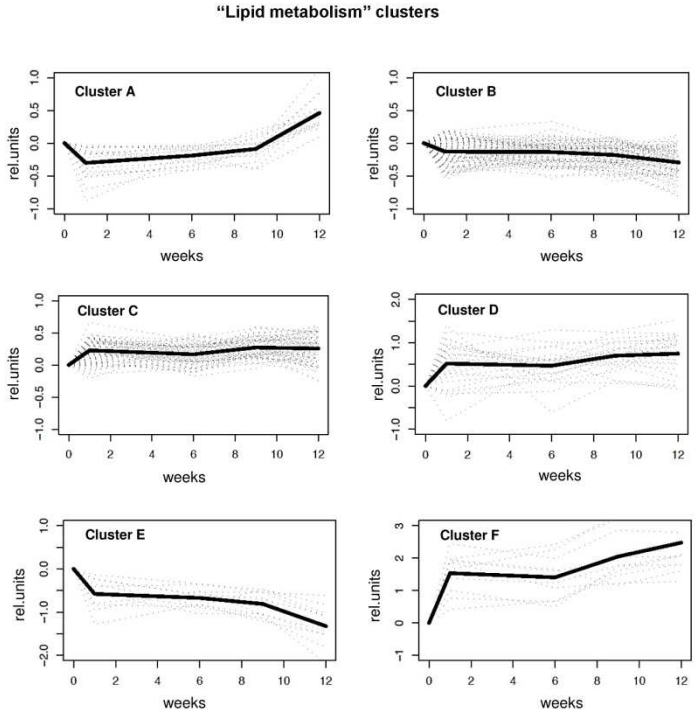

Figure 2: Cluster analysis of genes of lipid metabolism. Bayesian cluster analysis of genes with 'lipid metabolism' gene ontology resulted in 6 clusters (A, B, C, D, E, and F) with distinct time profiles. Individual gene expression profiles are shown as dotted lines. The bold line represents the cluster average.

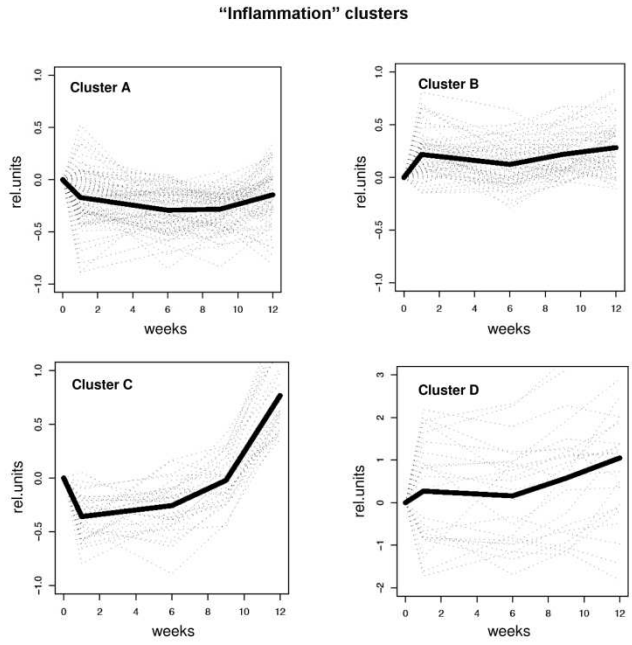

Figure 3: Cluster analysis of inflammatory genes. Bayesian cluster analysis of genes with 'inflammation' gene ontology resulted in 4 clusters A, B, C and D with distinct time profiles. Individual gene expression profiles are shown as dotted lines. The bold line represents the cluster average.

In contrast to the genes involved in lipid metabolism, the mRNA expression level of inflammatory genes increased markedly after week 6 (inflammation clusters C and D in **Figure 3**). This suggests that factors encoded by these genes may reflect or contribute to the observed onset of WAT inflammation. Indeed, among the upregulated genes were the complement factors C1qa, C1qb, C1qc, C3a receptor-1 and C5a receptor-1, the cytokines Cxcl1/KC, Ccl5/Rantes, Ccl6, Ccl7/Mcp3 and Ccl9/Mrp2, the inflammation markers orosomucoid-1, orosomucoid-3, granzyme A and neutrophil cytosolic factor 1 (Nrf1/p47/phox), the macrophage-associated markers CD11b/Mac1, CD11c, CD18/integrin beta-2, the inflammasome component ASC and the chemokine CXC motive receptor-2 (Ccr2), which is consistent with the observed accumulation of Ccr2-positive cells. Gene enrichment analysis confirmed that these genes belong to processes that promote WAT inflammation such as leukocyte mediated immune response, cytokine activity, complement activation, acute inflammatory response, and cell adhesion (**Table 2**). Some of the genes encode for inflammatory factors that can be secreted into plasma and may promote inflammation in other tissues.

Prediction of transcription factors that control the WAT response to HFD feeding

To identify transcription factors that can orchestrate the observed changes in gene expression profiles in WAT, we analyzed the promoter regions of clustered genes to identify putative common (shared) transcriptional regulators (last column of **Tables 1 and 2**). Transcriptional binding sites for Jun, Sp1, Stat1, Nfκb and Pparγ were frequently identified in the promoter regions of the 'lipid metabolism' genes in cluster A, i.e. the genes that are related to sphingolipid and ceramide metabolism. Srebf1, Srebf2, Pparγ and Hnf4α were identified as common regulators of the 'lipid metabolism genes' of cluster F. Transcriptional master regulators of the inflammatory genes in cluster D are Pparγ, Sfpi1, Stat6 (cluster C), and Sp1, Fos, Vdr, Esr1, Creb1, Gata1, Smad2 (**Table 2**).

Table 1: Genes of lipid metabolism with dynamic changes over time. Only the genes of cluster A, D, E and F show dynamic changes in expression during the study period. The pattern of the expression changes is described in the second column. Gene clusters are associated with specific biological processes (obtained by gene enrichment analysis) and clustered genes share common transcriptional regulators. These common transcription factors were predicted by promoter analysis and are listed in the last column.

Cluster	Pattern of time profile	Enrichment analysis of biological processes	TF
Cluster A: 20 genes	slight decrease in week 1;	Sphingolipid metabolic process	Jun
	slight increase > week 9	Ceramide metabolic process	Sp1
			Stat1
			Nfκb1
			Pparγ
Cluster D: 29 genes	slight increase in week 1	Steroid biosynthetic process	Pparα
		Cholesterol biosynthetic process	Nfκb1
		Cholesterol metabolic process	Pparγ
		Isoprenoid metabolic process	
		Oxidoreductase activity	
Cluster E: 11 genes	Continuous decrease	Steroid metabolic process	Esr1
		Hormone metabolic process	Stat5β
		Reproduction	
		Oxidoreductase activity	
Cluster F: 10 genes	pronounced increase in	Cholesterol absorption	Srebf2
	week 1, then slight increase	Cholesterol metabolic process	Nr1h2
		PPAR signaling pathway	Pparγ
		Lipid binding	Srebf1
		Lipid transport	Hnf4α
		Lipoprotein metabolic process	Sp1
		Glucose metabolic process	Nr1h3
			Nr5a1

Table 2: Inflammatory genes with dynamic changes over time. The genes of cluster C and D are characterized by dynamic changes in expression during HFD feeding. The pattern of the expression changes is described in the second column. Gene clusters are associated with specific biological processes (obtained by gene enrichment analysis) and clustered genes share common transcriptional regulators. Common transcription factors (TF) predicted by promoter analysis are provided in the last column.

Cluster	Description	Enriched processes	TF
Cluster C: 34 genes	slight decrease in first week; pronounced increase >week 8	Inflammatory response; Leukocyte mediated immune response; Cytokine activity; Extracellular region; B cell mediated immunity; Complement activation	Pparγ Sfpi1 Stat6 Pax5 Etv6 Pparα
Cluster D: 25 genes	slight increases early in time; pronounced increase >week 6	Inflammatory response; Acute inflammatory response; Extracellular space; Cytokine activity; T cell proliferation; Cell adhesion	Sp1 Fos Creb1 Myc Vdr Rarα Esr1 Ar Gata1 Smad2

Of note, some transcription factors like Pparγ, Esr1 and Sp1 have a dual role and regulate the expression of genes involved in lipid metabolism *and* inflammatory genes indicating that these transcription factors operate at the interface of metabolism and inflammation which are thus molecularly interlinked at the level of transcription.

Key regulators predicted in WAT are also involved in altered liver gene expression

The livers of the same mice used for the above WAT analysis were examined histologically and using microarrays. **Figure 4** shows that HFD feeding but not chow feeding resulted in pronounced micro- and macrovacuolization as well as hepatocellular hypertrophy, demonstrating onset of NAFLD at 12 weeks. Analysis of hepatic gene expression revealed that the genes of lipid metabolism and inflammatory genes were hardly affected until week 6 but thereafter (**Figure 5A/5B**). To evaluate whether this response to HFD feeding is related to the effects observed in WAT, we compared the gene expression changes in both tissues over time.

Until week 6, only a few differentially expressed genes were found in both tissues, but the number and percentage of common genes (see intersections of **Figure 5A and 5B**) strongly increased in week 9 and 12, i.e. when WAT becomes overloaded and expression of inflammatory genes of cluster C is observed. Together, these data are in line with the

concept that WAT serves as a first buffer to cope with metabolic overload and that the hepatic response is delayed and resembles that of WAT when the storage capacity of WAT is exceeded [5, 6]. At week 12, more than 50% of the liver genes with 'lipid metabolism' or 'inflammation' ontology are also affected in WAT. Analysis of all DEGs irrespective of their ontology confirms the relationship between both tissues (245 genes in intersection, 484 liver-specific, 784 WAT-specific in week 12; data not shown).

At the level of transcriptional regulators, the response of both tissues was even more comparable as demonstrated by Bayesian clustering analysis and, as an alternative approach, analysis of target genes. Cluster analysis showed that the gene expression changes until week 9 were modest in liver in comparison with WAT (Figure S1). Similar to WAT, some clusters showed an immediate response to HFD and gene expression did not further change thereafter. Lipid metabolism gene cluster D in the liver had a comparable profile to cluster F of WAT and the predicted transcriptional regulators (Pparγ, Nr1h2, Srebf2, Hnf4α, Nr1h3) were the same. The predicted transcriptional regulators for the inflammatory genes of cluster C in the liver (Ar, Creb1, Esr1, Fos, Myc, Pparγ, Rarα, Sfpi1, Stat6) also overlapped with those predicted for inflammatory genes in WAT.

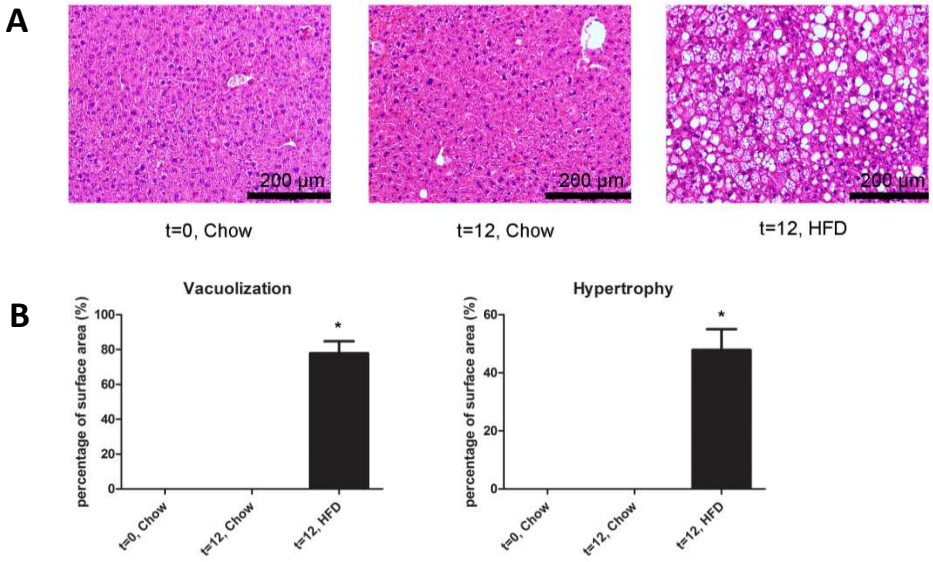

Figure 4: Histological analysis of livers. Hallmarks of non-alcholic fatty liver disease were scored in the livers of the mice that were used for WAT analysis. A, Representative photomicrographs of liver cross-sections after 12 weeks of HFD shows pronounced liver steatosis characterized by micro- and macrovacuolization and hepatocellular hypertrophy. B, Quantitative analysis of total vacuolization and hypertrophy. Data are presented as mean ± SEM. *P<0.05.

In addition to this, we analyzed the target genes of the master regulators predicted in WAT and tested whether they were differentially expressed in the liver. Statistical testing

of the effect on target gene expression showed that the transcription factors Hnf4α, Esr1, Fos, Myc, Pparα, Pparγ, Srebf1 and Srebf2 affected their target genes significantly (all P<0.05), and Creb1 and Jun with borderline significance (P=0.07). Biochemical analysis of the transcriptional binding activity of Hnf4α in liver protein homogenates confirmed its activation (**Figure 5C**). Of note, a particular transcription factor may affect a different set of genes in WAT and the liver as illustrated in **Figure 5D** for Srebf2.

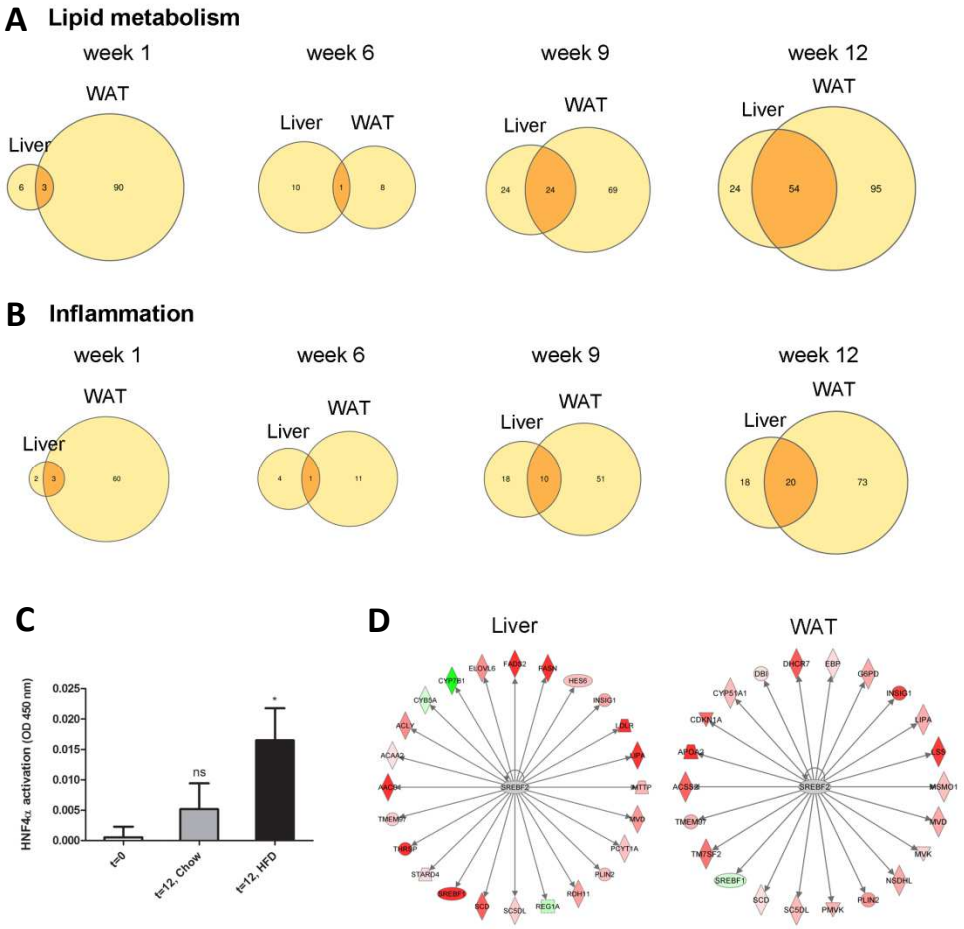

Figure 5: Comparison of gene expression in liver and WAT over time and analysis of transcriptional regulators. Venn diagrams of genes with A, 'lipid metabolism' gene ontology or B, 'inflammation' gene ontology. Time course analysis of the genes that were differentially expressed genes at a particular time point. The intersection represents the number of 'overlapping genes', ie. genes that were affected in both tissues. C, Quantitative analysis of the transcriptional activity of HNF4α by TransAM analysis at t=0 and t=12 weeks of HFD feeding relative to reference mice on chow to correct for aging. *P<0.05. D, Differentially expressed target genes of Srebf2 in WAT and liver. Srebf2 is significantly involved in the control of target genes (P<0.05 for both WAT and liver). In both tissues, the calculated Z-score was positive (3.7 for liver and 4.3 for WAT) indicating that Srebf2 is activated. Genes colored in red (green) are upregulated (downregulated).

Overall, the gene expression effects evoked by HFD in WAT and liver become increasingly comparable showing similar transcriptional responses in both tissues. This indicates that the factors that sense metabolic overload are highly conserved among metabolically active tissues.

DISCUSSION

The effect of metabolic overload on WAT and liver was analyzed in a mouse model that responds to HFD feeding with WAT expansion, metabolic stress, inflammation and development of NAFLD. Using Bayesian hierarchical clustering we showed that the expression of genes of lipid metabolism is rapidly adjusted upon HFD feeding (already within one week). Cluster analysis revealed that these genes hardly change in expression later in time, despite the observed pronounced WAT expansion and the onset of inflammation from week 6 onward. By contrast, many inflammatory genes strongly increase in their expression at >6 weeks (e.g. inflammatory clusters C and D), and these genes also encode for inflammatory factors that can be secreted into the circulation. This inflammatory response is observed when adipocytes become hypertrophic suggesting that adipose tissue expandability becomes inadequate and the storage capacity of WAT reaches its limit [5, 6]. Promoter analysis defined a rather small set of about 25 transcriptional master regulators including Pparγ, Hnf4α, Sp1, Jun/Fos, Esr1, Srebf2, Nr1h2, Sfpi1, Fos, Smad2, Sp1, Gata1 that orchestrate the adaptation of lipid metabolism and induce inflammation. Some of the identified transcription factors (Pparγ, Esr1, Jun/Fos) control the adjustment of lipid metabolism-related and inflammatory genes supporting the view that metabolism and inflammation are molecularly interlinked in WAT [29].

Notably in liver, only a small number of genes of lipid metabolism and inflammation are affected up to week 6. Thereafter, when WAT has become inflamed, a marked increase in the number of differentially expressed genes involved in hepatic lipid metabolism and inflammation was observed. Comparison of liver and WAT revealed a remarkable overlap in gene expression and transcriptional regulation at >6 weeks. Together this shows that HFD feeding results in rapid adaption of WAT lipid metabolism which is not further adjusted during fat storage. When WAT inflammation begins, the gene expression and transcriptional responses of WAT and liver start to resemble each other. This indicates that the fundamental principles of how metabolically active organs cope with HFD overload are conserved.

We found that Pparγ [30], Srebf1 and Srebf2 [31], and Nr1h3/Nr1h2 (also referred to as Lxrα/Lxrβ [32, 33] may explain the observed gene expression changes. Indeed, these transcription factors are well-established regulators of lipid metabolism and their identification confirms the validity of the approach applied. The ‘lipid metabolism’ genes with the largest changes grouped in lipid gene cluster F. Genes in this cluster are not only involved in lipid metabolism but also in lipid absorption and glucose metabolism and could reflect a reprogramming of WAT from early time points onward to cope with HFD overload. Potential transcription factors regulating this reprogramming include Srebf1, Srebf2, Pparγ, Lxrα, Lxrβ and Hnf4α. In a previous study, we indeed identified

transcription factor HNF4α as a regulator of energy metabolism in human adipose tissue [34], and activation of LXRα and LXRβ has been shown to affect lipid and glucose metabolism as well as the inflammatory state simultaneously [28, 35].

We also identified several transcription factors typically associated with inflammation (Jun, Stat1, Stat5β) in the promoter elements of genes associated with general sphingolipid metabolism and, more specifically, ceramide metabolism. This finding supports the notion that molecular links exist between lipid metabolism and inflammatory signaling cascades and that these processes are interlinked and hence, may influence each other [23, 29, 36]. Boini and coworkers have shown that HFD-treated mice have increased levels of ceramide in WAT and in plasma [37, 38]. In another study, the ceramide concentrations in human WAT were positively correlated with the inflammatory state of the tissue, independent of obesity [39].

The inflammatory/immune response genes of the inflammatory gene clusters C and D showed a pronounced increase in expression from week 6 onward. One of the genes encodes for Ccl5/Rantes which promotes macrophage recruitment in adipose tissue [40]. Indeed, the gene expression levels of CD11b/Mac1, a marker expressed on macrophages and neutrophils, were also increased showing a similar time pattern. Of note, the expression of another inflammatory gene, Cxcl1/KC, intensified also from week 6 onwards. This coincides with the development of insulin resistance in WAT of APOE*3Leiden mice under the experimental conditions employed herein [13]. Cxcl1/KC stimulates the infiltration of neutrophils into WAT [41] and represents the mouse ortholog of human interleukin-8, but the exact role of this factor in the pathogenesis of insulin resistance remains to be established. The observation that neutrophil cytosolic factor 1 (Nrf1/p47/phox) expression levels also increase suggests that (infiltrating) neutrophils may have a role early in the disease process. Of note, also the expression levels of granzyme A, a protease present in granules of cytotoxic T-cells and NK cells, increased strongly from week 6 onwards. Because immune cells accumulate in WAT during HFD feeding, it is thus likely that changes in inflammatory gene expression may, at least partly, be a reflection of the changes in cellular composition of the tissue. Interestingly, we also found a gradual increase in expression of the inflammasome adaptor ASC. ASC is necessary for assembly of inflammasome complexes, which activates the inflammatory cytokines IL1 and IL18 from their propeptides in response to saturated fatty acid overload, thereby linking lipid metabolism and inflammation and promoting the development of insulin resistance in T2DM [42]. Promoter analyses of clustered inflammatory genes revealed that a large number of these genes share Fos, Smad2, Stat6 and Pparα as transcriptional regulators, which is in accordance with their established roles in inflammatory signaling cascades [43-46].

In several clusters, the transcriptional regulators Pparγ, Sp1, estrogen receptor 1 (Esr1) and Jun/Fos were identified as central underlying transcriptional regulators that may explain the gene expression changes of both lipid metabolism genes and inflammation-related genes. In accordance with their suggested overarching role, Pparγ, Sp1 and Esr1 are indeed involved in cell differentiation, cell cycle and growth *and* immune response processes [23, 30, 47, 48]: Pparγ is implicated in adipogenesis and insulin signaling of adipocytes as well as in the control of the inflammatory state of infiltrating monocytes/macrophages [49]. Esr1 forms complexes with DNA-bound Sp1 to regulate the

transcription of low density lipoprotein receptor (LDLR) [50], retinoic acid receptor-alpha (Rarα) [51] and c-Fos [52]. Another transcription factor that may constitute a link between lipid metabolism and inflammation is c-Jun as established previously for WAT and liver [23, 36, 53].

A limitation of the present study is that the transcriptional regulator prediction method predicts the binding of the transcription factors only from the existence of the binding motifs in the regulatory elements of genes, i.e. it employs available knowledge about the regulation of these genes. Although the results of this bioinformatical approach are certainly indicative, the involvement of many of these transcription factors has not been experimentally proven under the experimental conditions employed and there is a recent recognition that only a small portion of the putative motif may actually be occupied by the transcription factors based on recent ChIP-seq studies.

Because WAT and liver tissue have evolved from common ancestral structures (mesoderm) it has been proposed that they may share similar functional units to control key metabolic and immune processes [29, 54]. Indeed, our results show that the factors important for regulation of gene expression in WAT were also affected in liver, suggesting a considerable consistency between both responses to HFD-induced metabolic overload. Some of the master regulators identified in WAT in the present study (Jun, Fos, Rarα, Pparα, Stat1, Stat5, Sp1) were also reported to control liver lipid metabolism and/or the inflammatory responses of the liver in experimental diet-induced cardiovascular disease [23]. A tight relationship between WAT dysfunction and the pathogenesis of NAFLD has been reported recently [55], suggesting comparable control of inflammatory gene expression in metabolically active organs [29]. This interrelationship could possibly be exploited in the future to monitor the condition of the liver via biopsies taken from WAT because they are more accessible. Our findings correspond with the view that the control mechanisms of metabolic and inflammatory homeostasis in WAT and liver share similarities and that a distortion of the mechanisms that control metabolic adaptation may also affect the inflammatory tone of a tissue [9, 29].

Collectively, this study demonstrates that high fat feeding evokes an immediate, stable response of lipid metabolism genes. Later in time, when the storage capacity of WAT becomes limited, inflammatory genes are induced in WAT (>6 weeks). When WAT began, genes of lipid metabolism and inflammation also became affected in corresponding livers. The hepatic response to HFD, in particular the underlying transcriptional responses, were remarkably similar to those detected in WAT. In all, WAT and liver respond to metabolic overload by adaptations in expression of (clusters of) genes controlling lipid metabolism and inflammatory processes in an orchestrated and interrelated manner.

ACKNOWLEDGEMENTS

The authors thank Nicholas Heard for help with the clustering algorithm. We thank Erik H. Offerman, Wim van Duyvenvoorde and Karin Toet for technical assistance.

REFERENCES

1. Chaput JP, Doucet E, Tremblay A. (2012) Obesity: A disease or a biological adaptation? an update. Obes Rev 13: 681-691.

2. Nolan CJ, Damm P, Prentki M. (2011) Type 2 diabetes across generations: From pathophysiology to prevention and management. Lancet 378: 169-181.

3. Lumeng CN, Saltiel AR. (2011) Inflammatory links between obesity and metabolic disease. J Clin Invest 121: 2111-2117.

4. Cohen JC, Horton JD, Hobbs HH. (2011) Human fatty liver disease: Old questions and new insights. Science 332: 1519-1523.

5. Sethi JK, Vidal-Puig AJ. (2007) Thematic review series: Adipocyte biology. adipose tissue function and plasticity orchestrate nutritional adaptation. J Lipid Res 48: 1253-1262.

6. Mollica MP, Lionetti L, Putti R, Cavaliere G, Gaita M, et al. (2011) From chronic overfeeding to hepatic injury: Role of endoplasmic reticulum stress and inflammation. Nutr Metab Cardiovasc Dis 21: 222-230.

7. Agarwal AK, Garg A. (2006) Genetic disorders of adipose tissue development, differentiation, and death. Annu Rev Genomics Hum Genet 7: 175-199.

8. Pihlajamaki J, Kuulasmaa T, Kaminska D, Simonen M, Karja V, et al. (2012) Serum interleukin 1 receptor antagonist as an independent marker of non-alcoholic steatohepatitis in humans. J Hepatol 56: 663-670.

9. Osborn O, Olefsky JM. (2012) The cellular and signaling networks linking the immune system and metabolism in disease. Nat Med 18: 363-374.

10. Grove KL, Fried SK, Greenberg AS, Xiao XQ, Clegg DJ. (2010) A microarray analysis of sexual dimorphism of adipose tissues in high-fat-diet-induced obese mice. Int J Obes (Lond) 34: 989-1000.

11. de Wit NJ, Boekschoten MV, Bachmair EM, Hooiveld GJ, de Groot PJ, et al. (2011) Dose-dependent effects of dietary fat on development of obesity in relation to intestinal differential gene expression in C57BL/6J mice. PLoS One 6: e19145.

12. Kreeft AJ, Moen CJ, Porter G, Kasanmoentalib S, Sverdlov R, et al. (2005) Genomic analysis of the response of mouse models to high-fat feeding shows a major role of nuclear receptors in the simultaneous regulation of lipid and inflammatory genes. Atherosclerosis 182: 249-257.

13. Kleemann R, van Erk M, Verschuren L, van den Hoek AM, Koek M, et al. (2010) Time-resolved and tissue-specific systems analysis of the pathogenesis of insulin resistance. PLoS One 5: e8817.

14. Strissel KJ, DeFuria J, Shaul ME, Bennett G, Greenberg AS, et al. (2010) T-cell recruitment and Th1 polarization in adipose tissue during diet-induced obesity in C57BL/6 mice. Obesity (Silver Spring) 18: 1918-1925.

15. Caesar R, Manieri M, Kelder T, Boekschoten M, Evelo C, et al. (2010) A combined transcriptomics and lipidomics analysis of subcutaneous, epididymal and mesenteric adipose tissue reveals marked functional differences. PLoS One 5: e11525.

16. Cooke EJ, Savage RS, Kirk PD, Darkins R, Wild DL. (2011) Bayesian hierarchical clustering for microarray time series data with replicates and outlier measurements. BMC Bioinformatics 12: 399-2105-12-399.

17. Hong C, Tontonoz P. (2008) Coordination of inflammation and metabolism by PPAR and LXR nuclear receptors. Curr Opin Genet Dev 18: 461-467.

18. Zadelaar AS, Boesten LS, Jukema JW, van Vlijmen BJ, Kooistra T, et al. (2006) Dual PPARalpha/gamma agonist tesaglitazar reduces atherosclerosis in insulin-resistant and hypercholesterolemic ApoE*3Leiden mice. Arterioscler Thromb Vasc Biol 26: 2560-2566.

19. Duivenvoorden I, Voshol PJ, Rensen PC, van Duyvenvoorde W, Romijn JA, et al. (2006) Dietary sphingolipids lower plasma cholesterol and triacylglycerol and prevent liver steatosis in APOE*3Leiden mice. Am J Clin Nutr 84: 312-321.

20. Wielinga PY, Harthoorn LF, Verschuren L, Schoemaker MH, Jouni ZE, et al. (2012)

Arachidonic acid/docosahexaenoic acid-supplemented diet in early life reduces body weight gain, plasma lipids, and adiposity in later life in ApoE*3Leiden mice. Mol Nutr Food Res 56: 1081-1089.
21. Kleiner DE, Brunt EM, Van Natta M, Behling C, Contos MJ, et al. (2005) Design and validation of a histological scoring system for nonalcoholic fatty liver disease. Hepatology 41: 1313-1321.
22. Verschuren L, Kooistra T, Bernhagen J, Voshol PJ, Ouwens DM, et al. (2009) MIF deficiency reduces chronic inflammation in white adipose tissue and impairs the development of insulin resistance, glucose intolerance, and associated atherosclerotic disease. Circ Res 105: 99-107.
23. Kleemann R, Verschuren L, van Erk MJ, Nikolsky Y, Cnubben NH, et al. (2007) Atherosclerosis and liver inflammation induced by increased dietary cholesterol intake: A combined transcriptomics and metabolomics analysis. Genome Biol 8: R200.
24. De Groot PJ, Reiff C, Mayer C, Muller M. (2008) NuGO contributions to GenePattern. Genes Nutr 3: 143-146.
25. Baccini M, Bachmaier EM, Biggeri A, Boekschoten MV, Bouwman FG, et al. (2008) The NuGO proof of principle study package: A collaborative research effort of the european nutrigenomics organisation. Genes Nutr 3: 147-151.
26. Catelan D, Lagazio C, Biggeri A. (2010) A hierarchical bayesian approach to multiple testing in disease mapping. Biom J 52: 784-797.
27. Huang da W, Sherman BT, Lempicki RA. (2009) Bioinformatics enrichment tools: Paths toward the comprehensive functional analysis of large gene lists. Nucleic Acids Res 37: 1-13.
28. Kleemann R, Bureeva S, Perlina A, Kaput J, Verschuren L, et al. (2011) A systems biology strategy for predicting similarities and differences of drug effects: Evidence for drug-specific modulation of inflammation in atherosclerosis. BMC Syst Biol 5: 125.
29. Hotamisligil GS. (2006) Inflammation and metabolic disorders. Nature 444: 860-867.
30. Anghel SI, Wahli W. (2007) Fat poetry: A kingdom for PPAR gamma. Cell Res 17: 486-511.
31. Eberle D, Hegarty B, Bossard P, Ferre P, Foufelle F. (2004) SREBP transcription factors: Master regulators of lipid homeostasis. Biochimie 86: 839-848.
32. Krasowski MD, Ni A, Hagey LR, Ekins S. (2011) Evolution of promiscuous nuclear hormone receptors: LXR, FXR, VDR, PXR, and CAR. Mol Cell Endocrinol 334: 39-48.
33. Ulven SM, Dalen KT, Gustafsson JA, Nebb HI. (2005) LXR is crucial in lipid metabolism. Prostaglandins Leukot Essent Fatty Acids 73: 59-63.
34. van Erk MJ, Pasman WJ, Wortelboer HM, van Ommen B, Hendriks HF. (2008) Short-term fatty acid intervention elicits differential gene expression responses in adipose tissue from lean and overweight men. Genes Nutr 3: 127-137.
35. Verschuren L, de Vries-van der Weij J, Zadelaar S, Kleemann R, Kooistra T. (2009) LXR agonist suppresses atherosclerotic lesion growth and promotes lesion regression in apoE*3Leiden mice: Time course and mechanisms. J Lipid Res 50: 301-311.
36. Tarantino G, Caputi A. (2011) JNKs, insulin resistance and inflammation: A possible link between NAFLD and coronary artery disease. World J Gastroenterol 17: 3785-3794.
37. Boini KM, Zhang C, Xia M, Poklis JL, Li PL. (2010) Role of sphingolipid mediator ceramide in obesity and renal injury in mice fed a high-fat diet. J Pharmacol Exp Ther 334: 839-846.
38. Shah C, Yang G, Lee I, Bielawski J, Hannun YA, et al. (2008) Protection from high fat diet-induced increase in ceramide in mice lacking plasminogen activator inhibitor 1. J Biol Chem 283: 13538-13548.
39. Kolak M, Westerbacka J, Velagapudi VR, Wagsater D, Yetukuri L, et al. (2007) Adipose tissue inflammation and increased ceramide content characterize subjects with high liver fat content independent of obesity. Diabetes 56: 1960-1968.
40. Keophiphath M, Rouault C, Divoux A, Clement K, Lacasa D. (2010) CCL5 promotes macrophage recruitment and survival in human adipose tissue. Arterioscler Thromb Vasc Biol 30: 39-45.

41. Elgazar-Carmon V, Rudich A, Hadad N, Levy R. (2008) Neutrophils transiently infiltrate intra-abdominal fat early in the course of high-fat feeding. J Lipid Res 49: 1894-1903.
42. Wen H, Gris D, Lei Y, Jha S, Zhang L, et al. (2011) Fatty acid-induced NLRP3-ASC inflammasome activation interferes with insulin signaling. Nat Immunol 12: 408-415.
43. Goenka S, Kaplan MH. (2011) Transcriptional regulation by STAT6. Immunol Res 50: 87-96.
44. Wagner EF, Eferl R. (2005) Fos/AP-1 proteins in bone and the immune system. Immunol Rev 208: 126-140.
45. Brown KA, Pietenpol JA, Moses HL. (2007) A tale of two proteins: Differential roles and regulation of Smad2 and Smad3 in TGF-beta signaling. J Cell Biochem 101: 9-33.
46. Pyper SR, Viswakarma N, Yu S, Reddy JK. (2010) PPARalpha: Energy combustion, hypolipidemia, inflammation and cancer. Nucl Recept Signal 8: e002.
47. Li L, He S, Sun JM, Davie JR. (2004) Gene regulation by Sp1 and Sp3. Biochem Cell Biol 82: 460-471.
48. Solomon SS, Majumdar G, Martinez-Hernandez A, Raghow R. (2008) A critical role of Sp1 transcription factor in regulating gene expression in response to insulin and other hormones. Life Sci 83: 305-312.
49. Tontonoz P, Spiegelman BM. (2008) Fat and beyond: The diverse biology of PPARgamma. Annu Rev Biochem 77: 289-312.
50. Li C, Briggs MR, Ahlborn TE, Kraemer FB, Liu J. (2001) Requirement of Sp1 and estrogen receptor alpha interaction in 17beta-estradiol-mediated transcriptional activation of the low density lipoprotein receptor gene expression. Endocrinology 142: 1546-1553.
51. Sun G, Porter W, Safe S. (1998) Estrogen-induced retinoic acid receptor alpha 1 gene expression: Role of estrogen receptor-Sp1 complex. Mol Endocrinol 12: 882-890.
52. Duan R, Porter W, Safe S. (1998) Estrogen-induced c-fos protooncogene expression in MCF-7 human breast cancer cells: Role of estrogen receptor Sp1 complex formation. Endocrinology 139: 1981-1990.
53. Hotamisligil GS. (2008) Inflammation and endoplasmic reticulum stress in obesity and diabetes. Int J Obes (Lond) 32 Suppl 7: S52-4.
54. Sondergaard L. (1993) Homology between the mammalian liver and the drosophila fat body. Trends Genet 9: 193.
55. Duval C, Thissen U, Keshtkar S, Accart B, Stienstra R, et al. (2010) Adipose tissue dysfunction signals progression of hepatic steatosis towards nonalcoholic steatohepatitis in C57BL/6 mice. Diabetes 59: 3181-3191.

PROTECTIVE EFFECT OF ROSIGLITAZONE ON KIDNEY FUNCTION IN HIGH-FAT CHALLENGED HUMAN CRP TRANSGENIC MICE: IS THERE A ROLE FOR ADIPONECTIN AND MIR-21?

Wen Liang*
Gopala K. Yakala*
Peter Y. Wielinga
Kanita Salic
Martine Morrison
Tushar Tomar
Robert Kleemann
Peter Heeringa
Teake Kooistra

* Both authors contributed equally

Submitted

ABSTRACT

Obesity-related albuminuria is associated with decline of kidney function and is considered a first sign of diabetic nephropathy. Suggested factors linking obesity to kidney dysfunction include low-grade inflammation, insulin resistance and adipokine dysregulation. Here, we investigated the effects of two pharmacological compounds with established anti-inflammatory properties, rosiglitazone and rosuvastatin, on kidney dysfunction during high-fat diet (HFD)-induced obesity. For this, human CRP transgenic mice were fed standard chow, a lard-based HFD, HFD + rosuvastatin or HFD + rosiglitazone for 42 weeks to study effects on insulin resistance; plasma inflammatory markers and adipokines; and renal pathology. Rosiglitazone but not rosuvastatin prevented HFD-induced albuminuria and renal fibrosis and inflammation. Also, rosiglitazone prevented HFD-induced KIM-1 expression, while levels were doubled with rosuvastatin. This was mirrored by miR-21 expression, which plays a role in fibrosis and is associated with renal dysfunction. Plasma insulin did not correlate with albuminuria. Only rosiglitazone increased circulating adiponectin concentrations. In all, HFD-induced albuminuria, and renal inflammation, injury and fibrosis are prevented by rosiglitazone but not rosuvastatin. These beneficial effects of rosiglitazone are paralleled by lowered miR-21 expression and selectively enhanced plasma adiponectin levels rather than lowered insulin levels or a reduction in chronic inflammation.

INTRODUCTION

Obesity rates are rapidly rising worldwide in almost all populations and age groups, largely due to increased availability and consumption of calorie-dense foods with a high-fat, high-sugar content and lack of physical activity (1). Obesity-related fat accumulation, especially in visceral depots, is associated with an increased risk of a number of pathologies, including insulin resistance (IR) (2) and (micro)albuminuria (3). Albuminuria has been associated with a decline of kidney function and is now being recognized not only as an important risk factor for future cardiovascular events (4, 5), but is also considered a first sign of diabetic nephropathy (6). With the recent rise in the prevalence of obesity, there is an urgent need for a better understanding of why a relationship exists between obesity and albuminuria and how obesity-related albuminuria develops. Suggested factors linking obesity to albuminuria include systemic chronic low-grade inflammation, IR, and specific adipocyte-derived adipokines.

Chronic low-grade inflammation, as evidenced by elevated plasma levels of acute-phase inflammatory markers, including C-reactive protein (CRP), a commonly used marker for systemic inflammation in humans (7), is thought to play an important role in the development of both IR and nephropathy. To show a causative relationship between these risk markers and kidney disease, an intervention directed at reduction of systemic inflammation should in turn at least partly diminish IR and prevent albuminuria. If that were true, interventions that reduce systemic inflammation and insulin are attractive candidates for preventive treatment of patients at risk for developing (diabetic) nephropathy.

Another explanation for renal disease in obesity may be related to the notion that adipocytes are an active endocrine cell type (8, 9). Adipocytes secrete several bioactive factors (adipokines) that reportedly play a role in maintaining metabolic health (reviewed in (9)). Obesity frequently leads to a dysregulation of adipokine secretion from fat depots (9) and thus may be associated with metabolic diseases. Of the numerous factors that are regulated with increased visceral obesity, one of the best characterized is adiponectin. Recent clinical studies suggest that lowered plasma levels of adiponectin may play a key role in the development of obesity-related albuminuria (10). Adiponectin is thought to regulate the function of podocytes, a renal cell-type that plays a significant role in the glomerular filtration barrier (11). Indeed, studies in adiponectin knockout mice indicate that absence of adiponectin can contribute to the initial development of albuminuria (10). Further evidence for beneficial effects of adiponectin on kidney functioning was sought by increasing plasma levels by administration of exogenous adiponectin, but these efforts were hampered by inherent difficulties in producing functional recombinant adiponectin, combined with the brief circulating half-life of adiponectin (12). Therefore, efforts to increase adiponectin levels have also been focused on increasing the production of endogenous adiponectin by adipose tissue. Since the human and mouse adiponectin promoter contains binding sites for peroxisome proliferator-activated receptor gamma (PPAR-γ), pharmacological activation of PPAR-γ offers the opportunity to enhance endogenous plasma levels of adiponectin and thereby to further substantiate a protective role of adiponectin in the development of kidney disease.

To gain more insight into the role of inflammation and adiponectin in metabolic-stress-induced albuminuria, renal inflammation and fibrosis in the context of IR, we used a human CRP transgenic (huCRPtg) mouse model. The huCRPtg mouse carries a transgene containing the human CRP gene, the 5' flanking promoter region and all known human CRP gene regulatory elements (13). These mice have been successfully employed to monitor systemic inflammation and to determine the effects and mechanisms of drugs like statins and fibrates in reducing inflammatory process (14). In a recent study (15), we demonstrated that by feeding a high-fat diet (HFD), huCRPtg mice showed metabolic-stress-induced systemic inflammation and developed osteoarthritis. Interventions with a statin (rosuvastatin) and a PPAR-γ activator (rosiglitazone) reduced systemic inflammation as indicated by decreased human CRP levels and concomitantly inhibited the development of osteoarthritis. Here we have used this mouse model to evaluate whether suppression of HFD-induced systemic inflammation by rosuvastatin and rosiglitazone also improves albuminuria, renal inflammation and fibrosis under conditions of obesity and IR. An integral part of the study was to assess a putative role of adiponectin, which is induced by rosiglitazone.

MATERIALS AND METHODS

Animal experiments

Experiments were approved by the institutional Animal Care and Use Committee of TNO and were in compliance with European Community specifications regarding the use of laboratory animals. All sample materials and organs required for this study were obtained from TNO-Biosciences, Leiden. Minor parts of the results (in particular body weight development over time) were published previously, where indicated, but are presented here as well for clarity (15).

HuCRPtg mice (13, 14) on a C57BL/6 background were characterized by PCR and ELISA for huCRP expression. Mice were housed in groups under standard conditions with a 12-h light-dark cycle and had free access to water and food. Mice of 12 weeks of age were fed either standard lab chow (ssniff® R/M-H, ssniff Spezialdiäten, Soest, Germany) or chow supplemented with 0.01% (w/w) rosuvastatin ("Crestor®", AstraZeneca, Zoetermeer, the Netherlands) (t=0). After 4 weeks (t=4) the diets were changed and mice were divided into 4 groups consisting of 9 mice per group. Mice that had been fed chow were randomly distributed into 3 groups. Group 1 consisted of control mice that remained on the standard chow diet. Group 2 was switched to a high-fat (lard) diet (HFD) (23.6% fat / 45% kcal% fat D12451, Research Diets, New Brunswick, New Jersey) and mice in group 3 were fed HFD containing 0.018% (w/w) rosiglitazone (HFD+Rosi) (Avandia, GSK, London, United Kingdom). Group 4 consisted of mice that had been fed standard chow supplemented with 0.01% (w/w) rosuvastatin (AstraZeneca), and were switched after 4 weeks to HFD containing 0.005% (w/w) rosuvastatin (HFD+Rosuva). The reason to lower the dose of rosuvastatin is the increased absorption of rosuvastatin in the context of HFD-feeding. The rosuvastatin and rosiglitazone doses were based on their anti-inflammatory effects observed in previous studies (42, 43). Mice on chow diet (group 1), mice on HFD without drugs (group 2) and drug-treated mice on HFD (groups 3 and 4) remained on their respective diets until the completion of the study at 54 weeks of age (t=42).

Body weight monitoring and blood sampling by tail incision after 4 hours of fasting was done at t=0 and weeks 2, 4, 5, 11, 34, and 42. Blood samples were collected in EDTA tubes (Sarstedt AG & Co, Nümbrecht, Germany) and centrifuged for 10 minutes at 6000 rpm, after which plasma was collected and immediately stored at −80°C until use. Spot urine and serum (after heart puncture) was collected from all animals at the time of sacrifice (t=42). Mice were sacrificed by CO2 asphyxiation after a 4-hour fast, and tissues were isolated and weighed. Left kidneys were fixed in formalin and embedded in paraffin, and right kidneys were snap frozen in liquid N2 and stored at −80°C until further use.

Histological, biochemical and gene expression analyses

A detailed description of biochemical, histological, and gene expression analyses is provided in **Supplement 3**. Briefly, plasma levels of human CRP, E-selectin and adiponectin were determined by ELISA (R&D Systems, Abingdon, United Kingdom) and urinary albumin/creatinine ratios were determined using commercially available kits (Bethyl laboratories, Montgomery, Texas and Exocell, Philadelphia, Pennsylvania). Renal gene expression and miR-21 analyses were performed by RT-PCR, using TaqMan® Gene Expression Assays (Life Technologies, Bleiswijk, the Netherlands) and changes in expression were calculated using the comparative Ct (ΔΔCt) method, expressed as fold-change relative to chow. Renal injury and fibrosis were determined histologically in Periodic acid-Schiff-, Masson's Trichrome-, and Sirius Red-stained kidney sections.

Statistical analysis

Data were analyzed with Graphpad Prism software (version 5.03, Graphpad Software Inc., La Jolla, California) and SPSS (version 22, IBM, Armonk, New York). Differences between groups at one specific time point were analyzed by 1-way ANOVA followed by LSD post-hoc analysis. To determine the correlation between two parameters, Spearman's correlation coefficients were calculated. A p-value ≤ 0.05 was considered statistically significant. All data are presented as mean $\pm$ SEM.

RESULTS

Body weight and fat distribution

HuCRPtg mice were fed a standard chow diet, a lard-based HFD, HFD+0.005% rosuvastatin or HFD+0.018% rosiglitazone for 42 weeks to study effects on insulin resistance, plasma inflammatory markers and adipokines, and renal pathology (albuminuria, inflammation and fibrosis). Body weight at baseline (t=0) was 28.5 ± 0.4 g. The three experimental groups that received HFD all showed a gradual increase in body weight over time and all had significantly higher average body weights at the end of the experimental period (t=42 weeks) compared with the group that remained on chow (35.1 ± 0.6 g). Mice treated with rosiglitazone had the highest body weight (57.7 ± 3.9 g), which was significantly higher than that of the HFD group (41.1 ± 1.6 g) and the rosuvastatin-treated group (46.1 ± 2.4 g) (15).

All mice fed HFD showed a clear increase in fat mass compared with chow-fed mice, but what was most striking were the observed differences in fat mass distribution over the various fat depots in the different groups (**Figure 1A-C**). Rosiglitazone treatment resulted

in a reduction in visceral fat mass and an increase in subcutaneous fat mass in comparison with the HFD group (visceral fat: 0.39 ± 0.06 g vs. 0.65 ± 0.09 g, p<0.01; subcutaneous fat: 2.93 ± 0.46 g vs. 0.83 ± 0.14 g, p<0.001). In the rosuvastatin group, an increase in epididymal fat mass was observed in comparison with both the HFD group (HFD+Rosuva vs. HFD, 2.02 ± 0.36 g vs. 1.54 ± 0.11 g, p=0.07) and the rosiglitazone group (HFD+Rosuva vs. HFD+Rosi, 2.01 ± 0.0.36 g vs. 1.27 ± 0.10 g, p<0.01).

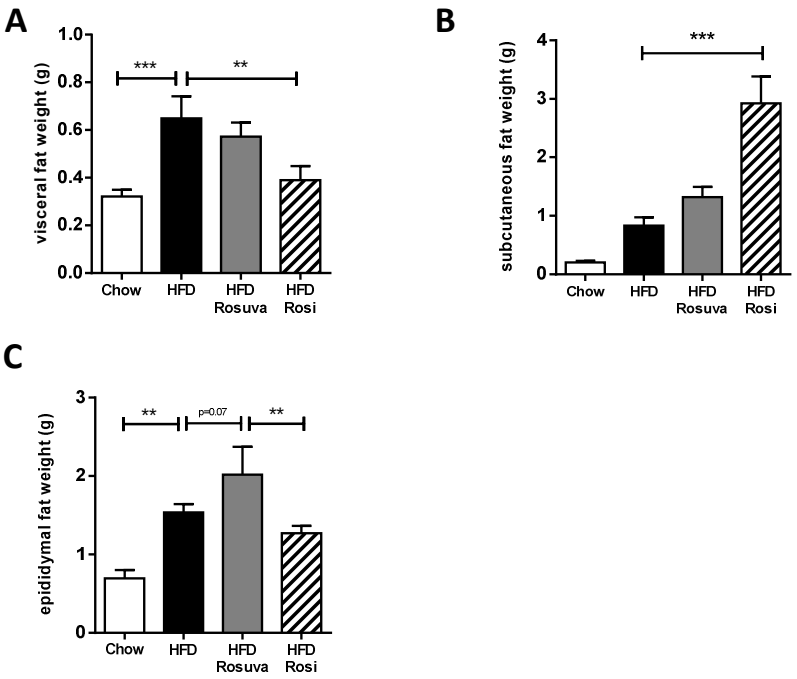

Figure 1: Effects of rosuvastatin and rosiglitazone on fat distribution. HuCRPtg mice mice were fed chow, high-fat diet (HFD), HFD+0.005% (w/w) rosuvastatin (HFD Rosuva) or HFD+0.018% (w/w) rosiglitazone for 42 weeks. A: visceral fat mass, B: subcutaneous fat mass, C: epididymal fat mass. Data are mean ± SEM. ** p<0.01, *** p<0.001.

Glucose and insulin levels

Plasma glucose levels were 9.8 ± 0.24 mM at the start of the experiment and increased steadily and significantly during the rest of the investigational period for all experimental groups: 13.6 ± 0.6 mM (chow), 15.9 ± 0.9 mM (HFD), 14.8 ± 0.8 mM (HFD+Rosuva), and 14.2 ± 0.7mM (HFD+Rosi) at t=42 (**Supplementary Figure 1A**). Compared with glucose levels, changes in insulin levels over time were more pronounced and differed between groups. Average insulin levels were 0.6 ± 0.1 ng/ml at t=0 and rose over time to 3.4 ± 0.6 ng/ml at t=42 weeks for the chow group and to 4.1 ± 0.3 ng/ml in HFD. Notably, the highest insulin levels were observed with rosuvastatin treatment (4.7 ± 0.4 ng/ml),

whereas rosiglitazone treatment markedly and significantly suppressed insulin levels to 2.3 ± 0.6 ng/ml (p<0.05 compared with HFD) (**Supplementary Figure 1B**).

Plasma adipokines

Leptin is an adipokine that is highly specific for adipose tissue. Several studies of obese humans have shown a strong and consistent positive relation between plasma leptin concentrations and adipose tissue mass (see (16) and references therein). At the start of the experiment, plasma leptin levels were low (0.15 ± 0.1 ng/ml) and they increased slightly over time in the chow group (4.7 ± 0.8 ng/ml at t=42 weeks) (**Figure 2A**). After starting the HFD, leptin levels gradually and strongly rose in all three groups (**Figure 2A**). At t=42 weeks, leptin levels in the rosiglitazone group had reached values of 35.9 ± 6.9 ng/ml, higher than those of the rosuvastatin group (30.1 ± 4.2 ng/ml) and the HFD group (21.8 ± 3.6 ng/ml, p<0.05). Correlation analysis revealed a strong positive relationship between body mass and leptin levels (R^2=0.8208, p<0.001, **Figure 2B**), in line with the reported correlation between plasma leptin levels and adipose mass in humans (16).

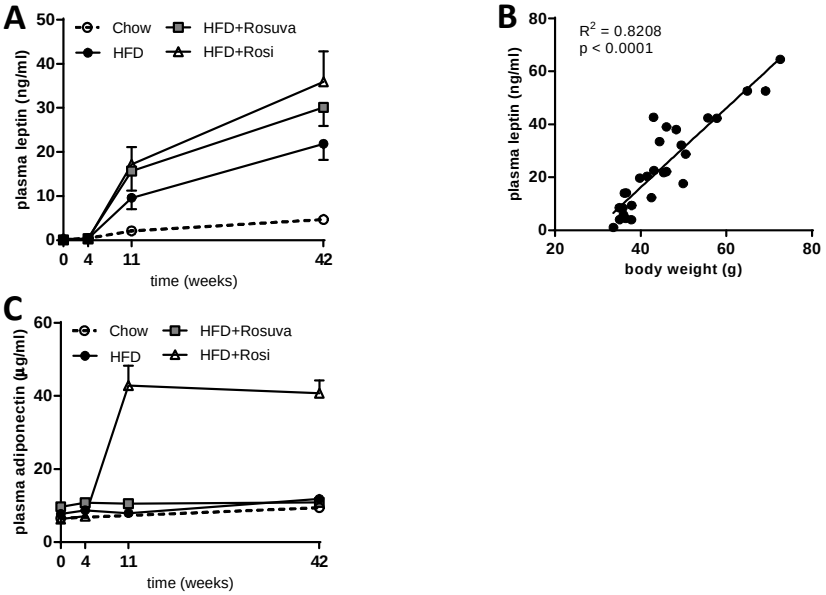

Figure 2: Effects of rosuvastatin and rosiglitazone on plasma leptin and adiponectin levels. HuCRPtg mice were fed chow, high-fat diet (HFD), HFD+0.005% (w/w) rosuvastatin (HFD Rosuva) or HFD+0.018% (w/w) rosiglitazone for 42 weeks. A: plasma leptin levels over time. B: correlation between plasma leptin and body weight. C: plasma adiponectin levels over time. Data are mean ± SEM.

In contrast to leptin, adiponectin levels are usually decreased with increasing obesity and associated comorbidities, such as type-2 diabetes (T2D) (17). Grosso modo, adiponectin levels remained relatively constant in all treatment groups during the entire experimental period (t=0: 7.4 ± 0.4 µg/ml, and t=42: 9.4 ± 1.1 µg/ml in chow, 11.9 ± 0.4

µg/ml in HFD, and 10.9 ± 1.1 µg/ml in HFD+Rosuva), except for the rosiglitazone group, which showed strongly increased plasma concentrations of adiponectin from t=4 weeks onward, reaching average levels of 40.8 ± 3.5 µg/ml ($p<0.001$ compared with all other groups at t=42, **Figure 2C**).

Renal inflammation and renal function

At the end of the experimental period, the chow group had an urinary albumin/creatinine ratio of 151 ± 22 µg/mg. Both the HFD group (396 ± 88 µg/mg, $p<0.01$) and the Rosuva group (361 ± 104 µg/mg, $p<0.05$) showed a comparable and significant increase in the albumin/creatinine ratio compared with the chow group (**Figure 3A**). In contrast, HFD-fed mice treated with rosiglitazone exhibited urinary albumin/creatinine ratios of 129 ± 7 µg/mg, i.e. similar to those of chow-fed mice, and well below the values seen for the HFD and Rosuva groups ($p<0.01$ compared with HFD, $p<0.05$ compared with HFD+Rosuva; **Figure 3A**). Notably, urinary albumin levels were not significantly correlated with plasma insulin levels (not shown).

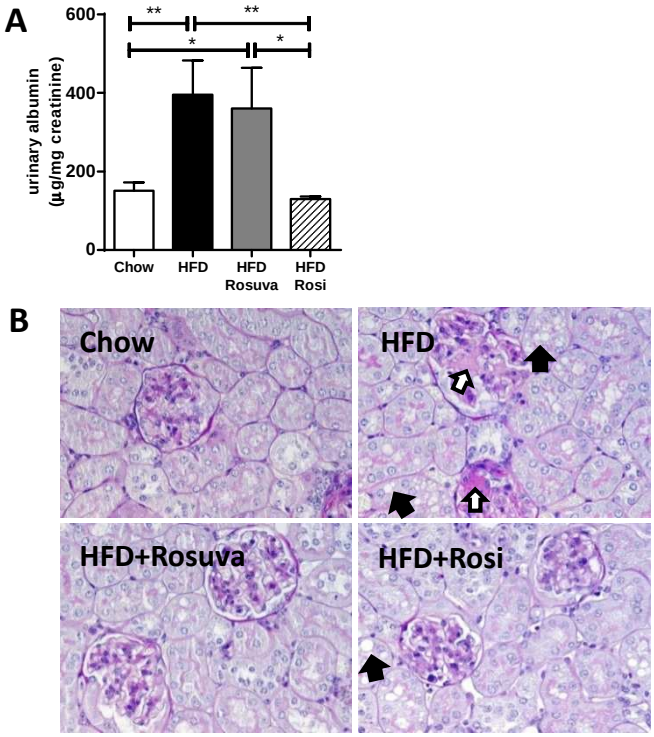

Figure 3: Effects of rosuvastatin and rosiglitazone on urinary albumin and kidney histology. HuCRPtg mice were fed chow, high-fat diet (HFD), HFD+0.005% (w/w) rosuvastatin (HFD Rosuva) or HFD+0.018% (w/w) rosiglitazone for 42 weeks. A: urinary albumin levels. B: representative photomicrographs of PAS-stained kidney sections showing mesanchial expansion (open arrows) and lipid droplets in tubuli (filled arrows). Data are mean ± SEM, * $p<0.05$, ** $p<0.01$.

Bright-field microscopy analysis revealed that HFD feeding induced development of mild mesangial area expansion and accumulation of lipid droplets in tubuli (**Figure 3B**). Both rosuvastatin and rosiglitazone prevented mesangial expansion. Tubular lipid accumulation was also observed in the rosiglitazone-treated group, but was absent in the rosuvastatin-treated mice.

Gene expression analysis revealed that relative mRNA expression levels (expressed as fold-change relative to chow) of kidney injury molecule 1 (KIM-1) were markedly upregulated in HFD (2.15 ± 0.30, p=0.08 vs. chow, **Table 1**). Notably, rosuvastatin markedly and significantly further increased KIM-1 expression levels (3.56 ± 0.89, p<0.05 vs. HFD), whereas rosiglitazone kept KIM-1 mRNA levels as low as those found for the chow group, i.e. strikingly below values seen for the HFD and HFD+Rosuva groups.

A similar picture emerged with respect to the renal mRNA expression levels of the endothelial activation marker E-selectin (**Table 1**). HFD feeding significantly upregulated E-selectin mRNA expression (2.41 ± 0.72, p<0.001 vs. chow), while rosuvastatin was unable to prevent this increase (2.22 ± 0.84, n.s. vs. HFD). In contrast, rosiglitazone treatment considerably downregulated E selectin mRNA expression (1.38 ± 0.53, p<0.01 vs. HFD), with expression levels similar to those observed in chow-fed mice.

The expression of CD68 mRNA, a marker for macrophage infiltration, and VCAM-1 mRNA, a vascular endothelial activation marker, did not differ significantly between the experimental groups (**Table 1**).

Table 1. Effects of rosiglitazone and rosuvastatin on renal mRNA expression. Renal mRNA expression levels of endothelial activation markers (E-selectin and VCAM-1), macrophage marker (CD68) and Kidney Injury Marker (KIM-1). *P<0.05 vs. HFD. Values are represented as means ± SD.

	Chow	HFD	HFD+Rosuva	HFD+Rosi
KIM-1	1.00 ± 0.24	2.14 ± 0.83	3.56 ± 2.17*	1.22 ± 0.54*
E-selectin	1.00 ± 0.33	2.41 ± 0.72	2.22 ± 0.84	1.38 ± 0.53*
CD68	1.00 ± 0.13	1.19 ± 0.32	1.31 ± 0.22	1.41 ± 0.33
VCAM-1	1.00 ± 0.22	0.82 ± 0.30	1.10 ± 0.37	0.93 ± 0.26

Plasma markers of systemic inflammation

HuCRP levels were measured to monitor the overall systemic inflammatory state induced by HFD, and the effect of interventions with rosuvastatin and rosiglitazone thereupon. As reported previously, both rosiglitazone and rosuvastatin exhibited anti-inflammatory effects (15). In contrast, only rosiglitazone markedly and significantly reduced the HFD-induced increase in plasma E-selectin levels at 42 weeks thus reflecting the renal mRNA data for E-selectin (**Supplementary Figure 2**).

Renal fibrosis and miR-21

Renal fibrosis is a frequent underlying cause of decreased renal function. To gain insight into fibrosis development, kidneys were stained with Masson Trichrome and Picro-Sirius Red, and analyzed for collagen deposition. **Figure 4A** shows Masson's trichrome staining

with the corresponding collagen quantification (as quantified in Picro-Sirius Red-staned sections) in **Figure 4B**. HFD induced the tubular interstitial collagen content (1.11 ± 0.15 %) compared with the chow group (0.57 ± 0.10 %; p<0.01, **Figure 4B**). Notably, while collagen content after rosuvastatin treatment was comparable to that in the HFD group (1.27 ± 0.17 %), rosiglitazone significantly prevented collagen deposition (0.74 ± 0.09 %; p<0.05 compared with HFD) with levels comparable to those in the chow group.

Since miR-21 has been shown to play a pathological role in many forms of fibrosis and since its increase is associated with microalbuminuria, inflammation and renal fibrosis (18, 19), we examined renal miR-21 expression (**Figure 4C**). Renal miR-21 expression was enhanced in HFD compared with chow group (fold-change 1.66 ± 0.29 in HFD, 1.00 ± 0.14 in chow). Rosuvastatin treatment nearly doubled miR-21 expression (fold-change 3.16 ± 0.53 relative to chow; p<0.01 compared with HFD) on top of HFD treatment. In contrast, rosiglitazone kept miR-21 levels low (fold-change 1.32 ± 0.39 relative to chow).

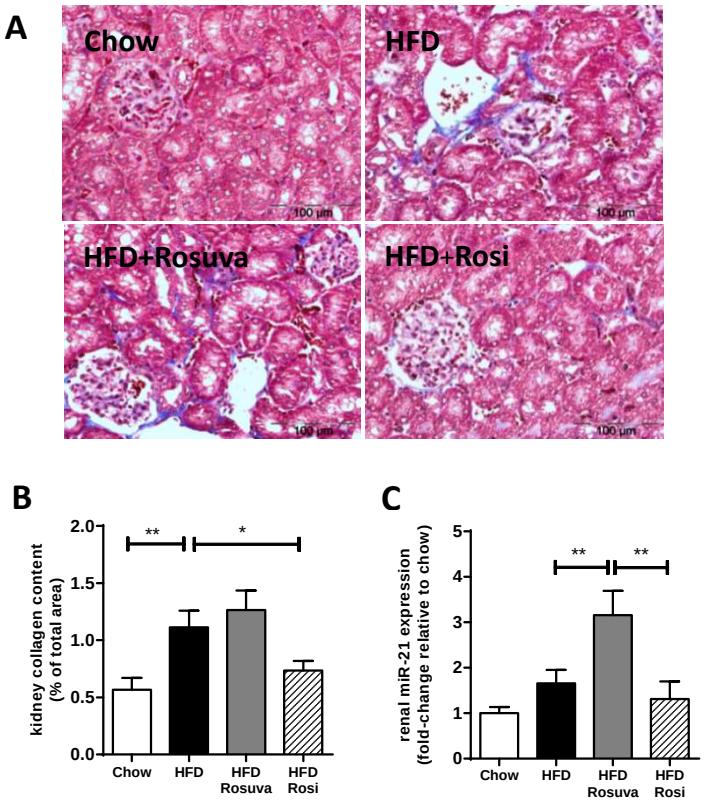

Figure 4: Effects of rosuvastatin and rosiglitazone on kidney fibrosis. HuCRPtg mice were fed chow, high-fat diet (HFD), HFD+0.005% (w/w) rosuvastatin (HFD Rosuva) or HFD+0.018% (w/w) rosiglitazone for 42 weeks. A: representative photomicrographs of kidney sections stained with Masson's Trichrome showing renal collagen deposition. B: quantification of tubular interstitial collagen (Sirius Red staining quantified by ImageJ analysis). C: renal miR-21 expression. Data are mean ± SEM. * p<0.05, ** p<0.01.

DISCUSSION

Obesity-related albuminuria is recognized as a sign of declined kidney function. Among the factors suggested to connect obesity to kidney dysfunction are low-grade systemic inflammation, IR/T2D and adipokine dysregulation. In the current study we sought evidence for the role of these obesity-linked factors in the development of aspects of renal pathology, viz. albuminuria, inflammation and fibrosis. For this, we employed huCRPtg mice under conditions of HFD-induced obesity in conjunction with two pharmacological interventions, rosiglitazone and rosuvastatin, with established anti-inflammatory properties (15), as exemplified by decreased huCRP levels. Our results demonstrate that anti-inflammatory rosiglitazone but not anti-inflammatory rosuvastatin prevented HFD-induced albuminuria and renal fibrosis, and inhibited expression of the renal inflammation marker, E-selectin. Rosiglitazone also prevented the HFD-enhanced mRNA expression of KIM-1, while rosuvastatin almost doubled KIM-1 mRNA levels. Notably, these beneficial effects of rosiglitazone were paralleled by absence of miR-21 induction and were associated with selectively enhanced plasma adiponectin levels. No correlation was found between plasma insulin levels and urine albumin/creatinine ratios.

In our study, we focused on human CRP levels as a marker for systemic inflammation. Recently, it has been reported that rosiglitazone treatment reduces plasma CRP levels in rats with induced T2D (20). Consistent with these findings, we observed that rosiglitazone treatment reduced human CRP levels in HFD-challenged huCRPtg mice indicating that rosiglitazone suppresses systemic inflammatory responses (15). Rosiglitazone is a PPAR-γ agonist that belongs to the thiazolidinedione class of drugs. It has been reported that in patients with T2D, treatment with another thiazolidinedione (pioglitazone) along with insulin therapy decreased human CRP levels when compared to insulin treatment alone (21, 22). In the current study, rosiglitazone reduced plasma insulin levels and hence reduced IR. In contrast, anti-inflammatory rosuvastatin treatment (15) failed to reduce circulating insulin levels, which is in line with a recent study showing that rosuvastatin failed to improve IR in patients on peritoneal dialysis (23).

Rosiglitazone treatment caused a significant increase in body weight in huCRPtg mice compared with HFD mice. More specifically, rosiglitazone-treated mice especially had increased subcutaneous fat mass compared with HFD mice. Consistent with these observations, treatment with PPAR-γ agonists has been shown to improve insulin sensitivity despite increasing body fat mass, in particular subcutaneously (22). In contrast, an increase in visceral fat has been reported to be highly associated with IR and T2D (21, 23). Here, we observed that rosiglitazone treatment decreased visceral fat mass. In contrast, in rosuvastatin-treated mice the mass and distribution of the fat depots were similar to those observed in untreated HFD-challenged mice.

We also observed that mice treated with rosiglitazone displayed markedly increased plasma levels of adiponectin, a protein predominantly secreted by adipocytes. It is now well documented that adiponectin is a cardioprotective adipokine, due to its anti-inflammatory and insulin-sensitizing properties (24, 25). An inverse relationship between adiponectin levels and CVD has been reported (2, 26) in patients with end-stage renal disease, and there is increasing evidence that adiponectin plays a protective role in T2D and IR. For example, adiponectin-deficient mice are prone to develop IR and vascular

damage after HFD challenge (27) whereas treatment with adiponectin inhibits renal fibrosis and albuminuria in adiponectin knock-out mice (28). Moreover, enhanced expression of adiponectin attenuates inflammation and diabetes development in db/db mice (29).

Obesity-related albuminuria is now being recognized not only as an indication of declined kidney function and a first sign of diabetic nephropathy (10), but also increases the risk of CVD (30). If left untreated, patients with albuminuria are more prone to CVD. Treatments that reduce albuminuria are therefore inherently renoprotective and would improve CVD outcomes (30). We observed that mice on HFD developed mesangial expansion, glomerulosclerosis, lipid accumulation and albuminuria. Furthermore, KIM-1, a marker of kidney injury (31), was upregulated in mice on HFD. Rosiglitazone treatment markedly diminished these HFD-induced renal effects and improved kidney function as evidenced by reduced urinary albumin/creatinine ratios and lowered KIM-1 expression. Moreover, rosiglitazone treatment strikingly reduced plasma E-selectin levels and, similarly, reduced renal E-selectin mRNA expression levels. Conversely, rosuvastatin treatment failed to exert any beneficial effects on markers of endothelial activation and inflammation in the kidney and did not improve albumin/creatinine ratios. In fact, the expression levels of some markers, including E-selectin and KIM-1 were increased in the kidneys of rosuvastatin-treated mice when compared with those of chow and HFD-challenged mice.

In a healthy individual, the kidney is able to reabsorb the majority of protein that enters the renal filtrate, with only traces being excreted in the urine. In the obese state there are two main sites involving two different processes that result in a loss of protein (mainly albumin) in the urine, viz. (i) structural changes to the glomerulus allowing more albumin to enter the filtrate and (ii) inability of the proximal tubules to endocytose the increased protein load (see (8) and references therein). The development of albuminuria is a typical characteristic of renal damage (nephropathy (32). Previous studies have demonstrated that statins can inhibit tubular reabsorption of filtered albumin (33, 34). Furthermore, this notion is supported by a recent study in hypertensive patients demonstrating that statin treatment was independently associated with the occurrence of microalbuminuria (35). Exposure to raised levels of albumin in the renal tubule has been linked to increased proinflammatory and profibrotic changes in the tubulointerstitium (36).

Diabetic patients with end-stage kidney disease have a 5-year survival rate of merely 20% (37). One of the major features of diabetic nephropathy is the presence of fibrosis. We observed increased collagen content in the HFD group. Notably, rosiglitazone, but not rosuvastatin treatment, prevented the increase in renal collagen deposition, suggesting a possible link between renal fibrosis and renal function. MiR-21 is the most substantial miRNA involved in many fibrotic diseases and is enhanced after initiation of myocardial and pulmonary fibrosis (38, 39). MiR-21 levels are also enhanced in human kidney fibrosis (18, 19). Experimental support for a causative role of miR-21 is provided by miR21 silencing experiments. Silencing of miR-21 by anti-miR-21 oligonucleotide treatment in a murine model of Alport nephropathy reduced glomerulosclerosis, interstitial fibrosis, tubular injury, and inflammation (41). Similarly, silencing miR-21 in diabetic kidneys of db/db mice ameliorated albuminuria, inflammation and renal fibrosis (40).

We observed highly enhanced miR-21 levels only after rosuvastatin treatment, whereas rosiglitazone prevented its expression and was comparable to the chow group. Notably, gene expression of pro-fibrotic genes like α-Sma and Col1α1 (results not shown) was unaffected suggesting that miR-21 could be an early marker of the initiating fibrosis in the kidneys.

In conclusion, our results demonstrate that rosiglitazone reduced HFD-induced insulin levels, suppressed the systemic inflammatory response and protected mice from the development of albuminuria. Despite its anti-inflammatory properties, rosuvastatin failed to improve IR and renal function. Although multiple mechanisms may be involved, rosiglitazone treatment was associated with a marked increase in circulating adiponectin levels suggesting that this adipokine may have contributed to these effects. Strikingly, the beneficial effects of rosiglitazone were paralleled by lowered renal expression levels of miR-21; an increase of miR-21 is associated with microalbuminuria development, inflammation and renal fibrosis. In all, our findings suggest that increasing adiponectin levels could be of clinical importance by improving kidney function and in turn improve cardiovascular health. Also the option of quenching miR-21 activity merits follow-up.

ACKNOWLEDGEMENTS

We thank Peter Zwiers, Wim van Duyvenvoorde and Karin Toet for their excellent technical assistance. MM and GY received funding from TI Food and Nutrition, a public-private partnership on pre-competitive research in food and nutrition. The authors' responsibilities were as follows: Conceived and designed the experiments: TK RK PYW. Performed the experiments: WL GKY KS PYW TT. Analyzed the data: WL GKY MM KS PYW RK TK PH. Wrote the paper: WL GKY MM TK PH. All authors read and approved the final manuscript.

REFERENCES

1. Swinburn BA, Caterson I, Seidell JC, James WP. Diet, nutrition and the prevention of excess weight gain and obesity. Public Health Nutr 2004; 7: 123-146.
2. Hajer GR, van Haeften TW, Visseren FL. Adipose tissue dysfunction in obesity, diabetes, and vascular diseases. Eur Heart J 2008; 29: 2959-2971.
3. Foster MC, Hwang SJ, Massaro JM, et al. Association of subcutaneous and visceral adiposity with albuminuria: the Framingham Heart Study. Obesity (Silver Spring) 2011; 19: 1284-1289.
4. Ritz E. Albuminuria and vascular damage--the vicious twins. N Engl J Med 2003; 348: 2349-2352.
5. Schmieder RE, Schutte R, Schumacher H, et al. Mortality and morbidity in relation to changes in albuminuria, glucose status and systolic blood pressure: an analysis of the ONTARGET and TRANSCEND studies. Diabetologia 2014; 57: 2019-2029.
6. Sharma K. The link between obesity and albuminuria: adiponectin and podocyte dysfunction. Kidney Int 2009; 76: 145-148.
7. Navarro JF, Mora C. Role of inflammation in diabetic complications. Nephrol Dial Transplant 2005; 20: 2601-2604.
8. Briffa JF, McAinch AJ, Poronnik P, Hryciw DH. Adipokines as a link between obesity and chronic kidney disease. Am J Physiol Renal Physiol 2013; 305: F1629-36.
9. Bluher M. Adipokines - removing road blocks to obesity and diabetes therapy. Mol Metab 2014; 3: 230-240.
10. Sharma K, Ramachandrarao S, Qiu G, et al. Adiponectin regulates albuminuria and podocyte

function in mice. J Clin Invest 2008; 118: 1645-1656.
11. Rutkowski JM, Wang ZV, Park AS, et al. Adiponectin promotes functional recovery after podocyte ablation. J Am Soc Nephrol 2013; 24: 268-282.
12. Halberg N, Schraw TD, Wang ZV, et al. Systemic fate of the adipocyte-derived factor adiponectin. Diabetes 2009; 58: 1961-1970.
13. Ciliberto G, Arcone R, Wagner EF, Ruther U. Inducible and tissue-specific expression of human C-reactive protein in transgenic mice. EMBO J 1987; 6: 4017-4022.
14. Kleemann R, Verschuren L, de Rooij BJ, et al. Evidence for anti-inflammatory activity of statins and PPARalpha activators in human C-reactive protein transgenic mice in vivo and in cultured human hepatocytes in vitro. Blood 2004; 103: 4188-4194.
15. Gierman LM, van der Ham F, Koudijs A, et al. Metabolic stress-induced inflammation plays a major role in the development of osteoarthritis in mice. Arthritis Rheum 2012; 64: 1172-1181.
16. Levine AS, Billington CJ. Do circulating leptin concentrations reflect body adiposity or energy flux?. Am J Clin Nutr 1998; 68: 761-762.
17. Ukkola O, Santaniemi M. Adiponectin: a link between excess adiposity and associated comorbidities?. J Mol Med (Berl) 2002; 80: 696-702.
18. Chau BN, Xin C, Hartner J, et al. MicroRNA-21 promotes fibrosis of the kidney by silencing metabolic pathways. Sci Transl Med 2012; 4: 121ra18.
19. Glowacki F, Savary G, Gnemmi V, et al. Increased circulating miR-21 levels are associated with kidney fibrosis. PLoS One 2013; 8: e58014.
20. Abdin AA, Baalash AA, Hamooda HE. Effects of rosiglitazone and aspirin on experimental model of induced type 2 diabetes in rats: focus on insulin resistance and inflammatory markers. J Diabetes Complications 2010; 24: 168-178.
21. Mattoo V, Eckland D, Widel M, et al. Metabolic effects of pioglitazone in combination with insulin in patients with type 2 diabetes mellitus whose disease is not adequately controlled with insulin therapy: results of a six-month, randomized, double-blind, prospective, multicenter, parallel-group study. Clin Ther 2005; 27: 554-567.
22. Fidan E, Onder Ersoz H, Yilmaz M, et al. The effects of rosiglitazone and metformin on inflammation and endothelial dysfunction in patients with type 2 diabetes mellitus. Acta Diabetol 2011; 48: 297-302.
23. Doh FM, Chang TI, Koo HM, et al. The effect of HMG-CoA reductase inhibitor on insulin resistance in patients undergoing peritoneal dialysis. Cardiovasc Drugs Ther 2012; 26: 501-509.
24. Pajvani UB, Scherer PE. Adiponectin: systemic contributor to insulin sensitivity. Curr Diab Rep 2003; 3: 207-213.
25. Ouchi N, Walsh K. Adiponectin as an anti-inflammatory factor. Clin Chim Acta 2007; 380: 24-30.
26. Zoccali C, Mallamaci F, Tripepi G, et al. Adiponectin, metabolic risk factors, and cardiovascular events among patients with end-stage renal disease. J Am Soc Nephrol 2002; 13: 134-141.
27. Nawrocki AR, Rajala MW, Tomas E, et al. Mice lacking adiponectin show decreased hepatic insulin sensitivity and reduced responsiveness to peroxisome proliferator-activated receptor gamma agonists. J Biol Chem 2006; 281: 2654-2660.
28. Ohashi K, Iwatani H, Kihara S, et al. Exacerbation of albuminuria and renal fibrosis in subtotal renal ablation model of adiponectin-knockout mice. Arterioscler Thromb Vasc Biol 2007; 27: 1910-1917.
29. Lee S, Zhang H, Chen J, et al. Adiponectin abates diabetes-induced endothelial dysfunction by suppressing oxidative stress, adhesion molecules, and inflammation in type 2 diabetic mice. Am J Physiol Heart Circ Physiol 2012; 303: H106-15.
30. Gaede P, Lund-Andersen H, Parving HH, Pedersen O. Effect of a multifactorial intervention on mortality in type 2 diabetes. N Engl J Med 2008; 358: 580-591.
31. Lim AI, Tang SC, Lai KN, Leung JC. Kidney injury molecule-1: more than just an injury marker of tubular epithelial cells?. J Cell Physiol 2013; 228: 917-924.
32. Gansevoort RT, Nauta FL, Bakker SJ. Albuminuria: all you need to predict outcomes in chronic kidney disease?. Curr Opin Nephrol Hypertens 2010; 19: 513-518.
33. Verhulst A, D'Haese PC, De Broe ME. Inhibitors of HMG-CoA reductase reduce receptor-mediated endocytosis in human kidney proximal tubular cells. J Am Soc Nephrol 2004; 15: 2249-2257.
34. Corna D, Sangalli F, Cattaneo D, et al. Effects of rosuvastatin on glomerular capillary size-selectivity function in rats with renal mass ablation. Am J Nephrol 2007; 27: 630-638.
35. van der Tol A, Van Biesen W, Van Laecke S, et al. Statin use and the presence of microalbuminuria. Results from the ERICABEL trial: a non-interventional epidemiological cohort study. PLoS One 2012; 7: e31639.
36. Wolf G, Schroeder R, Ziyadeh FN, Stahl RA. Albumin up-regulates the type II transforming

growth factor-beta receptor in cultured proximal tubular cells. Kidney Int 2004; 66: 1849-1858.
37. Rychlik I, Miltenberger-Miltenyi G, Ritz E. The drama of the continuous increase in end-stage renal failure in patients with type II diabetes mellitus. Nephrol Dial Transplant 1998; 13 Suppl 8: 6-10.
38. Thum T, Gross C, Fiedler J, et al. MicroRNA-21 contributes to myocardial disease by stimulating MAP kinase signalling in fibroblasts. Nature 2008; 456: 980-984.
39. Liu G, Friggeri A, Yang Y, et al. miR-21 mediates fibrogenic activation of pulmonary fibroblasts and lung fibrosis. J Exp Med 2010; 207: 1589-1597.
40. Zhong X, Chung AC, Chen HY, et al. miR-21 is a key therapeutic target for renal injury in a mouse model of type 2 diabetes. Diabetologia 2013; 56: 663-674.
41. Gomez IG, MacKenna DA, Johnson BG, et al. Anti-microRNA-21 oligonucleotides prevent Alport nephropathy progression by stimulating metabolic pathways. J Clin Invest 2014;
42. Kleemann R, Princen HM, Emeis JJ, et al. Rosuvastatin reduces atherosclerosis development beyond and independent of its plasma cholesterol-lowering effect in APOE*3-Leiden transgenic mice: evidence for antiinflammatory effects of rosuvastatin. Circulation 2003; 108: 1368-1374.
43. Tao L, Wang Y, Gao E, et al. Adiponectin: an indispensable molecule in rosiglitazone cardioprotection following myocardial infarction. Circ Res 2010; 106: 409-417.

SUPPLEMENTARY DATA

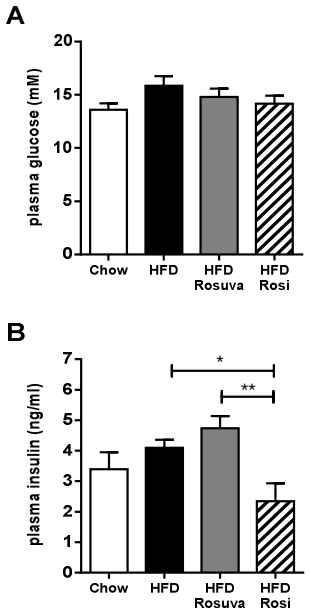

Supplementary Figure 1: Effects of rosuvastatin and rosiglitazone on plasma glucose and insulin. HuCRPtg mice mice were fed chow, high-fat diet (HFD), HFD+0.005% (w/w) rosuvastatin (HFD Rosuva) or HFD+0.018% (w/w) rosiglitazone for 42 weeks. A: plasma glucose levels, B: plasma insulin levels. Data are mean ± SEM. * p<0.05, ** p<0.01.

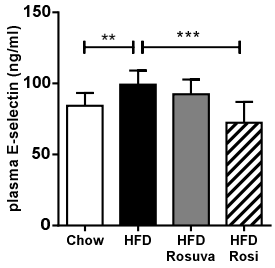

Supplementary Figure 2: Effects of rosuvastatin and rosiglitazone on plasma E-selectin. HuCRPtg mice were fed chow, high-fat diet (HFD), HFD+0.005% (w/w) rosuvastatin (HFD Rosuva) or HFD+0.018% (w/w) rosiglitazone for 42 weeks. Data are mean ± SEM. ** p<0.01, *** p<0.001.

SUPPLEMENT 3: DETAILED MATERIALS AND METHODS

Plasma analyses

Human CRP in plasma was quantified by established ELISA (R&D Systems, Abingdon, United Kingdom) at t=0 and weeks 2, 4, 5, 11, 34, and 42. Plasma levels of E-selectin (R&D Systems), leptin (R&D Systems), and adiponectin (R&D systems) were quantified up to t=42 weeks. Plasma insulin levels were determined by ELISA (Mercodia, Uppsala, Sweden) and plasma glucose levels were determined by enzymatic assay (glucose hexokinase method, Instruchemie, the Netherlands).

Renal RNA and miRNA extraction and gene expression analysis

Total RNA was extracted from 35-µm thin cryo-sections from kidney using RNeasy Plus Mini Kit (Qiagen N.V., Venlo, the Netherlands) according to the manufacturer's instructions. Integrity of RNA was determined by agarose gel electrophoresis. RNA quantity (OD-260) and quality (OD-260/OD-280) were determined using a NanoDrop1000 UV-Vis spectrophotometer (NanoDrop Technologies, Rockland, DE, USA) as described previously (1).

Total RNA was reverse-transcribed using SuperScript® III Reverse Transcriptase (Invitrogen, Breda, the Netherlands) and random hexamer primers (Promega, Leiden, the Netherlands). TaqMan® Gene Expression Assays (Life Technologies, Bleiswijk, the Netherlands) were used to detect the expression of selected target genes. Endogenous PPIA (Mm02342430_g1) was used as a housekeeping gene along with the following probes for CD68 (Mm00839636_g1), VCAM-1 (Mm00449197_m1), E-selectin (Mm00441278_m1), and Kidney Injury Molecule-1 (KIM-1, Mm00506686_m1). Real-time PCR was performed in duplicate and the obtained threshold cycle (Ct) values were averaged. Relative mRNA levels were calculated using the comparative Ct (ΔΔCt) method, expressed as fold-change relative to chow as described previously (2, 3).

For miRNA analysis, TaqMan® microRNA Reverse Transcription Kit (Life Technologies) and specific miR-21 (002493) TaqMan® probe was used for reverse transcription using 10 ng of total RNA. Real-time PCR was performed in a 7500 Fast Real-Time PCR machine using miRNA TaqMan® probes for miR-21(002493) and the endogenous control sno-202 (001232). Each sample was run in duplicate and relative miRNA levels were calculated using the comparative Ct (ΔΔCt) method, expressed as fold-change relative to chow.

Histology and immunohistochemistry

For light microscopic examinations, 3-µm renal paraffin sections were stained with Periodic acid-Schiff (PAS). In short, paraffin sections were deparaffinized and re-hydrated in distilled water. Sections were placed in 0.5% periodic acid solution for 5 minutes. After rinsing in distilled water, sections were incubated in Schiff's reagent (Sigma-Aldrich, Zwijndrecht, the Netherlands) for 15 minutes, followed by rinsing in lukewarm water for 5 minutes. Sections were counterstained with Mayer's haematoxylin for 1 minute and washed in tap water. Images were taken with a Leica microscope using QwinV3 software (Qwin V3 software, Leica Microsystems Imaging Solutions Ltd., Cambridge, UK). For direct visualization of collagen fibers in kidney, a trichrome staining was performed using the

Masson's Trichrome Staining kit (Accustain HT15, Sigma-Aldrich). To quantify renal fibrosis, sections were stained with Picro-Sirius Red for collagen content, and the extent of fibrosis was quantified at 40x magnification using an automated macro in the image processing software ImageJ (version 1.48, NIH, Bethesda, MD, USA). Collagen content was expressed as the percentage of the total tissue area that was positively stained. Glomeruli and vessels larger than the size of adjacent tubules were excluded when assessing the images.

Kidney function measured by albumin/creatinine ratio

To assess renal function, urinary albumin and creatinine levels were measured using commercially available kits. For this, Mouse Albumin ELISA Quantitation Set (Bethyl laboratories, Montgomery, Tx, USA) and The Creatinine Companion assay (Exocell, Philadelphia, PA, USA) were applied according to the manufacturer's instructions.

References

1. Wielinga PY, Yakala GK, Heeringa P*, et al*. Beneficial effects of alternate dietary regimen on liver inflammation, atherosclerosis and renal activation*. PLoS One* 2011; **6**: e18432.

2. Yakala GK, van der Heijden R, Molema G*, et al*. Beneficial effects of an alternating high- fat dietary regimen on systemic insulin resistance, hepatic and renal inflammation and renal function*. PLoS One* 2012; **7**: e45866.

3. Yakala GK, Wielinga PY, Suarez M*, et al*. Effects of chocolate supplementation on metabolic and cardiovascular parameters in ApoE3L mice fed a high-cholesterol atherogenic diet*. Mol Nutr Food Res* 2013;

GENERAL DISCUSSION AND FUTURE PERSPECTIVES

GENERAL DISCUSSION

Non-alcoholic fatty liver disease (NAFLD) has become the most common chronic liver disease in modern societies and constitutes an important global health problem. NAFLD is a multifactorial disease and encompasses a spectrum of pathologies that range from simple hepatic steatosis to nonalcoholic steatohepatitis (NASH) and fibrosis. Metabolic overload from excessive intake of calorie-dense diets and associated chronic inflammation ('metabolic inflammation') are thought play a critical role in the development NASH and fibrosis. A better understanding of the complex etiology of NAFLD, including the sequence of events over time, identification of NASH-promoting disease pathways and the inflammatory cross-talk between liver and adipose tissue, is needed to develop tools for studying the disease and to come up with first treatment regimens for patients.

This chapter discusses the major findings of this thesis in the following order: 1) Chronic inflammation exists in various forms and induction of metabolic inflammation depends on the nature and intensity of the inflammatory triggers employed; 2) Interrelated inflammatory responses in metabolically active tissues and their coordination; 3) Implications for human pathophysiology: human data versus data from experimental models.

Chronic inflammation exists in various forms and induction of metabolic inflammation depends on the nature and intensity of the inflammatory triggers employed

In 2006, Hotamisligil (1) studied chronic inflammation in metabolic diseases and proposed a new term for this type of inflammation, 'metaflammation'. Metaflammation refers to inflammation which is metabolically induced or amplified. Obesity is considered to be closely associated with sub-acute chronic inflammation, which develops systemically but also on tissue level, and this low-grade inflammation is thought to promote the development of metabolic diseases. There is strong link between excess calorie intake resulting in a condition of chronic energy surplus, and the induction of chronic inflammation. Therefore, diet-evoked chronic metaflammation may constitute a crucial factor in the progression of bland liver steatosis to NASH. The nature of this chronic inflammatory component that drives this transition towards NASH has long been unclear.

In ***Chapter 3*** we compared the effects of different inflammatory triggers, among which were metabolic inflammatory triggers (dietary carbohydrate, cholesterol) and non-metabolic (classical) inflammatory triggers (IL-1β, LPS). All these inflammatory triggers exhibited a comparable NFκB-activating effect but this property appeared to be insufficient to induce NASH, even when superimposed on HFD feeding. While HFD feeding alone merely induced bland liver steatosis, non-metabolic inflammatory triggers superimposed on HFD also did not induce a human-like NASH pathology, although additional inflammatory pathways (e.g. STAT3) were activated. Surprisingly, metabolic triggers of inflammation did promote the progression towards NASH. A common denominator the effect of metabolic triggers was the additional activation of the pro-inflammatory transcriptional master regulator AP-1 and the pronounced infiltration of neutrophils, both of which could be causative factors in the development of NASH. The

data of ***Chapter 3*** thus demonstrate that chronic liver inflammation exists in different forms and that the progression from steatosis to NASH depends on a specific type of inflammation, which can be evoked with calorie-dense diets (metabolically inflammatory triggers).

A next question is related to the dynamics of diet-inducible metabolic inflammation, i.e. whether metainflammation is induced gradually up to at a stable, elevated level or whether it has a more dynamic patter. In ***Chapter 3, Chapter 4 and Chapter 6***, studies with different time periods of HFD+cholesterol feeding were performed. There is a positive association between the severity of steatosis and fibrosis and the time of treatment with these cholesterol-containing diets. However, the extent of lobular inflammation as reflected by the number of inflammatory cells aggregates in liver lobes (including neutrophils) showed a more complex pattern over time. In the early phase of the pathogenesis (e.g. t=8 w or t=12 w of diet-feeding the number of inflammatory cell aggregates strongly increased with time. However, the number of these inflammatory foci decreased once fibrosis occurred at the more late stages of the disease, that is after t=20w of diet feeding. This counter-intuitive finding could be explained by the phenomenon of inflammation resolution (reviewed in (2)) which is frequently associated with the process of wound healing. In the early phases of inflammation, infiltrating neutrophils reach peak levels and these cells are gradually replaced by other types of inflammatory cells (from the macrophages/monocytes lineage) (2). In the late phase of tissue inflammation, macrophages or monocytes take a dominant role and the numbers neutrophils may decline. Finally, tissue repair mechanisms are mounted including the deposition of collagen to stabilize damaged areas within an organ. Consistent with this, we observed a decrease of inflammatory cells aggregates and neutrophils alongside with an increase of fibrosis in those studies with prolonged HFD+cholesterol feeding, e.g. in ***Chapter 6***. Although the studies which are part of this thesis may suggest to some readers that inflammation and fibrosis develop independently during the pathogenesis of NASH, it is more likely that, during the resolution phase of inflammation, inflammatory processes and pro-fibrotic processes are tightly interconnected. Studies of this thesis as well as those reported in literature indicate that the interrelationship between diet-induced inflammation and fibrosis is very complex and that the dose of the trigger of the inflammatory insult in liver (e.g. cholesterol) is critical for processes showing high dynamics such as lobular cellular inflammation. For instance, in ***Chapter 5***, we used a much lower dose of cholesterol (0.1% w/w) than in ***Chapter 6*** (1% cholesterol, w/w), while the length of both studies was comparable (20 weeks). We found that a higher dose of cholesterol (1% w/w) did not affect the induction of microvesicular steatosis (±10%) but led to two times more macrovesicular steatosis (20% vs 10%), thus a more severe form of human-like hepatic steatosis. Furthermore, the higher dose of cholesterol decreased the level of hepatic lobular inflammation, which may be unexpected when the concept of inflammation resolution is ignored, and increased the level of hepatic fibrosis.

Although the mechanism underlying the relationship of hepatic inflammation and fibrosis during the progressive stages of NASH is unclear, our studies have demonstrated that induction of metabolic inflammation is very dynamical process and that it largely depends on the quality and quantity of inflammatory triggers employed. Since these metabolic inflammatory triggers are employed for very long periods (up to 40 weeks), the

interpretation of the results of such studies should consider that an organism mounts counter-regulatory processes to resolve inflammation and to restore organ functions. Therefore, the outcomes of such studies (and interventions) should not only be interpreted and discussed in the light of a pro-inflammatory metabolic condition but should also consider that anti-inflammatory processes and tissue-repair pathways can take place.

Interrelated inflammatory responses in metabolically active tissues and their coordination

After investigating how inflammation develops in the liver in the context of diet-induced obesity, it is intriguing to explore the effects of metabolic overload on other metabolically active organs, the more so because it has been unclear in which tissue inflammation does start and whether organ-organ cross-talk may contribute to the pathogenesis of NASH.

Tracing back the development history of biology, interestingly, in the lower organisms, such as *Drosophila melanogaster*, the metabolic and immune responses are controlled by a single organ, the fat body (reviewed in (1)). In higher organisms, this association (and hence molecular interaction) between metabolism and inflammation is preserved and also can be found in the major metabolic tissues. For example, the liver and white adipose tissue (WAT) share the similar immune effector cells, e.g. Kupffer cells and macrophages which constitutively reside in these tissues, as well as metabolic cells, such as hepatocytes and adipocytes. Many gene expression studies and microarray analyses demonstrated that the expression of genes involved in (lipid) metabolism and inflammation is adjusted extensively after long periods of HFD feeding (3, 4). However, significant effects on gene expression are likely to start early and may change over time, i.e. may be much more dynamical than assumed.

Therefore, in ***Chapter 7***, we performed a refined HFD induced time course study in which we investigated *the early dynamical events* of metabolic adaptation in a) the expanding WAT and b) the liver. This allowed us to demonstrate that the adjustment of lipid metabolism genes is related to the onset of inflammatory gene expression during diet-induced obesity, and that a relationship exists between the processes in WAT and those occurring later in time in the liver. By means of gene expression analysis and histology, we found that lipid metabolism genes in WAT were adjusted in the first place. Later in time, when the storage capacity of WAT reached its limit, inflammatory genes were expressed in WAT. When WAT inflammation started, genes involved in lipid metabolism and inflammation in the liver were adjusted, as demonstrated by analysis of gene expression time profiles of WAT and corresponding livers. We showed that the transcriptional regulators Jun, Fos, Rarα, Pparα, Stat1, Stat5, Sp1 controlled lipid metabolism and the inflammatory responses to HFD feeding in both liver and WAT, which is in line with the evolutionary relationship of both tissues described above and the view that transcriptional control mechanisms of the metabolic-inflammatory network are highly preserved (1). Because WAT inflammation precedes NAFLD, our studies support the view that inflammatory factors released by WAT contribute to the pathogenesis of NAFLD. Experimental evidence for a causal role of WAT in the development of NASH has not been provided so far and studies on the role of inflamed WAT are subject to future investigations of our group. Because inflammatory factors secreted by WAT and liver may

affect other tissues, and because chronic HFD-induced metabolic overload is unlikely to be restricted to the expanding WAT and the liver only, we investigated whether other organs (in particular those with a high blood flow and high density of capillaries) may be effected affected as well. As shown in ***Chapter 8***, kidney function deteriorated significantly after long-term (40 weeks) HFD feeding and this deterioration appears to be caused, at least partly, by chronic inflammation.

Hence, metabolic overload evoked inflammation starts locally in WAT and affects, as time proceeds, more and more tissues. This concept is visualized in the figure below (***see* Figure 1**): metabolic overload (from overnutrition, HFD) leads to expansion of adipocytes in WAT. Once further expansion is not possible anymore, low-grade inflammation develops which is characterized by local expression of inflammatory mediators (e.g. TNF-α, IL-1β, CCL2) and related inflammatory pathways, such as IKK and JNK. Factors released by WAT and/or spill-over of lipids now stored in other organs such as liver and kidney subsequently triggers a pro-inflammatory response in these tissues. Over time, this local chronic inflammation (in WAT, liver and other organs) may intensify and further induce recruitment and activation of inflammatory cells. This metaflammation, which is in first place a consequence of metabolic overload of the entire organism, is typically not noticed for decades and, without resolution, may lead to chronic metabolic disease, such as NAFLD/NASH and chronic kidney disease.

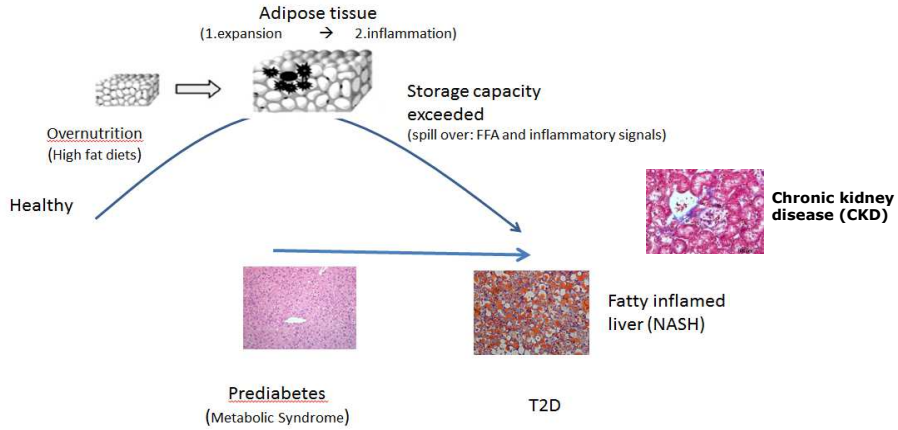

Figure 1: How different tissues are affected by metabolic overload and metabolic inflammation.

Implications for human pathophysiology: human data versus data from experimental models

'Translational research' has been discussed and debated in academia, industry and government for many decades. In 2008, a report 'Translational research: Crossing the valley of death' was published in *Nature* (5) and the author, Declan Butler, addressed the chasm that exists between biomedical research and the needs of patients. Due to the ethical issues and the inaccessibility of many tissues in humans, experimental studies are performed in models of disease in biomedical research. The most important question

related to these models is 'Does the model reflect the human situation?'. Experimental models are frequently performed in rodents which differ from humans with respect to metabolic activity as well as drug metabolism, immunological properties etc. However, when it comes to underlying mechanisms of disease, models can be very similar to human pathology, provided that the inducers of the pathogenic pathways are comparable and physiologically relevant. We and others have demonstrated that diet-inducible models of NAFLD/NASH share defining characteristics of the human pathology, and that there are many commonalities between humans and experimental models in animals. In this thesis, APOE*3 mice, APOE*3Leiden.huCETP mice or human CRP transgenic mice were used. The APOE*3 background allows to mimic human lipid metabolism and animals develop a more human-like lipoprotein profile as well as the risk factors that promote the development of NAFLD in the context of visceral obesity and dyslipidemia (6).

Furthermore, important hallmarks of human NASH (as defined in human biopsies) should be validated in experimental NAFLD/NASH models. It is remarkable that a direct comparison between the human NAFLD pathology and the experimentally induced NAFLD pathology has not been made, and that there was no generally accepted well-documented grading system for experimental NAFLD/NASH. That is why we first characterized the steatotic and inflammatory components of NAFLD/NASH in human biopsies (in ***Chapter 3***), and evaluated the same components in our experimental NASH model. This resulted in a general scoring system for experimental NAFLD/NASH for rodent models of the disease which is generic and applicable for a broad spectrum of models (***Chapter 2***). More specifically, the critical histopathological criteria for grading and scoring of macrovesicular and microvesicular steatosis, inflammatory cells aggregates, ballooning cells and fibrosis were defined by us. Application of the scoring system for examination the longitudinal development of disease stages and the efficacy of interventions, allowed us to further validate and implement the grading system.

In ***Chapter 4***, we, furthermore, tried to establish a link between specific features of histopathology and biomedical parameters relevant for the progression of NASH. We showed that a correlation exists between macrovesicular steatosis and cellular lobular inflammation, and that there is a correlation between microvesicular steatosis and NFκB activation in liver. Our findings shows that the specific forms of steatosis (macrovesicular and microvesicular) develop have a distinct developmental pattern over time and that they are associated with different cellular and molecular inflammatory events, which probably involve different pathways.

Conclusions and future perspectives

The studies presented in this thesis have generated more insight in the pathogenic mechanisms which contribute to obesity-induced NAFLD, in particular the transition from NAFL to NASH, and the development of fibrosis. The complex interactions between metabolic and inflammatory pathways in key metabolic organs were investigated in detail and, overall, our analyses support an involvement of the inflamed WAT in the pathogenesis of NAFLD/NASH which adds another layer of complexity. As outlined in detail, there are clear differences between NAFLD in humans and the pathology in experimental models and experimental models cannot mimic the full spectrum of diversity and variation that is typically observed in human patients. A part of the

complexity in humans arises from genetic and ethnic differences, but different dietary habits and different preference to nutritional components such as dietary fat (e.g. consumer oils) both in quality and quantity, as well as differences in organ-crosstalk between humans, all of which can hardly be mimicked in a single model of disease. In NASH research, the most fundamental questions, which are related to the lipid component of the disease and to the complex etiology of the disease still needs to be answered. For example, what is the actual potential of steatosis to induce toxic effects in liver?, what is the actual cascade of pathologic processes leading to inflammation and fibrosis?, and how are these processes related to the events of steatosis? Furthermore, observed phenotypic difference in human NASH patients raise the fundamental question whether the different phenotypic features that exist in humans are appropriately reflected (with respect to the specific molecular events and pathways) in the models?

Research can answers questions, but, if well conducted, will lead to more detailed questions which will also open new opportunities for better understanding and/or treatment of diseases.

Let us keep on thinking, as the honored 19th century scientists, trying to find out the explanation of the phenomenon in order to truly understand Nature we live in!

REFERENCES

1. Hotamisligil GS. Inflammation and metabolic disorders. *Nature* 2006;444(7121):860-7.

2. Serhan CN. Pro-resolving lipid mediators are leads for resolution physiology. *Nature* 2014;510(7503):92-101.

3. Grove KL, Fried SK, Greenberg AS, et al. A microarray analysis of sexual dimorphism of adipose tissues in high-fat-diet-induced obese mice. *Int J Obes (Lond)* 2010;34(6):989-1000.

4. Kreeft AJ, Moen CJ, Porter G, et al. Genomic analysis of the response of mouse models to high-fat feeding shows a major role of nuclear receptors in the simultaneous regulation of lipid and inflammatory genes. *Atherosclerosis* 2005;182(2):249-57.

5. Butler D. Translational research: Crossing the valley of death. *Nature* 2008;453(7197):840-2.

6. van den Hoek AM, van der Hoorn JW, Maas AC, et al. APOE*3Leiden.CETP transgenic mice as model for pharmaceutical treatment of the metabolic syndrome. *Diabetes Obes Metab* 2014;16(6):537-44

.

SUMMARY AND NEDERLANDSE SAMENVATTING

10

SUMMARY

Overload of nutrients can lead to diet-induced inflammation, also called metabolic inflammation, which is thought to play an important role in many metabolic diseases, including the development of nonalcoholic fatty liver disease (NAFLD). NAFLD has become the most common chronic liver disease and encompasses a spectrum of pathologies that range from simple hepatic steatosis to nonalcoholic steatohepatitis (NASH) and fibrosis. The pathogenesis of NAFLD, including the sequence of events in time and the underlying mechanisms that initiate the transition from a fatty liver to NASH and fibrosis, remain poorly understood. Effective and reliable therapeutic approaches that are based on the understanding of the pathogenesis of NASH are therefore still lacking.

After a general introduction of human NASH and experimental NASH in ***Chapter 1***, we systematically compared in ***Chapter 2*** human NAFLD liver pathology, using human liver biopsies, with liver pathology of several NAFLD mouse models. Based on the features pertaining to mouse NAFLD, we aimed at establishing a modified generic histological scoring system for NASH that is applicable to broad spectrum of rodent models.

In the ***second*** part of the thesis, we investigated the progression of NAFL to NASH in more detail using diet-induced NASH mouse models. In ***Chapter 3***, we examined the effect of metabolic inflammatory triggers (dietary carbohydrate, cholesterol) and non-metabolic (classical) inflammatory chronic triggers (IL-1β, LPS) on the progression of bland liver steatosis to NASH using high fat diet (HFD)-induced obese APOE*3Leiden.CETP mice. We showed that HFD feeding followed by metabolic triggers induced extensive steatosis and specific inflammatory components (neutrophils, AP-1) which results in a human-like NASH phenotype, while chronic administration of non-metabolic triggers, LPS and IL-1β, did not.
Because patients remain asymptomatic during the early stages of the disease, NAFLD is often diagnosed at a late stage which is accompanied by irreversibly liver damage (liver fibrosis, cirrhosis). Hence, little is known about the early, potentially reversible, disease processes and their relationship over time. Therefore, in ***Chapter 4***, we concentrated on the early events of NAFLD development and the processes 'steatosis' and 'onset of inflammation' with regards to their occurrence and progression over time as well as their role in the transition of NAFL to NASH. Based on a systematical and longitudinal analysis of liver histology in conjunction with biochemical measurements and microarray data of this time course study, we demonstrated that links exist between microvesicular and macrovesicular steatosis and specific facets of liver inflammation. We show that the two types of steatosis have a distinct time pattern and are associated with the activation of specific cellular and molecular inflammatory events.

In the ***third*** part of the thesis, we aimed to test potential therapeutics for NASH. In ***Chapter 5***, a nutritional intervention was performed by treating APOE*3Leiden mice fed a high cholesterol diet with a moderate dose of an anthocyanin-rich standardized bilberry extract (Mirtoselect). We found that Mirtoselect remarkable attenuates NASH and associated fibrosis as shown by an improvement of histological outcomes (steatosis, hepatic inflammation and fibrosis) and suppression of hepatocellular inflammation which can be explained by an effect on cholesterol handling. In ***Chapter 6***, a pharmaceutical intervention was performed by treating APOE*3Leiden.CETP mice fed a high fat, high cholesterol diet with salsalate, an anti-inflammatory agent hat was recently found to

exhibit beneficial metabolic effects on glucose and lipid metabolism. Salsalate exerted a preventive effect on onset and progression from NAFL to NASH and fibrosis. More specifically, our results showed an improvement of lipid metabolism by increasing β-oxidation and decreasing lipogenesis. Furthermore, inflammation was reduced (down-regulation of the NFκB pathway) and fibrosis development was prevented (down-regulation of TGF-β signaling).

In the ***last*** part of the thesis, the effects of metabolic overload and metabolic inflammation on other tissues were investigated. The effect of metabolic overload on white adipose tissue (WAT) and liver was analyzed in ***Chapter 7***, using HFD fed APOE*3Leiden mice. These mice respond to HFD feeding with WAT expansion, metabolic stress, inflammation and development of NAFLD. In WAT transcriptomics data showed that metabolic overload induced an immediate, stable response on clusters of lipid metabolism genes and induced inflammatory genes later in time. When WAT inflammation began, the hepatic response to HFD resembled that in WAT. Our study suggests WAT and liver respond to metabolic overload by adaptations in expression of gene clusters that control lipid metabolism and inflammatory processes in an orchestrated and interrelated manner.

Finally, in ***Chapter 8***, we investigated 1) how metabolic stress-induced inflammation exerted an effect on kidney dysfunction, and 2) whether pharmacological interventions aimed at suppressing metabolic stress-induced inflammation could improve renal function in high fat challenged transgenic mice. We demonstrated that human C-reactive protein transgenic (huCRPtg) mice with a HFD feeding showed metabolic stress-induced systemic inflammation and developed NASH. Interventions with a PPAR-γ activator (rosiglitazone) reduced systemic inflammation, prevented insulin resistance, increased plasma adiponectin, and diminished renal fibrosis and improved renal function. In contrast, a statin (rosuvastatin) treatment reduced systemic inflammation but did not affect insulin resistance or renal function.

Taken together, in order to gain more insight into the mechanisms of NASH pathogenesis, we started with comparison of human NASH and experimental NASH. Subsequently, we provided evidence that activation of AP-1 and associated neutrophil infiltration is important for NAFL progression towards NASH and this can be induced experimentally by 'metabolic' dietary triggers of inflammation. We demonstrated that specific links exist between microvesicular/macrovesicular steatosis and cellular/molecular inflammation in liver. Furthermore, we explored novel nutritional and pharmacological agents as potential strategies to combat NASH. Finally, we investigated the effects of high fat diet-induced metabolic overload on the liver in relation to inflammation in white adipose tissue and kidney, and the dysfunction of these tissues.

NEDERLANDSE SAMENVATTING

Een overmaat aan voedingsstoffen kan leiden tot dieet-geïnduceerde ontsteking. Dit wordt metabole ontsteking genoemd en hiervan wordt gedacht dat het een belangrijke rol speelt in veel stofwisselingsziekten, waaronder de ontwikkeling van niet-alcoholische leververvetting (non-alcoholic fatty liver disease, NAFLD). NAFLD is de meest voorkomende chronische leverziekte en omvat een spectrum van ziektebeelden die variëren van alleen leververvetting tot niet-alcoholische leververvetting met ontsteking (non-alcoholic steatohepatitis, NASH) en bindweefselvorming (fibrose). De ontstaanswijze van NAFLD en de onderliggende mechanismen die ten grondslag liggen aan de overgang van leververvetting naar NASH en fibrose zijn onduidelijk. Om deze reden ontbreken effectieve en betrouwbare behandelingsstrategieën die ingrijpen op de ontstaanswijze van NASH.

Na een algemene introductie over humaan en experimenteel NASH in ***hoofdstuk 1***, hebben we in ***hoofdstuk 2*** de leverpathologie van humaan NAFLD met behulp van humane leverbiopten systematisch vergeleken met de leverpathologie van enkele NAFLD muismodellen. Op basis van de kenmerken van NAFLD van muizen, beoogden we een aangepast algemeen histologisch scoresysteem voor NASH te definiëren dat toepasbaar is voor knaagdiermodellen.

In het ***tweede*** deel van het proefschrift bestudeerden we meer in detail de progressie van NALFD naar NASH met behulp van dieet-geïnduceerde NASH muismodellen. In ***hoofdstuk 3*** onderzochten we het effect van stimuli van metabole ontsteking (koolhydraten en cholesterol in dieet) en chronische, niet-metabole (klassieke) stimuli (IL-1β, LPS) op de progressie van louter leververvetting naar NASH in door hoog vet-geïnduceerde obese APOE*3Leiden.CETP muizen. We toonden dat een hoog vet dieet gevolgd door stimuli van metabole ontsteking, vervetting (steatose) en specifieke ontstekingscomponenten (neutrofielen, AP-1) induceert. Dit resulteert op een NASH dat lijkt op dat van de mens, terwijl een langdurige toediening van niet-metabole stimuli, LPS en IL-1β hier niet toe leidt.

Doordat patiënten asymptomatisch blijven tijdens de vroege stadia van NAFLD, wordt het vaak in een later stadium pas gediagnostiseerd, waarbij al onomkeerbare leverschade is ontstaan (leverfibrose, cirrhose). We weten nog weinig over de vroege, potentieel reversibele ziekteprocessen en hun tijdsbeloop. Daarom vestigden we onze aandacht in ***hoofdstuk 4*** op de vroege stadia van NAFLD ontwikkeling, het tijdsbeloop en de progressie van 'steatose' en 'ontsteking' en de rol van deze processen in de overgang van NAFLD naar NASH. Op basis van een systemische en longitudinale analyse van leverhistologie, biochemische metingen en microarray data, laten we zien dat microvesiculaire, macrovesiculaire steatose en specifieke kenmerken van leverontsteking aan elkaar gerelateerd zijn. We tonen dat de twee soorten steatose een verschillend tijdsbeloop hebben en geassocieerd zijn met de activatie van specifieke cellulaire en moleculaire ontstekingsprocessen.

In het ***derde*** deel van het proefschrift bestudeerden we potentiële therapieën van NASH. In ***hoofdstuk 5*** werden APOE*3Leiden muizen gevoed met een hoog cholesterol dieet met een gestandaardiseerde dosis van een anthocyaninine-rijk bosbessenextract (Mirtoselect). We vonden dat Mirtoselect NASH en fibrose aanmerkelijk verminderde,

gemeten aan de hand van een verbetering van de histologische resultaten (steatose, leverontsteking en fibrose) en een onderdrukking van levercelontsteking, wat kan worden verklaard door een effect van cholesterolverwerking. In ***hoofdstuk 6*** werden APOE*3Leiden.CETP muizen op een hoog vet, hoog cholesterol dieet gezet dat salsalaat bevat, een anti-inflammatoir middel waarvan recentelijk is aangetoond dat het gunstige metabole effecten heeft op het glucose- en vetmetabolisme. Salsalaat voorkwam de progressie van NAFLD naar NASH en fibrose en - meer specifiek- verbeterde het vetmetabolisme door toename van β-oxidatie en afname van lipogenese. Bovendien was ontsteking verminderd (minder activatie van de NFκB signaleringsroute) en werd fibrose ontwikkeling voorkómen (minder activatie van de TGF-β signaleringsroute).

In het ***laatste*** gedeelte van het proefschrift werden de effecten van metabole overbelasting en metabole ontsteking op andere weefsels onderzocht. De effecten van metabole overbelasting op wit vetweefsel en lever in APOE*3Leiden muizen op hoog vet dieet werd bestudeerd in ***hoofdstuk 7***. Deze muizen reageerden met een toename van wit vetweefsel, metabole stress, ontsteking en de ontwikkeling van NAFLD. mRNA analyse van wit vetweefsel toonde dat metabole overbelasting leidde tot een onmiddellijk optredend, stabiele respons op clusters van genen van het vetmetabolisme en later in de tijd ontstekingsgenen induceerde. Op het moment dat ontsteking van wit vetweefsel ontstond, leek de respons van de lever op hoog vet dieet op dat van wit vetweefsel. Onze studie impliceert dat wit vetweefsel en de lever op een samenhangende manier reageren op metabole overbelasting door aanpassingen in expressie van genclusters die het vetmetabolisme en ontstekingsprocessen reguleren.

Tenslotte onderzochtten we in ***hoofdstuk 8*** 1) hoe metabole stress-geïnduceerde ontsteking een effect heeft op de nierfunctie en 2) of farmacologische interventies die metabole stress-geïnduceerde ontsteking verminderen ook de nierfunctie in transgene muizen op een hoog vet dieet kunnen verbeteren. We toonden dat humaan C-reactief eiwit transgene (huCRPtg) muizen op een hoog vet dieet metabole stress-geïnduceerde systemische ontsteking en NASH ontwikkelden. Interventie met een PPAR-γ activator (rosiglitazon) verlaagde de systemische ontsteking, voorkwam insuline resistentie, leidde tot een toename van plasma adiponectin, verminderde nierfibrose en verbeterde de nierfunctie. Een statine (rosuvastatine) daarentegen, verminderde wel systemische ontsteking maar had geen effect op insuline resistentie of nierfunctie.

Samenvattend, hebben we ten eerste humaan en experimenteel NASH vergeleken om meer inzicht te verkrijgen in de mechanismen van de ontwikkeling van NASH. Vervolgens hebben we aangetoond dat activatie van AP-1 en de hiermee geassocieerde neutrofiel infiltratie belangrijk zijn voor NAFLD progressie naar NASH en dat dit geïnduceerd kan worden door 'metabole' stimuli voor ontsteking in het dieet. We hebben laten zien dat microvesiculaire/macrovesiculaire steatose en cellulaire/moleculaire ontsteking in de lever aan elkaar gerelateerd zijn. Daarnaast hebben we een nieuwe interventie in voeding en een farmacologisch middel onderzocht als potentiële strategieën om NASH tegen te gaan. Tenslotte bestudeerden we de effecten van hoog vet-geïnduceerde metabole overbelasting op de lever en ontsteking en functie van wit vetweefsel en de nieren.

ACKNOWLEDGEMENT

Finally the time has come, my thesis is finished. Here is the good opportunity to express my gratitude to everyone who supported me throughout the journey of my PhD. It is no doubt that my fancy book would never be able to come out without aspiring guidance, constructive criticism and friendly advice from my colleagues and friends. I am sincerely grateful to all of you for sharing your truthful and enlightening views on a number of issues related to the project.

Prof. Louis Havekes, ***Dr. Anita van den Hoek*** and ***Dr. Robert Kleemann***, thanks for being my promotor and supervisors. ***Louis,*** I would like to thank you for encouraging and supporting me throughout my PhD studies, and giving your suggestions for improving my researches and orientating my future career. ***Anita, Robert,*** you are tremendous mentors for me! Thanks for giving me more time and space to grow up to be an independent scientific researcher. Thank you, your advice on researches as well as on career has been priceless to me. I feel so lucky to work with you, learn from you, and develop myself in a good way.

Thanks all my dear colleagues at **Metabolic Health Research TNO**. ***Simone, Annie Jie, Christa, Marijke, Elly,*** thanks for your technical assistant of my experiments. ***Pascalle, Kirsty, Susanna and Marjolein***, thanks for your professional help in DEC application and taking care of my mice. ***Ageeth, Adri***, our secretary, I cannot imagine how our department looks like without your contribution. ***Erik, Frits,*** thank for your excellent technical assistant, you added a great value to my project. ***Wim,*** thanks for bringing fun to us and make us laugh all the time. ***Hans,*** thanks for recruiting me working here as a PhD. ***Reinout, Peter, Robert O., Hans,*** thanks for sharing your business perspective regarding to my job hunting and my future career plan. ***José,*** thanks for your positive energy. I let me know how to challenge myself and walk out from my comfortable zone. ***Karin,*** thanks for your laboratory assistant and support. ***Elsbet***, you are the best gift of MHR, you have created lots of beautiful memory for us! Dank je wel! Thanks for your help for everything. ***Kanita,*** thanks for your help with my research, especially, your support when I had a hard time. ***Lars,*** thanks for helping with omics data analysis and let me know how to go through my PhD successfully. ***Teake,*** thanks for your suggestion about how to think as a scientist, and I always feel happy to discuss my career with you. ***Coen,*** thanks for your advice and helps on my personal development. It has always been a good time to share my career goal with you. My dear **AIOs** fellows, ***Anne, Susan, Lobke, Rob, Martine and Petra***, I do enjoy the time with all of you, sharing our happy time and supporting each other in the hard time. Also our interns, ***Mara, Anne-Pauline, Simone, Mark,*** it is nice to work on some interesting projects together with you at TNO.

Dear ***Ko***, ***Patrick***, thanks for your supporting from **LUMC ENDO**. ***Man-Chi, Mariëtte, Nancy, Jimmy, Padmini, Sam, Mieke, Edwin, Claudia, Onno, Sander, Mattijs, Janna, Irene, Hanna, Illiana,*** thanks for sharing the good time with me, giving the presentation and discussing in our Monday Endo meetings, travelling to the congresses etc. Thanks for all of you! ***Jan,*** thanks for your great support from **LUMC Pathology**. ***Adri,*** thanks for teaching me how to perform a good immunostaining in lab.

Dear ***Jong TNOers***, ***Silja, Jacco, Wietske, Jeroen***, thanks for your supporting and I am happy to work with you guys. ***Jiongwei, shengxia, Yang, Guangyu, Chenwei, Chengcheng, Yao, Minglu, Qingyang, Yuanjie, Yongchang,*** my dear friends at **CALN *and* ECBBF**, thanks for your supporting. I am so proud of working together with you, doing something good, as a communication channel between China and The Netherlands.

My **mentors** Prof. ***Wang Mao, Wang Li, Eva, Susanne, May, Mei, Jan, Ivo, Kim,*** I feel lucky meeting you at the different stages of my life, from China, Sweden, to The Netherlands. Thanks for sharing your life experience and inspiring advice about my career and my life.

Dadi, the No.1 photographer, thanks for taking photos on my big day. I could keep today's good memory forever. ***Li Wen, Beijia, Lijing, Jiahui,*** my best friends, thanks for sharing happiness and sadness in the past, discussing our career and life in the future. Thanks for being my best friends, and I feel very happy to have you in my life. ***Bangwen, Haifeng, Haiyu, Ancong, Li Ji, Jinghui, Yuning, Meng He, Yifan, Xi Wen, Kaihua, Zhang Juan, Xiaolei, Xinyi, Yanan, Yongyi, Xiaohong, Qi Fang, Qin Yu, Yuntao, Wei-Min, Jen Huang, Shi Zheng, An Na, Shi Jing, Pan Wen, Shengfa, Guo Dong, Lizi, Chen bo, Ma Tao, Xiunan, Yanju, Xiaodong, Yang Yang, Zhou Zhao, Rongfang, Tiantian, Cui Chao, Xia Ji,*** my dearest friends, I am happy to meet you in the Netherlands, which is far away from our mother land. We had spent a good time being together, joys, also tears. Thanks for being a part of my life.

Peter, Ligia, Laura, Barbara, Yorick, my dear **NLP coaching** friends***.*** Thanks for sharing your personal stories with me. Sharing deeply emotional feelings to each other, enjoying cheerful or even suffering painful experience in a frank way, is one of the wonderful gifts I got in my life.

This thesis is dedicated to my great parents who have given me termless supports throughout my life. Letting me go wherever I want and do whatever I want, which means 'freedom', is an amazing gift you give to me. Importantly, I have learned the most important thing in life – believe myself and help people to have a better life. Here, I show my deepest gratitude to you, I love you, my ***MAMA*** and ***PAPA*** forever!

此博士论文特别献给这个世界上我最爱的人- 老爸老妈，姥姥姥爷！老爸老妈，谢谢你们用伟大而深沉的爱，让我这个咿呀学语的孩童，长大成人。如今的我，能自信地站立在这个世界上，呼吸自由的空气；能用自己的双手触摸大自然的神奇，感受尘世的繁华；这一切都是源于你们。"儿行千里，母担忧"，是你们努力压抑自己亲情地召唤，一次一次成全我的梦想；曾几何时，当你们看到别人膝下儿女成群，享受天伦的时候，一定是羡慕的。。。每每想到这里，愧疚感总是会阵阵袭来。。。老爸老妈，是你们用无私的爱给我撑起了这片纯净明媚的天空，让我看到了世界的色彩缤纷，感受到了生命的独特神秘。感谢你们如此无私的爱！慈母手中线，游子身上衣；谁言寸草心，报得三春晖。我永远爱你们！！

Aan het einde van mijn promotie reis, dat ik je ontmoette, mijn lieve, ***Rob***. Jij bent er "gewoon" altijd voor me. Je bent in mijn hart gekomen als de warmste en het helderste deel van mijn leven. Bedankt, ***Matty, Emmo, Maaike, Jelle, Koen, Geertje, Emme, en Rienk,*** Ik voel me altijd warm en gelukkig met jullie.

Dear all, I am very happy to share one of the most important life times with all of you! With such a beautiful memory, I am ready to start a new Journey!

Wen Liang

LIST OF PUBLICATIONS

Wen Liang, Lars Verschuren, José W.A. van der Hoorn, Joanne Verheij, Andrea D. van Dam, Mariette R. Boon, Hans M.G. Princen, Louis M. Havekes, Robert Kleemann, Anita M. van den Hoek. Salsalate attenuates diet induced non-alcoholic steatohepatitis by decreasing lipogenic and inflammatory processes. (Submitted)

Wen Liang, Lars Verschuren, Karin Toet, Louis M. Havekes, Anita M. van den Hoek, Robert Kleemann. Development of microvesicular and macrovesicular steatosis is associated with distinct inflammatory events in liver: a time-course study of cholesterol-induced NASH. (Submitted)

Wen Liang*, Gopala K. Yakala*, Peter Y. Wielinga, Kanita Salic, Tushar Tomar, Robert Kleemann, Peter Heeringa, Teake Kooistra. Protective effect of rosiglitazone on kidney function in high-fat challenged human CRP transgenic mice: is there a role for adiponectin and anti-miR-21? (Submitted)
[* Both authors contributed equally]

Petra Mulder, Martine Morrison, Wen Liang, Lars Verschuren, Hajo van Bockel, Teake Kooistra, Peter Wielinga, Robert Kleemann. Pharmacological intervention in white adipose tissue inflammation attenuates development of NAFLD in obese LDLr-/- mice. (Submitted)

Wen Liang, Aswin L. Menke, Ann Driessen, Ger H. Koek, Jan. H. Lindeman, Reinout Stoop, Louis M. Havekes, Robert Kleemann, Anita M. van den Hoek. Establishment of a General NAFLD Scoring System for Rodent Models and Comparison to Human Liver Pathology. **PLoS One 2014;** 9(12):e115922

Wen Liang, Jan H. Lindeman, Aswin L. Menke, Debby Koonen, Louis M. Havekes, Anita M. van den Hoek, Robert Kleemann. Metabolically induced liver inflammation leads to NASH and differs from LPS- or IL-1β-induced chronic inflammation. **Lab Invest. 2014;** 94(5):491-502

Martine Morrison, Wen Liang, Petra Mulder, Karin Toet, Peter Heeringa, Peter Wielinga, Teake Kooistra, Robert Kleemann. Mirtoselect, an anthocyanin-rich bilberry extract, attenuates non-alcoholic steatohepatitis and associated fibrosis in ApoE∗3Leiden mice.
J Hepatol. 2014; S0168-8278(14): 00929-5

Lovisa Holm, Wen Liang, Annika Thorsell, Susanne Hilke. Acute effects on brain cholecystokinin-like concentration and anxiety-like behaviour in the female rat upon a single injection of 17β-estradiol. **Pharmacol Biochem Behav. 2014;** 122:222-7.

Wen Liang*, Giulia Tonini*, Petra Mulder, Thomas Kelder, Marjan van Erk, Anita M. van den Hoek, Rob Mariman, Peter Y. Wielinga, Michela Baccini, Teake Kooistra, Annibale Biggeri, Robert Kleemann. Coordinated and interactive expression of genes of lipid

metabolism and inflammation in adipose tissue and liver during metabolic overload. **PLoS One 2013;** 8(9):e75290
[* Both authors contributed equally]

Sofia Gustafsson, Wen Liang, Susanne Hilke. Effects of voluntary running in the female mice lateral septum on BDNF and corticotropin-releasing factor receptor 2. **International J. Peptides 2011**:932361.

Wen Liang. The Functional Dead Cells in Plants. **Plant Science**. **2001**: 16: 22(6)

CURRICULUM VITAE

Wen Liang was born on May 8th, 1981 in Xi'an, China. In 2000, she graduated from the Gao Xin First High School in Xi'an. In September 2000, she entered the bachelor program 'Basic Biological Sciences' at China Agricultural University, Beijing, China, which she successfully completed in June 2004. Later on, she started her traineeship on clinical nutrition, which specialized in nutrition intervention in obesity and type 2 diabetes patients in the hospital of the Fourth Military Medical University, Xi'an, China. In 2007, she decided to go aboard and worked on her master study in Neuroscience (problem-based learning, PBL), Linköping University, Sweden. Two years later, she successfully earned master degree (Medical Bioscience). In January 2010, she worked as a PhD candidate in the Department of Metabolic Health Research at TNO (Netherlands Organization for Applied Scientific Research), Leiden, the Netherlands. Under her promoter Prof. Dr. Louis Havekes, the supervision of Dr. Anita M. van den Hoek and Dr. Robert Kleemann, her research aimed at investigating the role of metabolic overload and metabolic inflammation in the development of Nonalcoholic Steatohepatitis (NASH). The results of her experimental studies are presented in this thesis. Wen is now working on Dutch-Chinese communication, Science-Business networking and Business development (B2B/B2C consultancy and documental affairs service) in life sciences.